Intensity Measures for Seismic Response Prediction and associated Ground Motion Selection and Modification

Yin Cheng

Rome, September 2013

Sapienza University of Rome

Department of Structural Engineering and Geotechnics

Dottorato di Ricerca in Ingegneria delle Strutture

Università di Roma “La Sapienza”

XXV Ciclo

Supervisor:

Prof. Eng. Giorgio MONTI

Co-supervisor:

Prof. Eng. Fabrizio MOLLAIOLI

Coordinator of the Doctoral School:

Prof. Eng. Giuseppe REGA

ABSTRACT

Based on the research of the first generation of Performance-Based Earthquake engineering methodology (PBEE), Pacific Earthquake Engineering Research Centre (PEER) has developed the second generation procedure aiming at a more robust methodology of PBEE where the process is broken into several logical elements that can be studied and resolved in a rigorous and consistent manner. Due to the inherent uncertainty properties of earthquake occurrence, e.g. earthquake intensity, ground motion features, nonlinear dynamic behaviour of structures and etc., it allows that the new generation of PBEE methodology should be formalized within a probabilistic basis. To apply this methodology it requires an interactive effort of multi-disciplinary experts, such as geology engineers, seismologist, structural engineers, loss experts and etc. For structural engineers the most interest can be relevant to the selection and estimation of two parameters in PBEE, i.e. Intensity Measures (IM) and Engineering Demand Parameters (EDP), which reflect ground motion hazard and structural response in terms of deformations, accelerations, or other response quantities of the building excited by input ground motions.

The EDPs are strongly dependent on the Intensity Measure (IM) used to perform the selection of ground motions. The IM as an intermediate variable connecting seismic analysis and structural analysis plays a very important role for structural engineers. An ideal IM should generally be of efficiency and sufficiency. The efficiency means it yields low dispersion of values of engineering demand parameter (EDP), while the sufficiency implies that EDP predicted with the candidate IM should be only dependent on this IM, not be conditionally dependent on properties of ground motions, like magnitude, source to site distance, fault mechanism etc. Therefore it implies the need of comparison among different intensity measures (IMs), in particular the comparison of dispersion of the EDP in relation to each IM. To this purpose a set of IMs 27 IMs, including those commonly adopted and some modified IMs based on the existed ones, are investigated in order to find optimum IMs for predicting various EDPs. Not only is IMs for predicting the structural response of widely

studied fixed base buildings are investigated, but also IMs for predicting structural response of the base-isolated buildings are initiatively studied. 80 ordinary and 59 pulse-like ground motion records are used to run nonlinear dynamic analyses on the 4-storey and 6-storey frame concrete buildings and these buildings equipped with base-isolation system on them. The EDPs considered in this study include the Maximum Inter-storey Drift Ratio (MIDR), the Maximum Roof Drift Ratio (MRDR) and the Maximum Base Displacement (MBD, only for base-isolated buildings).

Base on the results from this study some energy-based intensity measures have been shown to be good predictors of both structural and non-structural damage for base-isolated structures. However, they are not usually employed in probabilistic seismic demand analyses because of the lack of reliable Ground Motion Prediction Equations (GMPEs). In order to define seismic hazard and thus to calculate demand hazard curves it is essential, in fact, to establish a GMPE for the earthquake intensity. In the light of this need, new GMPEs are proposed here for the energy-based intensity measure, in particular elastic input energy equivalent velocity spectra i.e. V_{EIa} and V_{EIr}. The new GMPE is developed by taking advantage of the more comprehensive NGA database with more completed meta-data compiled in recent years. This prediction equation has a wider magnitude and distance applicable range, considers the effect of soil site by V_{S30} and fault mechanism, and etc.

However when the energy-based IMs are used in the selection and modification of ground motions for structural dynamic analyses, the uniform hazard spectrum derived from their GMPEs only gives the marginal distribution without information of joint occurrence of spectral values at different periods. In fact the uniform hazard spectrum of spectral acceleration is widely demonstrated to cause conservative results. Therefore the correlation of the elastic input energy spectral values at different periods is initiatively evaluated and the analytical predictive equation is also proposed to calculate the correlation of elastic input energy spectral values. Using the correlation their conditional mean spectrum recognized as a more appropriate target spectrum for ground motions selections can be developed. On the other hand this correlation also can be used to calculate the predicted mean value and the

dispersion of some integral intensity measures (such as $V_{EIa}SI$, $V_{EIr}SI$, $MV_{EIa}SI$, $MV_{EIr}SI$), achieving the application of these IMs in Performance-Based Earthquake Engineering.

Finally, we made a practical Matlab implementation for ground motion selection and modification. Here it is called RELACS (REaL ACcelerogram Selection). The total ground motion database used in RELACS, with more available ground motion records, is composed of three large ground motion database, i.e. NGA (Next Generation Attenuation) database, SISMA (Site of Italian Strong Motion Accelerograms) database, and ESGM (European Strong Ground Motion) Database. The RELACS brings to engineers and researchers more convenience to select ground motion accelerograms, using nowadays widely adopted GMSM methods in terms of not only some commonly used acceleration-based IMs and some other scalar intensity measures but also some energy-based IMs that have been approved good predictors for the response of base-isolated buildings. The RELACS contains two consecutive steps: selection according to the geophysical parameters; and selection according to the elastic response parameters (IMs). The user can easily obtain the acceleration time-history, and the acceleration spectrum, the velocity spectrum and the displacement spectrum of the ground motion record selected using the RELACS.

ACKNOWLEDGEMENT

First and foremost, I would like to thank my advisor, Professor Giorgio Monti. His insight, advice and enthusiasm have been always inspiring me to do the research throughout my PhD. It was an honour to be his student.

I would like to thank my co-advisor, Professor Fabrizio Mollaioli, for his patience and invaluable suggestions that improved this thesis significantly. Without his guide the dissertation could not have been finished.

I have very sincere thanks to extend to Dr. Andrea Lucchini for helping and advising me in academic experience in Rome. I appreciate that he devoted much time in working with me. His attitude and enthusiasm to research will inspire me for the following years to come.

I would like to thank Professor Paolo Franchin for his valuable and precious comments on the dissertation.

I also would like to express my gratitude to my friends in Rome, Zhixiong Chen, Vincenzo Bianco, Quan Zhou, Hao Wang, Hao Ji, Huanyu Yang, Sanjeev Prajapati and etc., for their sincere help to me in academic or living field in Rome.

Last, but absolutely not the least, I would like to express my gratefulness to my parents for their unconditional support and love that they have always showered on me.

INDEX

NOTATION

EDP = Engineering Demand Parameter

IM = Intensity Measure

GMPE = Ground Motion Prediction Equation

GMSM = Ground Motion selection and Modification

M = Magnitude

R = Source to site distance

$Sa(T_1)$ = Spectral acceleration at natural period of structure

PGA = Peak ground acceleration

AI = Arias intensity

CAV = Cumulative absolute velocity

I_a = Compound acc.-related IM

I_c = Characteristic intensity

PGV = Peak ground velocity

FI = Fajfar intensity

I_v = Compound vel.-related IM

CAD = Cumulative absolute displacement

IV = Incremental velocity

SED = Specific energy density

PGD = Peak ground displacement

I_d = Compound disp.-related IM

ID = Incremental displacement

S_a = Spectral acceleration at isolation period

E_{Ir} = Relative input energy at isolation period

E_{Ia} = Absolute input energy at isolation period

V_{EIa} = Absolute input energy equivalent velocity

V_{EIr} = Relative input energy equivalent velocity

ASI = Acceleration spectrum intensity

VSI = Velocity spectrum intensity

I_H = Housner intensity

$V_{EIr}SI$ = Relative input equivalent velocity spectrum intensity

$V_{EIa}SI$ = Absolute input equivalent velocity spectrum intensity

MASI = Modified ASI

MVSI = Modified VSI

MI_H = Modified I_H

$MV_{EIr}SI$ = Modified $V_{EIr}SI$

$MV_{EIa}SI$ = Modified $V_{EIa}SI$

MIDR = Maximum inter-story drift ratio

MRDR = Maximum roof drift ratio

MFA = Maximum floor acceleration

MBD = Maximum bearing displacement

PBEE = Performance-Based Earthquake Engineering

PEER = Pacific Earthquake Engineering Research

USGS = United States Geological Survey

$\rho_{\varepsilon(T_1),\varepsilon(T_2)}$ = Correlation coefficient of epsilon at two different periods in the same horizontal direction

$\rho_{\varepsilon_x(T),\varepsilon_y(T)}$ = Correlation coefficient of epsilon in the same horizontal direction at the same period

$\rho_{\varepsilon_x(T_1),\varepsilon_y(T_2)}$	=	Correlation coefficient of epsilon at two different periods in horizontal orthogonal direction
NGA	=	Next generation attenuation
SISMA	=	Site of Italian Strong Motion Accelerograms
ESGM	=	European Strong-motion Database
CMS	=	conditional mean spectrum
CDF	=	Conditional density function
UHS	=	Uniform Hazard Spectrum
S	=	Site soil conditions
F	=	Fault rupture

List of Tables

List of Figures

1 Introduction

1.1 Motivation

Quantifying the seismic risk of a structure at a specified seismic-oriented site is a main objective but significant challenge in the earthquake engineering field. In recent years the Pacific Engineering Research Center, PEER, (e.g. reference to Moehle 2004) has developed the second generation of Performance-based Earthquake Engineering (PBEE) mode, which is divided into four rigorous, consistent and independent stages linked with four intermediate output variables. These variables include intensity measure (IM), engineering demand parameter (EDP), damage measure (DM) and decision variable (DV). Due to inherent uncertainty and variability in seismic response, the performance-based methodology is formalized within a probabilistic basis. The procedure of this methodology is illustrated in Fig. 1.1.

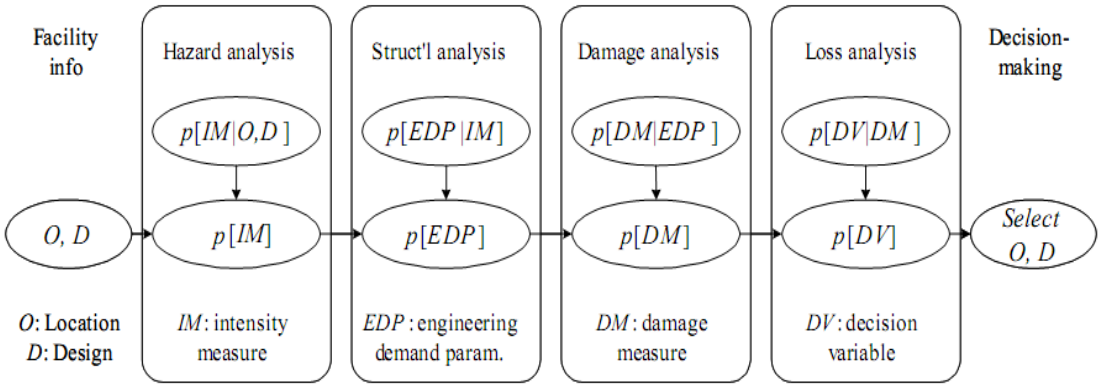

Fig. 1.1 The illustration of the methodology of the probabilistic performance-based earthquake engineering (the figure is from Moehle 2004)

The probabilistic PBEE methodology also can be expressed in terms of a triple integral based on the total probability theorem, shown in Equation 1.1. The decision variable (DV) that is meaningful to decision makers can be obtained with this equation (the further details could refer to the paper of Moehle 2004).

$$\lambda(DV) = \iiint G(DV \mid DM)dG(DM \mid EDP)dG(EDP \mid IM)d\lambda(IM) \qquad 1.1$$

In the light of the implication from Fig. 1.1 it is shown that the IM plays an important role for structural engineers, since it links Probabilistic Seismic Hazard Analysis (PSHA) to structural analysis. The result of PSHA is mean annual frequency of exceeding a certain level of IM, which reflect the seismic risk of ground motion for a specific site. This result then can be coupled with the result of nonlinear dynamic structural analysis to estimate the mean annual frequency of exceeding a certain level of nonlinear structural response or Engineering Demand Parameter (EDP). In the structural analysis the main cause of the variability of the structural response derived from the use of different ground motion accelerograms. However the uncertainty of ground motions can be represented by the IMs, some of which are well known e.g. PAG, PGV, PGD and etc. The uncertainties of EDPs are highly dependent on the variable adopted as intensity measure. It suggests that the characteristic of the IM plays an important role in the evaluation of the nonlinear structural response of structures. Therefore this flows the need of comparison among different Intensity Measures (IMs), in particular the comparison of the dispersions of the EDP associated to various IMs.

Although many of studies on IMs focusing on the fixed base reinforced concrete frame buildings can be found, few of works investigated the functional relationship between EDP and IM in the framework of Performance-based Earthquake Engineering for base-isolated structures that has become an over increasingly applied technique for protecting building located in highly seismic areas in recent years. Therefore the functional relationship between EDP and IM for base-isolated buildings can also should be emphasized and researched. In order to determine better IMs used in the context of PBEE, generally adopted IMs and some modified IMs, including some modified energy-based IMs, are analyzed as well in this study.

Along these lines based on the observation from the investigation of the functional relationship between EDP and IM for both base-isolated buildings and fixed base buildings, the application of some potential IMs in PBEE is achieved through a convenient Matlab implementation of the associated Ground Motion Selection and Modification (GMSM).

1.2 **Research Objectives**

The purpose of this work is to widely investigate on the Intensity Measures (IMs) in terms of their properties, i.e. efficiency, sufficiency and sensitivity, in order to find some potential IMs for predicting the seismic response of different structural types, i.e. fixed base and base-isolated buildings. In the further the application of these IMs in PBEE can be realized in terms of a convenient Matlab implementation of the associated Ground Motion Selection and Modification (GMSM). The development of the GMPEs and correlation of some potential IMs found in this study also have been focused, which is the premise of the application of these IMs. Therefore this general purpose is achieved according to identifying several specific objectives, which can be summarized in the following key points:

(1) Investigation of the prediction performance of the intensity measures for seismic response of fixed base buildings as well as base-isolated buildings in the framework of PBEE.

(2) Development of Ground Motion Prediction Equations for energy-based IMs found to be potential IMs in this study.

(3) Development of the correlation of energy-based spectral values for ground motions.

(4) Development of a Matlab implementation of Ground Motion Selection and Modification (GMSM) using widely used GMSM methods in terms of IMs investigated in this study.

1.3 **Organization**

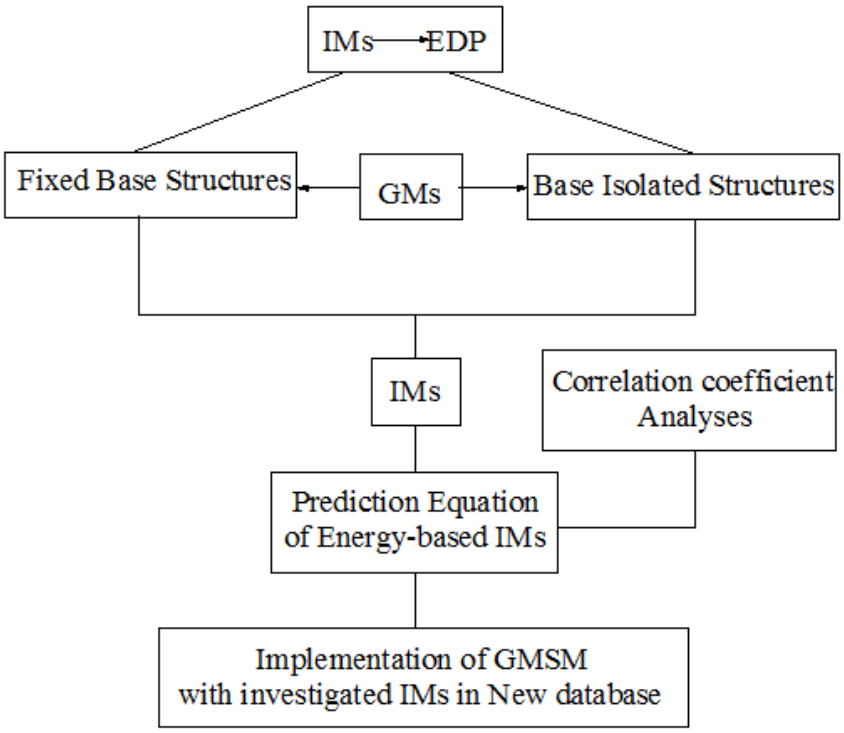

Fig. 1.2 The flow chart of this dissertation

Fig. 1.2 shows the flow-process of this dissertation. Firstly, basing the correlation between IMs and EDPs, we excite the same group of ground motions (ordinary and pulse like ground motions) to two different structural types of buildings (fixed base and base-isolated buildings), in order to investigate the performance of IMs for predicting various EDPs. After this investigation we find some potential IMs, such as energy-based IMs underlined in this dissertation. Then necessary Ground Motion Prediction Equations (GMPE) are developed for energy-based IMs, and the correlation coefficients of energy-based spectral values are initiatively calculated and modelled, which is also necessary to their application in GMSM of the framework of PBEE. Finally, it is programmed that the Matlab implementation of selection and modification of ground motions for structural dynamic analyses using widely used GMSM methods with the IMs investigated in this study. This implementation achieves the application of these investigated IMs in the field of PBEE and brings to engineers and

researchers the convenience to apply these IMs in the PBEE. In particular the content of every chapter of this dissertation is described as following.

Chapter 1 presents motivation, research objectives, and a brief organization of this study.

Chapter 2 focuses on the study of the performance of various IMs in terms of efficiency and sufficiency for predicting the structural seismic response (or EDP, Engineering Demand Parameters) of fixed base buildings in the framework of PBEE. Two concrete frame buildings, 4-storey and 6-storey building, are investigated in the study cases. The investigated IMs are categorized into two groups: 14 non-structure-specific IMs and 13 structure-specific IMs. Some modified IMs based on the existing ones are proposed and some Energy-based IMs are researched as well in this chapter. Three EDPs, namely Maximum Roof Drift Ratio (MRDR), Maximum Inter-storey Drift Ratio (MIDR) and Maximum Floor Acceleration (MFA), are studied. The ground motions are divided into two sets, ordinary ground motions and near-fault pulse-like ground motions, in order to observe the effect of pulse-like records on the properties (i.e., efficiency and sufficiency) of intensity measures.

Chapter 3, on the other hand, investigates the same intensity measures with little modification for predicting structural response of base-isolated buildings in terms of efficiency, sufficiency and sensitivity as well. In addition to the EDPs investigated in chapter 2, Maximum Bearing Displacement (MBD) is involved as well. Two multi-story buildings studied in chapter 2 are isolated at the base with isolation systems characterized with different properties are studied in this chapter. Overall, 32 different structures are analyzed. For each of them, the seismic response is calculated through non-linear dynamic analyses considering two different sets of ground motions consisting of ordinary and pulse-like records.

Chapter 4 focuses on developing the Ground Motion Prediction Equations for elastic input energy, on the basis of the founding of its good prediction capability in the chapter 2 and chapter 3, and the fact that there are relative few researches on the GMPE of elastic input energy IMs. The comparison between the proposed GMPE of elastic input energy and those previously developed is also performed in this chapter.

Chapter 5 evaluates the correlation of input energy spectral values for ground motions. The correlations include those of spectral values: at different periods for the same direction; at the same periods in horizontal perpendicular directions; and at different periods in horizontal perpendicular directions. The new analytical predictive equations of the correlation coefficients of the input energy are proposed based on the modification of the existing ones. Some applications of the correlations are also introduced in this chapter.

Chapter 6 presents a Matlab implementation, called RELACS (REaL ACcelerogram Selection). The RELACS compiles three large ground motion database, NGA (Next Generation Attenuation) database, SISMA (Site of Italian Strong Motion Accelerograms) database, and ESGM (European Strong Ground Motion) Database, thus provides larger available ground motion data. This Matlab implementation also provides the values of various IMs of the ground motions in the new database and realizes the application of these IMs for selecting and scaling ground motions used in structural analyses in the context of PBEE. The results of Chapter 4 and Chapter 5 are also used in developing the RELACS.

Chapter 7 makes a summary of the conclusions obtained on each of the discussed issues and presents some suggestions for the future studies as well. Several appendices with tables and images processed and used during the study are shown at the end of this dissertation.

2 Intensity measures for seismic response prediction of fixed base buildings

2.1 Introduction

Many researchers (e.g. Padgett et al. 2008) argued that a desirable IM should be one which is not only with efficiency and sufficiency but also have scaling robustness and have hazard computability. The efficiency means that the given IM yields the EDP with relatively small variability. The benefit of using an efficient IM can be observed that with more efficient IM the less number to perform nonlinear dynamic analyses is required to obtain the same accurate EDP. Regarding the sufficiency, the EDP should be only dependent on IM, not be conditionally dependent on the properties of ground motions, e.g., magnitude, source to site distance, fault mechanism and etc. An insufficient IM will lead to a biased estimation of the seismic performance if the ground motions have not been carefully selected presenting hazard at the specified site. Conversely, if a sufficient IM is used the detailed ground motion selection (without considering the magnitude and distance and etc.) is not necessary and more real records of database are available. The scaling robustness of IM can be defined as the degree of structural response bias induced by the ground motions scaled by means of IM compared to the results obtained from un-scaled records having the same intensity. This property of ground motions greatly impact on the result of the structural seismic response evaluated by means of Incremental Dynamic Analysis (IDA), because the bias can be induced when the ground motions that have been scaled to get a certain level of IM are used as input. The hazard computability of the IM can be defined, e.g., in the study of Giovenale et al.(2004), as the level of effort required to determine the probabilistic seismic hazard curve of the IM. Now Hazard maps and hazard curves are readily available for peak ground acceleration (PGA) and acceleration spectral values (Sa) in some region (e.g. on the USGS website http://earthquake.usgs.gov/hazards/products/). However the effort required the calculation of the hazard curves of the IM should be taken into account when it comes to decide which IM can be used in the probabilistic seismic performance assessment.

Many researches regarding the efficiency of IMs for predicting the seismic response can be widely found (e.g., Shome et al. 1998, Cordova et al. 2000, Akkar and Özen 2005, Riddell 2007, Yakut et al. 2008, Bianchini et al. 2009, Jayaram et al. 2010 and Mollaioli et al. 2011). Shome et al. (1998) was to aim at establishing accurate and efficient estimation of post-elastic damage measures for MDOF structure subjected to a specified earthquake scenario, e.g., a given magnitude and distance. They finding that the bin of records chosen from a narrow magnitude and distance interval results in a wide variability of nonlinear structural response but when the records in each bin are normalized or scaled to the bin-median spectral acceleration at fundamental period of the structure, the same median nonlinear structural response with reduced dispersion is obtained compared to the results obtained with the un-scaled records. In the light of this founding it is suggested that the best way to estimate the nonlinear structural response from a given seismic scenario (M and R) is firstly to establish the median spectral acceleration with GMPE, and then to scale ground motions so that they have roughly the same magnitude of spectral acceleration, and finally to get the structural response by performing nonlinear dynamic analysis with these scaled records. The authors pointed out this procedure can reduce the number of runs by a factor of 4. They also found that scaling records to the elastic pseudo-spectral acceleration at the fundamental period of the structure ($S_a(T_1)$) is better than scaling records to PGA. It should be noticed that all the conclusions were derived from the study of a single MDOF structure dominated by the first model of vibration. These conclusions need a further verification or modification when they are extended to other types of MODF structures.

Cordova et al. (2000) have developed a new two-parameter earthquake hazard intensity measure, i.e., $S^* = S_a(S_a(cT_1)/S_a(T_1))^{\alpha}$ ($c = 2, \alpha = 0.5$ for general use), taking into account the strength softening. It was found that this proposed IM significantly reduced the large record-to-record variability of seismic response, typically observed in inelastic time-history analyses. In other words, the proposed IM can lead an improvement on the accuracy of the seismic assessment and a reduction of necessary record number of run to gain a given confidence in the result.

Akkar and Özen (2005) investigated the effect of PGV on single-degree-of-freedom (SDOF) deformation demands and correlation with certain ground-motion features (earthquake magnitude, effective ground-motion duration and frequency content of ground motions) that play a role in the seismic demand of structures using a total of 60 soil site records. In the light of statistical results obtained from non-linear response history analyses on SDOF system the PGV correlates better with the deformation demands with respect to other ground motions (including PGA, PGV/PGA and $S_a(T_1)$), especially in the short period range. It should be noticed that the conclusion is based on the study only using ordinary records, since the author excluded the pulse-signal that are mostly observed in near-fault records with forward directivity.

Riddell (2007) divided 23 considered intensity measures into three groups: acceleration-related, velocity-related and displacement-related intensity measures and then investigated their correlation with four different structural response variables, which are elastic and inelastic deformation demands, input energy and hysteretic energy. Nonlinear responses are calculated using elastic-plastic, bilinear, and bilinear with stiffness degradation SDOF models. The results indicated that no single intensity measure has satisfactory correlation with nonlinear structural response in all period range simultaneously. In fact it was observed that acceleration-related intensity measures are more efficient for rigid systems, velocity-related intensity measures for intermediate-frequency systems, and displacement-related intensity measures for more flexible system. Housner's intensity was found to be the best index in the velocity region in terms of the correlation with both spectral ordinates and energy responses. It also should be noticed that the author did not give detailed information about record selection criteria (e.g., whether pulse-signal is taken account or the magnitude and distance range) about records used for analyses although a list of ground motion records are reported in this study.

In the work of Yakut et al. (2008) a comprehensive study was formed in order to investigate the correlation between a series of commonly used ground motion intensity measures and maximum inter-storey drift ratio (MIDR) of frame structures. A set of records containing 80 ground motions is used to perform nonlinear time-history analyses. The statistical result

obtained from the regression of the MIDR with these intensity measures indicated that spectrum intensity measures, such as Housner Intensity (I_H) and velocity spectrum intensity (VSI), more correlate with the MIDR with respect to other intensity measures, such as PGA, PGV, and $S_a(T_1)$. However it should be noticed that the author did not account for the near-fault effect of ground motions and the classification of soil type, which have significant effects on the structural response.

Bianchini et al. (2009) presented a desirable intensity measure, $S_{a,avg}(T_1,\ldots,T_n)$, geometric mean of pseudo-spectral acceleration ordinates over a certain range of periods, to predict the inelastic structural response of buildings subjected to recorded ground motions. It shows that the proposed IM have better prediction capability than $S_a(T_1)$ and PGA especially for inelastic structural systems. In addition the author indicated that it is simpler to evaluate the seismic hazard in terms of this proposed IM with respect to some vector-values and inelastic IMs.

Jayaram et al. (2010) investigated the correlation of a wide range of intensity measures (i.e., peak values, spectral quantities, duration and energy-based quantities) with both force-based and displacement-based responses for four story reinforced concrete frame buildings with and without infill. The force-based responses contain maximum base shear, maximum story shear and maximum overturning moment; the displacement-based responses consist of peak (over time) inter-story drift ratio, maximum (over all stories) peak inter-story drift ratio and roof drift ratio. It was observed that: in general the deformation-based responses seem to have better correlation with ground motion intensity measures than force-based response such as base shear; the velocity-based intensity measures, such as Housner Intensity (I_H) and the incremental velocity (IV), appear to be better correlated with deformation-based response.

Mollaioli et al. (2011) studied the degree of correlation of intensity measures, including PGA, PGV, $S_a(T_1)$, Arias Intensity (AI), Housner Intensity (I_H) and input energy-equivalent velocity (V_{EI}) with the maximum inter-story drifts. Nonlinear dynamic analyses were carried out for ten two-dimensional multi-story structural systems (2, 4, 6, 8, 10, 12, 14, 16, 20 and 24 storey) subjected to a large number of strong ground motions (around 900 records from 40 earthquakes). The near-fault ground motions were considered in this work. The $S_a(T_1)$

constitutes an efficient IM for medium-rise structures. However its strong correlation with structural response is limited for moderately inelastic structures, whose behaviour is not governed by the first mode of vibration. On the other hand Input Energy-equivalent Velocity V_{EI} can markedly improve the correlation with the maximum inter-story drifts for high-rise buildings with respect to low-rise buildings, since it reflects the effect of inelasticity and duration of ground motions, in fact, it directly relates to the number and amplitude of the cycles of the oscillator response.

In addition to the investigation of the efficiency of the aforementioned scalar intensity measures for predicting structural damage, some vector intensity measures with efficiency are also proposed to predict structural response. The representative researches carried out in recent years on scalar intensity measures include those of Shome (1999), Baker (2005), Baker and Cornell (2005) and Baker and Cornell (2007).

The objective of this chapter is aim to investigate the predictive capacity of a wide range of scalar intensity measures for structural response. Two properties of the intensity measures, i.e., efficiency and sufficiency, for predicting seismic response of fixed base buildings are discussed herein. In order to achieve this objective, author first performs nonlinear dynamic analyses on two multi-storey buildings, i.e., 4-storey and 6-storey, with two sets of records containing ordinary and pulse-like ground motions.

Then regression analyses are carried out to examine the linear relationship between the seismic response of buildings and the variable investigated IMs, i.e., some most commonly used elastic scalar IMs in literatures. Finally, the statistical data from the regression results are used to evaluate the efficiency and sufficiency of IM for predicting various seismic structural responses. Only scalar IMs are investigated, since vector IMs are frequently considered to be still not sufficiently practical because of the high evaluation efforts they usually require in the assessment analyses. New IMs are also proposed, obtained by modifying existing ones in the literature, so as to obtain better correlation with the considered predicted EDPs.

2.2 **Case studies**

2.2.1 Studied buildings

The selected case studies are two reinforced concrete buildings consisting of a 4-storey and a 6-storey three-bay frame designed according to a past code (DM 96; 1996). They are representative of existing buildings located in a high seismic zone (i.e., "zone 1" according to the seismic hazard classification of DM 96). In this study we only investigated the buildings with 4-storey and 6-storey buildings, since this study is mainly to exam the existing building in the Mediterranean area, where those taller than 8-10 storeys are not so common. A schematic representation of the two frames with information of the span length and the storey height is reported in Fig. 2.1(see the Appendix for details on cross-sections dimensions and reinforcement of the structural members). The periods of the first three modes of vibration of the frames, obtained with a reduced cracked stiffness of the structural elements (equal to half the initial elastic one), are given in Table 2.1 .

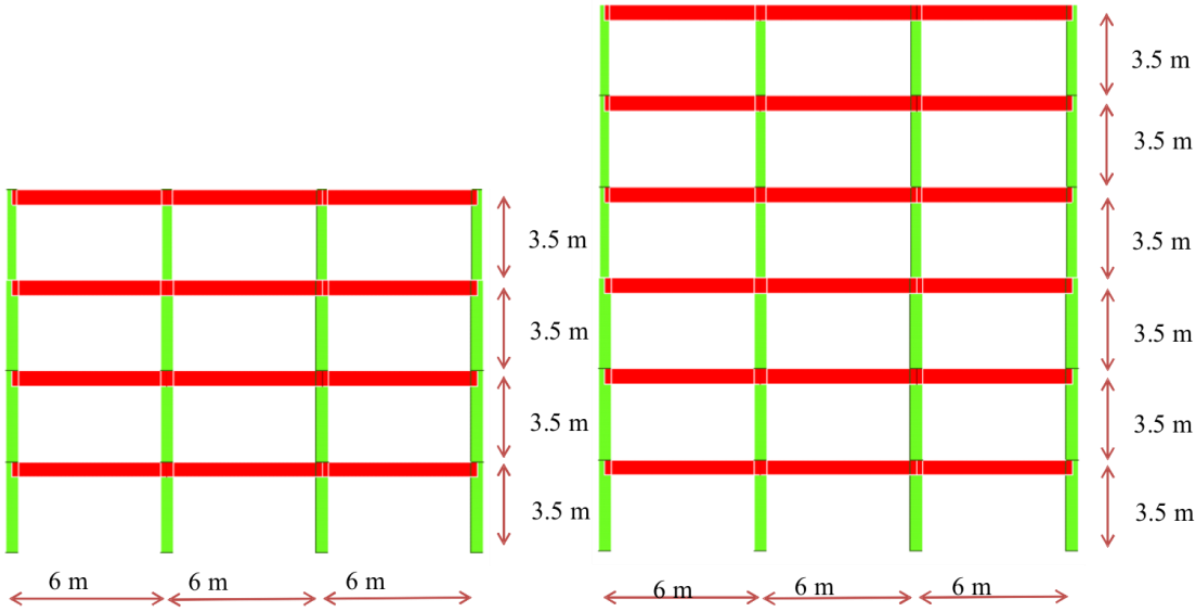

Fig. 2.1 Schematic representation of the frame structures analysed in the study.

Table 2.1Periods (T_i) of the first three modes of vibration of the analysed frames, obtained with a reduced cracked stiffness of the structural elements equal to half the initial elastic one.

frame	**T_1** [s]	**T_2**[s]	**T_3**[s]
4-storey	0. 97	0. 33	0. 20
6-storey	1. 17	0. 40	0. 24

2.2.2 Ground motion database

139 earthquake ground motions (GMs) are selected from the Next Generation of Attenuation project database (PEER 2005) and used as input for non-linear dynamic analyses on fixed base buildings. In order to highlight the effect of pulse-type motions, the above suite of GMs is divided into two groups: ordinary GMs (80 records, with closest distance ranging from 0.34 km to 87.87 km, and magnitude from 5.74 to 7.9) and pulse-like near-fault GMs (59 records, with closest distance ranging from 0.07 km to 20.82 km, and magnitude from 5 to 7.62). The latter are identified from the suite by using the pulse identification method based on the wavelet analysis approach proposed by Baker (2007). The horizontal component of each of them used in the analyses is the following: for ordinary GMs, the component having larger spectral acceleration at the fundamental period of the considered structure; for pulse-like near-fault GMs, the fault-normal rotated component. All the time histories are recorded on soil classified as type C or D, according to the NEHRP site classification based on the preferred V_{S30} values. The choice of selecting these soil conditions merely depend on the large number of records which is available for this type of soils (especially for the case of pulse-like records). The magnitude of all earthquakes ranges from 5 to 7.9 and the site-to-rupture closest distance varies from 0.07 km to 87.87 km (see Fig. 2.2). The details of each record are reported in the Appendix of the study.

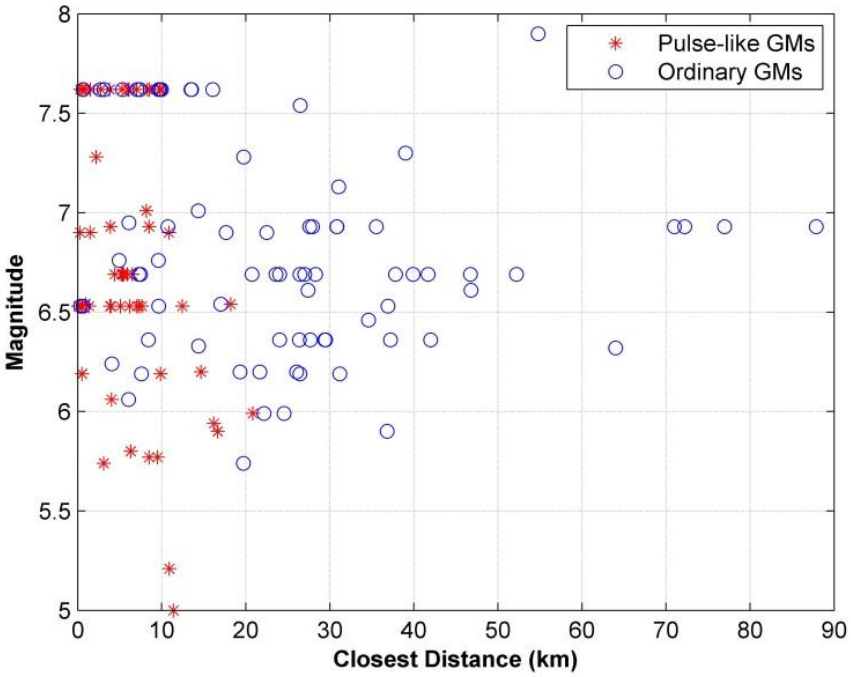

Fig. 2.2 Earthquake magnitude and distance range for the 139 ground motions used in the analyses.

2.3 **Intensity measures and engineering demand parameters**

2.3.1 Intensity measures

In this study, the intensity measures under investigation from the literature are categorized into two groups: i) non-structure-specific IMs calculated directly from ground motion time histories, given in Table 2.2; ii) structure-specific IMs obtained from response spectra of ground motion time histories depending on the period of the structure, defined in Table 2.3. The first group of IMs is further classified into three categories: acceleration-related, velocity-related and displacement-related IMs. The second group is further sorted into two groups: IMs obtained from the response spectral ordinate at certain periods and from integration of response spectra over a defined period range.

PGA (Peak Ground Acceleration), PGV (Peak Ground Velocity), PGD (Peak Ground Displacement), IV (incremental velocity) and ID (incremental displacement), AI (Arias

intensity) are included in the first group. PGA, PGV and PGD are the most common time domain parameters of strong ground motion. IV is the area under the maximum acceleration pulse, while ID is the area under the maximum velocity pulse (Anderson and Bertero 1987). AI was proposed by Arias (1970) and accounts for duration and amplitude but does not reflect the frequency content. AI tends to overestimate the intensity of long duration motions with high amplitude and a broad range of frequency content. The other IMs of the first group considered in the study are presented in Table 2.2.

S_a (5% damped pseudo acceleration spectral value at specified period), E_{Ia} (5% damped absolute input energy spectral value at specified period) and E_{Ir} (5% damped relative input energy spectral value at specified period) (Uang and Bertero 1990) are considered as structure-specific IMs. In this study, S_a, E_{Ia} and E_{Ir} are calculated at the fundamental periods of analysed fixed base buildings (in Chapter 2) or at isolation periods of the analysed base-isolated structures (in Chapter 3). IMs evaluated by integration of the structural response in a given period range can explicitly account for higher modes effects as well as period lengthening due to structural softening. Those considered in this study, which are classified as the second group of investigated IMs, are: ASI (Acceleration Spectrum Intensity), VSI (Velocity Spectrum Intensity), I_H (Housner Intensity), $V_{EIr}SI$, and $V_{EIa}SI$ (relative and absolute Input Equivalent Velocity Spectrum Intensity, respectively). The definitions of all these IMs are given in Table 2.3. In this study, ASI has been used as proposed by Von Thun et al. (1988), while the period range considered for VSI (Von Thun et al. 1988) was lengthened to include velocity-spectrum-sensitive structures. The main difference between VSI and I_H (Housner 1952) is that the absolute velocity spectrum is used for computing VSI, while the pseudo velocity spectrum is used for I_H. $V_{EIr}SI$, and $V_{EIa}SI$ are parameters obtained from integration of the energy response spectra in the period range 0.1-3.0 sec, deemed as more appropriate for near-fault signals (Decanini and Mollaioli 1998; 2001).

Modified versions of the second group of structure-specific IMs are also considered (see Table 2.3). The modified IMs are obtained from the existing ones by changing the period range of integration into 0.2T-1.5T, where T is the fundamental period of the fixed base structures in this chapter. This period range is based on the fact that many codes states that

response spectra for the suite of motions is not less than the design response spectrum for the site for periods ranging from $0.2T_1$ to $1.5T_1$ (ASCE/SEI 7). In the code of Eurocode 8 (2003) the matching period ranges from $0.2T_1$ to $2.0\ T_1$, but some researchers indicated that in most case the upper bound of $2.0T_1$ seems to be excessive (e.g., Katsanos et. al 2009). Basing on the above reason, the integration period range of modified integral intensity measures for the fixed base buildings are finally chosen to be from $0.2T_1$ to $1.5T_1$.

Table 2.2 Non structure-specific intensity measures considered in this study

		Notation	Name	Definition
Non-structure-specific intensity measures	**Acceleration-related**	PGA	Peak Ground Acceleration	$PGA = \max \lvert \ddot{u}_g(t) \rvert$ $\ddot{u}_g(t) =$ acceleration time history
		AI	Arias Intensity (Arias, 1970)	$AI = \frac{\pi}{2g}\int_0^{t_f} \ddot{u}_g^2(t)dt$ $t_f =$ total duration
		CAV	Cumulative Absolute Velocity (EPRI, 1988)	$CAV = \int_0^{t_f} \lvert \ddot{u}_g(t) \rvert dt$
		I_a	Compound Acc.-Related IM (Riddell and Garcia, 2001)	$I_a = PGA \cdot t_d^{1/3}; t_d = t_2 - t_1;$ $t_1 = t(5\%AI); t_2 = t(95\%AI)$
		I_c	Characteristic Intensity (Park et al., 1985)	$I_c = (a_{rms})^{3/2}\sqrt{t_d}$ $a_{rms} = \sqrt{\frac{1}{t_d}\int_{t_1}^{t_2} \ddot{u}_g(t)^2 dt}$
	Velocity-related	PGV	Peak Ground Velocity	$PGV = \max \lvert \dot{u}_g(t) \rvert$ $\dot{u}_g(t) =$ velocity time history
		FI	Fajfar Intensity (Fajfar et al., 1990)	$FI = PGV \cdot t_d^{0.25}$
		I_v	Compound Vel.-Related IM (Riddell and Garcia, 2001)	$I_v = PGV^{2/3} \cdot t_d^{1/3}$
		CAD	Cumulative Absolute Displacement (Mackie and Stojadinovic, 2003)	$CAD = \int_0^{t_f} \lvert \dot{u}_g(t) \rvert dt$
		IV	Incremental Velocity (Anderson and Bertero, 1987)	

		SED	Specific Energy Density	$SED = \int_0^{t_f} [\dot{u}_g(t)]^2 dt$
	Displacement –related	PGD	Peak Ground Displacement	$PGD = \max \lvert u_g(t) \rvert$
		I_d	Compound Disp.-Related IM (Riddell and Garcia, 2001)	$I_d = PGD \cdot t_d^{1/3}$
		ID	Incremental Displacement (Anderson and Bertero, 1987)	

Table 2.3 Structure-specific intensity measures considered in this study

		Notation	**Name**	**Definition**
Structure –specific intensity measures	**Spectral**	S_a	Spectral Acceleration at Fundamental or Isolation Period	$S_{pa}(T)$ S_{pa} = 5% damp. pseudo acc. spectrum T = fundamental periods(Chapter 2) or isolation period (Chapter 3)
		E_{Ir}	Relative Input Energy (Uang and Bertero, 1990) at Fundamental or Isolation Period	$E_{Ir} = -\int_0^{t_f} \ddot{u}_g(t)\dot{u}_r(t)dt$ $\ddot{u}_g(t)$ = ground acceleration time history $\dot{u}_r(t)$ = relative velocity time history of a $(\xi = 5\%, T)$ SDOF
		E_{Ia}	Absolute input energy (Uang and Bertero, 1990) At Fundamental or isolation period	$E_{Ia} = \int_0^{t_f} \ddot{u}_t(t)du_g = \int_0^{t_f} \ddot{u}_t(t)\dot{u}_g(t)dt$ $\dot{u}_g(t)$ = ground velocity time history $\ddot{u}_t(t)$ = absolute acceleration time history of a $(\xi = 5\%, T)$ SDOF
	Integral	ASI	Acceleration Spectrum Intensity	$ASI = \int_{0.1}^{0.5} S_{pa}\, dT$
		VSI	Velocity Spectrum Intensity	$VSI = \int_{0.1}^{2.5} S_v\, dT$ S_v = 5% damp. velocity spectrum
		I_H	Housner Intensity (Housner, 1952)	$I_H = \int_{0.1}^{2.5} S_{pv}\, dT$ S_{pv} = 5% damp. pseudo velocity
		$V_{EIr}SI$	Relative input equivalent velocity spectrum	$V_{EIr}SI = \int_{0.1}^{3.0} \sqrt{2E_{Ir}}\, dT$

			intensity	
		$V_{EIa}SI$	Absolute input equivalent velocity spectrum intensity	$V_{EIa}SI = \int_{0.1}^{3.0} \sqrt{2E_{Ia}}\, dT$
		MASI	Modified ASI	$MASI = \int_{0.2T}^{1.5T} S_{pa} dT$
		MVSI	Modified VSI	$MVSI = \int_{0.2T}^{1.5T} S_{v}\, dT$
		MI_H	Modified I_H	$MI_H = \int_{0.2T}^{1.5T} S_{pv}\, dT$
		$MV_{EIr}SI$	Modified $V_{EIr}SI$	$MV_{EIr}SI = \int_{0.2T}^{1.5T} V_{EIr}\, dT$
		$MV_{EIa}SI$	Modified $V_{EIa}SI$	$MV_{EIa}SI = \int_{0.2T}^{1.5T} V_{EIa}\, dT$

2.3.2 Engineering demand parameters

The Engineering Demand Parameters (EDPs) considered for fixed base buildings in this chapter are the following:

- Maximum Roof Drift Ratio (MRDR), namely, the ratio of the peak lateral roof displacement (with respect to the base) to the building height;
- Maximum Inter-story Drift Ratio (MIDR), namely, the maximum value of the peak inter-story drift ratio (drift normalized by the story height) over all stories;
- Maximum Floor Acceleration (MFA), namely, the maximum value of the peak floor absolute acceleration over all stories of structures;

MIDR was widely used as EDP for evaluating the degree of structural damage. In particular, this measure was shown to be closely related to local damage, instability, and story collapse. MRDR is a measure well correlated to the overall structural damage, and also related to the global stability of the moment-resisting frame. MFA is considered to be a measure that reflects the level of non-structural damage of the buildings.

2.4 **Regression analysis**

2.4.1 Predictive models

Several are the properties that are usually investigated for evaluating the predictive capabilities of an IM (e.g., see Tothong and Luco, 2007). Those considered in this chapter are the efficiency and the sufficiency. An efficient IM is defined as one that yields relatively small variability of predicted EDP for a given IM level. A sufficient IM is one for which the conditional probability distribution of EDP given IM is independent of the other parameters involved in computing the seismic hazard (only magnitude and closest distance will be considered in this study). These properties can be evaluated by first running non-linear dynamic analyses on the structure, and then by carrying out regression analyses between the obtained EDP values and the IM values of the used earthquake records.

It was observed by many researchers (e.g., Cornell et al., 2002) that EDP-IM relationships, in general, typically follow a standard power law. Therefore, all regressions are performed according to the following functional form:

$$\mathrm{EDP} = a(\mathrm{IM})^b \tag{2.1}$$

The Equation 2.1can be also expressed in the following format:

$$\ln(\mathrm{EDP}) = \ln(a) + b \cdot \ln(\mathrm{IM}) \tag{2.2}$$

where ln(a) and b are model parameters to be determined by simple linear regression on ln(EDP) and ln(IM).

Among the statistical parameters evaluated in regression analyses, the standard error of residuals σ_ε is considered as a measure of predictive efficiency of the IM. IMs resulting in EDPs standard errors of the order of 0.20-0.30 are normally considered as having a good efficiency, while the range 0.30-0.40 is still considered as reasonably acceptable. The regression residuals $\varepsilon|_{IM}$, instead, are used for evaluating the IM sufficiency. If the following predictive models are used for correlating $\varepsilon|_{IM}$ with magnitude (M) and distance (R):

$$\varepsilon|_{IM} = \alpha_M + \beta_M \cdot M, \ \varepsilon|_{IM} = \alpha_R + \beta_R \cdot R \tag{2.3}$$

the sufficiency can be directly measured by the p-value for the estimated slope coefficient β. The p-value is defined as the likelihood of observing a slope coefficient equal to or greater than the estimated β (absolute) value, if the underlying (true) value of β is in fact zero (Cornell, 1970). A smaller p-value of β indicates a less sufficient IM, where M or R has significant influence on residuals of EDP. Generally, IM is considered sufficient when the p-value is more than 0.05.

2.4.2 Evaluation results

2.4.2.1 Efficiency

The standard deviation of residuals, $\sigma_{\varepsilon,}$ of MRDR, MIDR and MFA obtained from the regression model of ln(MRDR)|ln(IMs), ln(MIDR)|ln(IMs) and ln(MFA)|ln(IMs), respectively, for 4-storey and 6-storey buildings subjected to ordinary and pulse-like ground motions, are shown in Fig. 2.3, Fig. 2.4 and Fig. 2.5. It is observed that σ_ε values obtained in the regression for the MIDR are generally larger than ones for MRDR. For 4-storey and 6-storey buildings S_a is always the most efficient IM among all considered IMs for predicting MRDR and MIDR by means of the comparison of σ_ε given by various IMs. This is probably because the structures considered in this study are significantly dominated by the first mode of vibration. In fact this is also held by many researches that have demonstrated that S_a is more efficient for first mode dominated structures. In general σ_ε of MRDR is less sensitive, especially for 4-storey building, to the pulse-like ground motions with respect to the MIDR according to the observation on the difference of σ_ε values obtained from the ordinary and the pulse-like records for the same IM. That is probably explained by the fact that the MRDR more reflects the overall deformation of structures comparing to the MIDR. In the light of Fig. 2.3 and Fig. 2.4 it is revealed that among all considered IMs, except CAD, the velocity-related non-structure-specific IMs are most influenced when the buildings are subjected to pulse-like GMs instead of ordinary GMs.

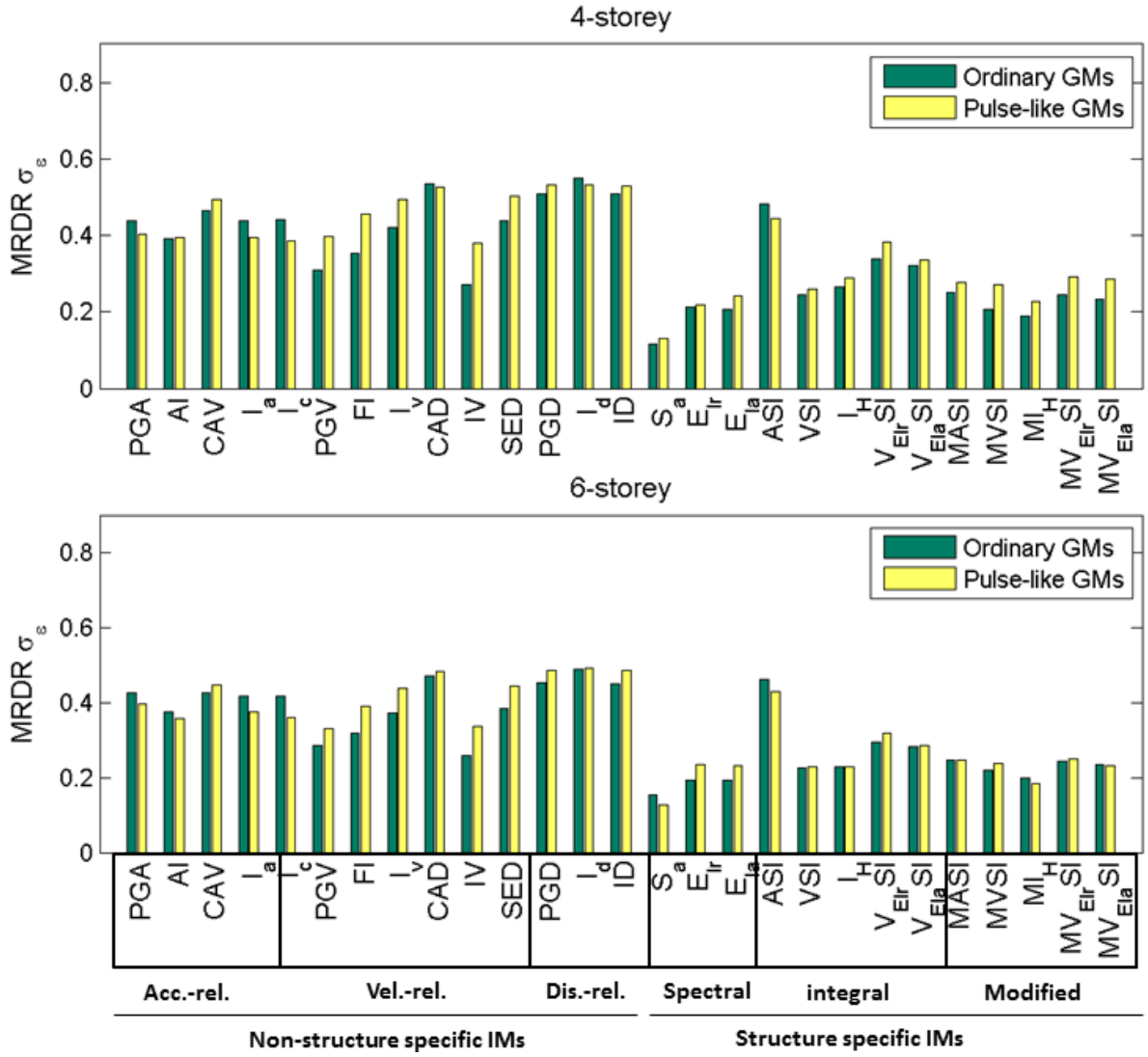

Fig. 2.3 Standard error of residuals σ_ε obtained in the ln(MRDR)|ln(IMs) regression of 4-storey frame (top panel) and 6-storey frame (bottom panel) subjected to ordinary ground motions and near-fault pulse-like ground motions

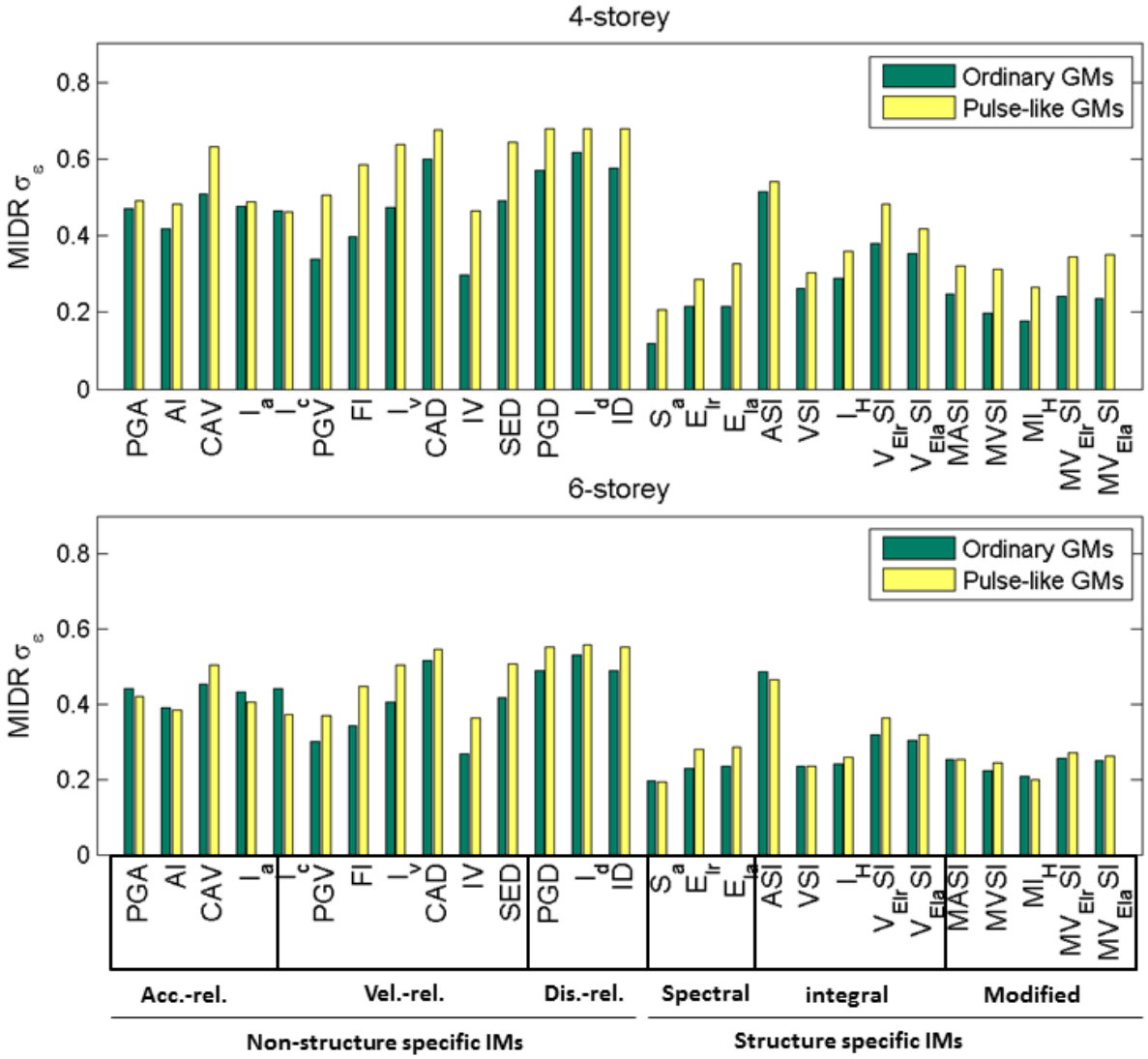

Fig. 2.4 Standard error of residuals σ_ε obtained in the ln(MIDR)|ln(IMs) regression of 4-storey frame (top panel) and 6-storey frame (bottom panel) subjected to ordinary ground motions and near-fault pulse-like ground motions.

From Fig. 2.4 it could be observed that the modified intenisty measures, such as MI_H, present competitively efficient with respect to the S_a for the 6-storey building that is more flexible and more influenced by higher mode of vibration comparing to the 4-storey building. One reasone of this observation can be that these modified intensity measures are defined by integration of spectral values in certain range of period, simutaneoulsy taking into account the effect at short preriod (higher mode influence) and at long period (lengthing period of structures due to inelasticity). It is also worth noticing that the modified intensity measures always result in less

disperion of residuals σ_ε of MRDR and MIDR obtained from regression analyses in the model ln(MIDR)|ln(IM) and ln(MRDR)|ln(IM) with respect to those of the corresponding IMs (e.g., VSI vs MVSI, I_H vs MI_H). That is probably due to the fact that by relating the integration period range to the fundamental period of the studied structure these modified intensity measures can more reflect the actual degree of influence from higher modes and soften situation when structure goes into the inelasticity.

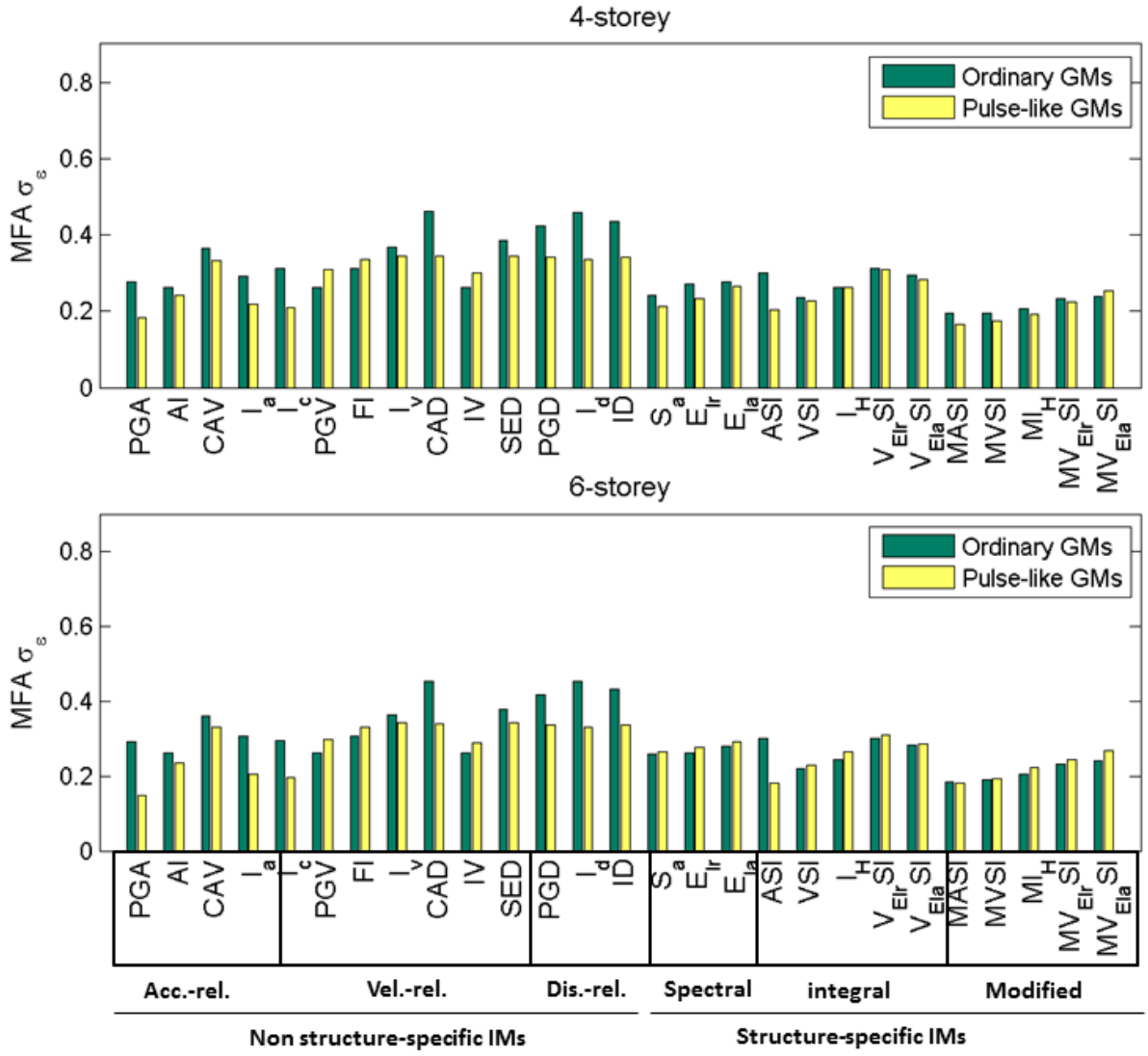

Fig. 2.5 Standard error of residuals σ_ε obtained in the ln(MFA)|ln(IMs) regression of 4-storey frame (top panel) and 6-storey frame (bottom panel) subjected to ordinary ground motions and near-fault pulse-like ground motions.

In the Fig. 2.5 statistical results of the ln(MFA)|ln(IMs) regression model are reported using the same process adopted above for the other two considered EDPs. It can be observed that PGA and modified intensity measures are the most efficient ones for predicting MFA among all considered IMs. PGA is very sensitive to pulse-like ground motions since the standard error of residuals, σ_{ε}, for PGA for ordinary records are significantly reduced when the pulse-like ground motions are considered. Compared to PGA, the modified intensity measures, such as MASI, MVSI, MI_H, $MV_{EIr}SI$ and $MV_{EIa}SI$, are less sensitive to the pulse-like ground motions. From Fig. 2.5 it is observed that the modified intensity measures are more efficient for predicting MFA than the corresponding spectrum intensities, which can also be found when predicting MIDR and MRDR.

In order to illustrate the distribution of IM values with respect to EDP values, the fitted line in the regression model, ln(EDP)|ln(IMs), and their cloud plot only for the 6-storey frame building are visualized in this chapter. In particular, Fig. 2.6, Fig. 2.7 and Fig. 2.8 report the cloud plot and fitted line of various representative IMs with respect to their EDPs (i.e., PGA, PGV, S_a, E_{Ir}, E_{Ia}, MI_H vs MRDR and MIDR, and PGA I_a, IV, S_a, MASI and MVSI vs MFA) for the 6-storey building subjected to the ordinary ground motions. In the same way the cloud plot and fitted line for the 6-storey building subjected to the near-fault pulse-like ground motions are given by Fig. 2.9, Fig. 2.10 and Fig. 2.11.

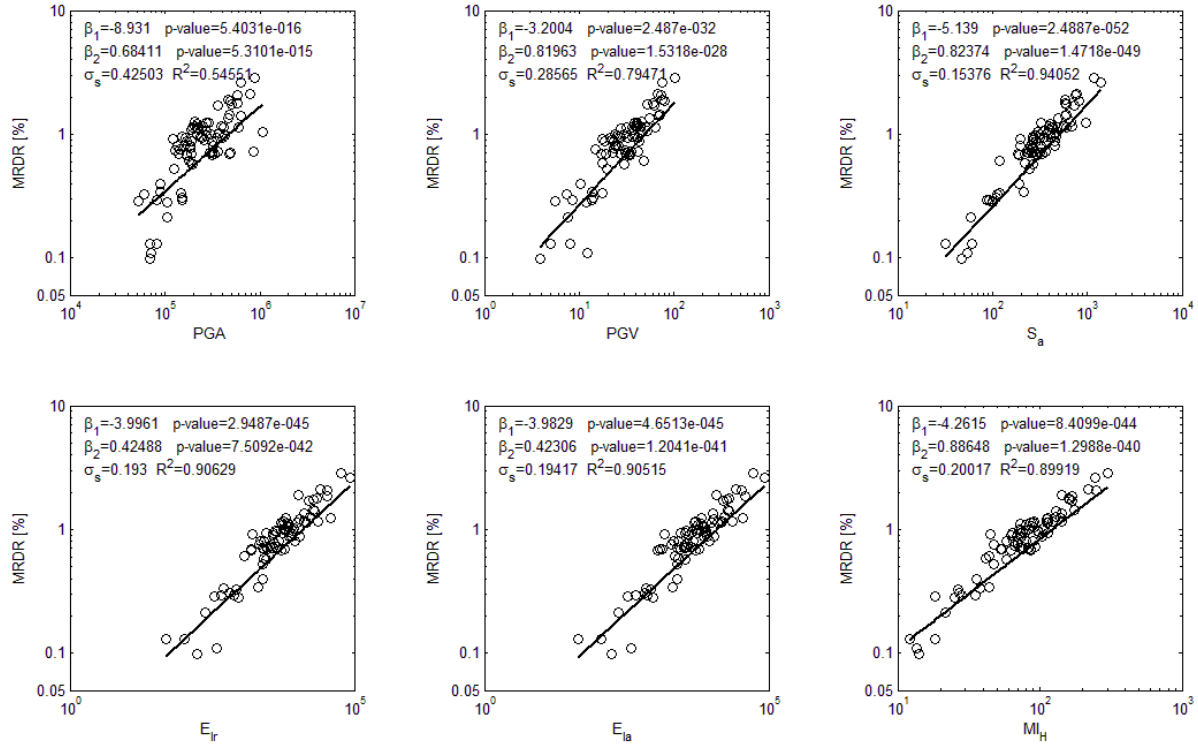

Fig. 2.6 Distribution of MRDR with IMs (i.e., PGA, PGV, S_a, E_{Ir}, E_{Ia} and MI_H) and the fitted lines, obtained from nonlinear dynamic analyses on the 6-storey building subjected to ordinary ground motions.

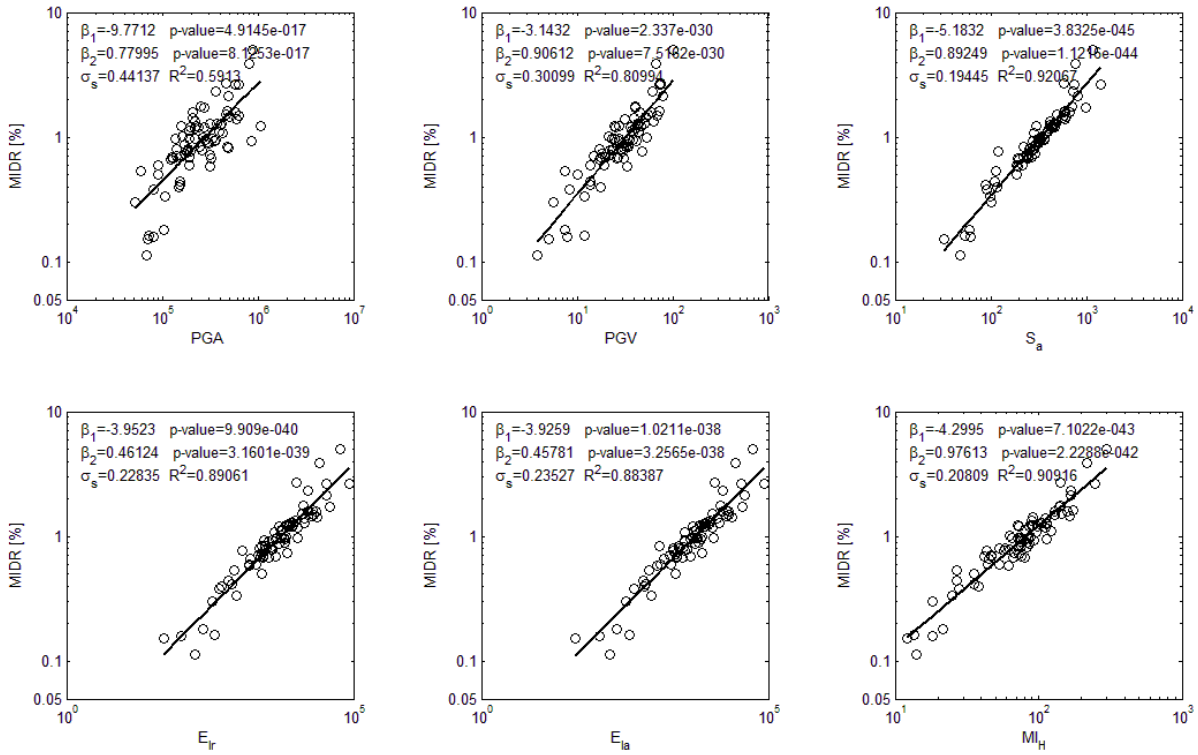

Fig. 2.7 Distribution of MIDR with IMs (i.e., PGA, PGV, S_a, E_{Ir}, E_{Ia} and MI_H) and the fitted lines, obtained from nonlinear dynamic analyses on the 6-storey building subjected to ordinary ground motions.

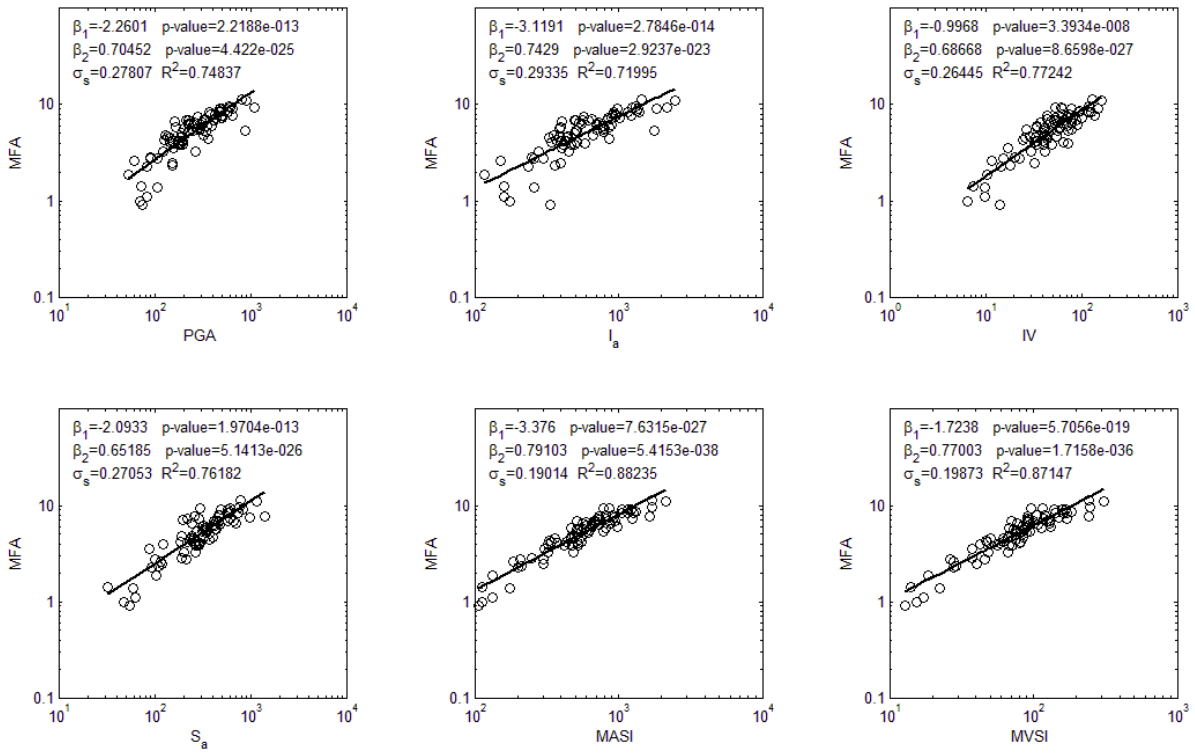

Fig. 2.8 Distribution of MFA with IMs (i.e., PGA, PGV, S_a, E_{Ir}, E_{Ia} and MI_H) and the fitted lines, obtained from nonlinear dynamic analyses on the 6-storey building subjected to ordinary ground motions.

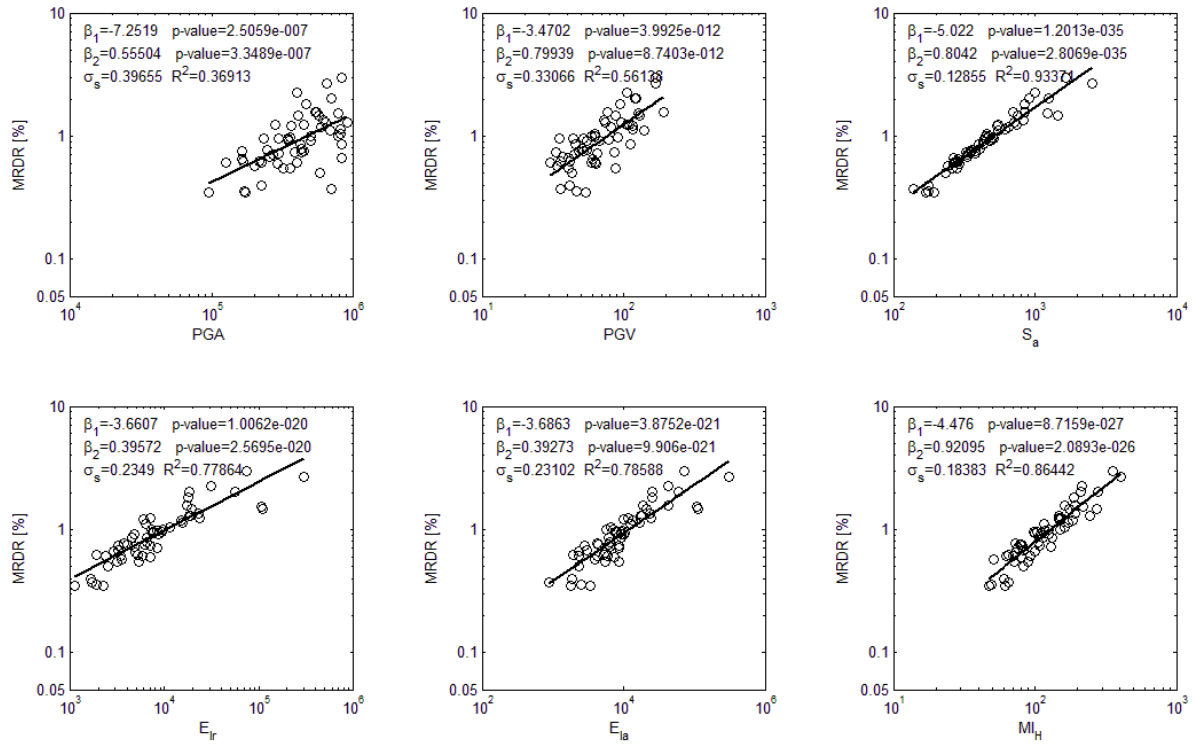

Fig. 2.9 Distribution of MRDR with IMs (i.e., PGA, PGV, S_a, E_{Ir}, E_{Ia} and MI_H) and the fitted lines, obtained from nonlinear dynamic analyses on the 6-storey building subjected to near-fault pulse-like ground motions.

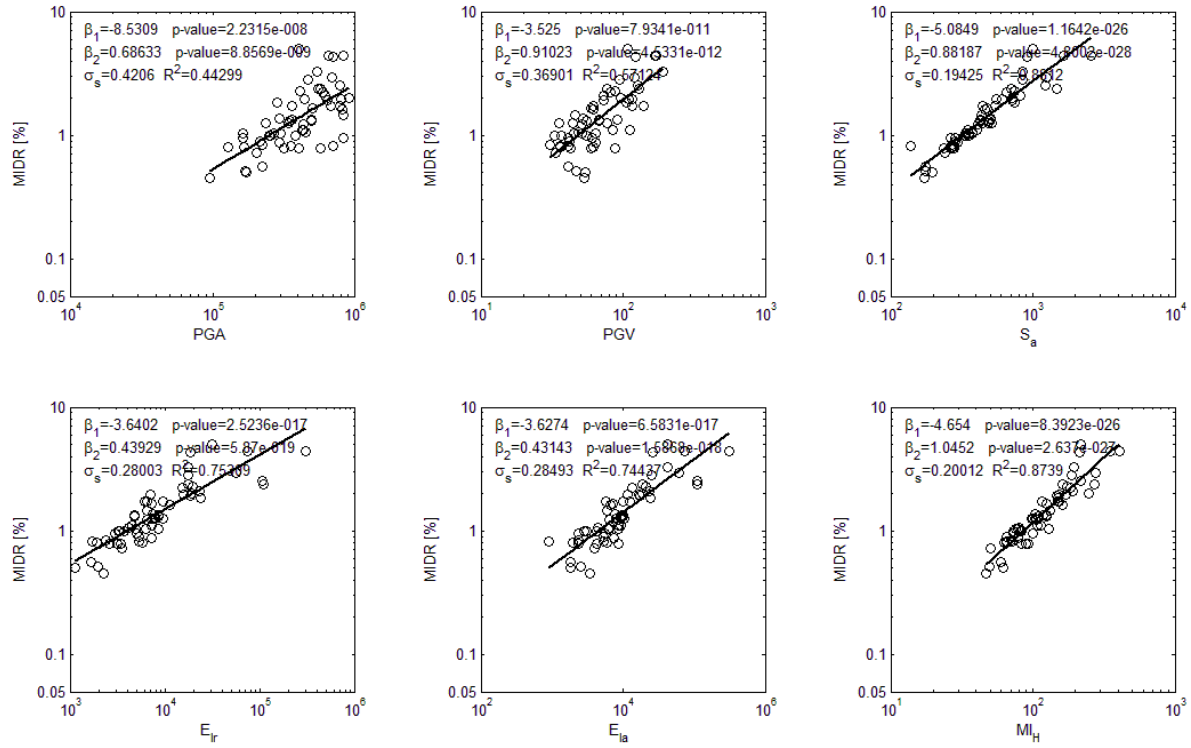

Fig. 2.10 Distribution of MIDR with IMs (i.e., PGA, PGV, S_a, E_{Ir}, E_{Ia} and MI_H) and the fitted lines, obtained from nonlinear dynamic analyses on the 6-storey building subjected to near-fault pulse-like ground motions.

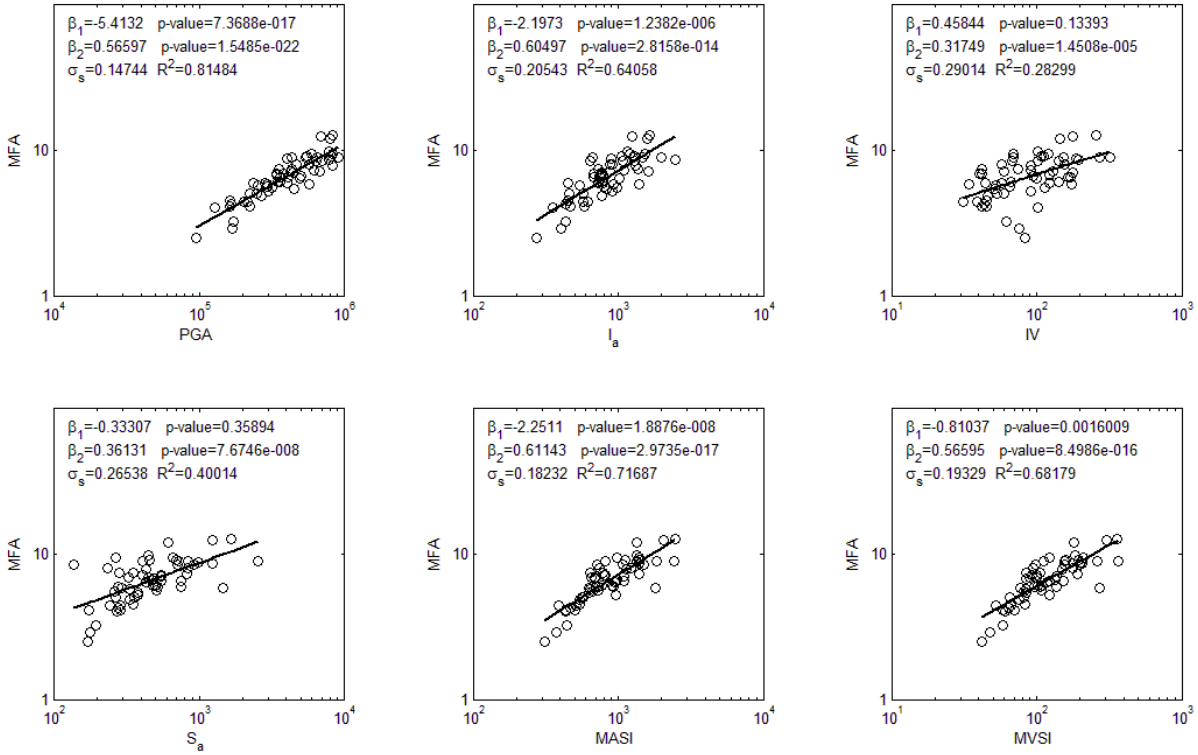

Fig. 2.11 Distribution of MFA with IMs (i.e., PGA, PGV, S_a, E_{Ir}, E_{Ia} and MI_H) and the fitted lines, obtained from nonlinear dynamic analyses on the 6-storey building subjected to near-fault pulse-like ground motions.

2.4.2.2 Sufficiency

In this subchapter the sufficiency of all considered IMs for predicting EDPs are evaluated in terms of p-value of β_R and β_M obtained in the regression of $\varepsilon|_{MRDR}$ on R and M (shown in Equation 2.3), where the $\varepsilon|_{MRDR}$ is obtained in the regression model ln(MRDR)|ln(IMs). The Table 2.4, Table 2.5 and Table 2.6 report these p-values for all considered IMs when MRDR, MIDR and MFA are predicted, respectively.

Based on the observation of Table 2.4, Table 2.5 and Table 2.6 it can be found that in general the sufficiency of IMs to distance is better than magnitude.

Table 2.7 reports, for each considered EDP, the most sufficient IMs for which the p-values are all more than 0.05 and more competitively sufficient IMs for which the p-value less than 0.05 only occurs in one case. It reveals that: the intensity measures, i.e. I_a, I_c, IV, S_a and MI_H, are considered as the most sufficient IMs for predicting MRDR since all the p-values of β_R and

β_M are more than 0.05; the intensity measures, i.e. I_a, I_c, IV, VSI and MI_H, are the most sufficient IMs for predicting MIDR because of the all p-values more than 0.05; PGA and ASI are most sufficient IMs for the prediction of MFA in terms of all p-values more than 0.05. AI, I_H, MASI and MVSI are of very sufficiency for predicting MRDR since in only one case the p-value is less than 0.05; in the mean while the intensity measures, consisting of MASI and MVSI, could be sufficient IMs for MFA since in only one case the p-value is less than 0.05.

In general the influence of pulse-like ground motions to the sufficiency of IMs is not significant, since the numbers of cases where p-values are less than 0.05 for ordinary GMs and pulse-like records are closed.

Table 2.4 p-value of R and M coefficient obtained in the regression of $\varepsilon|_{MRDR}$ on R and M, where the $\varepsilon|_{MRDR}$ is obtained in the regression model ln(MRDR)|ln(IMs). The p-values less than 0.05 are made in bold.

	Ordinary GMs				Pulse-like GMs			
	Distance		Magnitude		Distance		Magnitude	
	4-storey	6-storey	4-storey	6-storey	4-storey	6-storey	4-storey	6-storey
PGA	0.26	0.26	**0.02**	**0.01**	0.05	**0.03**	0.09	**0.01**
AI	**0.04**	**0.03**	0.64	0.93	0.80	0.70	**0.10**	0.65
CAV	0.58	0.39	0.06	0.10	0.13	0.15	**0.01**	**0.04**
I_a	0.14	0.12	0.51	0.34	0.19	0.11	0.46	0.63
I_c	0.59	0.49	0.23	0.15	0.52	0.38	0.89	0.16
PGV	0.15	0.07	0.08	0.16	0.52	0.27	**0.00**	**0.02**
FI	0.41	0.19	**0.01**	**0.01**	0.62	0.89	**0.00**	**0.00**
I_v	0.99	0.68	**0.01**	**0.01**	0.15	0.22	**0.01**	**0.01**
CAD	0.09	0.18	0.12	0.08	**0.02**	**0.04**	0.19	0.21
IV	0.27	0.14	0.29	0.53	0.90	0.86	0.29	0.85
SED	0.73	0.92	**0.01**	**0.01**	0.20	0.38	**0.02**	**0.02**
PGD	0.56	0.87	0.17	0.14	**0.01**	**0.04**	0.40	0.38
I_d	0.26	0.46	0.28	0.23	**0.00**	**0.01**	0.61	0.57
ID	0.36	0.60	0.14	0.12	**0.01**	**0.04**	0.35	0.35
S_a	0.34	0.39	0.53	0.02	0.80	0.99	0.17	0.15
E_{Ir}	0.67	0.73	0.06	0.63	0.98	0.80	**0.00**	**0.04**
E_{Ia}	0.61	0.93	0.02	0.67	0.14	0.28	**0.00**	**0.00**
ASI	0.41	0.41	**0.01**	**0.01**	**0.02**	**0.01**	0.17	**0.02**

VSI	0.06	**0.02**	0.43	0.69	0.96	0.84	0.39	0.29
I_H	0.19	0.04	0.13	0.18	0.36	0.25	**0.01**	0.29
$V_{EIr}SI$	0.54	0.23	**0.01**	**0.01**	0.55	0.34	**0.00**	**0.00**
$V_{EIa}SI$	0.32	0.12	**0.01**	**0.01**	0.38	0.32	**0.00**	**0.01**
MASI	**0.03**	**0.03**	0.14	0.21	0.19	0.29	0.13	**0.01**
MVSI	**0.03**	**0.03**	0.11	0.22	0.06	0.09	0.15	**0.01**
MI_H	0.08	0.06	0.34	0.68	0.52	0.95	0.69	0.22
$MV_{EIr}SI$	**0.03**	0.05	0.12	0.14	0.76	0.99	0.05	0.20
$MV_{EIa}SI$	0.05	0.06	**0.04**	**0.04**	0.24	0.10	**0.00**	**0.00**

Table 2.5 p-value of R and M coefficient obtained in the regression of $\varepsilon|_{MIDR}$ on R and M, where the $\varepsilon|_{MIDR}$ is obtained in the regression model ln(MIDR)|ln(IMs). The p-values less than 0.05 are made in bold.

	Ordinary GMs				Pulse-like GMs			
	Distance		Magnitude		Distance		Magnitude	
	4-storey	6-storey	4-storey	6-storey	4-storey	6-storey	4-storey	6-storey
PGA	0.32	0.30	**0.03**	**0.00**	0.07	**0.02**	0.11	**0.01**
AI	0.06	0.05	0.43	1.00	0.98	0.72	**0.03**	0.35
CAV	0.75	0.55	**0.03**	0.10	0.15	0.12	**0.00**	**0.02**
I_a	0.20	0.14	0.67	0.29	0.25	0.10	0.28	0.91
I_c	0.67	0.64	0.34	0.10	0.72	0.41	0.88	0.24
PGV	0.31	0.17	**0.04**	0.21	0.44	0.31	**0.00**	**0.01**
FI	0.68	0.40	**0.00**	**0.01**	0.66	0.72	**0.00**	**0.00**
I_v	0.70	1.00	**0.01**	**0.01**	0.15	0.14	**0.00**	**0.01**
CAD	0.05	0.09	0.11	0.11	**0.02**	**0.03**	0.14	0.16
IV	0.52	0.32	0.16	0.67	0.90	0.85	0.14	0.81
SED	0.50	0.77	**0.01**	**0.01**	0.22	0.29	**0.01**	**0.01**
PGD	0.38	0.63	0.15	0.17	**0.01**	**0.02**	0.31	0.30
I_d	0.16	0.30	0.28	0.27	**0.00**	**0.01**	0.53	0.52
ID	0.22	0.39	0.15	0.15	**0.01**	**0.02**	0.30	0.29
S_a	**0.03**	0.08	0.13	**0.01**	0.92	0.59	0.06	0.07
E_{Ir}	0.29	0.59	**0.01**	0.36	0.91	0.59	**0.00**	**0.01**
E_{Ia}	0.25	0.35	**0.00**	0.92	0.15	0.54	**0.00**	**0.00**
ASI	0.46	0.47	**0.02**	**0.00**	**0.03**	**0.01**	0.19	**0.03**
VSI	0.15	0.06	0.22	0.91	0.70	0.76	0.14	0.62
I_H	0.39	0.15	0.06	0.29	0.24	0.36	**0.00**	0.09
$V_{EIr}SI$	0.83	0.49	**0.00**	**0.01**	0.45	0.47	**0.00**	**0.00**
$V_{EIa}SI$	0.56	0.30	**0.00**	**0.02**	0.26	0.39	**0.00**	**0.00**
MASI	0.04	0.08	0.25	0.10	0.27	0.22	0.20	**0.02**

MVSI	0.05	0.12	0.21	0.10	0.08	0.05	0.24	**0.02**
MI_H	0.16	0.23	0.64	0.41	0.70	0.87	0.90	0.62
$MV_{EIr}SI$	0.05	0.16	**0.02**	0.21	0.98	0.89	**0.01**	0.05
$MV_{EIa}SI$	0.09	0.21	**0.00**	0.07	0.13	0.15	**0.00**	**0.00**

Table 2.6 p-value of R and M coefficient obtained in the regression of $\varepsilon|_{MFA}$ on R and M, where the $\varepsilon|_{MFA}$ is obtained in the regression model ln(MFA)|ln(IMs). The p-values less than 0.05 are made in bold.

	Ordinary GMs				Pulse-like GMs			
	Distance		Magnitude		Distance		Magnitude	
	4-storey	6-storey	4-storey	6-storey	4-storey	6-storey	4-storey	6-storey
PGA	0.26	0.74	0.22	0.34	0.77	0.76	0.86	0.88
AI	0.10	0.29	**0.01**	**0.00**	0.09	0.11	**0.00**	**0.00**
CAV	0.76	0.46	**0.00**	**0.00**	0.56	0.41	**0.00**	**0.00**
I_a	0.17	0.56	0.29	0.26	0.43	0.47	**0.00**	**0.00**
I_c	0.95	0.65	0.84	0.59	0.08	0.07	**0.01**	**0.00**
PGV	0.88	0.45	**0.00**	**0.00**	0.47	0.45	**0.00**	**0.00**
FI	0.53	0.26	**0.00**	**0.00**	0.63	0.55	**0.00**	**0.00**
I_v	0.20	0.09	**0.00**	**0.00**	0.19	0.13	**0.01**	**0.00**
CAD	**0.01**	**0.00**	0.08	0.05	0.04	0.02	0.15	0.12
IV	0.44	0.17	**0.03**	**0.02**	0.72	0.70	**0.00**	**0.00**
SED	0.12	0.05	**0.00**	**0.00**	0.19	0.14	**0.01**	**0.00**
PGD	0.12	0.05	**0.04**	**0.02**	**0.02**	**0.01**	0.24	0.15
I_d	**0.04**	**0.02**	0.11	0.07	**0.01**	**0.00**	0.53	0.43
ID	0.05	**0.02**	0.06	**0.04**	**0.01**	**0.01**	0.28	0.19
S_a	**0.01**	**0.00**	0.20	0.68	0.30	0.77	**0.00**	**0.00**
E_{Ir}	**0.03**	**0.01**	0.04	0.19	0.33	0.82	**0.00**	**0.00**
E_{Ia}	**0.03**	**0.00**	**0.03**	0.11	0.25	0.70	**0.00**	**0.00**
ASI	0.27	0.59	0.17	0.26	0.63	0.53	0.81	0.97
VSI	0.78	0.38	**0.03**	**0.01**	0.19	0.32	**0.00**	**0.00**
I_H	0.51	0.22	**0.01**	**0.00**	0.21	0.34	**0.00**	**0.00**
$V_{EIr}SI$	0.35	0.16	**0.00**	**0.00**	0.59	0.80	**0.00**	**0.00**
$V_{EIa}SI$	0.51	0.25	**0.00**	**0.00**	0.29	0.46	**0.00**	**0.00**
MASI	0.66	0.57	0.58	0.10	0.22	0.22	0.06	**0.00**
MVSI	0.84	0.24	0.60	0.10	0.60	0.60	0.05	**0.00**
MI_H	0.41	0.10	0.34	**0.03**	0.19	0.26	**0.00**	**0.00**
$MV_{EIr}SI$	0.96	0.28	**0.00**	**0.00**	0.22	0.35	**0.00**	**0.00**
$MV_{EIa}SI$	0.75	0.20	**0.00**	**0.00**	0.10	0.26	**0.00**	**0.00**

Table 2.7 The list of IMs which are considered as the most sufficient and competitively sufficient IMs for predicting each considered EDP.

EDP	p-values are more than 0.05 in all cases	p-value is less than 0.05 in one case
MRDR	I_a, I_c, IV, S_a and MI_H	VSI, I_H and $MV_{EIr}SI$
MIDR	I_a, I_c, IV, VSI and MI_H	AI, I_H, MASI and MVSI
MFA	PGA and ASI	MASI and MVSI

2.5 **Summary and conclusions**

The prediction capability of a wide range of intensity measures for fixed base structural responses, i.e. MRDR, MIDR and MFA, is investigated in terms of efficiency and sufficiency in this chapter. 80 ordinary and 59 pulse-like ground motion records are used to run nonlinear dynamic analyses on the 4-storey and 6-storey frame concrete buildings which are dominated by the first mode of vibration.

S_a (T_1) results in the smallest dispersion of residuals of the MRDR and MIDR obtain from the regression model $\ln(MRDR)|\ln(S_a(T_1))$ and $\ln(MIDR)|\ln(S_a(T_1))$. In other words, it is demonstrated that $S_a(T_1)$ is the most efficient IM among all considered IMs for predicting MIDR and MRDR of fixed base buildings. But it may not be sufficient to distance and Magnitude. That implies that more attention to the distance and magnitude of the records should be paid when the record selection is performed in terms of $S_a(T_1)$. On the other hand the intensity measure, i.e. MI_H, present competitive efficiency especially when higher storey buildings are considered. In the mean while the MI_H show the most sufficient property for predicting MIDR. Therefore the author suggests use MI_H for predicting MIDR because of its desirable efficiency and sufficiency, especially when the influences of the higher mode of vibration and the deep inelasticity of structures are significant. For predicting MFA the intensity measures, i.e., PGA and MASI, are both very good predictors because of desirable

efficiency and sufficiency. However the author still suggests PGA as the predictor of MFA because of its simplicity to evaluate.

Another important finding is that the proposed modified intensity measures are always more efficient than the corresponding spectrum intensity measures for predicting each considered EDP. The reason for this could be due to that the integral period range of the proposed modified intensity is dependent on the structural fundamental period, which could be more representative of the influence of higher-mode vibration and the inelastic effect of structures with respect to the spectrum intensity measures with fixed integral period range.

3 Intensity measures for the seismic response prediction of base-isolated buildings

3.1 Introduction

A key issue in the seismic assessment procedure for buildings proposed by PEER within the framework of Performance-Based Earthquake Engineering (see Moehle and Deierlein 2004), is the evaluation of the p[EDP/IM] probabilities. The p[EDP/IM] are defined as the probabilities of exceeding certain Engineering Demand Parameter (EDP) values, conditioned to given earthquake intensity levels, namely, different values of a selected ground motion Intensity Measure (IM). These conditioned probabilities can be used together with the results of a probabilistic seismic hazard analysis for calculating mean annual frequencies of exceedance of specified EDP values of interest (e.g., see Cornell and Krawinkler 2000; Cornell et al. 2002), representing different seismic performance levels of the building. The stronger the correlations of the selected IM with respect to the predicted EDP, the more accurate the result of the assessment analysis.

Many studies have been carried out to evaluate the predictive capability of the IMs currently available in the literature, and efforts for understanding how to improve these IMs have also been spent. Due to the large number of hazard curves available for Peak Ground Acceleration (PGA) and Spectral acceleration at the fundamental period of the structure ($S_a(T_1)$), these two parameters are in general the most widely investigated intensity measures. Unfortunately, numerous works have shown that in some cases $S_a(T_1)$ may not be a good predictor, since it does not account for the lengthening of period, as the structure goes well into the inelastic range, and does not consider the influence of the higher modes. Consequently, some scalar measures have been proposed in order to explicitly take into account such aspects (e.g., Cordova et al. 2000; Bianchini et al. 2009). In recent years, some other IMs including spectrum intensity measures have been investigated and proved having better predictive abilities than PGA and $S_a(T_1)$ especially in the case of medium-period frame structures (Yakut and Yilmaz 2008; Jayaram et al. 2010). Vector intensity measures have also been proposed

(e.g., by Baker and Cornell 2005; Luco et al. 2005) by adding to $S_a(T_1)$ other parameters for improving the correlations with respect to the predicted EDPs.

Analyses on many different types of buildings have been carried out (e.g., see the recent works on torsional and tall buildings by Lucchini et al. 2011a,b; Asgarian et al. 2012; respectively). However, only a few have focused on base isolated structures. Among these studies deserve to be mentioned those of Ryan and Chopra (2004a,b), Narasimhan et al. (2009) and Avşar and Özdenmir (2011). Ryan and Chopra (2004a,b) showed that the Peak Ground Velocity (PGV) is in general an effective IM for predicting the response of base-isolators. Narasimhan et al. (2009) demonstrated that the predictions using this scalar IM can be significantly improved by considering a vector IM that includes, in addition to the PGV, also the PGA, and the following parameters: Ia, E_v and P_D, as defined in Arias (1970), Nau and Hall (1984), and Araya and Saragoni (1980), respectively. In particular, they found that the standard error of the predicted maximum displacement at the base isolation level can be reduced from values equal to 0.4-0.6 to values equal to 0.3-0.35. The case studies used in their analyses were mainly simple 2DOF models excited only by ordinary ground motions. In Avşar and Özdenmir (2011), the interesting results of a systematic investigation of the predictive capability of a large number of IMs from the literature are reported. The predictive capability of the considered IMs is evaluated with respect to the seismic response of isolated bridges (not of buildings) characterized by different isolation periods and strengths. Modified IMs from existing ones are proposed in order to improve the correlation with the observed response of interest, that is, the maximum displacement of the isolation system. In the analyses, both ordinary and pulse-like near-fault records are used. The latter are studied due to their potential to be particularly destructive for isolated structures in general (e.g., as demonstrated by Jangid and Kelly 2001). It is shown that the predictive capability of the IMs significantly depends on the isolation period of the structure when pulse-like ground motions are considered. For such type of records, the velocity-related IMs are those that more strongly correlate with the response of the isolation system. In particular, the best predictor among the velocity-related IMs considered from the literature results in the PGV. The good predictive capabilities of PGV when dealing in general with pulse-like records are also confirmed by the

results of analyses carried out by Yang et al. (2009) on simple non-linear elasto-plastic single-degree-of-freedom systems.

The aim of this chapter is to contribute to the current knowledge on still unclear aspects related to the IMs and the seismic response prediction of base-isolated buildings. The intent is to focus on specific topics that have still not received much research attention. In particular, the objective of the work is to:

*investigate on the predictive capability of the IMs with respect to EDPs related not only to damage in the isolation system but also to EDPs that can be used for describing damage in the building (such as the maximum inter-storey displacement and the maximum floor acceleration);

*evaluate the predictive efficiency of the IMs, and also their sensitivity with respect to both the elastic and post-elastic properties of the isolation system;

*evaluate the different predictive capability of the IMs when ordinary or pulse-like near-fault ground motions are used for exciting the base-isolated building.

In order to achieve this objective, the responses of two multi-storey buildings isolated at the base with systems characterized by different properties are studied. Overall, 32 different structures are analysed. For each of them, the seismic response is calculated through non-linear dynamic analyses considering two different sets of ground motions consisting of ordinary and pulse-like records used in the last chapter. A large number of IMs representative of those most commonly used in the literature for predicting the response of fixed-base buildings are evaluated. IMs proposed for the prediction of base-isolated structures in general are studied as well. Only scalar IMs are investigated, since vector IMs are frequently considered to be still not sufficiently practical because of the high evaluation efforts they usually require in the assessment analyses. New IMs are also proposed, obtained by modifying existing ones from the literature so as to obtain better correlation with the considered predicted EDPs.

3.2 **Case studies**

3.2.1 Studied buildings

The selected case studies are two reinforced concrete buildings consisting of a 4-storey and a 6-storey three-bay frame retrofitted with base-isolation. The 4-storey and 6-storey buildings investigated in the chapter 2 are adopted as the superstructures of the base-isolated buildings in this chapter. Therefore the schematic representation of these superstructures showing the information of the span length and the storey height is presented in Fig. 2.1 or Fig. 3.1. The periods of the first three modes of vibration of superstructures, modelled with a reduced cracked stiffness of the structural elements (equal to half the initial elastic one), are given in Table 2.1. The further details of the superstructures refer to the Appendix.

For each frame, base-isolation systems characterized by 16 different isolation properties are considered. Fig. 3.2 reports the constitutive law used for representing the cyclic response of the generic isolation system. This is characterized by no stiffness degradation under cyclic loading. The parameters that define the bi-linear backbone curve of the constitutive law are the characteristic strength F_d, the elastic limit displacement D_y and the post-elastic stiffness K_d. For all of the considered isolation systems the characteristic strength F_d is set equal to 0.03 the seismic weight W of the structure. Different design values for D_y and K_d are used for defining isolation systems with differences in both the elastic and the post-elastic properties. In particular, four different values are considered for the elastic limit displacement D_y: 0, 10, 25 and 50 mm. These values can be considered representative of isolation systems consisting of friction pendulum isolators (D_y=0) or lead rubber bearings having different initial stiffness (D_y>0). For K_d also, four different values for each building are considered. They are calculated so as to obtain isolation periods T defined as follows

$$T = 2\pi\sqrt{\frac{W}{K_d \cdot g}} \tag{3.1}$$

equal to 2.5, 3.0, 3.5 and 4.0 sec for the 4-storey building, and equal to 3.0, 3.5, 4.0 and 4.5 sec for the 6-storey. The notation used hereafter for identifying these different isolation systems is reported in Table 3.1.

Table 3.1 Notation for the structures with reference to their isolation period and yield displacement

Isol. Period / Yield Disp.	2.5 sec/4-storey	3.0 sec/4-storey	3.5 sec/4-storey	4.0 sec/4-storey
	3.0 sec/6-storey	3.5 sec/6-storey	4.0 sec/6-storey	4.5 sec/6-storey
0 mm	a1	a2	a3	a4
10 mm	b1	b2	b3	b4
25 mm	c1	c2	c3	c4
50 mm	d1	d2	d3	d4

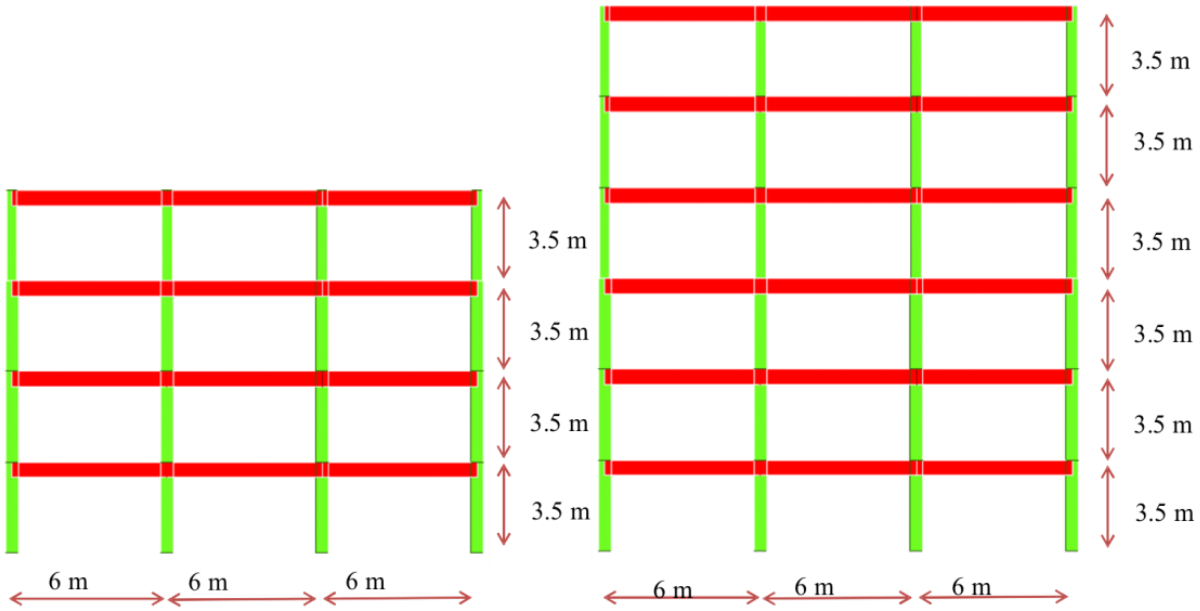

Fig. 3.1 Schematic representation of the frame structures analysed in the study

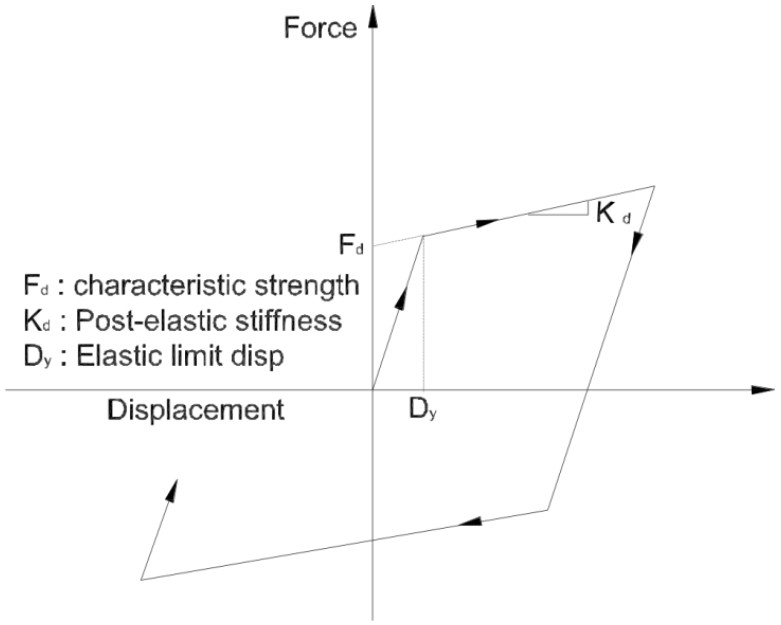

Fig. 3.2 Bi-linear hysteretic law used for representing the lateral constitutive behaviour of the isolation system

3.2.2 Ground motion database

Ground motions used as input to perform dynamic analyses of the base-isolated building are the same as those used in chapter 2 for fixed base buildings. The details about the selection of ground motions are referred to chapter 2.2.2.

3.3 **Non-linear modelling and analysis**

The response of the selected case studies is evaluated via non-linear dynamic analyses run in OpenSees 2.2.2 (2010). The models of the structures are built using Beam with Fibre-Hinges Elements for modelling beams and columns of the frames, and with Elastomeric Bearing Elements for modelling the isolators. The masses are concentrated at the nodes representing the beam-column joints, and the stiffness of the floors is modelled with rigid diaphragm constraints. A Rayleigh damping proportional to the mass and tangent stiffness matrix is used, with coefficients calibrated to provide a 5% damping at the first and second mode periods of the undamaged structures. The effects of geometric nonlinearities are not considered in the analyses. All the other missing details on the modelling of both the superstructures and the isolators are given in the Appendix.

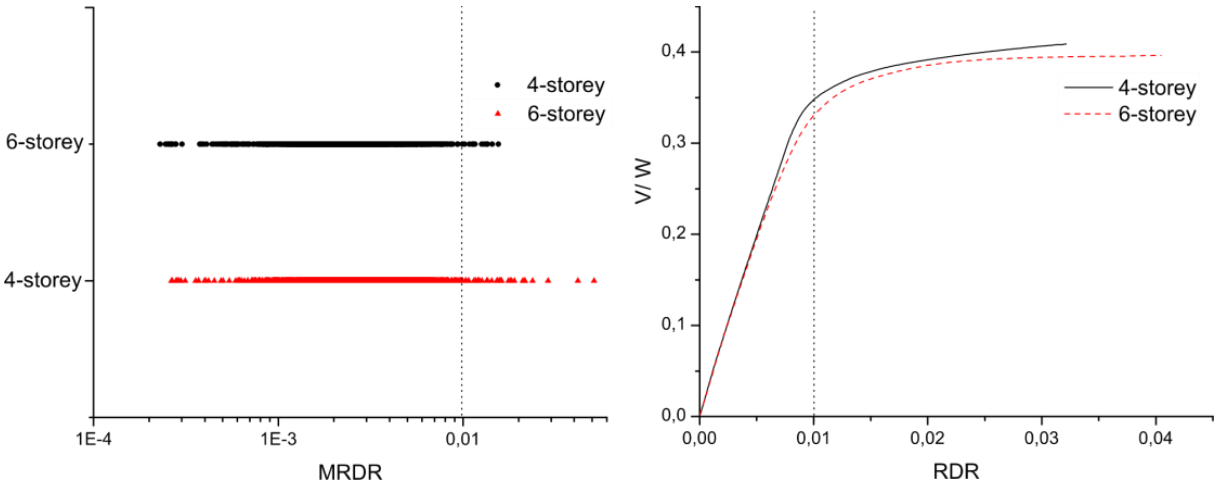

Fig. 3.3 Response of the frames obtained for all the investigated cases, and pushover curves of the two studied superstructures (left and right plot, respectively).

In the left plot of Fig. 3.3, the results of the dynamic analyses carried out with the full set of the selected GMs applied to all the studied base-isolated structures are reported. The plot reports the responses obtained for the 4-storey and 6-storey building expressed in terms of the Maximum Roof Drift Ratio (MRDR), that is, the maximum displacement of the roof with respect to that of the base divided by the height of the building. This parameter can be easily used to approximately identify the non-linear level of the seismic response investigated for the studied superstructures. The right plot of the same Figure reports the pushover curves of the two buildings obtained using fixed-base models and lateral pushing forces proportional to the floor masses. In the plot, RDR denotes the Roof Drift Ratio, while V and W the base shear and the seismic weight of the structure, respectively. It can be observed that a significant reduction of the lateral stiffness occurs for both structures at a value of the RDR equal to circa 0.01. Thus, the selected records do not produce damage to the studied isolated superstructures, with the exception of some of them which are able to excite the frames also well deep into the non-linear range.

3.4 **Intensity measures and engineering demand parameters**

3.4.1 Intensity measures

The definition of Intensity Measures used in this chapter can be referred to the Chapter 2. But there are two differences: the definition of period T in this chapter is changed with the isolation period instead of fundamental period of structure in chapter 2; the modified IMs are obtained from the existing ones by changing the period range of integration into 0.5T-1.25T, where T is the isolation period of the structure. A similar modification has been also considered by Avşar and Özdenmir (2011) when investigating the capability of IMs in predicting the seismic response of base-isolated bridges.

3.4.2 Engineering demand parameters

The EDPs considered in this chapter are MRDR, MIDR, MFA and MBD (Maximum Bearing Displacement). Among them MRDR, MIDR and MFA are introduced in chapter 2. The relevant content can be referred to Chapter 2.4.2. MBD is Maximum Bearing Displacement (MBD), which is a key index for base-isolated structures as a measure of the damage at base isolation level.

3.5 **Regression analyses**

3.5.1 Predictive models

The predictive models used for investigation of seismic response prediction of base-isolated buildings have been introduced in the chapter 2. The relevant content can be referred to chapter 2.5.1. In addition to the study on the efficiency and sufficiency of intensity measures for predicting seismic response of fixed based buildings, in the chapter the sensitivity of correlation between EDPs and IMs to varying isolation properties is investigated as well. In this chapter, sensitivity reflects the robustness of the IM in predicting, with the same efficiency, the response of structures, regardless of their properties. In particular, the efficiency trend of the IM of base isolation systems with different yield displacements and isolation periods is evaluated.

3.5.2 Evaluation results

3.5.2.1 Efficiency

Prediction of MIDR and MRDR

Fig. 3.4 reports the σ_ε values obtained in the regressions on the MIDR of the c2 structures (refer to Table 3.1 for the acronym). The predictive efficiencies of the IMs obtained for these two specific case studies are representative of the general trends observed in all the studied base-isolated buildings. By looking at the σ_ε values of Fig. 3.4, for both 4- and 6-storey buildings, the following conclusions can be drawn. The MIDR is more efficiently predicted when ordinary records rather than pulse-like near-fault records are used. MVSI, PGV, $V_{EIr}SI$, $MV_{EIr}SI$ and I_H are in general the most efficient IMs. In particular, for ordinary GMs the most efficient predictors are the structure-specific IMs, PGV, MVSI and I_H, while for pulse-like near fault GMs are PGV, MVSI, $V_{EIr}SI$ and $MV_{EIr}SI$. Among the non-structure-specific IMs, the velocity-related IMs, with the exception of CAD, are the most efficient predictors. Integral IMs, except for ASI, are more efficient than spectral IMs, while modified IMs have in general better efficiency than the corresponding existing ones only for the case of pulse-like near-fault GMs.

Table 3.2 σ_ε Values of the most efficient IMs for predicting MIDR.

MIDR				
Most efficient IMs	4-storey buildings		6-storey buildings	
	Ordinary GMs	Near-fault pulse-like GMs	Ordinary GMs	Near-fault pulse-like GMs
PGV	0.18-0.25	0.22-0.56	0.16-0.24	0.22-0.30
I_H	0.17-0.22	0.26-0.48	0.15-0.24	0.25-0.36
$V_{EIr}SI$	0.18-0.22	0.24-0.43	0.18-0.24	0.24-0.28
MVSI	0.17-0.22	0.23-0.40	0.18-0.24	0.19-0.24
$MV_{EIr}SI$	0.21-0.25	0.24-0.43	0.20-0.27	0.23-0.28

Fig. 3.5 and Fig. 3.6 report the σ_ε values obtained with some IMs for all the studied buildings in this chapter. In general, it can be observed that for pulse-like near-fault GMs the prediction errors on the 6-storey buildings are smaller than those on the 4-storey buildings. For ordinary

GMs, instead, the results of the predictions are much more similar. The ranges of values for σ_ε obtained for the most efficient IMs are reported in Table 3.2.

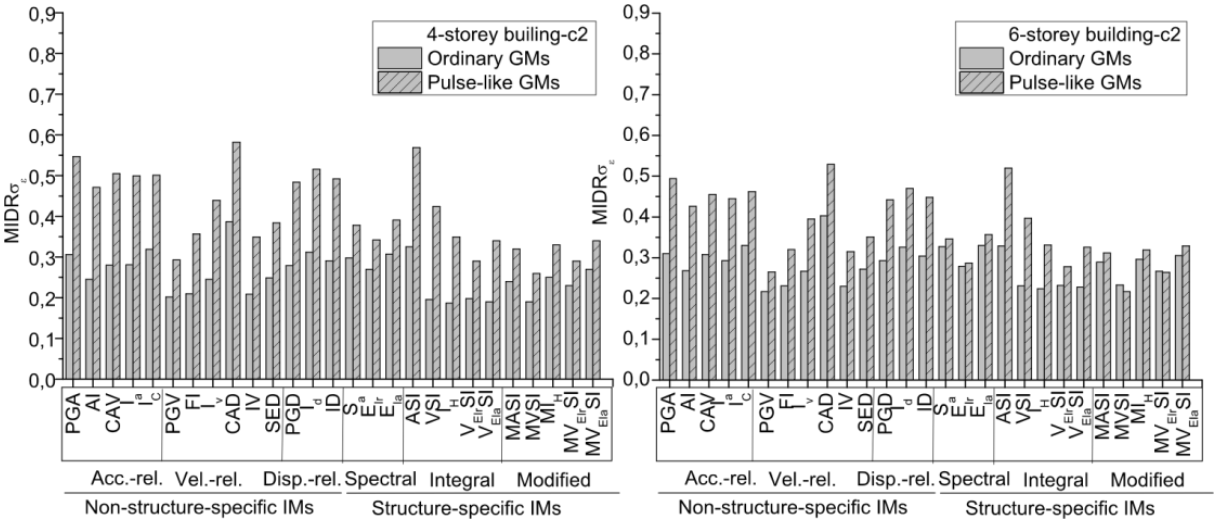

Fig. 3.4 Standard error of residuals σ_ε obtained in the IMs-MIDR regression of the c2 buildings (refer to Table 3.1).

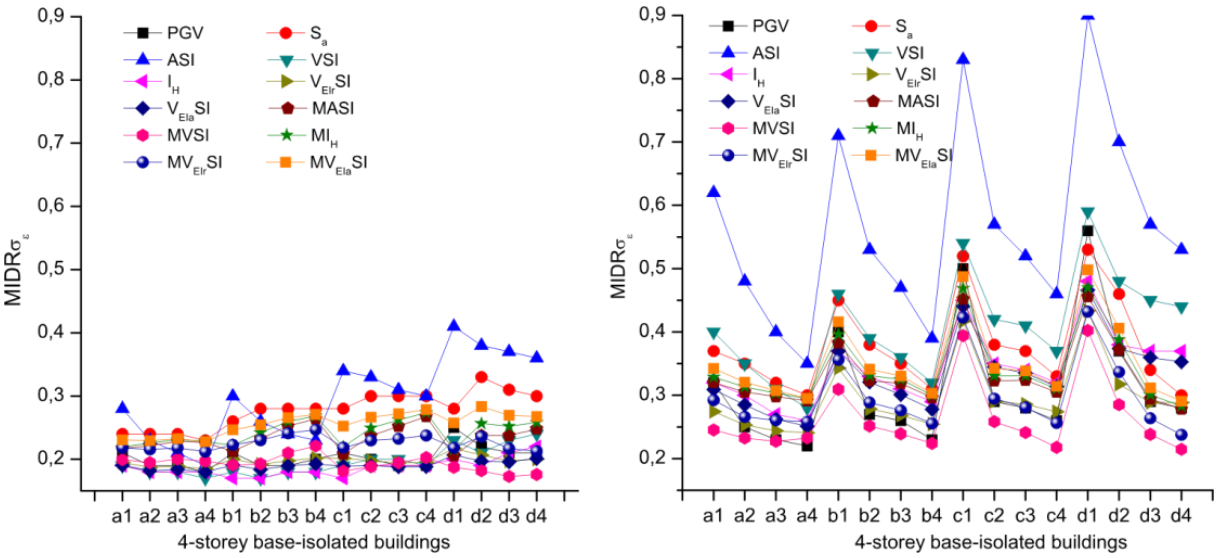

Fig. 3.5 Standard error of residuals σ_ε obtained in the IMs-MIDR regression of the 4-storey buildings using ordinary GMs (left plot) and pulse-like near-fault GMs (right plot).

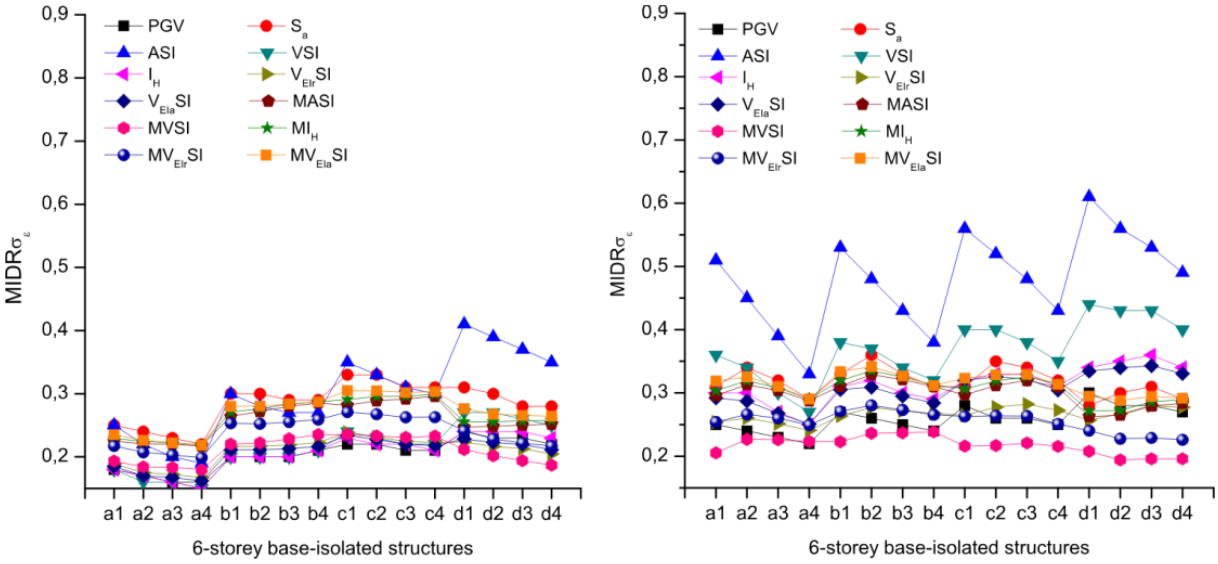

Fig. 3.6 Standard error of residuals σ_ε obtained in the IMs-MIDR regression of the 6-storey buildings using ordinary GMs (left plot) and pulse-like near-fault GMs (right plot).

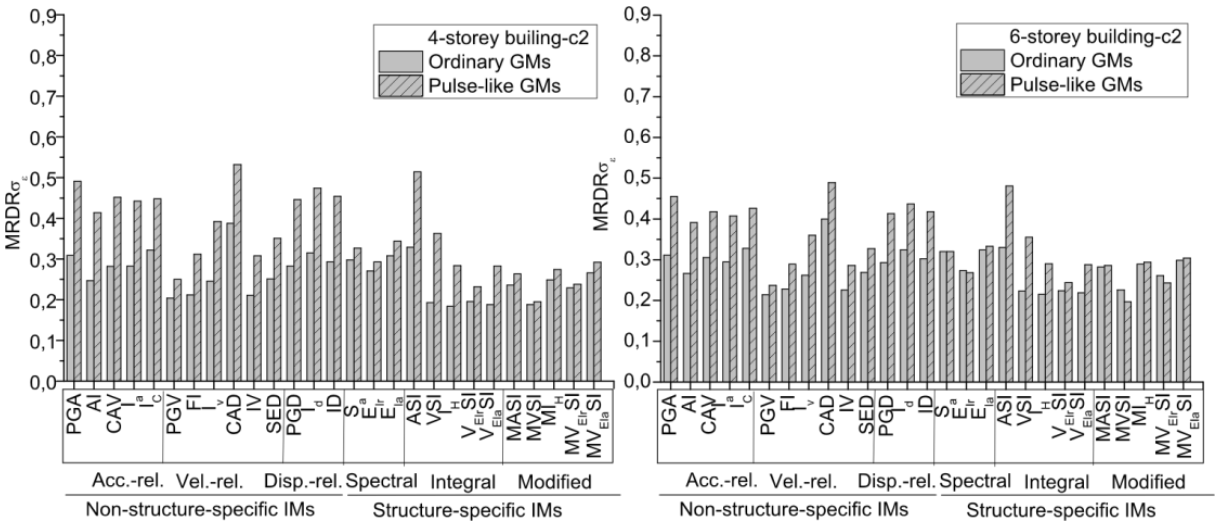

Fig. 3.7 Standard error of residuals σ_ε obtained in the IMs-MRDR regression of the c2 buildings (refer to Table 3.1).

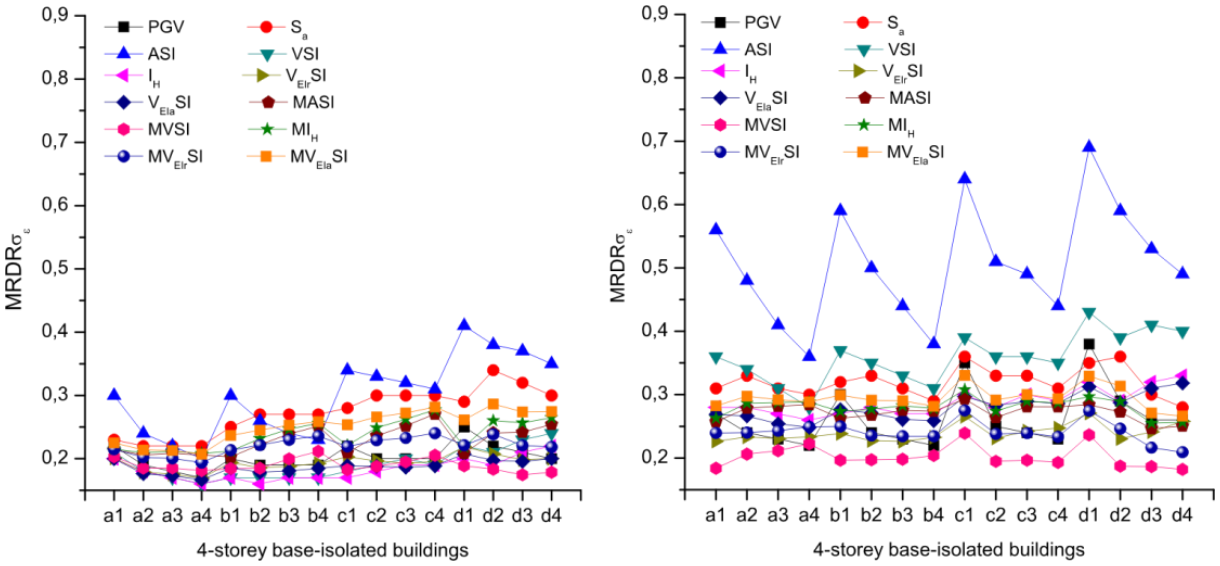

Fig. 3.8 Standard error of residuals σ_ε obtained in the IMs-MRDR regression of the 4-storey buildings using ordinary GMs (left plot) and pulse-like near-fault GMs (right plot).

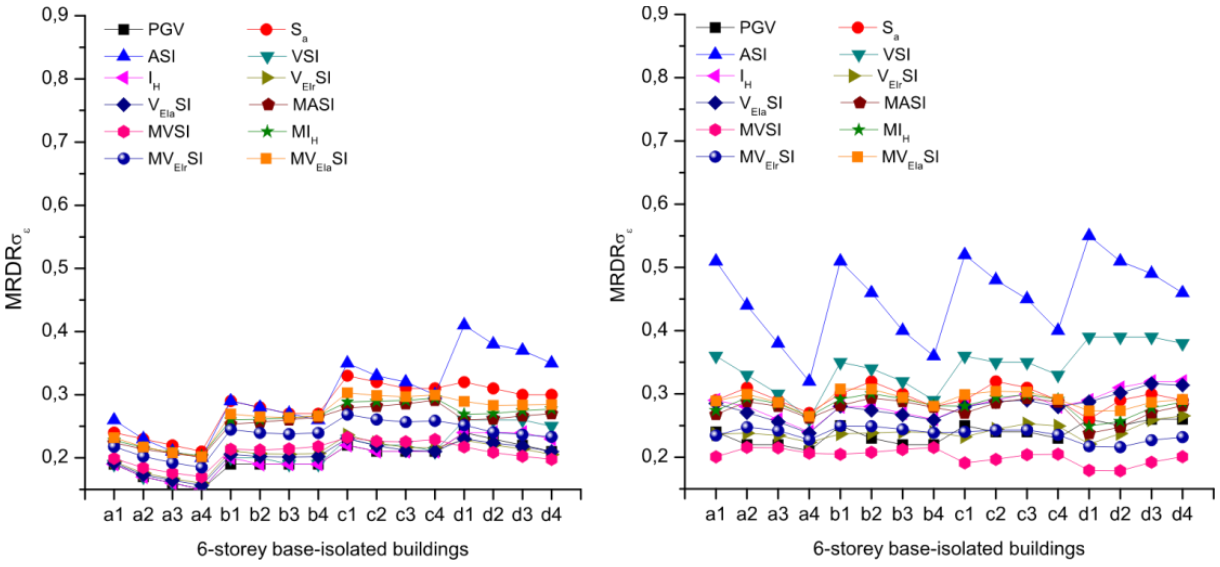

Fig. 3.9 Standard error of residuals σ_ε obtained in the IMs-MRDR regression of the 6-storey buildings using ordinary GMs (left plot) and pulse-like near-fault GMs (right plot).

The results of the regressions on the MRDR are summarized in the plots of Fig. 3.7, Fig. 3.8 and Fig. 3.9. It can be noticed that the trends of the IMs efficiencies are the same as those observed in the MIDR predictions. The only significant difference is that the obtained σ_ε values are in general lower. This is in accordance with the expectation that it is more difficult to predict local EDPs than global EDPs.

Prediction of MFA

The results obtained in the regressions on MFA demonstrate that non-structure-specific acceleration-related IMs are in general the most efficient IMs for this EDP. This is clearly shown in the plots of Fig. 3.10 reporting the σ_ε values obtained from the analyses of the c2 structures (once again, refer to Table 3.1 for the acronym). By considering the results of the analyses carried out on all the studied structures (see Fig. 3.11 and Fig. 3.12), it can be stated that the most efficient IMs are in particular PGA, AI, I_a and I_c. In Table 3.3, the ranges of σ_ε values obtained for these IMs are reported. Integral IMs are also efficient predictors of MFA. Differently from what observed for MIDR and MRDR, for MFA the use of modified IMs does not lead to improved predictions. Another different trend that can be observed in the regressions of MFA with respect to those of MIDR and MRDR is that the IMs efficiencies for ordinary and pulse-like near-fault records are almost the same.

Table 3.3 σ_ε values of the most efficient IMs for predicting MFA.

MFA				
Most efficient IMs	4-storey buildings		6-storey buildings	
	Ordinary GMs	Near-fault pulse-like GMs	Ordinary GMs	Near-fault pulse-like GMs
PGA	0.21-0.29	0.23-0.33	0.23-0.33	0.21-0.30
AI	0.22-0.32	0.21-0.31	0.24-0.36	0.23-0.29
I_a	0.23-0.31	0.21-0.32	0.25-0.34	0.23-0.29
I_c	0.24-0.34	0.23-0.32	0.26-0.34	0.20-0.30

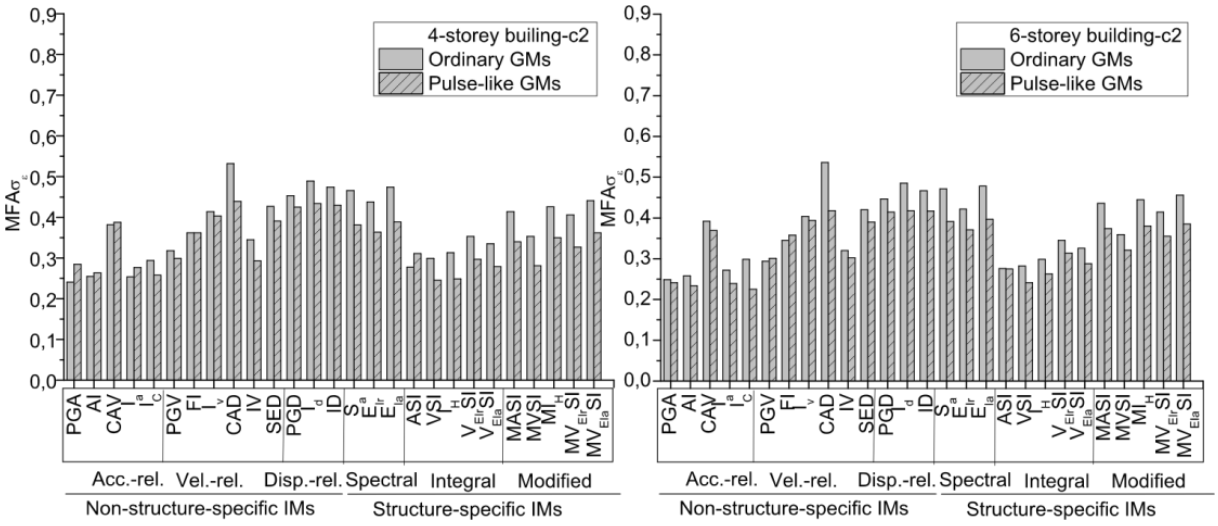

Fig. 3.10 Standard error of residuals σ_ε obtained in the IMs-MFA regression of the c2 buildings (refer to Table 3.1).

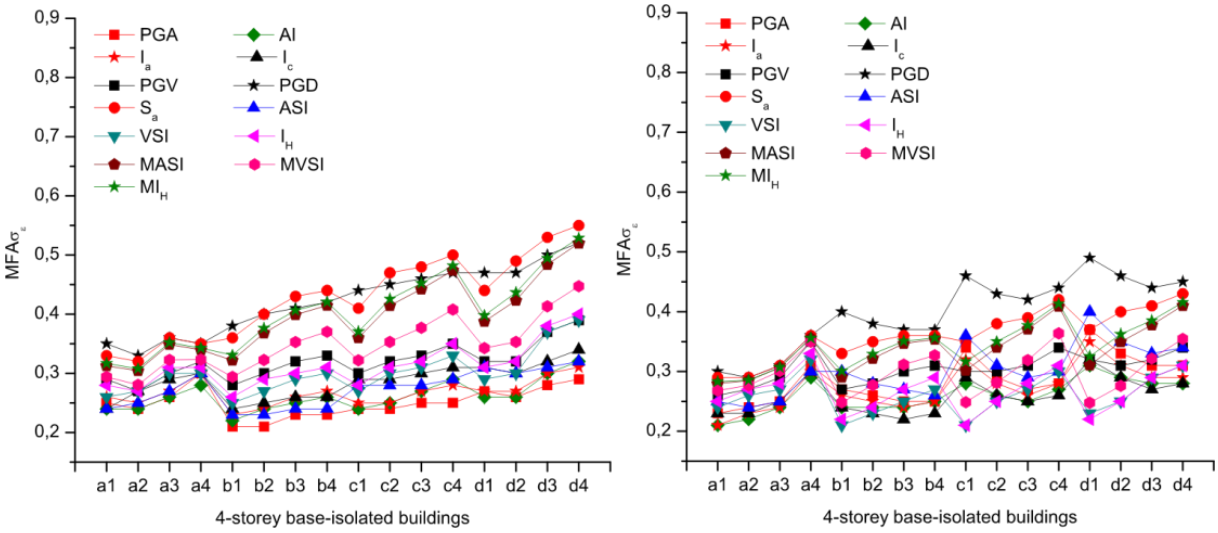

Fig. 3.11 Standard error of residuals σ_ε obtained in the IMs-MFA regression of the 4-storey buildings using ordinary GMs (left plot) and pulse-like near-fault GMs (right plot).

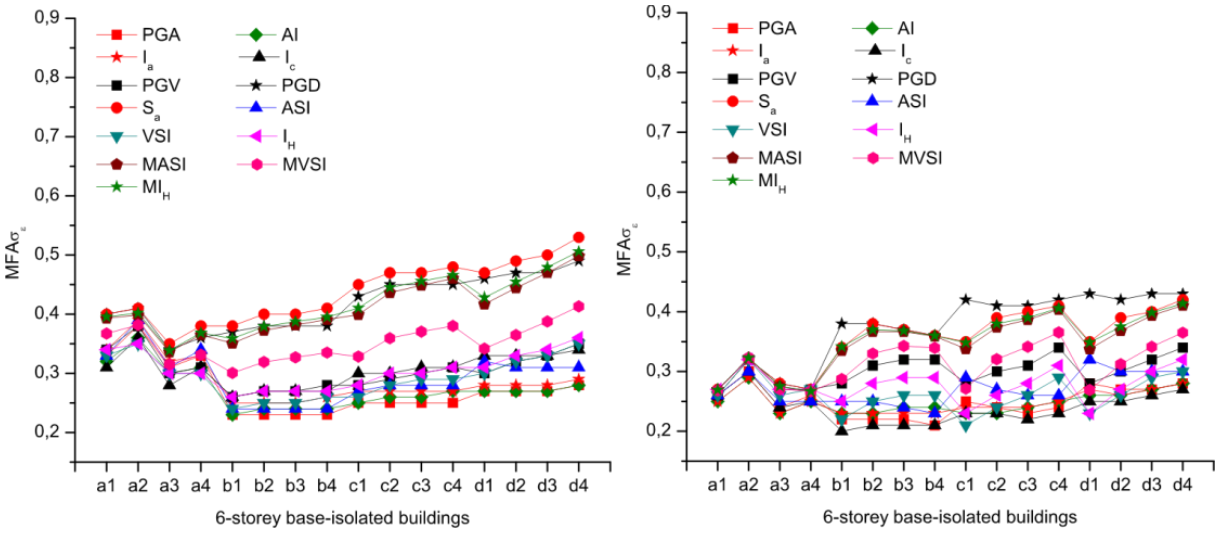

Fig. 3.12 Standard error of residuals σ_ε obtained in the IMs-MFA regression of the 6-storey buildings using ordinary GMs (left plot) and pulse-like near-fault GMs (right plot).

Prediction of MBD

In Fig. 3.13, Fig. 3.14 and Fig. 3.15 the results of the IMs-MBD regressions are reported using the same format adopted above for the other two considered EDPs. It can be observed that also for MBD, the results of the analyses on the 4-storey and the 6-storey base-isolated buildings follow similar trends. The only difference is that for ordinary GMs the errors are slightly larger when the responses of the 6-storey buildings than those of the 4-storey buildings are predicted. By comparing σ_ε values obtained with the different groups of IMs, the following main trends can be identified. Among the non-structure-specific IMs, PGV and FI are the most efficient ones. Except for CAD, velocity-related IMs result to be more efficient than both acceleration-related and displacement-related IMs. Spectral and modified IMs are those which in general produce the lowest σ_ε values, with the latter being the most efficient predictors especially when pulse-like near-fault GMs only are considered. This observation agrees with the fact that the period range used for calculating the modified IMs corresponds to a significant damage of the isolation system, and that for the considered case studies the MBD highest values have been recorded for pulse-like near-fault records. For all the IMs the less efficient predictions for the ordinary records are those corresponding to buildings with isolation systems characterized by an yield displacement equal to 0mm (the a

buildings, in accordance to the notation given in Table 3.1). This is due to the fact that, in these cases, zero or small bearing displacements values have been recorded. Finally, the most efficient predictor among all the considered ones is MVSI, with MI_H, MASI and $MV_{EIr}SI$ being also very efficient. The range of σ_ε values obtained with these IMs for the b, c and d structures only are reported in Table 3.4.

Table 3.4 Regressions of the MBD obtained for the b, c and d buildings: σ_ε values of the most efficient IMs.

MBD σ_ε				
Most efficient IMs	4-storey buildings		6-storey buildings	
	Ordinary GMs	Near-fault pulse-like GMs	Ordinary GMs	Near-fault pulse-like GMs
MASI	0.17-0.36	0.17-0.30	0.26-0.46	0.18-0.32
MVSI	0.23-0.28	0.23-0.28	0.29-0.36	0.23-0.31
MI_H	0.16-0.38	0.15-0.31	0.27-0.47	0.16-0.33
$MVE_{Ir}SI$	0.21-0-32	0.22-0.28	0.30-0.41	0.23-0.27

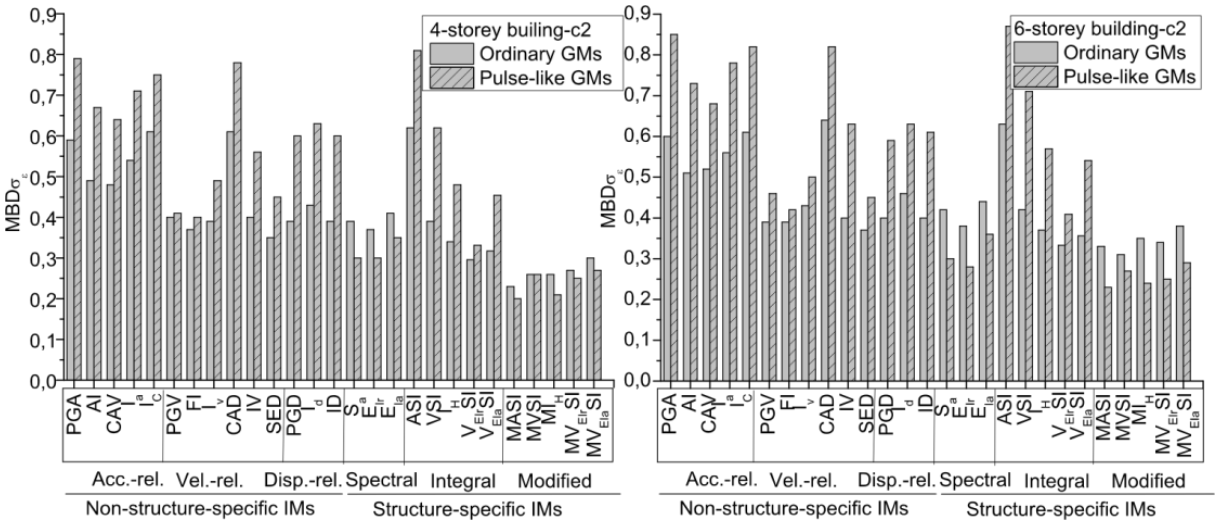

Fig. 3.13 Standard error of residuals σ_ε obtained in the IMs-MBD regression of the c2 buildings (refer to Table 2).

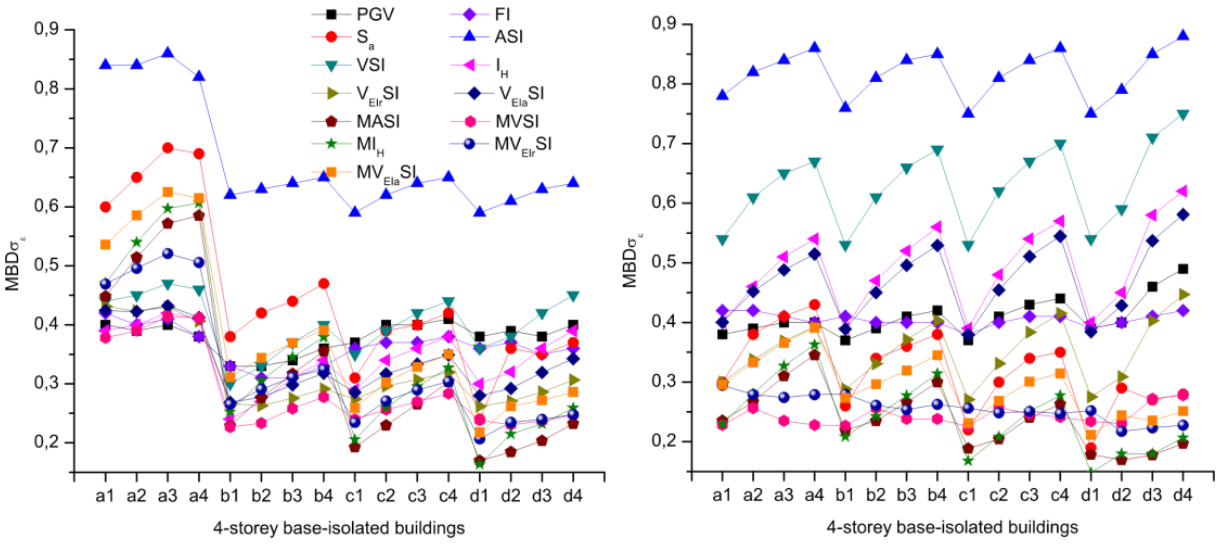

Fig. 3.14 Standard error of residuals σ_ε obtained in the IMs-MBD regression of the 4-storey buildings using ordinary GMs (left plot) and pulse-like near-fault GMs (right plot).

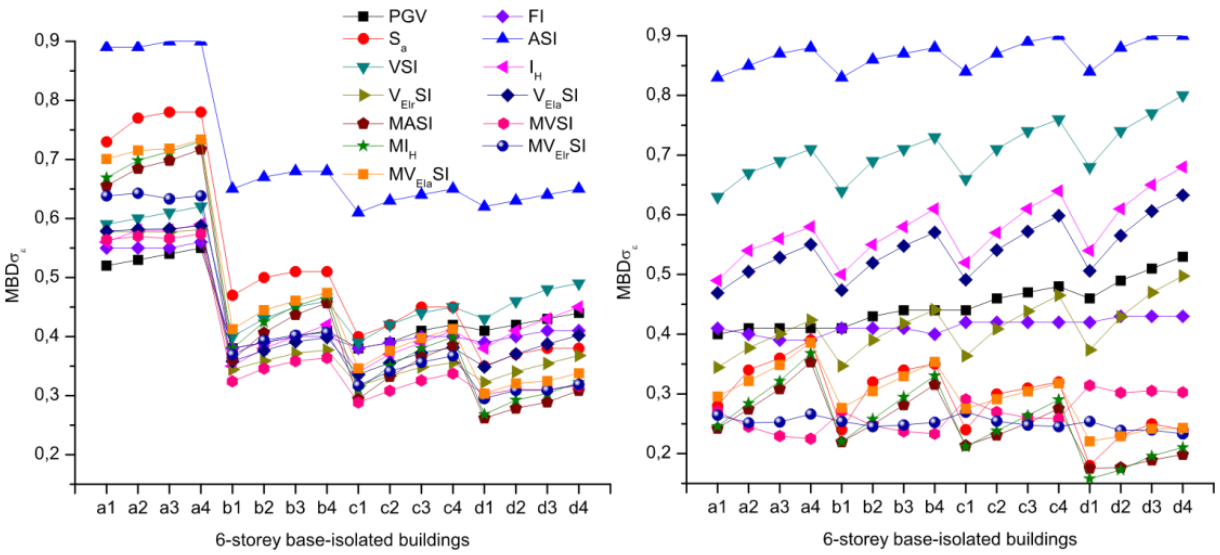

Fig. 3.15 Standard error of residuals σ_ε obtained in the IMs-MBD regression of the 6-storey buildings using ordinary GMs (left plot) and pulse-like near-fault GMs (right plot).

3.5.2.2 Sufficiency

The Figures of this subsection shortly report the results of the analyses carried out for evaluating the sufficiency of the investigated IMs. For each considered EDP, the analyses results obtained for the most efficient IMs only are reported. Thus, for MIDR and MRDR the sufficiency of PGV, $V_{EIr}SI$, MVSI and $MV_{EIr}SI$ only is discussed, for MFA that of PGA, AI, I_a and I_c, and for MBD that of PGV, MASI, MVSI, MI_H and $MV_{EIr}SI$.

In Fig. 3.16 and Fig. 3.17, the p-values of β_M and β_R obtained in the regression analyses of the MIDR and the MRDR residuals are given. From these values it can be stated that PGV and MVSI are the most sufficient IMs. In particular, PGV results to be conditionally independent on both M and R for all the studied cases. MVSI, instead, is conditionally dependent on M and R, but for some few cases only (some 6-storey buildings under pulse-like near fault GMs and some 4-storey buildings under ordinary GMs).

From the plots of Fig. 3.18 it can be clearly noticed that the most sufficient IMs for predicting MFA is I_c, resulting to be conditionally independent on both M and R for all the studied cases except for one. I_a is conditional dependent on R but for some cases of buildings under pulse-like ground motions only. The p-values of the β coefficients obtained with PGA and AI are much lower than 0.05, especially when pulse-like near-fault GMs are considered.

The results of the analyses for the evaluation of the IMs sufficiency with respect to the MBD prediction are reported in Fig. 3.19. It can be observed that all the IMs result to be dependent on M and/or on R for some of the studied cases. However, the p-values of the β coefficients obtained with $MV_{EIr}SI$ are significantly high, being in seven cases only lower than the limit value of 0.05.

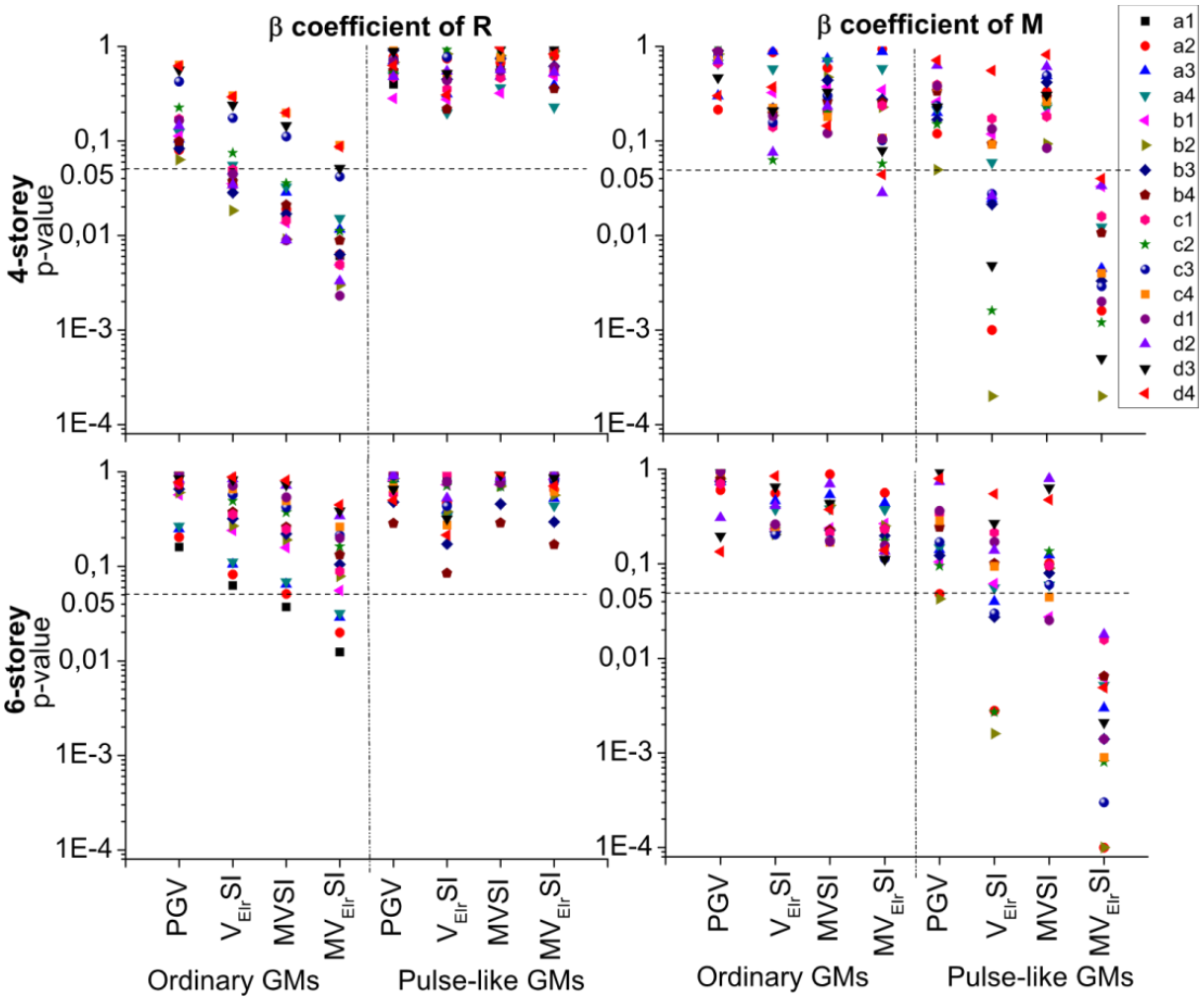

Fig. 3.16 Prediction of the $\varepsilon|_{IM}$ residuals obtained in the regressions of MIDR with the most efficient IMs (i.e., PGV, $V_{EIr}SI$, MVSI and $MV_{EIr}SI$): p-values of the R and M β coefficient (left and right plots, respectively) estimated for all the 4-storey and the 6-storey buildings (top and bottom plots, respectively).

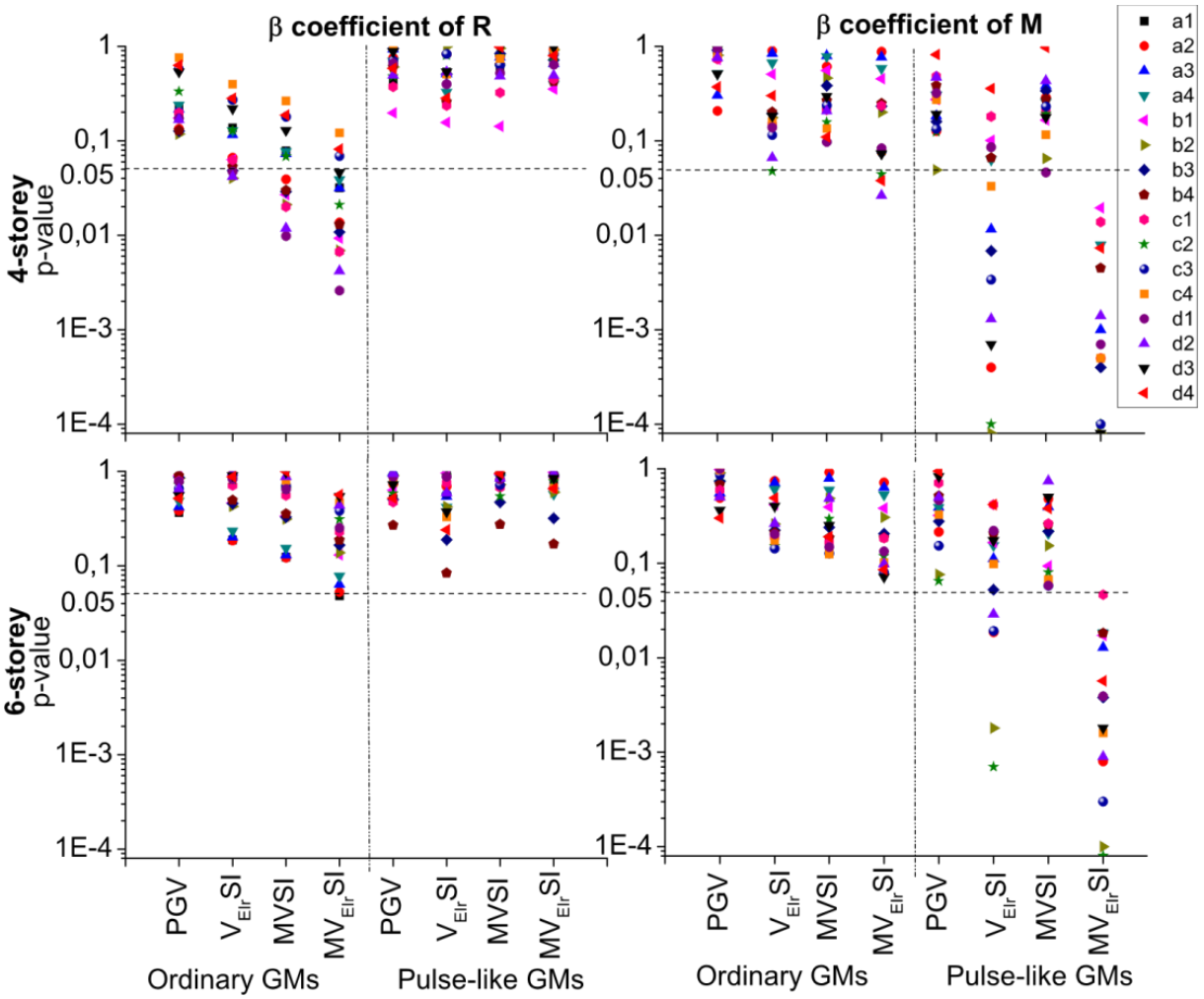

Fig. 3.17 Prediction of the $\varepsilon|_{IM}$ residuals obtained in the regressions of MRDR with the most efficient IMs (i.e., PGV, $V_{EIr}SI$, MVSI and $MV_{EIr}SI$): p-values of the R and M β coefficient (left and right plots, respectively) estimated for all the 4-storey and the 6-storey buildings (top and bottom plots, respectively).

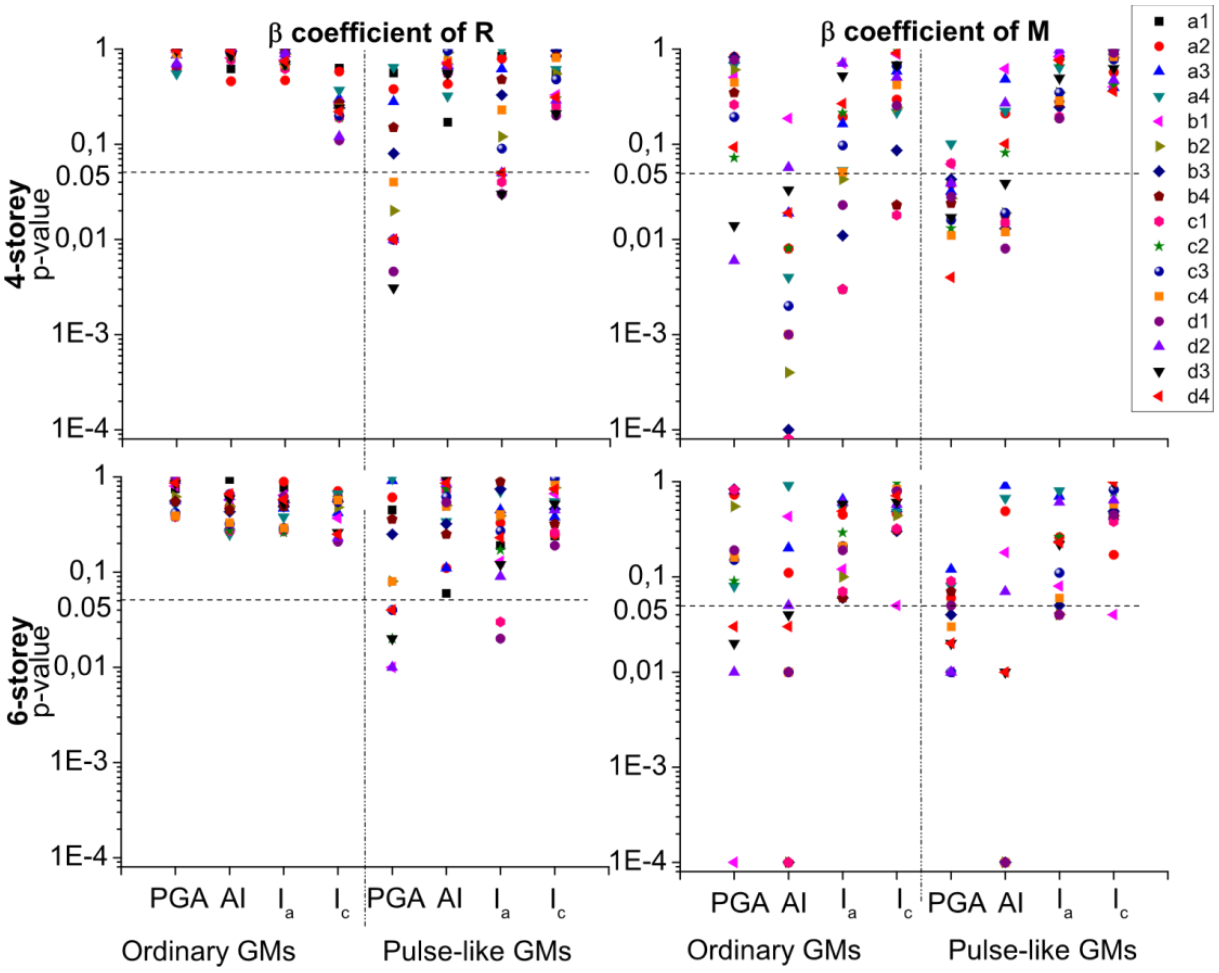

Fig. 3.18 Prediction of the $\varepsilon|_{IM}$ residuals obtained in the regressions of MFA with the most efficient IMs (i.e. , PGA, AI, I_a and I_c): p-values of the R and M β coefficient (left and right plots, respectively) estimated for all the 4-storey and the 6-storey buildings (top and bottom plots, respectively).

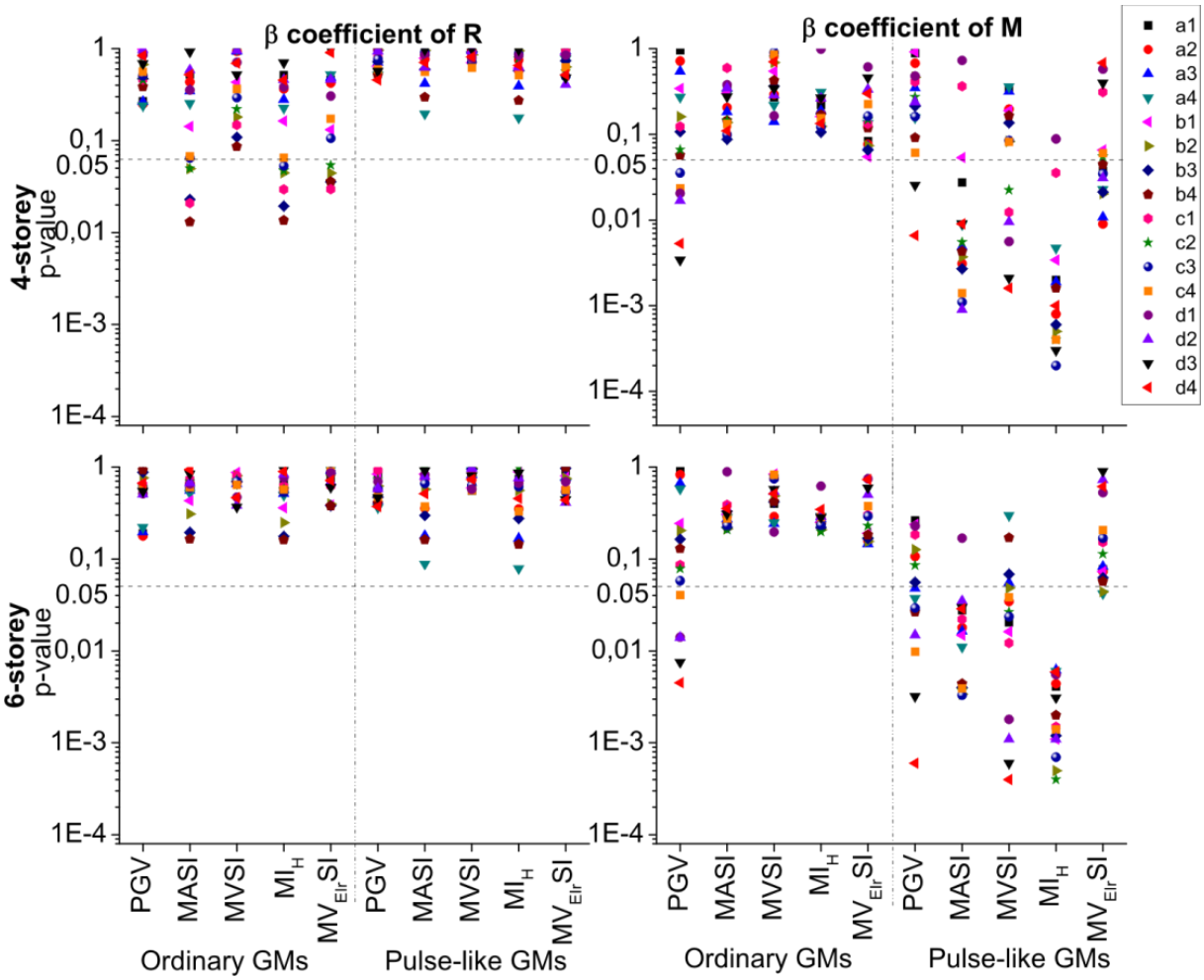

Fig. 3.19 Prediction of the $\varepsilon|_{IM}$ residuals obtained in the regressions of MBD with the most efficient IMs (i.e., PGV, FI, MVSI, MI_H, $MV_{EIr}SI$ and $MV_{EIa}SI$): p-values of the R and M β coefficient (left and right plots, respectively) estimated for all the 4-storey and the 6-storey buildings (top and bottom plots, respectively).

3.5.2.3 Sensitivity

In this subsection, the results of the analyses on the IMs efficiencies are reported again but with a different format than that used in subsection 3.5.2.1 so as to more clearly show the predictive sensitivity of the IMs to varying isolation properties. For each IM, the comparison of the efficiencies towards the response of structures with isolation systems having the same isolation period but different yielding displacements is used for evaluating the sensitivity to varying D_y values. Analogously, the sensitivity to varying T values is evaluated by comparing the efficiencies obtained in the response prediction of structures with isolation systems having

the same yielding displacement but different isolation periods. Because no significant differences have been found between the results of the analyses carried out on the 4-storey and the 6-storey buildings, only those obtained for the 4-storey buildings are shown. In particular, the results of the analyses of the a3, b3, c3 and d3 structures and those of the b1, b2, b3 and b4 structures (again, refer to Table 3.1 for the acronym) are used for showing the IMs sensitivity with respect to varying D_y and T values, respectively. The trends observed for these specific cases, in fact, can be considered as representative also of those found for all the other studied structures.

By observing the plots of Fig. 3.20 and Fig. 3.21, the following conclusions about the IMs sensitivity in predicting the MIDR can be drawn. The most efficient IMs, namely, MVSI, PGV, $V_{EIr}SI$ and $MV_{EIr}SI$ are not so much sensitive to the variation of both D_y and T. Among them, the only one showing a slight significant variation of the efficiency with the variation of the isolation properties is PGV. PGA, CAD and ASI, which are the least efficient IMs, are those which result to be also the most sensitive ones. The same trends have been also observed for the sensitivity of these IMs with respect to the MRDR prediction.

The plots of Fig. 3.22 and Fig. 3.23 show that also for the MFA the most efficient IMs, which in this case are PGA, AI, I_a and I_c, are the least sensitive predictors. The PGA only exhibits a significant variation of the predictive efficiency to D_y for pulse-like near-fault GMs. Integral IMs are robust as well, except for the case of the sensitivity to D_y when ordinary GMs are considered.

Among the most efficient IMs for predicting the MBD, the most robust ones are MVSI and $MV_{EIr}SI$ (see the plots of Fig. 3.24 and Fig. 3.25). MI_H and MASI result to be more sensitive also if compared to the less efficient PGV and FI. For all of these IMs, the more significant sensitivity can be observed for the case of ordinary GMs and varying D_y values.

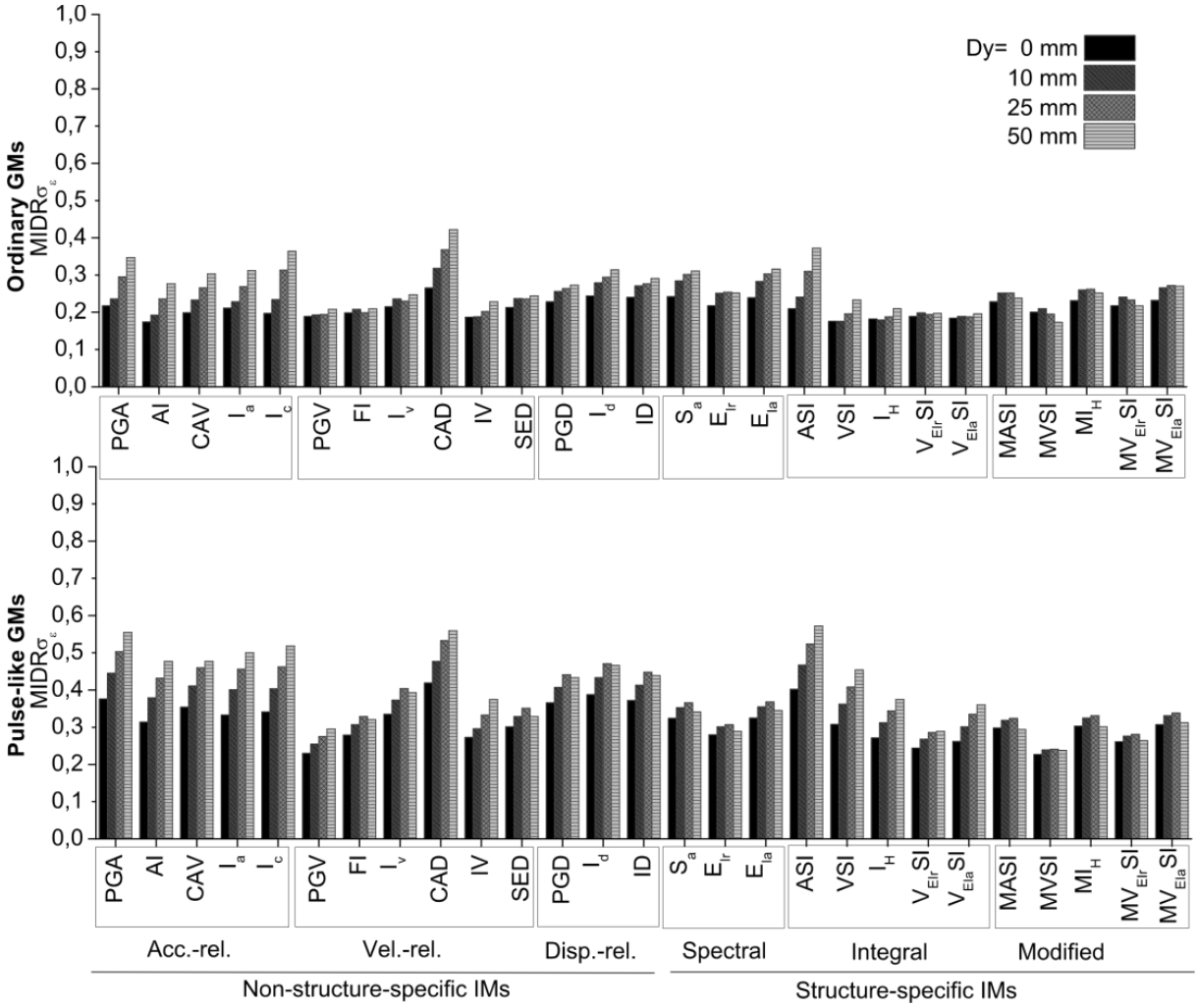

Fig. 3.20 Results of the IMs-MIDR regressions for the a3, b3, c3 and d3 4-storey building (refer to Table 3.1 for the acronym) under ordinary and pulse-like near-fault GMs (top and bottom plot, respectively): predictive sensitivity of the IMs to varying D_y values.

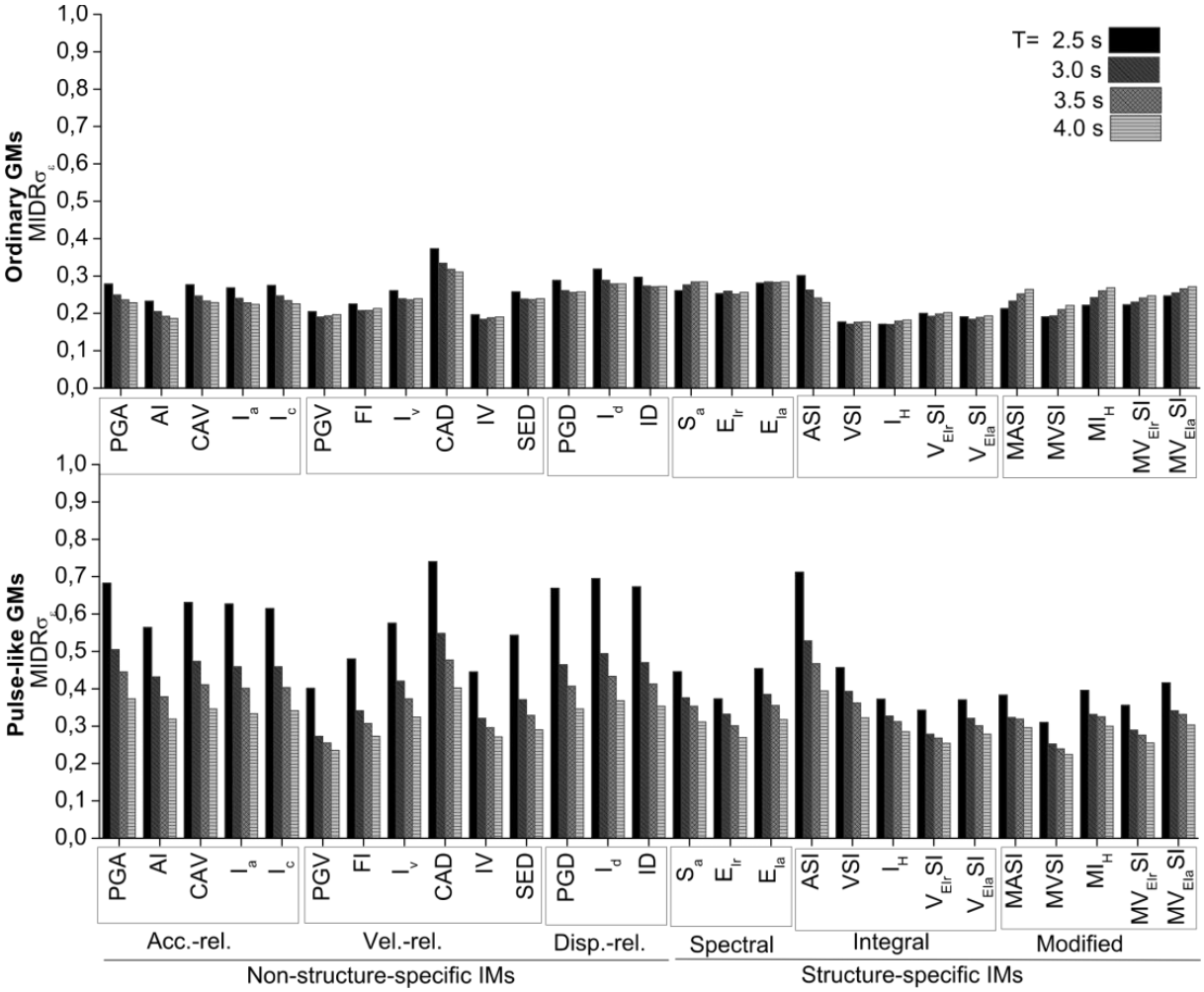

Fig. 3.21Results of the IMs-MIDR regressions obtained for the b1, b2, b3 and b4 4-storey building (refer to Table 3.1for the acronym) under ordinary and pulse-like near-fault GMs (top and bottom plot, respectively): predictive sensitivity of the IMs to varying T values.

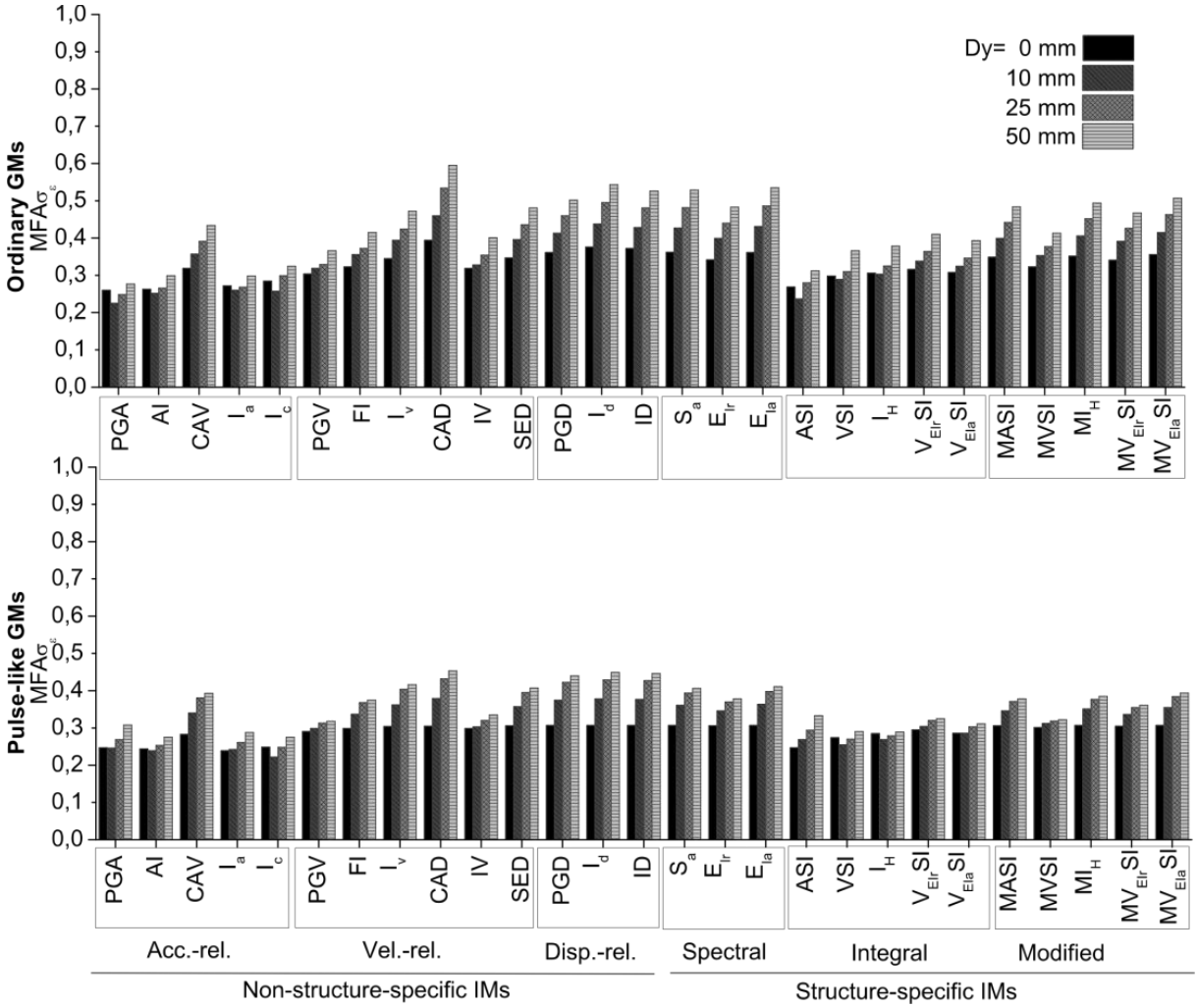

Fig. 3.22 Results of the IMs-MFA regressions obtained for the a3, b3, c3 and d3 4-storey building under ordinary and pulse-like near-fault GMs (top and bottom plot, respectively): predictive sensitivity of the IMs to varying D_y values.

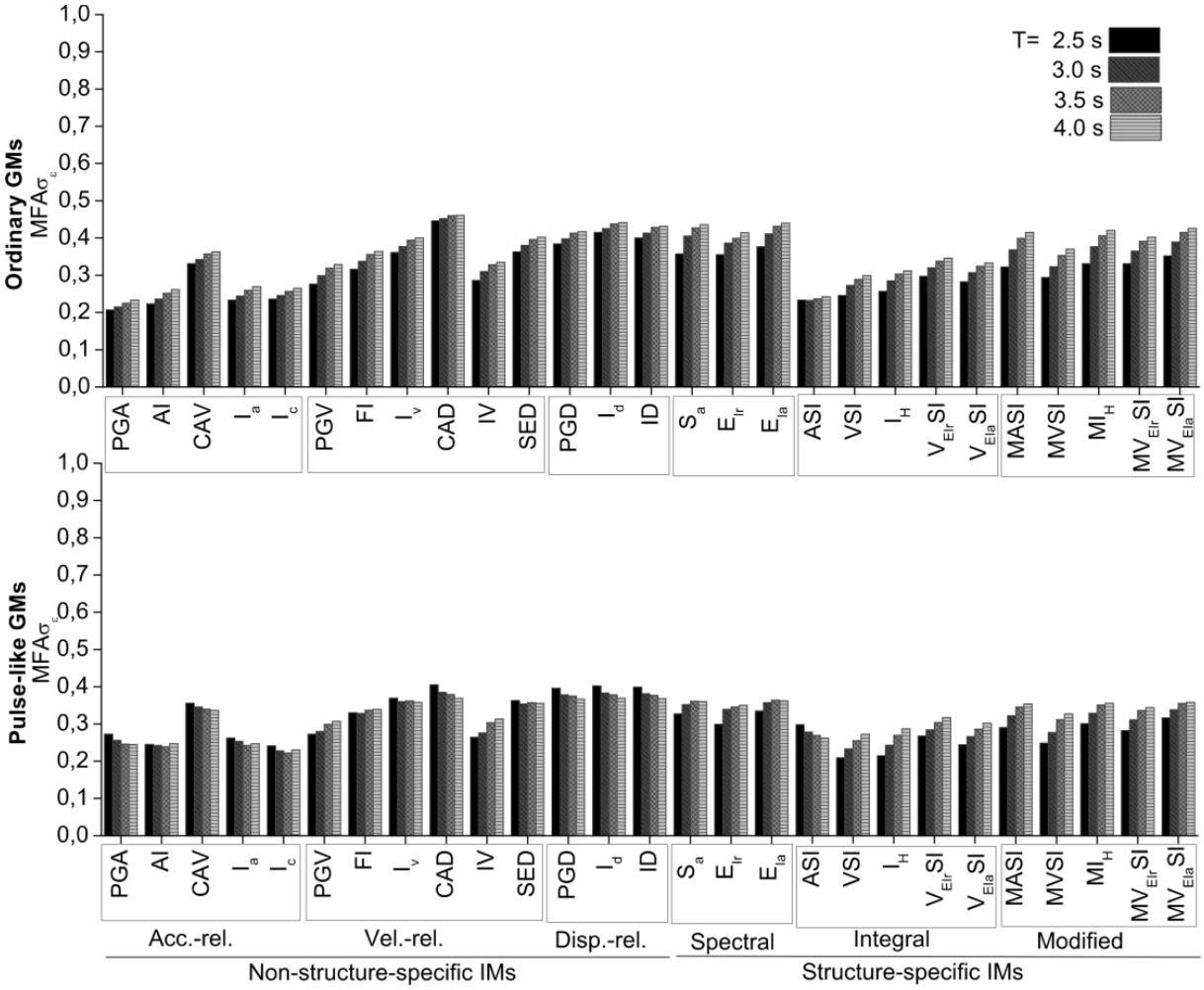

Fig. 3.23 Results of the IMs-MFA regressions obtained for the b1, b2, b3 and b4 4-storey building under ordinary and pulse-like near-fault GMs (top and bottom plot, respectively): predictive sensitivity of the IMs to varying T values.

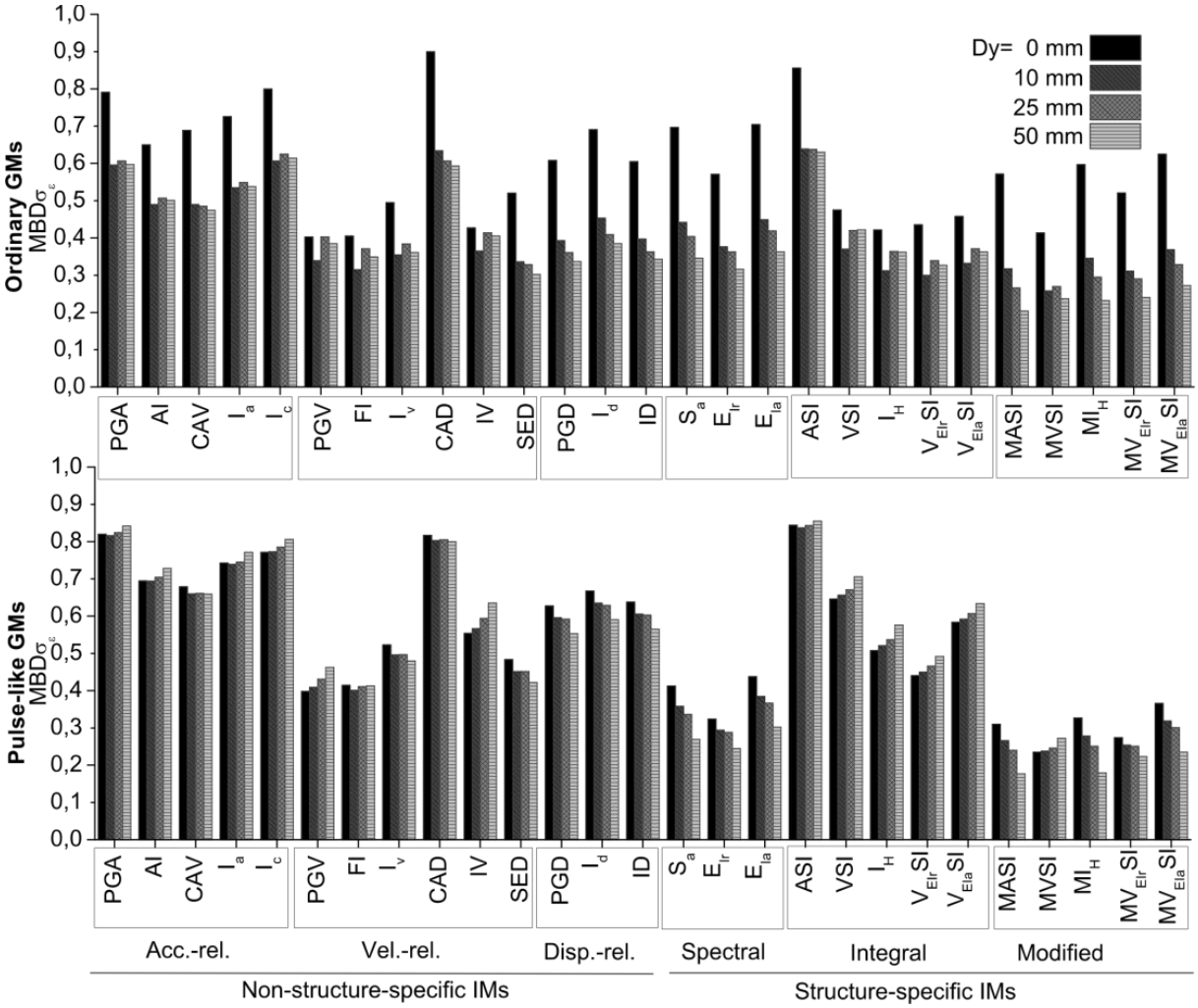

Fig. 3.24 Results of the IMs-MBD regressions obtained for the a3, b3, c3 and d3 4-storey building under ordinary and pulse-like near-fault GMs (top and bottom plot, respectively): predictive sensitivity of the IMs to varying D_y values.

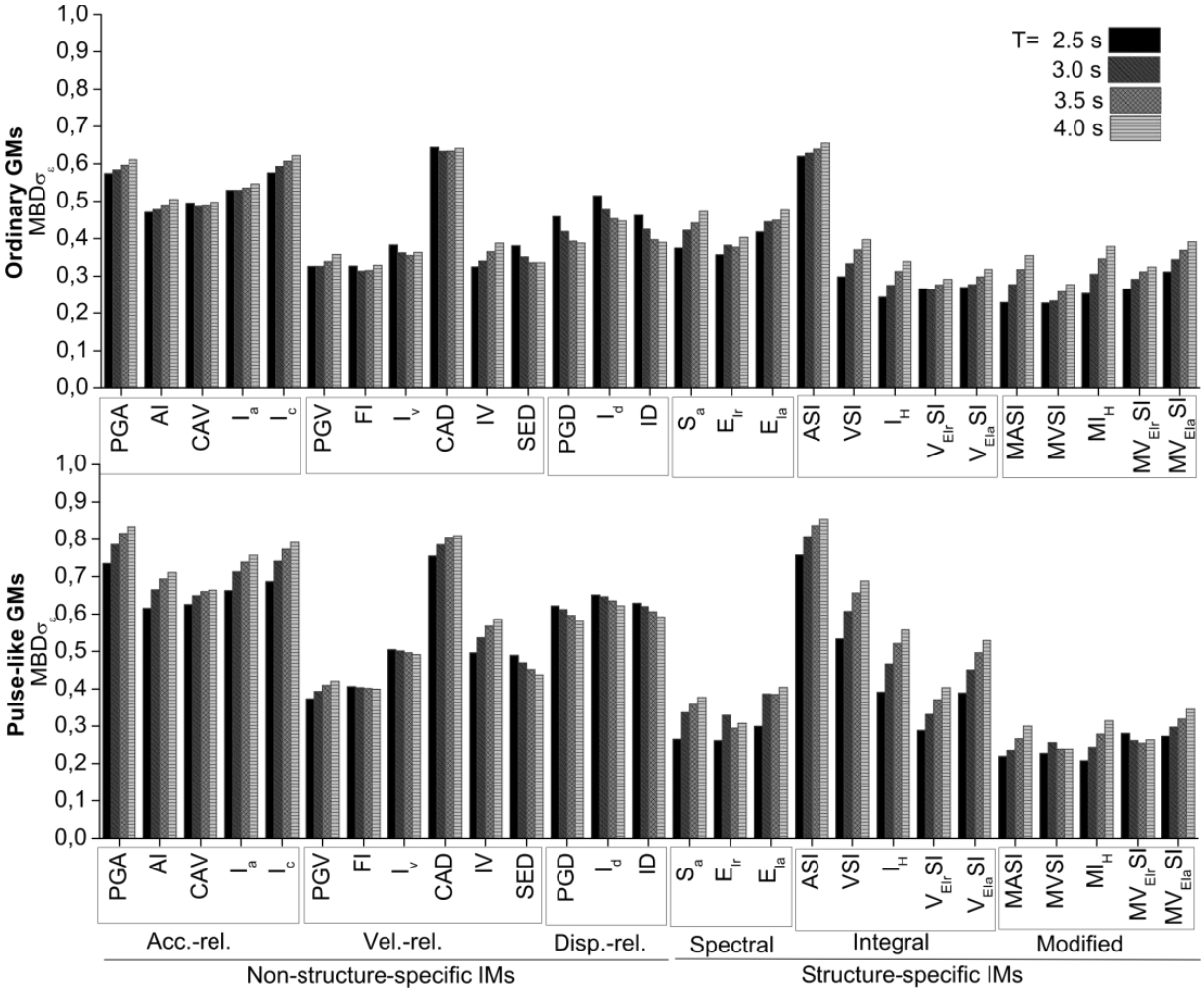

Fig. 3.25 Results of the IMs-MBD regressions obtained for the b1, b2, b3 and b4 4-storey building under ordinary and pulse-like near-fault GMs (top and bottom plot, respectively): predictive sensitivity of the IMs to varying T values.

3.6 **Summary and conclusions**

The aim of the work was to identify the Intensity Measure (IM) that better predict the seismic response of base-isolated buildings. In order to fulfil to this objective, the prediction capability of existing IMs were investigated by studying the response of two multi-storey RC frame structures protected at the base with systems characterized by different isolation properties. Non-linear dynamic analyses were carried out by using a large number of exciting ground motions. Different parameters were considered for measuring the seismic response observed in both the building and the isolation system. The investigated IMs were correlated

with the obtained structural responses and their predictive capabilities finally evaluated. The properties of the IMs considered in the evaluation analyses were the efficiency, the sufficiency and the robustness. The latter were considered for studying the sensitivity of the IMs to varying isolation properties.

Depending on the structure, the considered response parameter and IM property, different optimal predictors can be identified. Among them, the one that in the opinion of the authors can be considered as the best IM for predicting base-isolated building is overall $MV_{EIr}SI$. This IM is a proposed modified version of the relative Input Equivalent Velocity Spectrum Intensity. The analyses results showed that $MV_{EIr}SI$ is a very efficient predictor for the deformation response of both the superstructure and the isolation system. In particular, it was found that $MV_{EIr}SI$ is well correlated with the Maximum Inter-storey Drift Ratio (MIDR), the Maximum Roof Drift Ratio (MRDR) and the Maximum Base Displacement (MBD). This IM is also a good predictor for the acceleration response of the building. Reasonably acceptable values of the standard error of residuals were in fact obtained in the prediction of the Maximum Floor Acceleration (MFA). Among the considered predictors, however, other IMs such as the widely used Peak Ground Acceleration were found to be more efficient. About the sufficiency, all the investigated IMs resulted to be dependent on magnitude and/or on distance. However, the p-values of the β coefficients obtained with $MV_{EIr}SI$ were found to be lower than the limit value of 0.05 only in some cases. Finally, the results of the sensitivity investigations showed that $MV_{EIr}SI$ is a very robust IM, especially when the maximum displacement of the isolation system is predicted.

Trends about the variation of the IMs predictive capabilities produced by the pulse-type properties of the exciting ground motions cannot be clearly identified. In most of the cases, both the efficiency and the sufficiency of the IMs reduce. For $MV_{EIr}SI$, it was found that the efficiency is actually not significantly influenced by the type of record. For most of the other considered IMs, instead, the efficiency considerably reduces, particularly when MIDR and MBD is predicted. Significant increases in the magnitude influence on the prediction of the regression residuals of MIDR, MRDR and MBD were observed, especially for the case of $MV_{EIr}SI$. In general, the obtained results showed that frequently the IMs cannot predict

properly the response of the base-isolated building when it is subjected to pulse-like records. Research efforts for modifying the IMs currently available in the literature and for improving their predictive performance when dealing with this type of ground motions are therefore needed. Alternatively, new predictors that explicitly account for parameters which have already been shown to appropriately characterize the intensity of near-fault pulse-like records, such as the shape and period of the dominant pulse (e.g., see Kalkan and Kunnath 2007; 2008), should be investigated.

It is important to underline that when the predictive capability of the IM is evaluated, as in the present study, with regression of responses obtained from dynamic analyses, the results can be only applied in principle to structures with dynamic properties similar to those of the studied ones. For this reason, in order to generalize the findings obtained in this study also to other types of buildings that can be suitable for base isolation (e.g., buildings designed without specific provisions for earthquake resistance or irregular structures) additional analyses are required.

4 Proposal for new prediction equations of elastic input energy equivalent velocity spectra

4.1 Introduction

In Performance-Based Earthquake Engineering (PBEE) the intensity of the earthquake is quantified through a parameter that is usually denoted as Intensity Measure (IM). A Ground Motion Prediction Equations (GMPE) is an equation for calculating the IM value as a function of different variables representative of the earthquake properties, such as, magnitude, fault mechanism, source-to-site distance and soil condition. The GMPE is a tool commonly used in Probabilistic Seismic Hazard Analysis (PSHA). It gives, in fact, a prediction of the expected (mean) value and standard deviation of the IM at a site, and thus can be used to calculate the annual rate of exceeding a specific earthquake level of interest.

In the literature, many different IMs can be found. Those that have been more largely investigated and that are most commonly used both in PSHA and Probabilistic Seismic Demand Analysis (PSDA) to predict the response of structures to earthquake are the following: the Peak Ground Acceleration (PGA), the Peak Ground Velocity (PGV), the Peak Ground Displacement, and the Spectral pseudo-acceleration (S_a). However, studies (e.g., Yakut and Yilmaz, 2008, Jayaram et al., 2010, Lucchini et al., 2013, and the Chapter 3 of this study) have recently evaluated these IMs and demonstrated the reduced predictive capabilities they have with respect to some types of structures and Engineering Demand Parameters (EDPs) commonly used to measure damage. It is also for such a reason that the interest in studying alternative IMs has been recently renewed (e.g., see the recent studies on design input energy spectra formulated in terms of velocity carried out by Benavent-Climent et al., 2010 and by López-Almansa et al., 2013).

Several studies proposing energy-based concepts for the definition of the earthquake IM have been carried out in the past (e.g., Uang and Bertero, 1990, and the most recent Kalkan and Kunnath, 2008). Among the different energy-based parameters that have been studied, the

relative and absolute elastic input energy and the corresponding equivalent velocities are those that more than others have been considered as potential measures of seismic demand in structures. These parameters have been shown to be good predictors due to their dependence on both amplitude and duration of the motion, and the properties of the structure as well.

Recently, due to increased number of strong motion records available, new GMPEs have been proposed. Many of them have been developed in the Next Generation Attenuation (NGA) projected for predicting shallow crustal earthquakes in active seismic regions. Details about these new NGA GMPEs can be found in Abrahamson and Silva (2008), Boore and Atkinson (2008), Campbell and Bozorgnia (2008), Chiou and Youngs (2008), and Idriss (2008). These GMPEs have been developed using ground motion database larger than those used in the past, and advanced functional forms requiring many input variables, namely, many information on the earthquake properties. The IMs predicted by these GMPEs are PGA, PGV, PGD, and S_a only. Studies that recently focused on energy-based intensity measures are really a few. Among them deserve to be mentioned those of Chapman (1999), Gong and Xie (2004), and Danciu and Tselentis (2007). In these studies, GMPEs for input energy equivalent velocities are developed, but only for specific seismic regions and by using a small number of strong ground motion data (due to the available databases at the time they have been proposed). In particular, 304 records from 23 earthquakes occurred in western North America, 266 records from 15 earthquakes in California, and 335 records from 151 Greek earthquakes are used in Chapman (1999), Gong and Xie (2004), and Danciu and Tselentis (2007), respectively. In these GMPEs very limited consideration is given to site effects, and dummy variables are usually used to represent site classes and soil conditions. Only in Danciu and Tselentis (2007) fault mechanism effects are taken into account in the development of the prediction equations. The aim of this study is to establish new GMPEs for both the absolute and the relative elastic input energy equivalent velocity spectrum. The equations will be derived using a large set of strong ground motions selected from the NGA database. Improvements with respect to the GMPEs currently available in the literature will be obtained by accounting for the effects of both fault mechanism and soil condition. The latter will not be evaluated with dummy variables but the commonly used parameter V_{S30}, namely, the value of the average shear-wave velocity between 0 and 30-meters depth. A random effects model for considering the variation

of records within-event and between-events (Abrahamson and Youngs, 1992) will be employed in the regression analyses for the development of the prediction equations.

4.2 **Strong motion database**

The NGA ground motion database (http://peer.berkeley.edu/peer_ground_motion_database/site) includes a very large number of strong ground motions recorded worldwide of shallow crustal earthquakes in active tectonic regions. This database, which has already been used by other researcher to develop GMPEs, provides records with comprehensive meta-data (such as earthquake source data and various site characterizations) that enable to constrain relatively complex functional forms for many different earthquake properties (e.g., fault mechanism and V_{S30}).

The subset of records selected from the NGA database and used to derive the proposed GMPEs consists of 1550 ground motions from 63 main shock earthquakes. Each of them represents a free-field motion, has two horizontal components and is characterized by a measured or estimated V_{S30}. The same general criteria used in Campbell and Bozorgnia (2008) to select records to derive prediction equations for the geometric mean horizontal component of PGA, PGV, PGD and S_a is applied. In particular, only earthquakes located within the shallow continental crust in a tectonically active region are selected. All data are from recordings at or near ground level and exhibits no known embedment or topographic effects. In addition, earthquakes having not enough records to reliably represent the mean horizontal ground motion in relation to their magnitude are excluded.

The distribution of the selected ground motions with respect to moment magnitude (in the range from 4.53 to 7.9) and site-rupture closest distance (varying from 0.1km to 199.3km) is shown in Fig. 4.1. In Table 4.1, a summary of these earthquakes is also are reported.

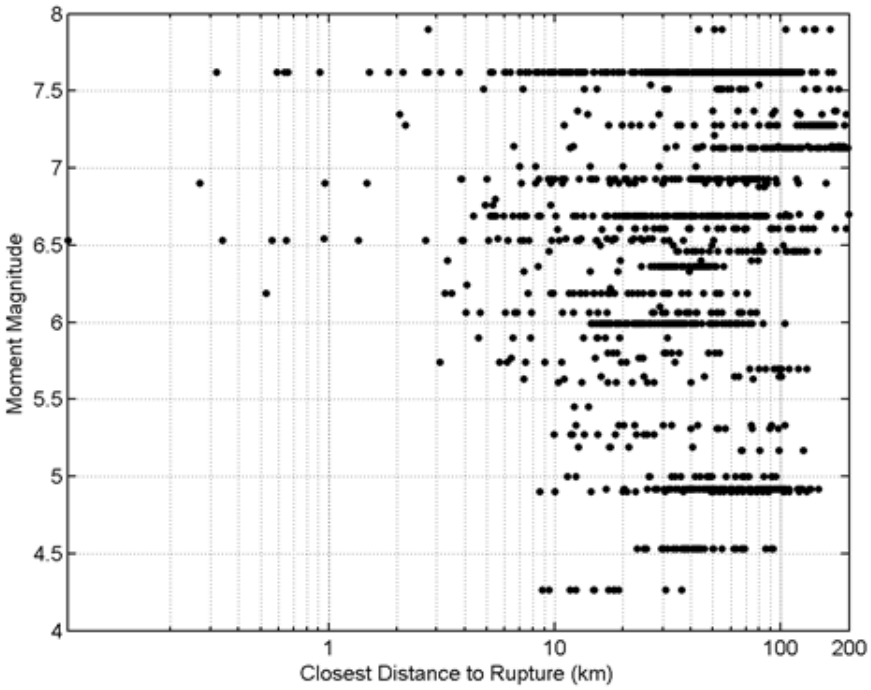

Fig. 4.1 Magnitude-Distance Distribution of Data Used in the Attenuation Regression

Table 4.1 Database of Strong Ground Motions Records Used in the Regression Analyses

Earthquake Name	Year	M	Mec.	Depth (km)	Rrup (km)		V_{S30} (m/s)		Number of recordings				Total No.
					Min.	Max.	Min.	Max.	AB	C	D	E	
Kern County	1952	7.36	R	16	117.8	117.8	316.5	316.5	0	0	1	0	1
Parkfield	1966	6.19	SS	10	9.6	17.6	256.8	527.9	0	2	2	0	4
Lytle Creek	1970	5.33	RO	8	12.4	103.6	302.0	813.5	1	7	2	0	10
San Fernando	1971	6.61	R	13	19.3	193.9	235.0	821.7	2	19	12	0	33
Managua. Nicaragua-01	1972	6.24	SS	5	4.1	4.1	288.8	288.8	0	0	1	0	1
Friuli. Italy-01	1976	6.5	R	5.1	15.8	102.2	274.5	659.6	0	3	2	0	5
Gazli. USSR	1976	6.8	R	18.2	5.5	5.5	659.6	659.6	0	1	0	0	1
Tabas. Iran	1978	7.35	R	5.75	2.1	194.6	274.5	766.8	1	2	4	0	7
Coyote Lake	1979	5.74	SS	9.6	3.1	33.8	221.8	1428.0	1	5	4	0	10
Norcia. Italy	1979	5.9	N	6	4.6	31.4	338.6	1000.0	1	1	1	0	3
Imperial Valley-06	1979	6.53	SS	9.96	0.1	50.1	162.9	659.6	0	2	30	1	33
Livermore-01	1980	5.8	SS	12	17.2	53.4	271.4	517.1	0	2	3	0	5
Anza (Horse Canyon)-01	1980	5.19	SS	13.6	12.7	40.6	329.0	724.9	0	3	2	0	5
Mammoth Lakes-01	1980	6.06	NO	9	4.7	15.5	338.5	370.8	0	1	2	0	3
Victoria. Mexico	1980	6.33	SS	11	7.3	39.3	274.5	659.6	0	1	3	0	4
Irpinia. Italy-01	1980	6.9	N	9.5	8.2	59.6	274.5	1000.0	5	5	2	0	12
Corinth. Greece	1981	6.6	N	7.15	10.3	10.3	338.6	338.6	0	0	1	0	1
Westmorland	1981	5.9	SS	2.3	6.5	19.4	191.1	362.4	0	1	5	0	6

Coalinga-01	1983	6.36	R	4.6	8.4	55.8	184.8	684.9	0	25	20	0	45
Borah Peak. ID-01	1983	6.88	N	16	79.6	84.8	424.8	659.6	0	3	0	0	3
Morgan Hill	1984	6.19	SS	8.5	0.5	70.9	116.4	1428.0	1	10	15	1	27
Lazio-Abruzzo. Italy	1984	5.8	N	14	18.9	51.3	200.0	659.6	0	1	4	0	5
Nahanni. Canada	1985	6.76	R	8	4.9	9.6	659.6	659.6	0	3	0	0	3
Hollister-04	1986	5.45	SS	8.72	12.2	14.1	215.5	684.9	0	1	2	0	3
N. Palm Springs	1986	6.06	RO	11	4.0	78.1	207.5	684.9	0	13	18	0	31
Chalfant Valley-01	1986	5.77	SS	6.7	6.4	24.5	271.4	345.4	0	0	5	0	5
Chalfant Valley-02	1986	6.19	SS	10	7.6	52.0	271.4	359.2	0	0	11	0	11
New Zealand-02	1987	6.6	N	6.4	16.1	68.7	424.8	424.8	0	2	0	0	2
Whittier Narrows-01	1987	5.99	RO	14.6	14.5	103.9	160.6	1222.5	3	49	56	1	109
Whittier Narrows-02	1987	5.27	RO	13.3	9.9	27.5	271.9	821.7	1	3	6	0	10
Superstition Hills-01	1987	6.22	SS	10	17.6	17.6	207.5	207.5	0	0	1	0	1
Superstition Hills-02	1987	6.54	SS	9	1.0	27.0	191.1	362.4	0	1	10	0	11
Loma Prieta	1989	6.93	RO	17.48	3.9	117.1	116.4	1428.0	7	37	28	5	77
Griva. Greece	1990	6.1	N	9.45	29.2	29.2	338.6	338.6	0	0	1	0	1
Erzican. Turkey	1992	6.69	SS	9	4.4	4.4	274.5	274.5	0	0	1	0	1
Cape Mendocino	1992	7.01	R	9.6	7.0	42.0	311.8	712.8	0	4	2	0	6
Landers	1992	7.28	SS	7	2.2	190.1	207.5	684.9	0	20	47	0	67
Big Bear-01	1992	6.46	SS	13	9.4	144.6	207.5	821.7	1	14	23	0	38
Northridge-01	1994	6.69	R	17.5	5.2	147.6	160.6	2016.1	13	67	68	1	149
Kobe. Japan	1995	6.9	SS	17.9	0.3	158.6	256.0	609.0	0	4	8	0	12
Kozani. Greece-01	1995	6.4	N	12.64	19.5	79.4	338.6	659.6	0	2	1	0	3
Dinar. Turkey	1995	6.4	N	5	3.4	44.2	219.8	338.6	0	0	2	0	2
Kocaeli. Turkey	1999	7.51	SS	15	4.8	180.2	175.0	811.0	1	9	11	1	22
Chi-Chi. Taiwan	1999	7.62	RO	6.76	0.3	169.9	124.3	1525.9	7	181	186	7	381
Duzce. Turkey	1999	7.14	SS	10	6.6	188.7	175.0	659.6	0	4	9	1	14
Caldiran. Turkey	1976	7.21	SS	10	50.8	50.8	274.5	274.5	0	0	1	0	1
St Elias. Alaska	1979	7.54	R	15.7	26.5	80.0	274.5	274.5	0	0	2	0	2
Upland	1990	5.63	SS	4.49	7.3	75.5	229.8	659.6	0	2	1	0	3
Manjil. Iran	1990	7.37	SS	19	12.6	174.6	274.5	724.0	0	1	6	0	7
Sierra Madre	1991	5.61	R	12	10.4	39.8	349.4	996.4	2	5	1	0	8
Little Skull Mtn.NV	1992	5.65	N	12	16.1	100.2	274.5	659.6	0	3	5	0	8
Hector Mine	1999	7.13	SS	5	11.7	198.1	202.9	724.9	0	30	47	0	77
Yountville	2000	5	SS	10.12	11.4	94.4	133.1	712.8	0	4	15	5	24
Big Bear-02	2001	4.53	SS	9.1	23.1	92.3	207.5	684.9	0	9	34	0	43
Mohawk Val. Portola	2001	5.17	SS	3.95	66.8	125.8	274.5	345.4	0	0	6	0	6
Anza-02	2001	4.92	NO	15.2	16.8	133.3	196.3	845.4	1	26	45	0	72
Gulf of California	2001	5.7	SS	10	72.8	130.0	196.3	345.4	0	0	11	0	11
CA/Baja Border Area	2002	5.31	SS	7	39.9	97.0	191.1	231.2	0	0	9	0	9
Gilroy	2002	4.9	SS	10.12	8.6	130.1	155.4	729.7	0	20	13	1	34
Yorba Linda	2002	4.265	SS	7	8.8	36.3	270.2	376.1	0	7	5	0	12

Nenana Mountain. Alaska	2002	6.7	SS	4.2	104.7	199.3	274.5	659.6	0	4	1	0	5
Denali. Alaska	2002	7.9	SS	4.86	2.7	164.7	274.5	963.9	2	4	3	0	9
Big Bear City	2003	4.92	SS	6.3	25.5	146.2	207.5	684.9	0	12	24	0	36

4.3 **Elastic input energy equivalent velocities**

For a damped SDOF system subjected to a ground acceleration $\ddot{x}_g$, the equation of motion can be simply written as follows

$$m(\ddot{x}_g + \ddot{x}) + c\dot{x} + f_s = 0 \tag{4.1}$$

or alternatively

$$m\ddot{x} + c\dot{x} + f_s = -m\ddot{x}_g \tag{4.2}$$

where x is the relative displacement of the SDOF system with respect to the ground, c is the viscous damping coefficient and f_s is the restoring force.

Integrating (4.1) and (4.2) with respect to x, and denoting with x_t the total displacement of the SDOF system, the two following equations can be obtained:

$$\frac{m\dot{x}_t^2}{2} + \int (c\dot{x})dx + \int f_s dx = \int m\ddot{x}_t dx_g \tag{4.3}$$

$$\frac{m\dot{x}^2}{2} + \int (c\dot{x})dx + \int f_s dx = -\int m\ddot{x}_g dx \tag{4.4}$$

Using equation (4.3) and (4.4), two different input energies can be defined (e.g., see Uang and Betero, 1990): the absolute input energy E_{Ia} (corresponding to the right side term of equation 3), which is equal to the work done by the total force applied to the base of the SDOF system mx_t in the ground displacement x_g, and the relative input energy E_{Ir} (corresponding to the right side term of equation 4.4), which is equal to the work done by the equivalent force $-m\ddot{x}_g$ in the displacement of the SDOF system relative to the ground x. In order to eliminate the dependence on mass, these two energy parameters can be conveniently converted into equivalent velocities using the following equation:

$$V = \sqrt{2E/m} \tag{4.5}$$

The maximum value of the velocities through the ground motion duration can be identified, and the absolute and relative input energy equivalent velocity spectra can be consequently defined as follows:

$$V_{EIa} = \sqrt{2E_{Ia} / m} \tag{4.6}$$

$$V_{EIr} = \sqrt{2E_{Ir} / m} \tag{4.7}$$

With the increase of the oscillator period of the SDOF system, V_{EIa} approaches zero whereas V_{EIr} points toward the maximum ground velocity. At low oscillator periods, instead, V_{EIr} approaches zero while V_{EIa} is asymptotic to the maximum ground velocity. Regardless of the considered oscillator period of the SDOF system, E_{Ia} and E_{Ir} converge to the same value at the end of the ground motion duration. However, their maximum value is different and do not usually occur at the end of the ground motion. Accordingly, V_{EIa} and V_{EIr} are in general characterized by different values.

4.4 **Proposed prediction equations**

The standard approach to develop GMPEs is to carry out a regression analysis on earthquake data by using a fixed- or a mixed-effects model. According to fixed-effects models, the *k-th* value of the IM can be in general expressed as follows:

$$\log(IM_k) = f(M_k, r_k, \theta) + \varepsilon_k \tag{4.8}$$

where $f\left(M_k, r_k, \theta\right)$ is a functional form consisting in the ground motion prediction equation, M_k is the earthquake magnitude of the *k-th* record, r_k is the distance, θ is a model coefficient matrix, and ε_k is an error term that is usually assumed to be normally distributed with zero mean. The main limit of this type of model is that can lead to bias if the data are not uniformly distributed among the predictor variables, that is, if data are dominated by many records from few earthquakes or recording sites.

In order to overcome this limit and to reduce the bias, a mixed-effects model can be adopted (e.g., see Brillinger and Preisler 1984 and 1985, Abrahamson and Youngs 1992, Özbey et al. 2004, Danciu and Tselentis 2007). In this model, the IM value for the *j-th* ground motion record from the *i-th* earthquake is expressed as follows:

$$\log(IM_{ij}) = f(M_i, r_{ij}, \theta) + \eta_i + \varepsilon_{ij} \quad (4.9)$$

where

M, r and θ denote again magnitude, distance and a model coefficient matrix,

ε_{ij} is the error term for the *j-th* ground motion record from the *i-th* earthquake,

η_i is the random effect for the *i-th* earthquake.

η_i and ε_{ij} are assumed to be independent and normally distributed with zero mean and variance equal to τ^2 and σ^2, respectively. Consequently, the total standard error for this model is equal to $\sqrt{\tau^2 + \sigma^2}$. Using the mixed-effects model, the earthquake-to-earthquake (inter-event) variability resulting from differences in the data recorded from different earthquakes can be accounted for, as well as the within-earthquake (intra-event) variability resulting from differences in data from records at different stations produced by the same earthquake.

In the present work, the following mixed-effects model, calibrated with the NLME package implemented in the statistical software R (Pinheiro et al. 2011), is employed for deriving the GMPEs:

$$\log(IM_{ij}) = f(M_i, R_{ij}, V_{S30ij}, NR_i, RS_i, \theta) + \eta_i + \varepsilon_{ij} \quad (4.10)$$

where

IM_{ij} is the considered IM (i.e., V_{EIa} or V_{EIr}) value for the *j-th* record and the *i-th* event,

M_i is again the moment magnitude of the *i*-th event,

R_{ij} is the closest distance to rupture from the *i*-th event to the station of the *j*-th recording,

V_{S30} is the value of the average shear-wave velocity between 0 and 30 meters depth,

and with the variables *NR* and *RS* given as follows

NR=1 for normal fault mechanism and normal-oblique, 0 otherwise,

RS=1 for reverse fault and reverse-oblique mechanism, 0 otherwise,

NR=0 and RS=0 for strike-slip fault mechanism.

The specific functional form used for the prediction of V_{EIa} or V_{EIr} is

$$f = a + b(M-6) + c(M-6)^2 + (d + fM)\ln\sqrt{R^2 + h^2} + e\ln(V_{S30}/1130) + m1NR + m2RS \quad (4.11)$$

with model coefficients

a, b, c, d, e, f, m1, m2, and the 'fictitious' focal depth *h* used to provide a better fit to the data at short distances (Abrahamson and Silva 1997 and Özbey et al. 2004)

Equation (4.11) is a modification of the following functional form

$$f = a + b(M-6) + c(M-6)^2 + d\log\sqrt{R^2+h^2} + eG_{ci} + fG_{di} \tag{4.12}$$

where

G_{ci}=1 for site class C, 0 otherwise, and

G_{di} =1 for site class D, 0 otherwise,

which has been originally proposed by Boore et al. (1993) to study the attenuation of S_a, and then used by Chapman (1999) and Gong and Xie (2005) to develop prediction equations for the input energy equivalent velocity V_{EIa} and V_{EIr}. It can be noted that in Equation (12) an additional magnitude-dependent slope in the distance term is included. This term, in fact, has been found to be necessary to extend the ground motion model to distances of 200km (e.g., see Campbell and Bozorgnia, 2008). V_{S30} is used to characterize the soil conditions instead of the indicator variables G_{ci} and G_{di} of Equation (12). Studies (e.g., Piggott and Stafford, 2012) showed in fact that use of the continuous predictor variable V_{S30} enables to more adequately capture the site response by eliminating bias of ground motions on the V_{S30} produced when only dummy variables are considered. Finally, in order to account for fault mechanism effects two other terms (i.e., *m1NR* and *m2RS*) are added at the end of the functional form.

4.5 **Regression analyses**

The results of the regression analyses carried out to calibrate the model coefficients of V_{EIa} and V_{EIr} for a damping value equal to 5% are reported in Table 4.2 and Table 4.3. In these Tables, the values of the stardard error τ and σ of the inter-event and intra-event residuals are also given, as well as the obtained total standard error values.

Table 4.2 Results of the regression analyses on V_{EIr} obtained for different values of the SDOF period T

T[s]	*a*	*b*	*c*	*d*	*e*	*f*	*h*	*m1*	*m2*	τ	σ	σ_T
0.05	4.555	0.423	-0.105	-2.023	-0.465	0.172	3.308	-0.212	0.246	0.209	0.474	0.518
0.1	5.107	0.312	-0.099	-2.023	-0.323	0.168	4.423	-0.079	0.236	0.206	0.452	0.496
0.15	5.531	0.304	-0.111	-1.945	-0.289	0.153	5.884	-0.048	0.228	0.196	0.441	0.483
0.2	5.375	0.569	-0.138	-1.457	-0.316	0.087	6.118	0.011	0.216	0.190	0.439	0.478
0.25	5.337	0.685	-0.159	-1.273	-0.381	0.061	6.135	-0.027	0.203	0.191	0.445	0.484
0.3	5.199	0.737	-0.168	-1.155	-0.443	0.048	5.509	-0.084	0.227	0.202	0.460	0.503
0.35	5.245	0.734	-0.162	-1.187	-0.459	0.053	5.456	-0.130	0.188	0.193	0.472	0.510
0.4	5.296	0.711	-0.156	-1.280	-0.469	0.067	5.499	-0.134	0.172	0.210	0.475	0.520
0.45	5.286	0.697	-0.159	-1.354	-0.511	0.079	5.348	-0.164	0.141	0.221	0.486	0.534
0.5	5.273	0.707	-0.161	-1.380	-0.552	0.083	5.369	-0.203	0.135	0.211	0.496	0.539
0.55	5.188	0.696	-0.176	-1.417	-0.583	0.092	4.910	-0.216	0.141	0.208	0.510	0.551
0.6	5.103	0.691	-0.188	-1.453	-0.612	0.099	4.617	-0.214	0.150	0.221	0.519	0.564
0.65	4.973	0.694	-0.197	-1.458	-0.644	0.104	4.060	-0.202	0.172	0.231	0.527	0.575
0.7	4.890	0.690	-0.197	-1.471	-0.670	0.107	3.509	-0.221	0.198	0.232	0.532	0.580
0.75	4.844	0.707	-0.199	-1.465	-0.688	0.107	3.213	-0.232	0.197	0.232	0.531	0.580
0.8	4.779	0.724	-0.203	-1.460	-0.700	0.107	3.143	-0.212	0.193	0.236	0.530	0.580
0.85	4.751	0.737	-0.209	-1.469	-0.706	0.109	3.099	-0.208	0.185	0.241	0.534	0.586
0.9	4.749	0.732	-0.207	-1.509	-0.715	0.114	3.115	-0.212	0.188	0.253	0.537	0.594
0.95	4.756	0.713	-0.211	-1.571	-0.726	0.124	3.118	-0.230	0.171	0.265	0.539	0.600
1	4.751	0.696	-0.220	-1.632	-0.745	0.133	3.102	-0.245	0.159	0.273	0.541	0.606
1.1	4.702	0.699	-0.242	-1.681	-0.794	0.141	-2.900	-0.299	0.130	0.292	0.544	0.617
1.2	4.679	0.716	-0.254	-1.710	-0.800	0.145	-2.716	-0.325	0.113	0.306	0.546	0.626
1.3	4.633	0.767	-0.253	-1.688	-0.816	0.141	-2.925	-0.390	0.079	0.313	0.548	0.631
1.4	4.573	0.827	-0.243	-1.634	-0.836	0.132	-3.141	-0.441	0.065	0.313	0.547	0.630
1.5	4.527	0.880	-0.236	-1.579	-0.845	0.123	3.338	-0.480	0.052	0.313	0.548	0.631
1.6	4.478	0.918	-0.234	-1.561	-0.852	0.120	3.319	-0.483	0.024	0.311	0.552	0.634
1.7	4.406	0.937	-0.233	-1.568	-0.869	0.122	3.163	-0.467	0.009	0.309	0.558	0.638
1.8	4.348	0.946	-0.233	-1.591	-0.883	0.125	3.037	-0.471	0.003	0.302	0.559	0.635
1.9	4.318	0.967	-0.228	-1.595	-0.881	0.125	-2.969	-0.476	-0.008	0.295	0.559	0.632
2	4.291	0.989	-0.225	-1.594	-0.880	0.125	-2.898	-0.489	-0.026	0.293	0.561	0.633
2.2	4.210	1.019	-0.219	-1.600	-0.879	0.126	-2.831	-0.535	-0.040	0.299	0.563	0.637
2.4	4.128	1.093	-0.221	-1.518	-0.880	0.113	-2.881	-0.561	-0.044	0.309	0.562	0.642
2.6	4.057	1.122	-0.205	-1.510	-0.875	0.111	-2.889	-0.568	-0.042	0.304	0.561	0.638
2.8	3.991	1.146	-0.186	-1.516	-0.870	0.112	-2.948	-0.548	-0.043	0.297	0.559	0.633
3	3.961	1.217	-0.171	-1.456	-0.860	0.101	3.256	-0.535	-0.054	0.287	0.561	0.630

3.5	3.875	1.314	-0.140	-1.372	-0.843	0.085	3.870	-0.534	-0.065	0.278	0.572	0.636
4	3.756	1.345	-0.114	-1.337	-0.819	0.081	4.006	-0.545	-0.076	0.271	0.570	0.631
4.5	3.657	1.367	-0.090	-1.303	-0.794	0.076	4.161	-0.556	-0.085	0.272	0.579	0.640
5	3.562	1.393	-0.070	-1.250	-0.770	0.068	4.262	-0.539	-0.081	0.274	0.592	0.652
5.5	3.479	1.407	-0.056	-1.221	-0.754	0.064	4.368	-0.526	-0.074	0.282	0.591	0.655
6	3.418	1.419	-0.049	-1.198	-0.742	0.060	4.403	-0.535	-0.084	0.288	0.590	0.657
6.5	3.394	1.451	-0.042	-1.140	-0.708	0.051	4.525	-0.558	-0.098	0.298	0.589	0.660
7	3.351	1.442	-0.039	-1.140	-0.677	0.052	4.494	-0.568	-0.103	0.306	0.586	0.661
7.5	3.293	1.403	-0.035	-1.190	-0.657	0.061	4.381	-0.564	-0.099	0.306	0.584	0.660
8	3.232	1.354	-0.030	-1.250	-0.641	0.072	4.266	-0.553	-0.090	0.305	0.580	0.655

Table 4.3 Regression coefficients and standard deviation for V_{EIa} at various SDOF periods

T[s]	*a*	*b*	*c*	*d*	*e*	*f*	*h*	*m1*	*m2*	τ	σ	σ_T
0.05	4.970	0.136	0.157	-2.233	0.034	0.148	11.085	-0.006	0.228	0.371	0.550	0.664
0.1	6.779	0.352	-0.127	-1.978	0.009	0.089	16.758	0.041	0.168	0.371	0.546	0.660
0.15	6.784	0.476	-0.133	-1.731	-0.089	0.069	15.798	0.030	0.168	0.314	0.513	0.602
0.2	6.108	0.733	-0.159	-1.217	-0.178	0.020	13.059	0.058	0.168	0.259	0.499	0.562
0.25	5.775	0.812	-0.176	-1.064	-0.284	0.011	10.777	0.017	0.175	0.234	0.489	0.542
0.3	5.456	0.802	-0.185	-1.018	-0.375	0.017	8.579	-0.055	0.211	0.228	0.492	0.542
0.35	5.421	0.782	-0.177	-1.076	-0.411	0.029	7.808	-0.110	0.179	0.209	0.493	0.536
0.4	5.448	0.719	-0.170	-1.235	-0.429	0.054	7.542	-0.112	0.166	0.223	0.492	0.540
0.45	5.396	0.683	-0.170	-1.337	-0.479	0.073	6.928	-0.141	0.144	0.234	0.497	0.549
0.5	5.364	0.658	-0.171	-1.417	-0.526	0.086	6.570	-0.177	0.145	0.220	0.504	0.550
0.55	5.259	0.628	-0.186	-1.479	-0.555	0.099	5.780	-0.191	0.154	0.215	0.516	0.559
0.6	5.176	0.602	-0.197	-1.548	-0.584	0.113	5.366	-0.188	0.165	0.227	0.523	0.570
0.65	5.029	0.602	-0.205	-1.554	-0.617	0.118	4.558	-0.180	0.188	0.235	0.529	0.578
0.7	4.925	0.597	-0.203	-1.566	-0.647	0.122	3.813	-0.196	0.218	0.236	0.531	0.581
0.75	4.888	0.608	-0.203	-1.569	-0.666	0.123	3.504	-0.210	0.215	0.233	0.529	0.578
0.8	4.838	0.619	-0.205	-1.574	-0.676	0.125	3.358	-0.196	0.208	0.236	0.525	0.576
0.85	4.820	0.621	-0.209	-1.599	-0.681	0.129	3.292	-0.194	0.201	0.240	0.528	0.580
0.9	4.819	0.612	-0.206	-1.641	-0.687	0.135	3.300	-0.194	0.206	0.252	0.533	0.589
0.95	4.832	0.594	-0.210	-1.701	-0.698	0.143	3.371	-0.208	0.194	0.263	0.535	0.596
1	4.837	0.577	-0.218	-1.760	-0.714	0.152	3.331	-0.221	0.184	0.271	0.535	0.599
1.1	4.790	0.571	-0.238	-1.816	-0.763	0.161	-3.052	-0.279	0.157	0.288	0.536	0.608
1.2	4.783	0.576	-0.245	-1.856	-0.766	0.167	-2.867	-0.301	0.141	0.297	0.535	0.612

1.3	4.761	0.616	-0.240	-1.843	-0.778	0.164	-3.015	-0.355	0.108	0.302	0.537	0.616
1.4	4.727	0.658	-0.227	-1.815	-0.797	0.158	-3.169	-0.400	0.100	0.299	0.535	0.613
1.5	4.708	0.684	-0.218	-1.795	-0.804	0.154	3.337	-0.432	0.093	0.295	0.536	0.612
1.6	4.670	0.699	-0.212	-1.794	-0.806	0.154	3.276	-0.428	0.077	0.292	0.540	0.613
1.7	4.615	0.706	-0.207	-1.808	-0.821	0.156	3.145	-0.407	0.069	0.290	0.542	0.615
1.8	4.584	0.700	-0.203	-1.848	-0.832	0.162	3.033	-0.404	0.071	0.282	0.542	0.611
1.9	4.581	0.699	-0.196	-1.875	-0.825	0.165	-2.983	-0.407	0.071	0.274	0.540	0.606
2	4.580	0.701	-0.192	-1.895	-0.821	0.167	-2.923	-0.417	0.062	0.272	0.542	0.606
2.2	4.549	0.693	-0.179	-1.942	-0.816	0.174	-2.844	-0.447	0.063	0.276	0.544	0.610
2.4	4.512	0.728	-0.174	-1.896	-0.809	0.166	-2.856	-0.454	0.080	0.284	0.545	0.615
2.6	4.470	0.726	-0.154	-1.913	-0.807	0.168	-2.845	-0.455	0.095	0.280	0.543	0.611
2.8	4.454	0.729	-0.134	-1.931	-0.796	0.169	-2.953	-0.438	0.107	0.273	0.541	0.606
3	4.469	0.773	-0.118	-1.887	-0.781	0.160	3.248	-0.421	0.104	0.261	0.542	0.601
3.5	4.481	0.814	-0.088	-1.859	-0.761	0.152	3.811	-0.394	0.105	0.241	0.550	0.600
4	4.455	0.813	-0.066	-1.858	-0.736	0.152	3.886	-0.382	0.103	0.230	0.547	0.593
4.5	4.446	0.810	-0.050	-1.849	-0.709	0.149	4.025	-0.379	0.103	0.227	0.554	0.599
5	4.417	0.816	-0.039	-1.820	-0.684	0.145	3.951	-0.356	0.110	0.227	0.563	0.607
5.5	4.382	0.811	-0.029	-1.811	-0.673	0.144	3.847	-0.342	0.121	0.231	0.562	0.607
6	4.360	0.814	-0.024	-1.788	-0.659	0.140	3.749	-0.342	0.119	0.235	0.558	0.606
6.5	4.366	0.826	-0.022	-1.750	-0.630	0.134	3.751	-0.355	0.117	0.242	0.554	0.605
7	4.364	0.805	-0.026	-1.762	-0.606	0.137	3.691	-0.361	0.118	0.247	0.549	0.602
7.5	4.359	0.773	-0.027	-1.796	-0.586	0.143	3.577	-0.358	0.125	0.246	0.544	0.597
8	4.351	0.728	-0.030	-1.846	-0.567	0.152	3.441	-0.352	0.133	0.243	0.540	0.592

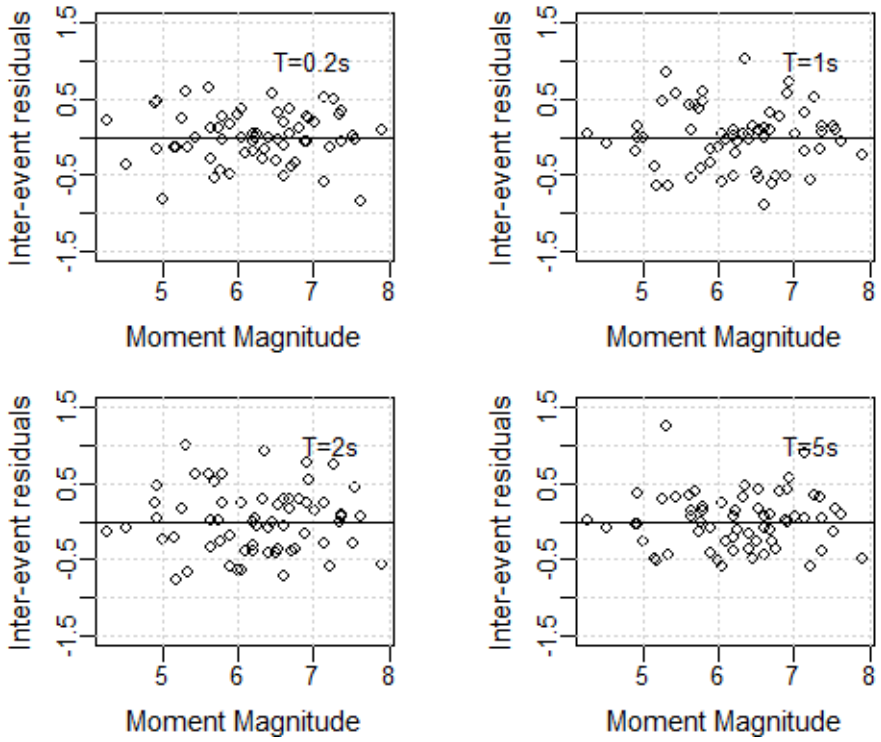

Fig. 4.2 Dependence of inter-event residuals of V_{EIa} on moment magnitude

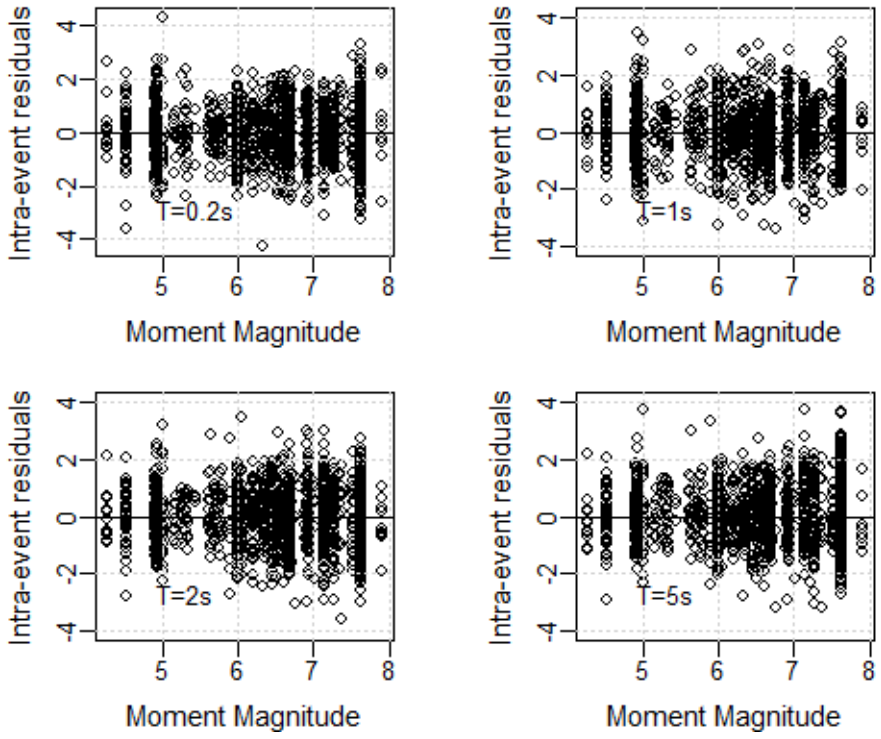

Fig. 4.3 Dependence of inter-event residuals of V_{EIr} on moment magnitude

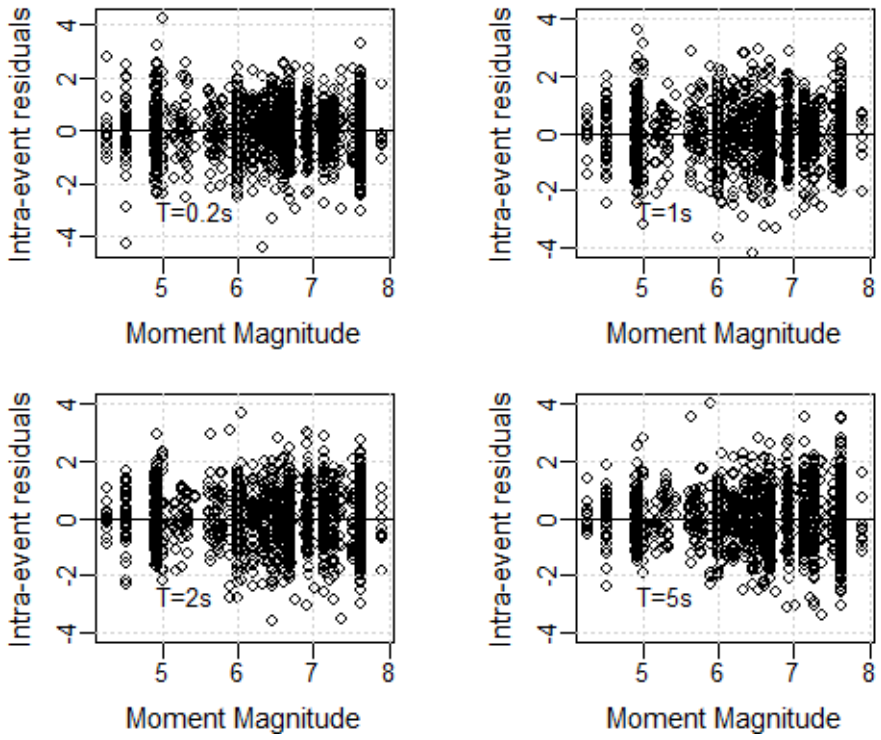

Fig. 4.4 Dependence of intra-event residuals of V_{EIa} on moment magnitude

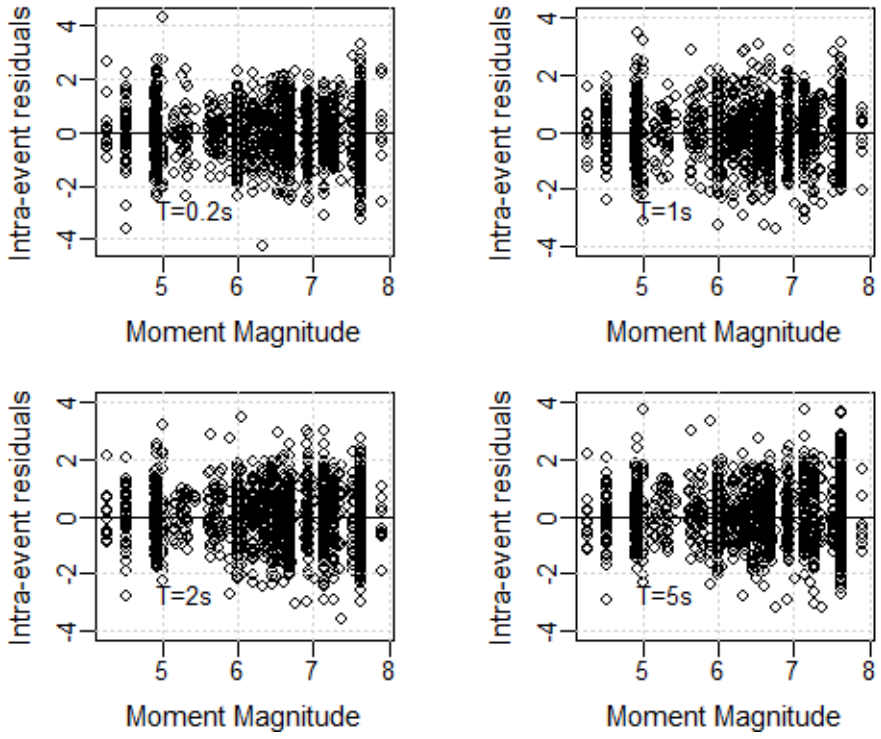

Fig. 4.5 Dependence of intra-event residuals of V_{EIr} on moment magnitude

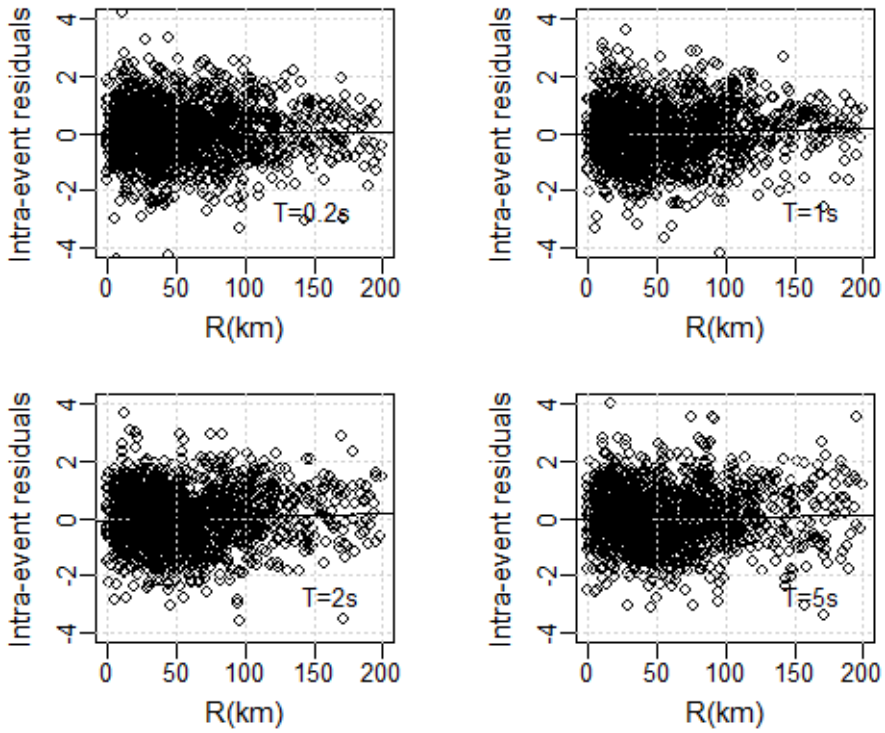

Fig. 4.6 Dependence of intra-event residuals of V_{EIa} on rupture distance (R)

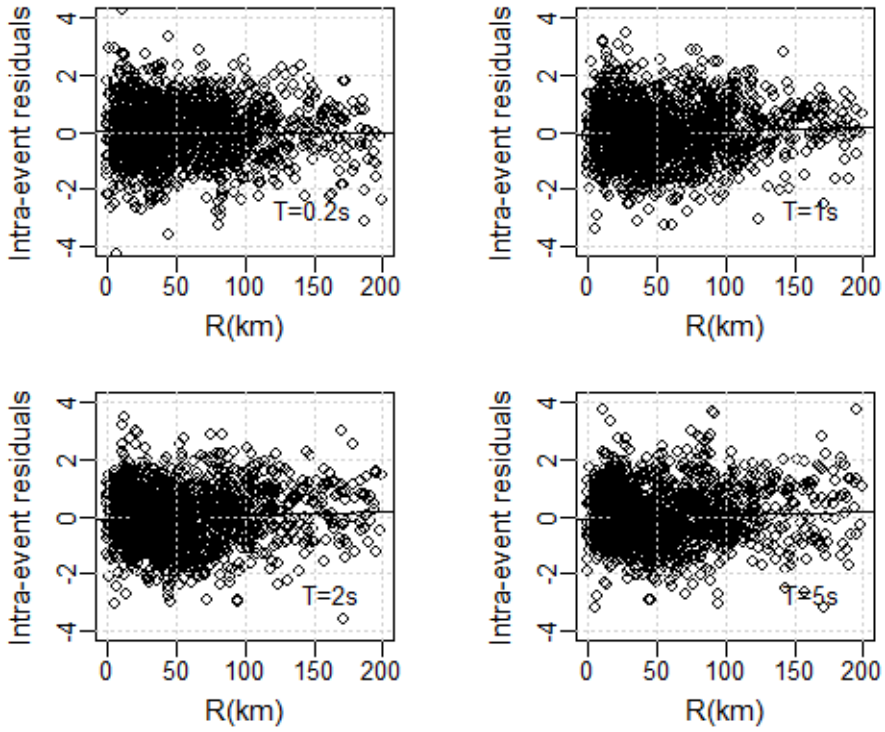

Fig. 4.7 Dependence of intra-event residuals of V_{EIr} on rupture distance (R)

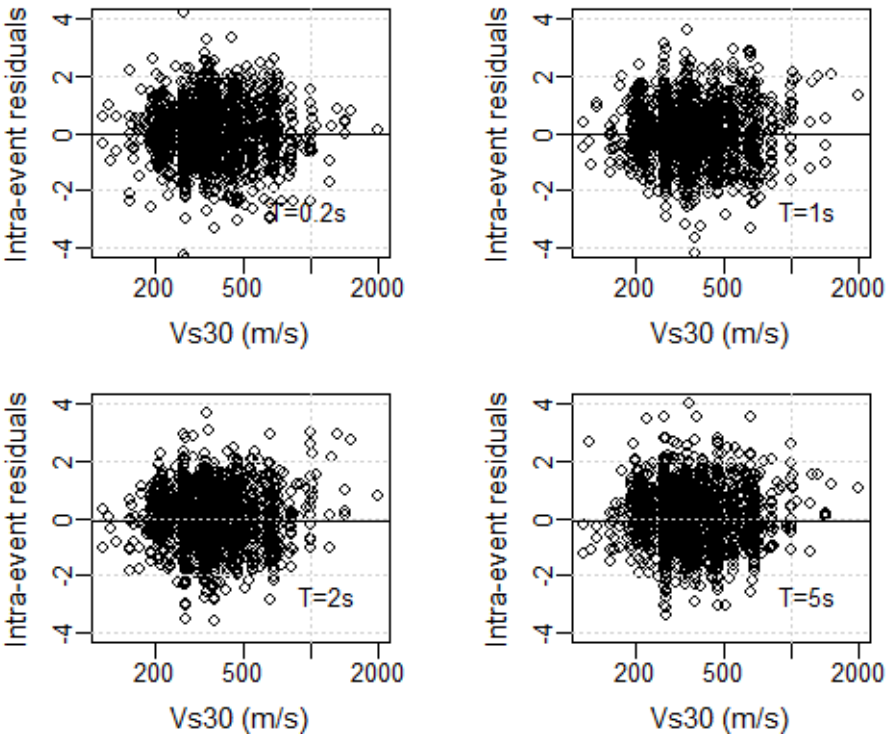

Fig. 4.8 Dependence of intra-event residuals of V_{EIa} on V_{S30}

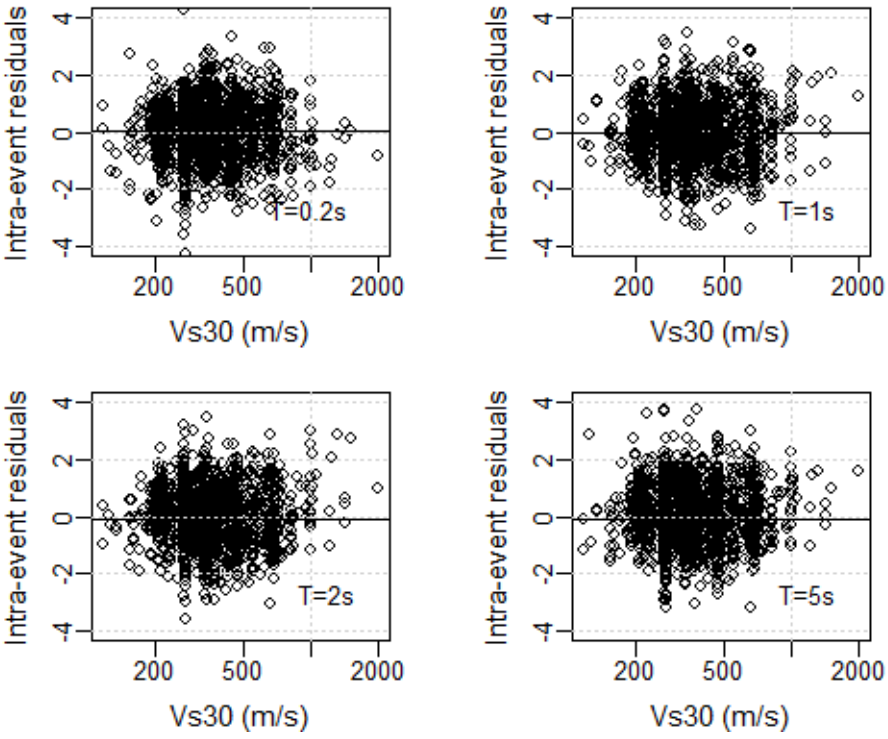

Fig. 4.9 Dependence of intra-event residuals of V_{EIr} on V_{S30}

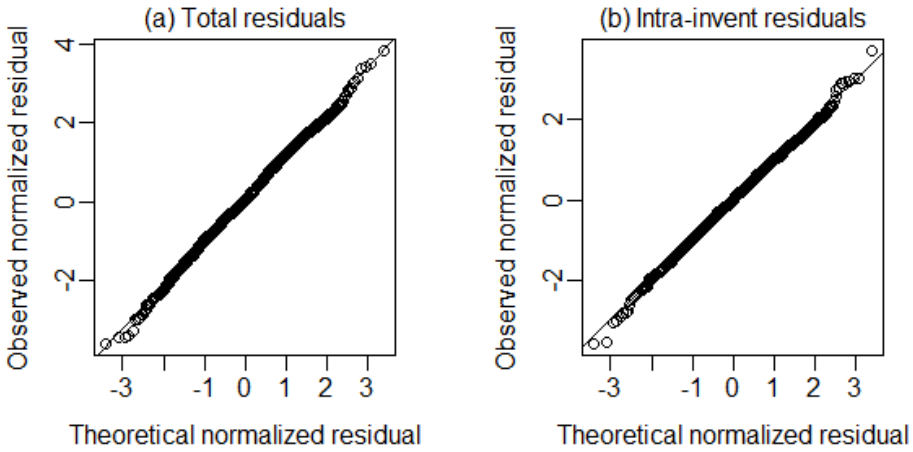

Fig. 4.10 Normal Q-Q plot for total residuals (a) and intra-event residuals (b) obtained for VEIa using the proposed GMPE

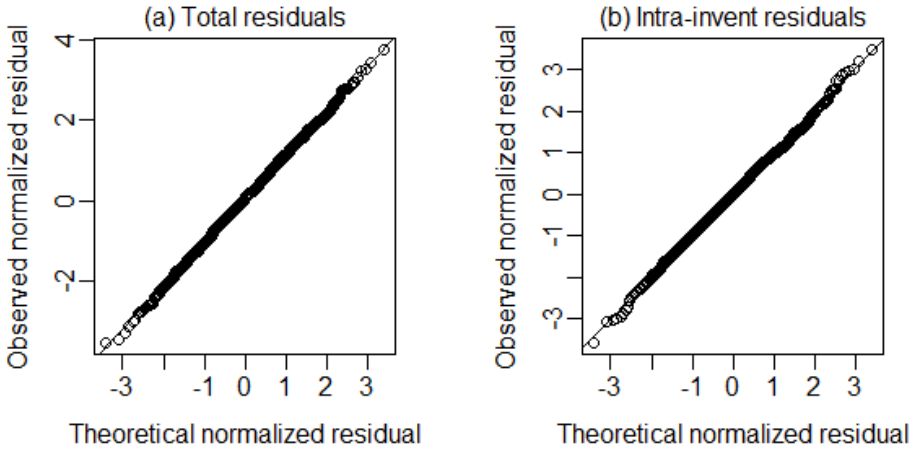

Fig. 4.11 Normal Q-Q plot for total residuals (a) and intra-event residuals (b) obtained for V_{EIr} using the proposed GMPE

Figures from Fig. 4.2 to Fig. 4.9 show the dependence of the inter-event and intra-event residuals on magnitude, distance and V_{S30}, respectively. It can be observed that for the case of both V_{EIa} and V_{EIr} there is no significant trends or bias that result from the use of the considered functional form, confirming the used function to be appropriate for the selected predictor variables. Results of other tests carried out to evaluate the prediction model are reported in Fig. 4.10 and Fig. 4.11. In these Figures, the normal Quantile-Quantile plots for

the residuals of V_{EIa} and V_{EIr} are reported, showing that both total and intra-event residuals, derived using the established GMPEs, have a very good fit to the assumed normal distribution.

In Fig. 4.12, the model coefficients of V_{EIa} and V_{EIr} calculated at different period values *T* are compared. It can be observed that at periods lower than around 1s, the linear and quadratic magnitude coefficients of the V_{EIa} and V_{EIr} functional forms are almost the same. This means that at short periods the scaling of the two velocities with magnitude is very similar. For period values lower than 1.5s, a similar trend can be also observed for the model coefficients *m1* and *m2*, denoting the same sensitivity of V_{EIa} and V_{EIr} on fault mechanism type in this period range. At short periods, distance coefficients *d* and *f* of the two velocities are nearly the same, but the *h* value is higher for V_{EIr} than for V_{EIa} indicating a faster intensity attenuation for V_{EIr} than for V_{EIa}. Independently from the period value, values of the model coefficient *e* of V_{EIa} and V_{EIr} are very close meaing site effects for the two velocities are almost the same. About standard errors, opposite trends can be identified for T values lower and higher than 1s. In particular, for T< 0.5s the values of τ and σ obtained for V_{EIr} are significantly higher than those found for V_{EIa}. On the other hand, for T>2s the values of the V_{EIa} stadard errors are higher than those obtained in the V_{EIr} predictions.

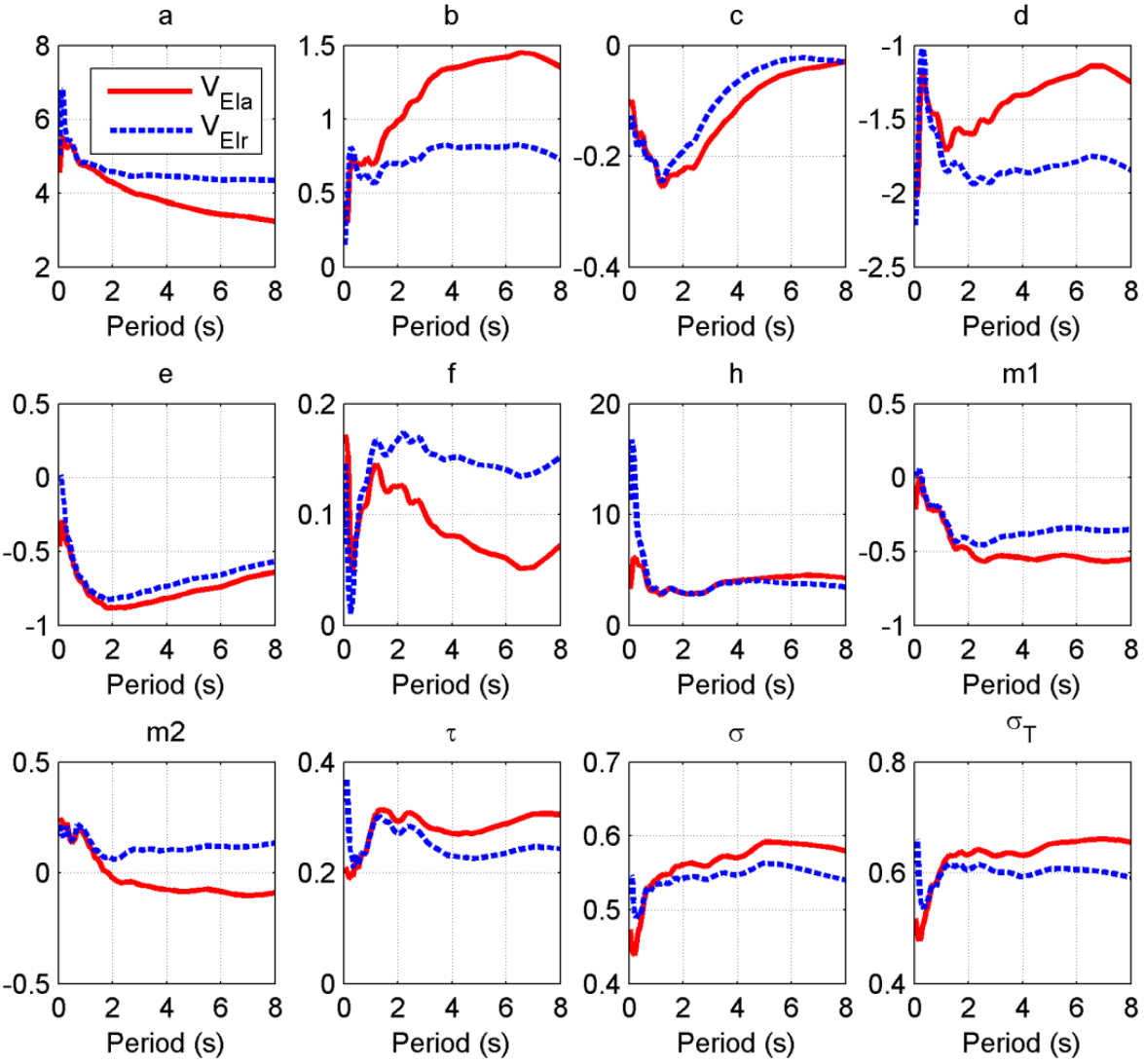

Fig. 4.12 Variation with period of the estimated model coefficients of the functional forms of V_{EIa} and V_{EIr}

4.6 **Predicted V_{EIa} and V_{EIr} spectra**

In Fig. 4.13, V_{EIa} and V_{EIr} spectra obtained with the proposed GMPEs for a strike-slip earthquake of 6.5 magnitude and a rupture distance equal to 30 km are reported. Spectra corresponding to different V_{S30} values show how soil condition affects these spectra. It is interesting to observe that while the intensity of V_{EIa} is always influenced by such variable, V_{EIr} does not depend on it at period values lower than 0.2s. In the same Figure, comparisons

between spectra produced by different types of fault mechanism are also reported. The two velocities show the same trend. For both of them, in fact, the intensity produced by an earthquake with a strike-slip fault mechanism ranges in between the intensities corresponding to normal and reverse-faulting earthquakes. In particular, at short periods (lower than 0.2s, in the reported case) the velocity values produced by strike-slip and normal fault earthquakes are pretty the same; at large periods (higher than about 1.5s), the velocity values produced by the strike-slip fault earthquake converge toward those of the reverse fault earthquake.

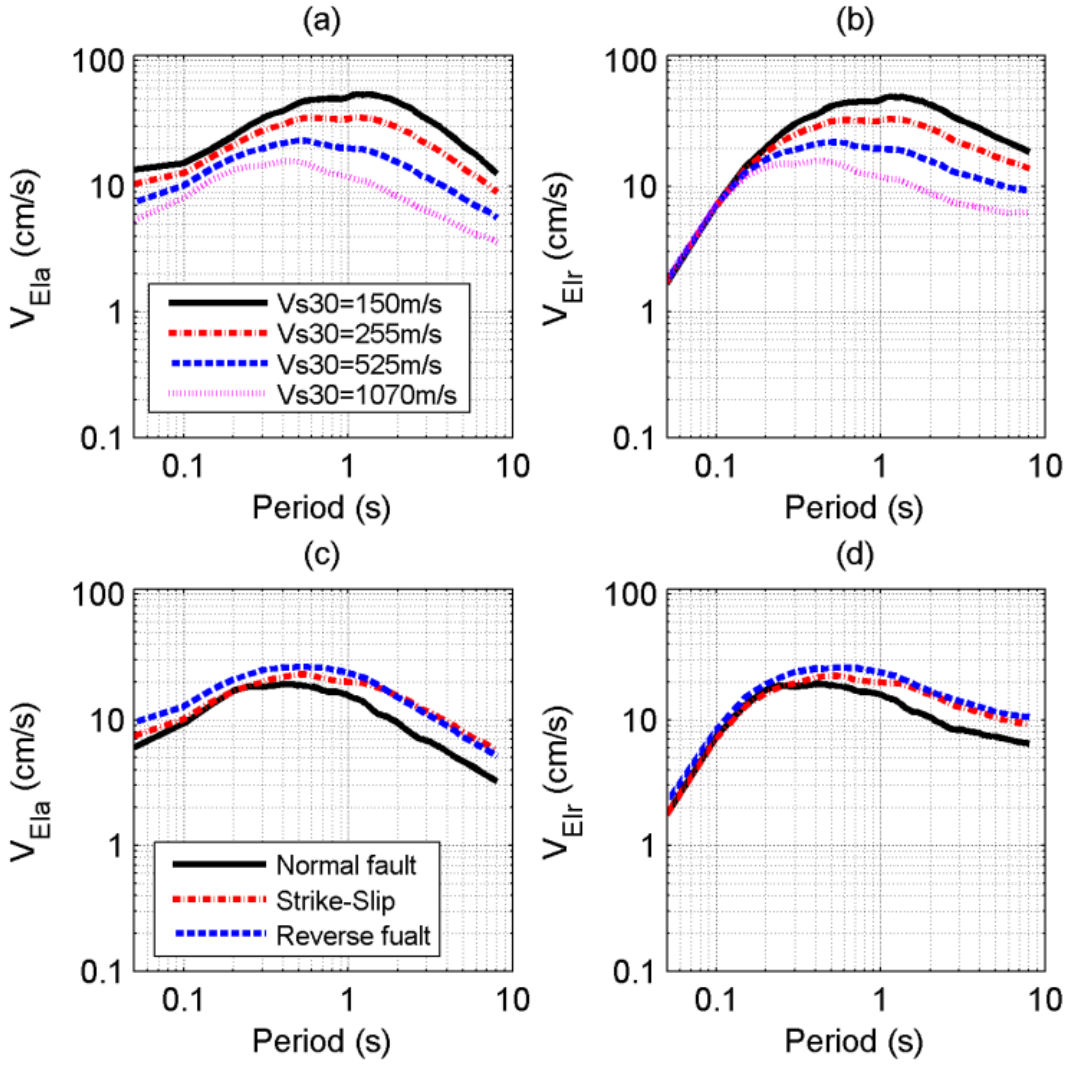

Fig. 4.13 Predicted V_{EIa} and V_{EIr} spectra for M=6.5 and R=30 km considering: different V_{S30} values (corresponding to different NEHRP soil conditions) for the same strike-slip fault mechanism (plots a and b), and different fault mechanisms for V_{S30}=525 m/s (plots c and d).

In Fig. 4.14 and Fig. 4.15 the two velocity spectra are compared considering different distances and soil conditions, respectively. In this case it can be observed that while at short periods (lower than about 0.2s) the difference between the V_{EIa} and V_{EIr} value is large, with the increase of magnitude at periods higher than 1s the difference reduces.

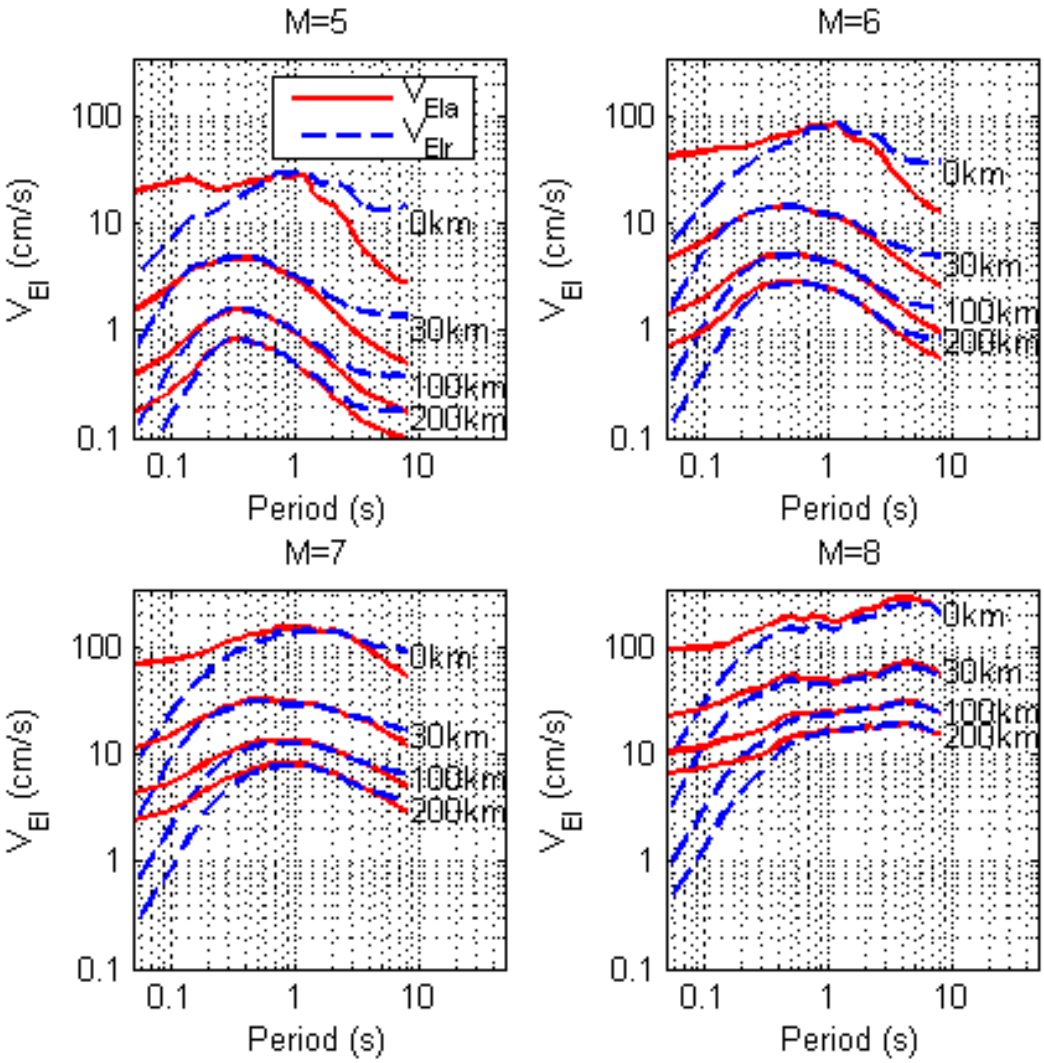

Fig. 4.14 Comparison between V_{EIa} and V_{EIr} spectra produced by a strike-slip earthquake, a V_{S30} equal to 525 m/s (corresponding to a soil type C, according to NEHRP classification), and various distance and magnitude values.

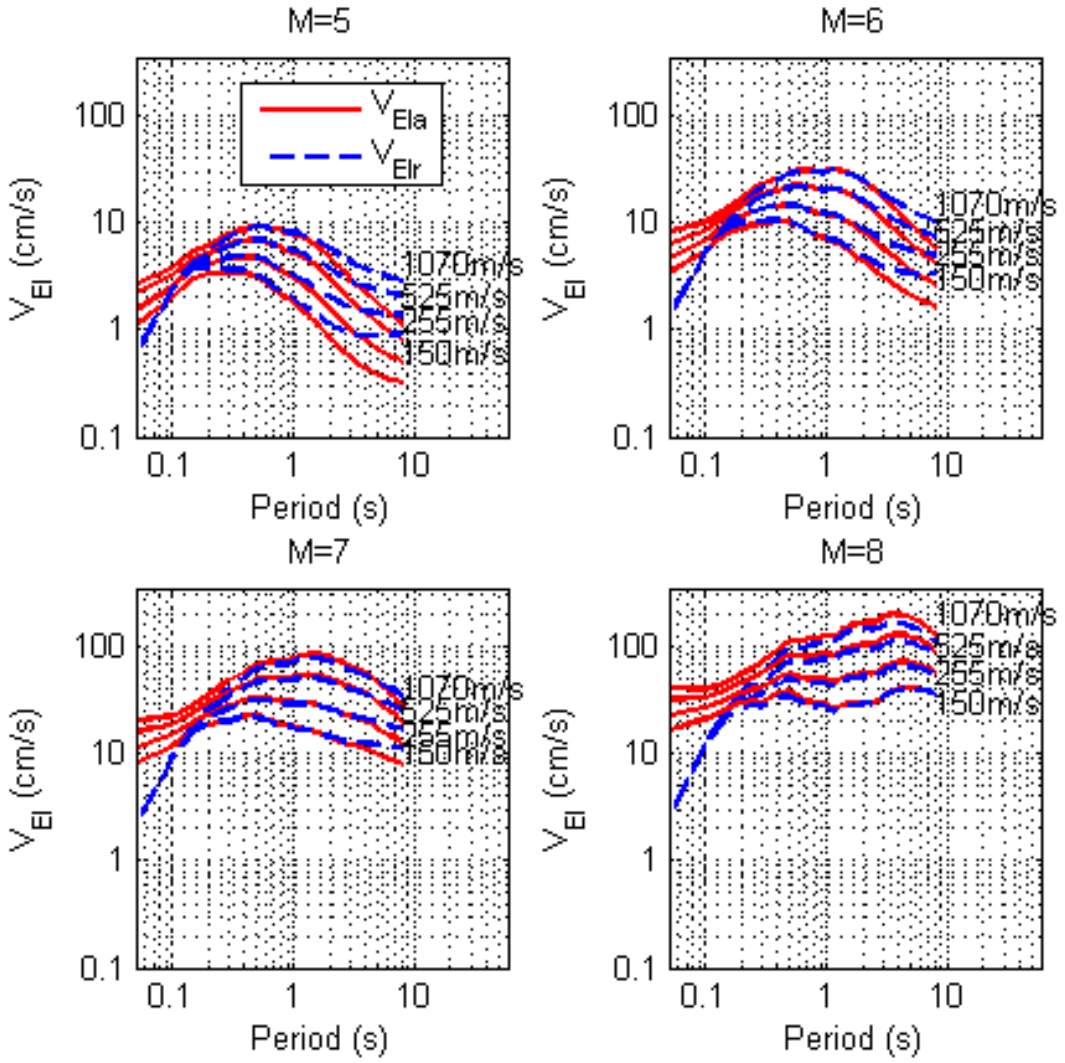

Fig. 4.15 Comparison between V_{EIa} and V_{EIr} spectra produced by a strike-slip earthquake, a distance equal to 30km, and various V_{S30} and magnitude values.

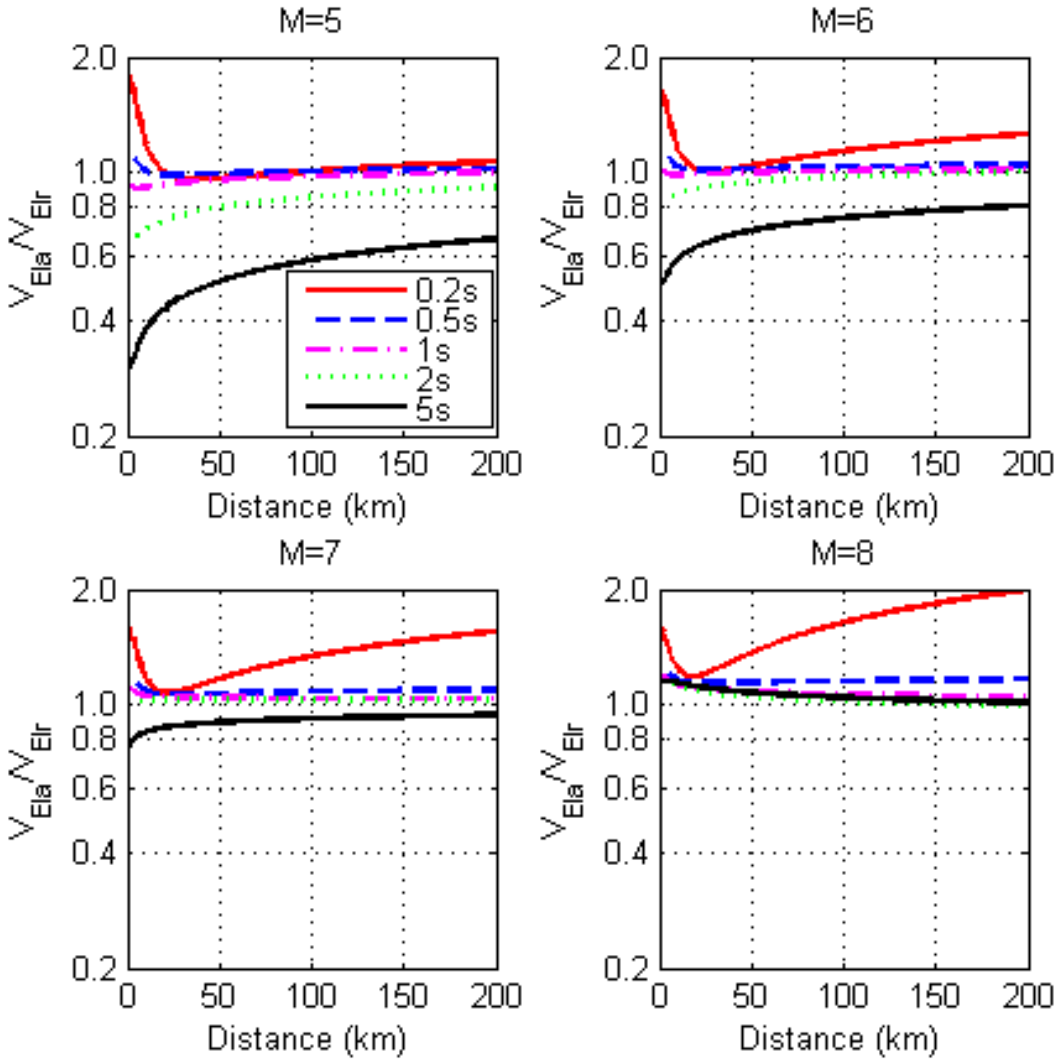

Fig. 4.16 V_{EIa} to V_{EIr} ratio vs distance (closest distance to the fault) calculated for a strike-slip earthquake with V_{S30}=525 m/s considering different magnitude and oscillator period values.

In order to clearly show differences in the intensity of the two velocities, the variation of the V_{EIa} to V_{EIr} ratio with distance is reported in Fig. 4.16. considering a strike-slip fault earthquake, and a V_{S30} value equal to 525 m/s. The most significant difference in the values of the two velocities can be observed at large periods and short distances for M=5, and short periods and large distances for M=8. For a period value equal to 1s, the V_{EIa} to V_{EIr} ratio is always around 1, while at periods much larger or lower than 1s is more sentive to distance.

With the increase of magnitude, however, all the V_{EIa} to V_{EIr} ratio values, excpet that corresponding to 0.2s (the red curve), approach 1. It is interesting to note that the curve corresponding to a T value equal to 0.2s is characterized by an inflection point at a distance of 15km circa, with a difference between the slope of the curve before and after this point which increases with the increase of magnitude. A similar trend has been also observed by Chapman (1999), but for the V_{EIa} to PSV (pseudo-velocity spectrum) ratio. The inflection is due to the difference in the value of *h* estimated for V_{EIa} and V_{EIr} at short periods. It is important to underline that *h* is not true focal depth, but simply a model parameter used in the functional form to represent the flattening of attenuation observed at small distances, especially for V_{EIr} at short periods.

4.7 **Comparison with models from the literature**

In this section of the paper, input energy equivalent velocity spectra obtained with the proposed GMPEs and models from the literature are compared. The prediction equations selected from the literature are those of Chapman (1999), Danciu and Tselentis (2007), and Gong and Xie (2005). The following different magnitude and source-to-site distance values are considered in the comparisons: M equal to 6 and 7, and R equal to 5, 30, 60 and 120 km. These values are consistent with the range of applicability of the prediction equations selected from the literature. The type of fault considered is the reverse. Although in Chapman (1999) and Gong and Xie (2005) fault mechanism effects are not accounted for, the records used to develop their prediction equations are dominated by reverse fault earthquakes, especially at magnitudes equal to 6 (e.g., dominated by Whittier 10/1/1987) and 7 (e.g., dominated by Northridge 1/17/1994 and Loma Prieta 10/18/1989). Since the prediction equations from the literature use different distance measures than the closest distance to rupture R considered in this study, a conversion is needed. The equations of Kaklamanos et al. (2011) are applied to convert R to the Joyner-Boore distance R_{JB}, that is, the closest distance to the surface projection of the fault rupture. R_{JB} is used in Chapman (1999) and Gong and Xie (2005), and can be considered a quite good approximation of the epicentral distance (Kaklamanos et al. 2011) which is used in Danciu and Tselentis (2007). It should be noted that while the difference between these distance measures is significant in the near source region, it becomes

negligible far from the field. The last comment before discussing the results of the comparisons is about the different definitions used in the prediction equations for the input energy equivalent velocity spectra. In Chapman (1999), Gong and Xie (2005) and the present study, each ordinate of the spectra is the geometric mean of the input energy equivalent velocities obtained for the two horizontal components of the ground motion, in Danciu and Tselentis (2007), instead, is the arithmetic mean.

In Fig. 4.17, V_{EIa} spectra corresponding to different magnitude and distance vales are plotted. The most significant discrepancy in the predictions can be observed between the spectra obtained with Danciu and Tselentis (2007) and those obtained with the other three GMPEs when the magnitude is equal to 7. This is probably due to the fact that in Danciu and Tselentis (2007) the magnitude saturation phenomenon is not explicitly taken into account, as it is in the other prediction equations which use a nonlinear magnitude scaling term in addition to a linear one. This may lead to an overestimation of V_{EIa} with the increase of magnitude. Differences between the spectra obtained with Chapman (1999) and the proposed GMPE can be observed at period values higher than about 0.6s. However, compared to both Chapman (1999) and Gong and Xie (2005), the proposed GMPE produces in general comparable spectra which become very similar for the case of magnitude 6 and distance equal to 30 km. This consistency in the predictions can be due to the large number of data used in the regression for this earthquake scenario.

In Fig. 4.18, V_{EIa} spectra corresponding to different soil conditions are shown.It can be noted that for the considered case studies using Danciu and Tselentis (2007) the predicted spectra do not significantly change with the type of soil. On the contrary, soil conditions clearly affect the spectra obtained with the other prediction equations, with the V_{EIa} values being almost the same at short periods. The most significant difference between the results obtained with the proposed GMPE and those of Chapman (1999) and Gong and Xie (2005) can be found for the case of soil type A+B and magnitude equal to 7. This can be due both to the lack of soil type A+B records in the databases used by Chapman (1999) and Gong and Xie (2005), and to the fact that they used different parameters(dummy variables instead of V_{S30}) with respect to the present study to account for the soil effects.

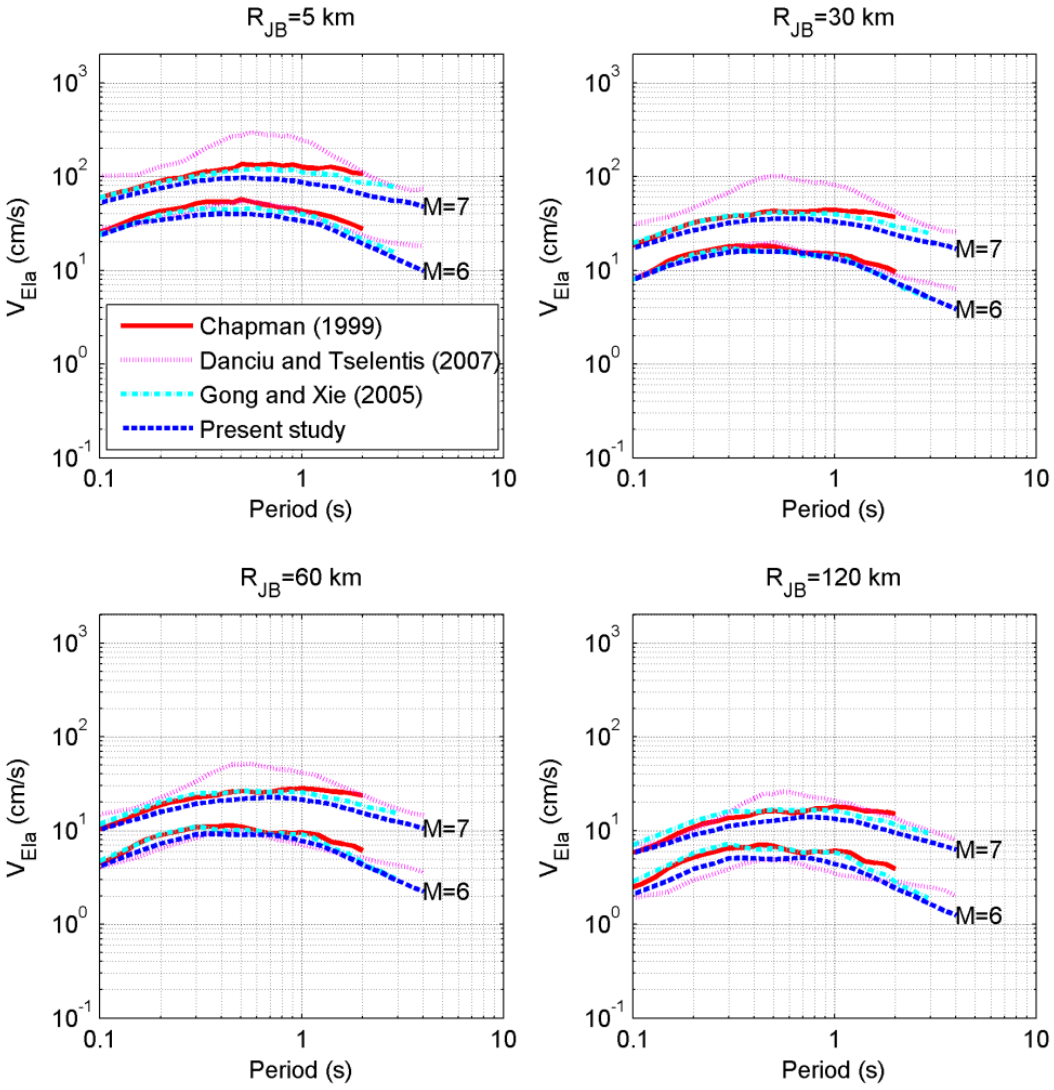

Fig. 4.17 V_{EIa} spectra predicted for different magnitude and Joyner-Boore distance values, corresponding to an earthquake with a reverse fault mechanism and a soil condition of NEHRP type C (modelled with a V_{S30} equal to 525m/s).

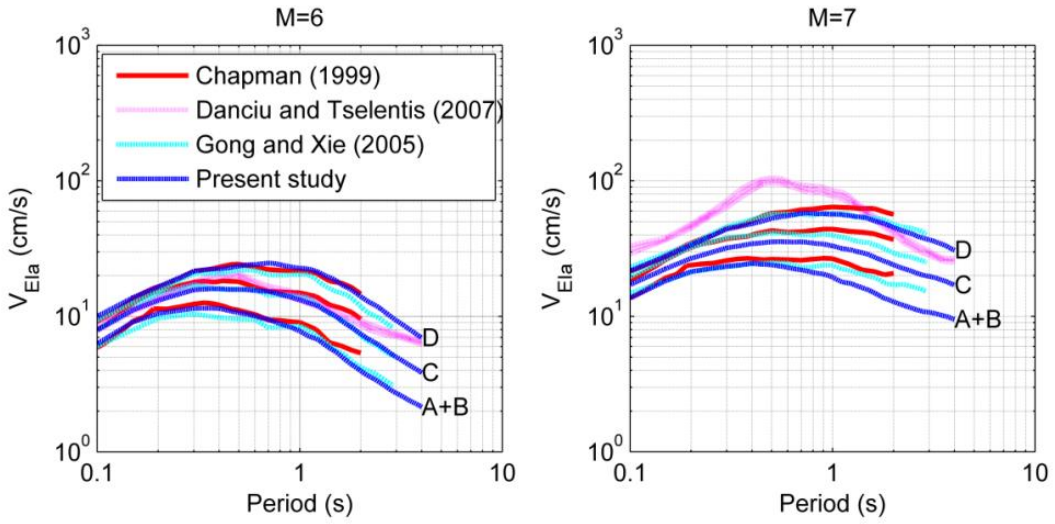

Fig. 4.18 V_{EIa} spectra predicted for different types of soil (NEHRP A+B, C, and D modelled with V_{S30} equals to 1070m/s, 525m/s, and 255m/s, respectively), corresponding to an earthquake with a reverse fault mechanism and a Joyner-Boore distance equal to 30km.

The V_{EIr} spectra are reported in Fig. 4.19 and Fig. 4.20. Since in Chapman (1999) and Danciu and Tselentis (2007) predictive equations for V_{EIr} are not developed, Gong and Xie (2005) only is used in the evaluation of the proposed GMPE. In these Figures, the same types of comparisons shown for V_{EIa} are reported and similar trends can be observed. In particular, by looking at the plots of Fig. 4.19 it can be stated that the spectra predicted with the two GMPEs are very similar, especially for the case of magnitude 6 and distance equal to 30 km. The effects of soil condition, shown in the plots of Fig. 4.20, are very similar except for the case of soil type A+B and magnitude equal to 7. Also in this case, the same explanations of those proposed for V_{EIa} can be given.

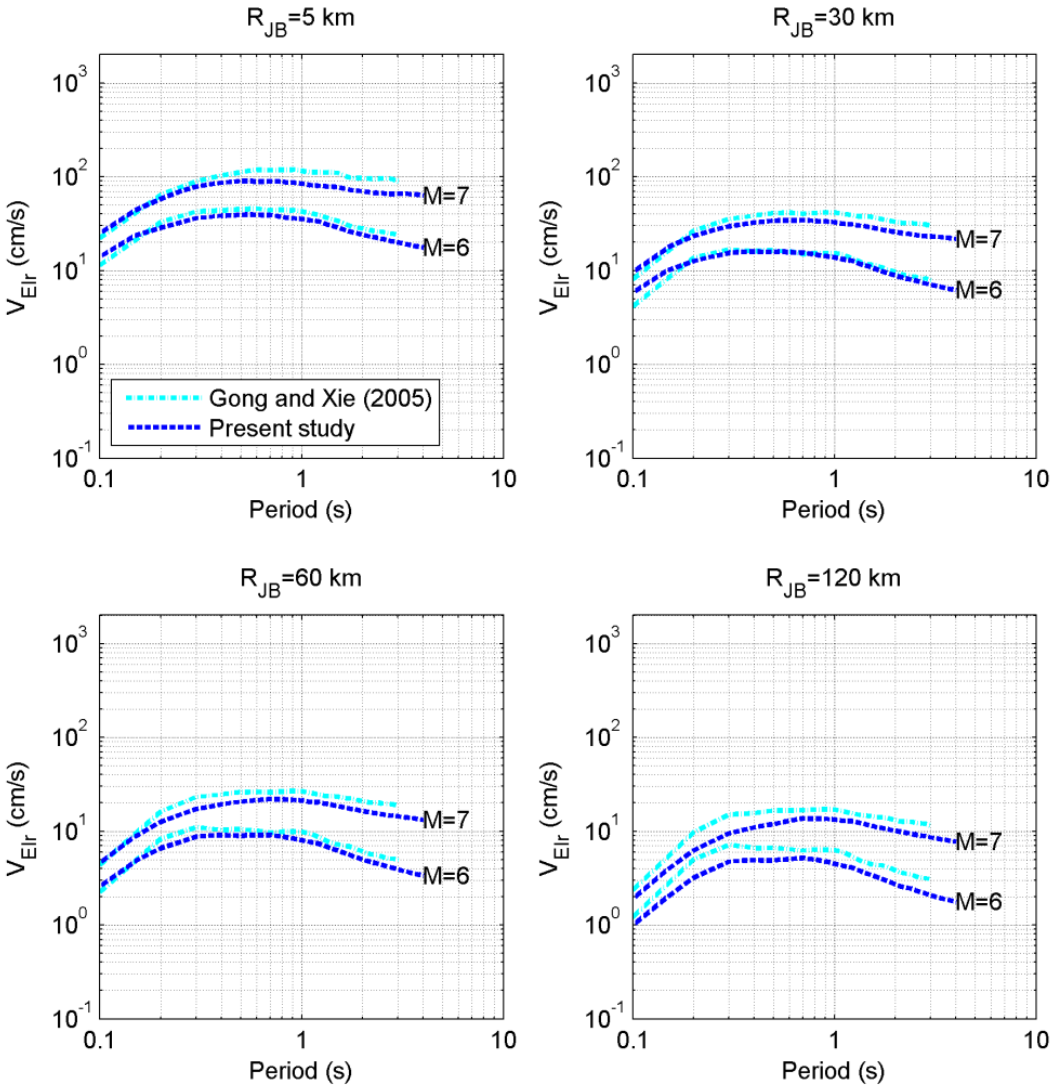

Fig. 4.19 V_{EIr} spectra predicted for different magnitude and Joyner-Boore distance values, corresponding to an earthquake with a reverse fault mechanism and a soil condition of NEHRP typeB (modelled with a V_{S30} equal to 525m/s).

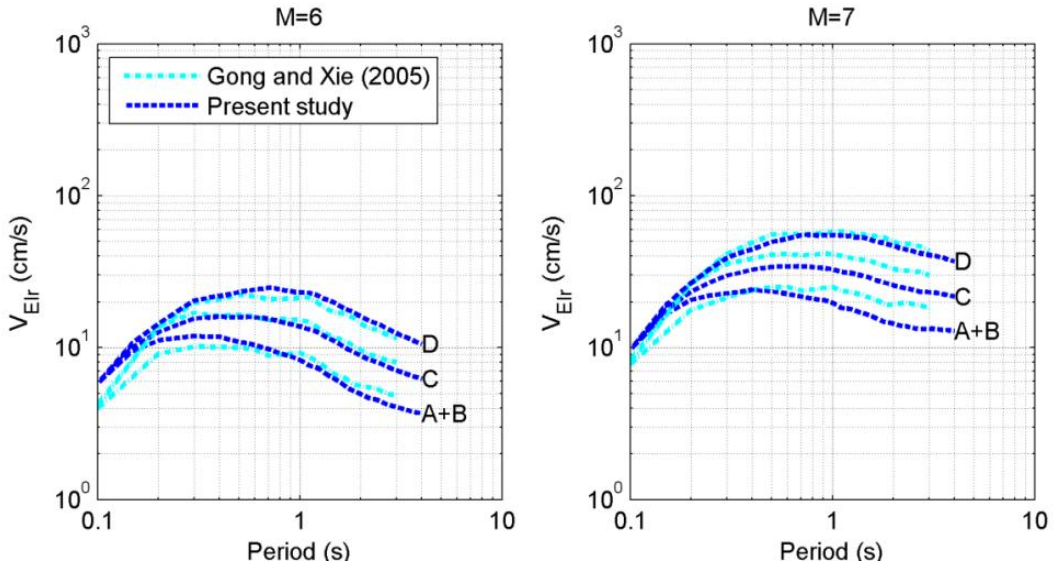

Fig. 4.20 V_{EIr} spectra predicted for different types of soil (NEHRP A+B, C, and D modelled with V_{S30} equals to 1070m/s, 525m/s, and 255m/s, respectively), corresponding to an earthquake with a reverse fault mechanism and a Joyner-Boore distance equal to 30km.

4.8 **Conclusion**

The previous chapters have shown that in order to predict the seismic response of the structures the absolute input energy equivalent velocity V_{EIa} and the relative input energy equivalent velocity V_{EIr} can be considered in some cases as good alternatives with respect to standard intensity measures commonly used in performance-based earthquake engineering, such as the peak ground acceleration or the pseudo-spectral acceleration. V_{EIa} and V_{EIr}, in fact, are intensity measures that are able to capture not only the duration and amplitude of the ground motion but also the dynamic properties of the structure.

In this chapter, empirical ground motion prediction equations developed based on a mixed-effect model are proposed for estimating both V_{EIa} and V_{EIr}. The model coefficients have been calibrated through regression analyses using records selected from the NGA database. The proposed equations can be applied to predict V_{EIa} and V_{EIr} for shallow crustal earthquakes occurring in active tectonic region, with a magnitude range of 5 to 8, a distance less than 200 km, and a V_{S30} value in the range of 150-1500m/s.

The improvements with respect to the prediction equations for input energy equivalent velocity spectra already available from the literature can be identified in the following: the proposed equations have been developed using a large number of records characterized by a wide range of magnitude and distance; they include a V_{S30} term that enables to better evaluate the effects of soil conditions than simple dummy variables; they also include terms to explicitly account for different types of fault mechanisms; a prediction equation for the relative input energy equivalent velocity, intensity measures that has not still received much research attention, has been also proposed.

Results of parametric analyses and comparisons with other prediction equations from the literature have been finally shown to discuss about the different effects that the variation of earthquake properties and site conditions have on these two intensity measures.

5 Correlation of elastic input energy equivalent velocity spectral values for ground motions

5.1 Introduction

In the framework of performance-based earthquake engineering, Intensity Measure (IM) plays a dominant role, especially for engineers, in evaluation of structural seismic performance. In recent years energy-based intensity measures (IMs) have received more attention. Several studies (e.g., Uang and Bertero, 1990, and the most recent Kalkan and Kunnath, 2008) have proposed the energy-based concepts for the definition of the earthquake IM. The relative and absolute elastic input energy and their corresponding equivalent velocities (V_{EIa} and V_{EIr}) have been considered as more potential measures of seismic demand in structures among the different energy-based IMs that have been researched in the past. In fact these IMs have been shown to have good prediction capabilities due to the fact that they are not only dependent on amplitude and duration of ground motions but also the properties of the structure.

The Ground Motion Prediction Equation (GMPE) of V_{EIa} and V_{EIr} has been developed by some researchers, which achieves their application in seismic hazard analysis in the context of performance-based earthquake engineering (see, Chapman 1999, Gong and Xie 2005, Danciu and Tselentis 2007 and chapter 4 of this study). But the GMPE of these energy-based IMs only consider the marginal distribution of individual spectral values without giving the any information about the joint distribution of their spectral values at different periods. Therefore their uniform hazard spectrum based on the GMPE used as the target spectrum for selecting and modification ground motions can induce conservative results. However the conditional mean spectrum with epsilon (CMS-ε), which is introduced by Baker and Cornell (2006) and takes into account the correlation of the spectral values at different periods, can address this issue (see, e.g., Haselton et al. 2009). Although the correlation of the S_a spectral values at different periods has been investigated in some studies (see Baker and Cornell 2006, Baker and Jayaram 2008, Abrahamson et al. 2003, and Cimellaro 2013), there is barely such evaluation of the correlation of the energy-based IMs in literatures.

Therefore the main purpose of this chapter is to evaluate the correlation of the energy-based spectral values for ground motions. It has been obtained by firstly calculating the empirical correlation coefficients of the energy-based spectral values, and then investigating the compatibility of the correlation prediction equations of S_a developed in the previous literatures to the empirical values of the energy-based spectral values, finally proposing new prediction for calculating the correlation coefficients of the energy-based spectral values. Three cases for the evaluations of correlation of the energy-based spectral values are taken into account: the case with different periods and the same component; the case with the same period and different perpendicular components; and the case with the different periods and different perpendicular components. Only horizontal components are considered in this study. Some applications of these correlations are also introduced in the end of this chapter.

5.2 **Development of correlation equations**

The detail of the definition of elastic input absolute and relative energy equivalent velocities can be referred to the chapter 4 or the study of Uang and Betero (1990).

In this study we only take into account the horizontal components due to the fact that the vertical effects are neglected in seismic evaluation of structures in many cases. The logarithm of input energy equivalent velocities of two horizontal components of each record can be expressed in the following equations:

$$\ln V_{EIx}(T) = f(M,R,T,\theta) + \sigma(T)\varepsilon_x(T) \tag{5.1}$$

$$\ln V_{EIy}(T) = f(M,R,T,\theta) + \sigma(T)\varepsilon_y(T) \tag{5.2}$$

, where

V_{EI} presents observed values of V_{EIa} or V_{EIr} for each record considered herein;

x and y represent the two perpendicular horizontal components, respectively;

$f(M,R,T,\theta)$ is the predicted mean of logarithmic V_{EIa} or V_{EIr} at a specific period T, evaluated through the GMPE that is a function of magnitude (M), source to site distance (R), period (T) and other parameters (θ);

$\sigma(T)$ is standard deviation of the predicted V_{EIa} or V_{EIr}, which is also provided by the GMPE. This variation could be also related with magnitude when nonlinear site effect is taken account, correspondingly, noted as $\sigma(M,T)$.

The above two equations can also be transferred and presented with the following equations:

$$\varepsilon_x(T) = \frac{\ln V_{EIx}(T) - f(M,R,T,\theta)}{\sigma(T)} \tag{5.3}$$

$$\varepsilon_y(T) = \frac{\ln V_{EIy}(T) - f(M,R,T,\theta)}{\sigma(T)} \tag{5.4}$$

Because in equation 5.3 and 5.4 $f(M,R,T,\theta)$ and $\sigma(T)$ account for the mean value and standard deviation of logarithm of elastic input energy, $\varepsilon_x(T)$ and $\varepsilon_y(T)$ accounting for the randomness of observation follow the distribution with mean of zero and unit standard deviation. In fact in some studies regarding the S_a, the $\varepsilon(T)$ associated with S_a has been revealed to be a good predictor of the shape of the response spectrum of ground motions. Since it is observed from the equation 5.1 and 5.2 that $\varepsilon(T)$ and $\ln V_{EI}(T)$ are simply linear correlation, the author calculated the correlation of $\varepsilon(T)$ values for appropriately representing the correlation of $\ln V_{EI}(T)$ values in this study.

The correlation of $\varepsilon(T)$ can be estimated with the equation 11using the Pearson product-moment correlation coefficient.

$$\rho_{\varepsilon(T_1),\varepsilon(T_2)} = \frac{\sum_{i=1}^{n}(\varepsilon_i(T_1) - \overline{\varepsilon(T_1)})(\varepsilon_i(T_2) - \overline{\varepsilon(T_2)})}{\sqrt{\sum_{i=1}^{n}(\varepsilon_i(T_1) - \overline{\varepsilon(T_1)})^2 \sum_{i=1}^{n}(\varepsilon_i(T_2) - \overline{\varepsilon(T_2)})^2}} \tag{5.5}$$

where

$\varepsilon_i(T_1)$ and $\varepsilon_i(T_2)$ are the *i*th observation of $\varepsilon(T_1)$ and $\varepsilon(T_2)$;

n is the number of observation of ε at period T

$\overline{\varepsilon(T_1)}$ and $\overline{\varepsilon(T_2)}$ are means of all n observations at T_1 and T_2, respectively.

Since the vertical component is not taken into account in the study, the correlation of $\varepsilon(T)$ can categorized into three cases: the correlation coefficient of $\varepsilon(T)$ for the different

periods but the same horizontal component, noted as $\rho_{\varepsilon(T_1),\varepsilon(T_2)}$; the correlation coefficient for the same period but different horizontal orthogonal components, noted as $\rho_{\varepsilon_x(T),\varepsilon_y(T)}$; the correlation coefficient for the different periods and different horizontal orthogonal components, noted as $\rho_{\varepsilon_x(T_1),\varepsilon_y(T_2)}$.

To confine the limitation of the correlation, some criteria are used to select the ground motion recordings in this chapter: the lower limit of magnitude of records is fixed as M=5; recordings with closest distance than 200 km are excluded; the site categorization of B, C and D, classified according to NEHRP are only considered here due to the rare quantities recorded on the A and E class site; only the records with two available horizontal components; the two horizontal orthogonal components with high-pass filter corner frequencies less than 0.2Hz and with low-pass filter corner frequencies great than 18 Hz. The strong ground motion records used in this chapter were collected from NGA database consisting of a large set of ground motions recorded in worldwide shallow crustal earthquakes. As the result 740 records recorded from 40 earthquakes with two horizontal perpendicular components are selected for running the correlation analysis.

Although the correlation coefficients can be tabulated, researchers prefer to fit them with an analytic equation for better and easier communication (see Baker and Cornell 2006, Baker and Jayaram 2008, Abrahamson et al. 2003, and Cimellaro 2013). In this work we also used the same nonlinear regression methods as the one used by Baker and Cornell (2006), where Fisher z transformation (Neter et al. 1996) was applied to correlation coefficients, expressed as Equation 5.6, and a simple least-squares regression is utilized to these z values. The Equation 5.7 shows the expression of minimum residuals when the least-squares regression is used. It is noticed that the Fisher z transformation is necessary since correlation coefficients evaluated in Equation 5.5 have non-constant standard errors (see Baker and Cornell 2006, Baker and Jayaram 2008).

$$z_{i,j} = 0.5\ln\left(\frac{1+\rho_{i,j}}{1-\rho_{i,j}}\right) \tag{5.6}$$

$$\min \sum_{i=1}^{n} \sum_{j=1}^{n} (z_{i,j} - \hat{z}_{i,j})^2 \tag{5.7}$$

, where

$\rho_{i,j}$ is the empirical correlation coefficient of ε at the period of T_i and T_j;

$z_{i,j}$ is the Fisher z transformation for the empirical correlation coefficient;

$\hat{z}_{i,j}$ is the Fisher z transformation for the predicted correlation coefficient.

5.3 **Observed correlation and correlation predictive equations**

5.3.1 Correlation of spectral values for different periods and the same component

5.3.2 Empirical correlation coefficients

The empirical correlation coefficients of V_{EIa} and V_{EIr} obtained with various GMPE models at different periods (i.e. T_1 and T_2) for the same horizontal component were computed through Equation 5.5, and presented in Figures from 5.1 to 5.4. The Fig.5.1 and Fig.5.2 show the contours of the correlation coefficients versus T_1 and T_2, while the Fig.5.3 and Fig.5.4 present the change of correlation coefficients as a function of T_1 for a set of periods T_2. The latter are plotted in the different way but use the same results as the former.

The correlation coefficients of V_{EIa} obtained with the GMPE models of Chapman (1999), Gong and Xie (2005), Danciu and Tselentis (2007) and Chapter 4 at different periods in the same orientation is shown in Fig. 5.1 and Fig. 5.3. It was observed that there is no significant influence of the choice of GMPE on the correlation coefficients. The largest difference occurs when the results obtained with the GMPE of Daciu and Tselentis (2007) is compared to those obtained with other GMPEs used in this chapter. That is probably due to the fact that the record data used to derive the GMPE of Daciu and Tselentis (2007) are specifically recorded in Greece, while the records used to develop other GMPEs are consistent to each other, where many California ground motion recordings exist. The Fig. 5.2 and Fig. 5.4 only give the empirical correlation coefficients of V_{EIr} based on the GMPEs of Gong and Xie (2005) and Chapter 4, since the other works did not develop the GMPE for the V_{EIr} parameter. By comparing among Fig. 5.1, Fig. 5.2, Fig. 5.3 and Fig. 5.4, it is shown that the correlation

coefficient values of V_{EIa} is larger than V_{EIr}. In other words, V_{EIa} values in the same component at different periods are more correlated than V_{EIr}.

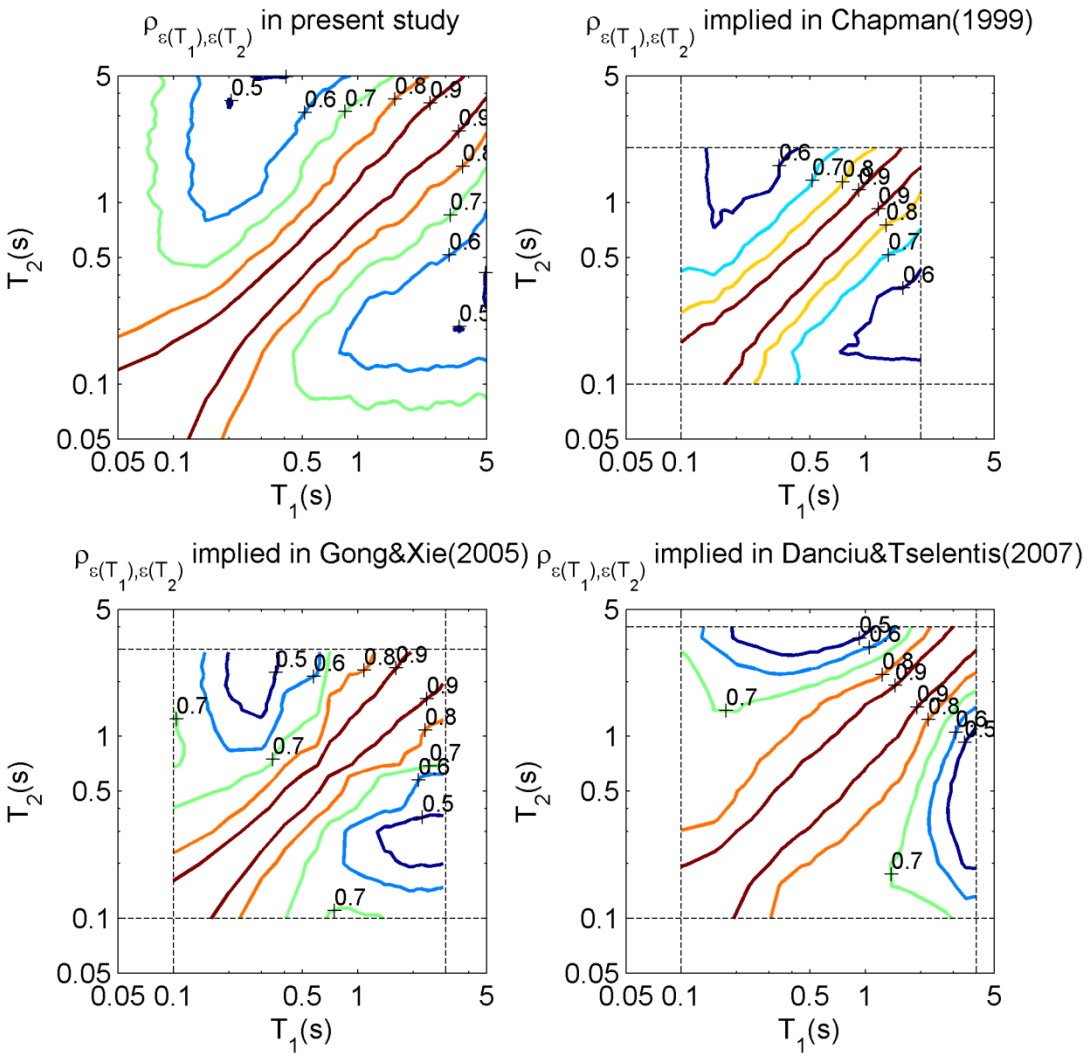

Fig. 5.1 Contours of empirical horizontal correlation coefficients of absolute input energy equivalent velocity (V_{EIa}) spectral values for four GMPEs versus T_1 and T_2.

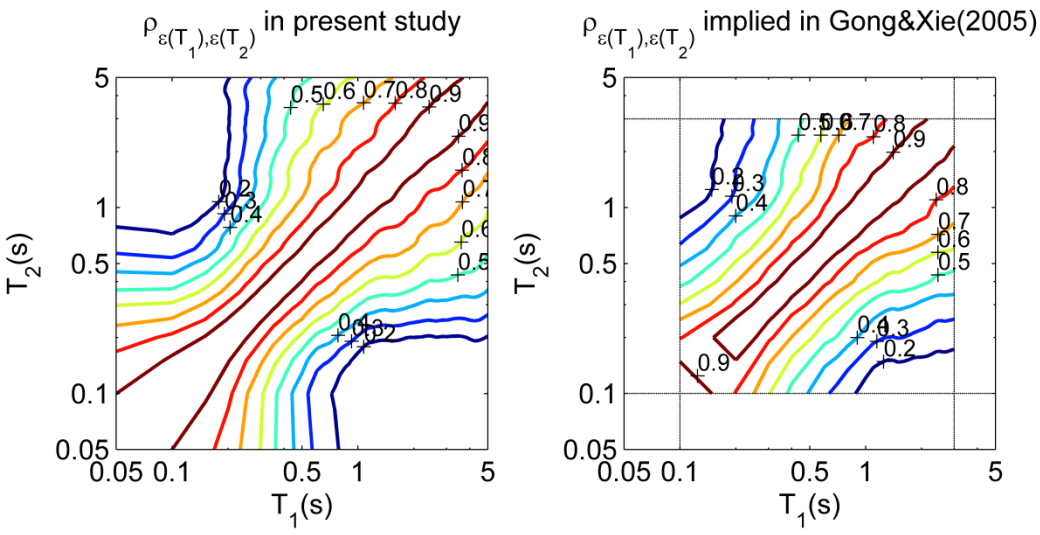

Fig. 5.2 Contours of empirical horizontal correlation coefficients of relative input energy equivalent velocity (V_{EIr}) spectral values for two GMPEs versus T_1 and T_2.

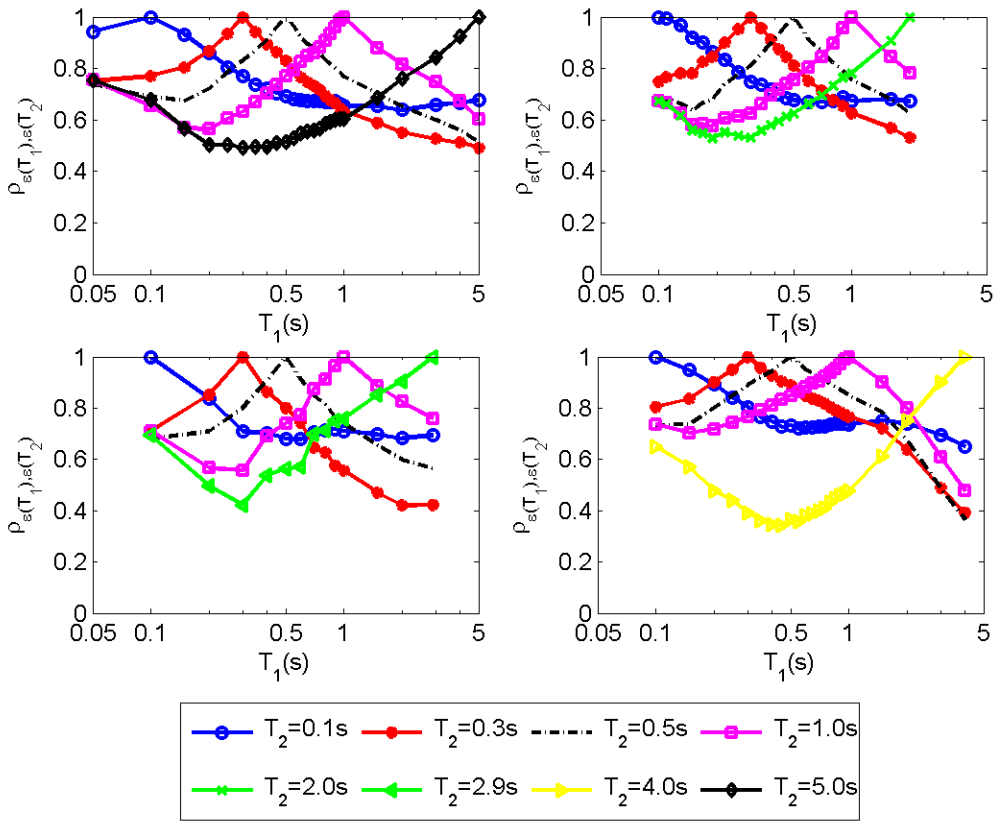

Fig. 5.3 Empirical horizontal coefficients of V_{EIa} spectral values versus T_1, for variable T_2 values, calculated with the GMPE developed by Chapter 4, Chapman (1999), Gong and Xie (2005) and Danciu and Tselentis (2007) (shown in left top, right top, left bottom and right bottom panel, respectively).

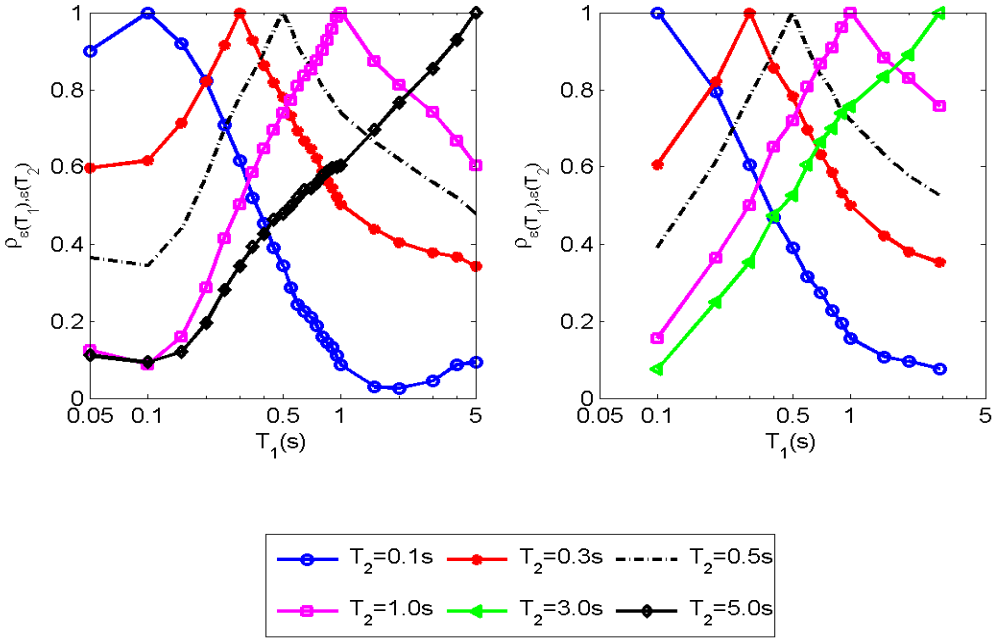

Fig. 5.4 Empirical horizontal coefficients of V_{EIr} spectral values versus T_1, for variable T_2 values, calculated with the GMPE of Chapter 4 (left panel) and Gong and Xie(2005) (right panel).

5.3.2.1 Predictive equations

Although some predictive models of correlation coefficient of Spectral acceleration values (S_a) are available in the literatures (see Baker and Cornell 2006, Baker and Jayaram 2008, Abrahamson et al. 2003, and Cimellaro 2013), there are few researches on the analytical predictive models of correlation coefficients of elastic input energy spectral values.

Therefore in this subsection we first use the predictive models of correlation coefficient of S_a spectral values to carry out the regression analysis to the observed (empirical) correlation coefficients of V_{EIa} and V_{EIr} spectral values in order to see whether the predictive models of correlation of S_a fit the observed correlation of V_{EIa} and V_{EIr}. Based the above observation,

then a new potential predictive is proposed for better predicting the correlation of V_{EIa} and $V_{EIr.}$

The predictive model of Baker Cornell (2006) that is widely used such as in the calculation of CMS and that of Cimellaro (2013) that shows the newest research are used to compare. The model of Abrahamson et al.(2003) is not taken into account in this study, since it does not possess the positive definiteness property that is necessary when one needs the joint distribution of spectral values at many periods simultaneously (Baker Cornell 2006). The present work only evaluates the correlation of spectral values in the range of 0.05-5s, since in the periods out of this range it is less engineering interest and it lacks of empirical data. The model of Baker and Jayaram (2008) is not considered in this study, since it mainly provides for a wide range period of 0.01-10s and it has complicated variables

The predictive model of correlation coefficients proposed by Backer and Cornell (2006) has been used to fit the observed S_a spectral values through nonlinear least square regression. This model is described as following:

$$\rho_{\varepsilon(T_1),\varepsilon(T_2)} = 1-\cos\left(\frac{\pi}{2}-(A0-A1\cdot I_{(T\min<A2)}\ln(\frac{T_{\min}}{A2}))\ln(\frac{T_{\max}}{T_{\min}})\right) \tag{5.8}$$

, where T_{min} =min(T_1, T_2) ; T_{max} =max(T_1, T_2) ; I(T_{min}<A2) is an indicator function equal to 1 if T_{min}<A2 and equal to 0 otherwise. The parameters of this model resulted from its curve fit to the observed V_{EIa} and V_{EIr} spectral values for the same horizontal component and different periods are listed in Table 5.1 and the contour of the observed (empirical) and predicted correlation coefficients are plotted in Figure 5.5 (top panels).

Cimellaro (2013) proposed a simpler predictive model, without indicator function, of correlation coefficients of S_a for the same horizontal or vertical component at two different periods, using records collected from a European ground motion database. It's an improved predictive model of correlation of S_a for earthquakes in Europe. The predictive model of correlation coefficients is presented by

$$\rho_{\varepsilon(T_1),\varepsilon(T_2)} = 1 - \left(\frac{a + b\ln(T_{\min}) + c(\ln(T_{\max}))^2}{1 + d\ln(T_{\max}) + e(\ln(T_{\min}))^2} \right) \ln\left(\frac{T_{\min}}{T_{\max}} \right) \tag{5.9}$$

In Equation 5.9, T_{min} =min(T_1, T_2) and T_{max} =max(T_1, T_2), where T_1 and T_2 are different periods in a single component. After fitting the observed correlation coefficients of V_{EIa} and V_{EIr} with this model, the parameters of this model are evaluated and listed in Table 5.2. The predicted correlation coefficients with the corresponding observed coefficients are presented in Fig. 5.5 (bottom panels).

It can be observed in Fig. 5.5 that the predicted correlation coefficients of V_{EIa} and V_{EIr} by the model of Jack Baker (2006) do not match well the corresponding observed values. On the other hand, the model of Cimellaro (2013) better fit the observed correlation coefficients than the model of Jack Baker (2006), especially when T_{min} is larger than a certain value. Based on the above observations, a new predictive model of correlation coefficients of V_{EIa} and V_{EIr} is proposed and given by following two equations:

$$\rho_{\varepsilon(T_1),\varepsilon(T_2)} = 1 - \cos\left(\frac{\pi}{2} - (B1 - A1 \cdot I_{(T\min<A2)} \ln\left(\frac{T_{\min}}{A2}\right)) \ln\left(\frac{T_{\max}}{T_{\min}}\right)\right) \tag{5.10}$$

$$B1 = -\frac{a + b\ln(T_{\min}) + c(\ln(T_{\max}))^2}{1 + d\ln(T_{\max}) + e(\ln(T_{\min}))^2} \tag{5.11}$$

, where I (T_{min} <A2) equal to 1when T_{min} <A2 and equal to 0 otherwise. This model is proposed by integrating the model of Baker and Cornell (2006) with the one of Cimellaro (2013). *.B1* expressed in equation 5.11 has the same form as a part of model of Cimellaro (2013) expressed in equation 5.9. The proposed model will become the same model as that of Cimellaro (2013) when T_{min} >A2. Conversely, when T_{min} <A2 the proposed model will have the same form as the model of Jack Baker (2006). The parameters obtained by fitting observed data to the proposed model expressed with equation 5.10 and 5.11 are listed in Table 5.3. The contour of observed and predicted correlation coefficients of V_{EIa} and V_{EIr} using the proposed model is shown in Fig. 5.6.

In order to compare the fitness of these three predictive models of correlation coefficients, AIC values are obtained by carrying out the nonlinear least-square fit to the observation

correlation coefficients of V_{EIa} and V_{EIr} with these models, and presented in Table 5.4. It shows that the proposed model in this study results in the smallest AIC value among all considered models. The model of Baker and Cornell (2006) shows the largest value of AIC. In other words, the proposed predictive model has better fitness to the observed correlation of V_{EIa} and V_{EIr}, especially when compared to the model of Baker and Cornell (2006). By comparing Fig. 5.5 to Fig. 5.6, it is also illustrated that the proposed predictive model of correlation coefficients of epsilon at different periods in the same direction better fits to the observed values when compared to other two models. Therefore it suggests that the proposed predictive model can be reasonably more robust to describe the correlation coefficients of V_{EIa} and V_{EIr}.

Table 5.1 Parameters of the predictive correlation coefficients model of Backer and Cornell (2006) for different periods and the same component

Parameters	A0	A1	A2
V_{EIa}	0.2665	0.1030	0.327
V_{EIr}	0.3535	0.1333	0.112

Table 5.2 Parameters of the predictive correlation coefficients model of Cimellaro (2013) for different periods and the same component

Parameters	a	b	c	d	e
V_{EIa}	-0.3741	-0.0628	0.0077	0.3854	0.0982
V_{EIr}	-0.4494	-0.0363	0.0393	0.1785	0.0287

Table 5.3 Parameters of the predictive correlation coefficients model in this study for different periods and the same component

Parameters	A1	A2	a	b	c	d	e
V_{EIa}	0.0459	0.228	-0.3464	-0.0359	0.0077	0.2796	0.0569
V_{EIr}	0.0801	0.1	-0.4368	-0.0215	0.0426	0.1109	0.0060

Table 5.4 AIC values resulted from the nonlinear curve fit to the observed correlation coefficients of epsilon at two different periods in the same direction for V_{EIa} and V_{EIr} using various predictive equation models.

AIC	Baker and Cornell 2006	Cimerallo 2013	Proposed in this study
V_{EIa}	-6314.254	-8272.737	-9087.155
V_{EIr}	-6599.84	-9053.089	-9069.951

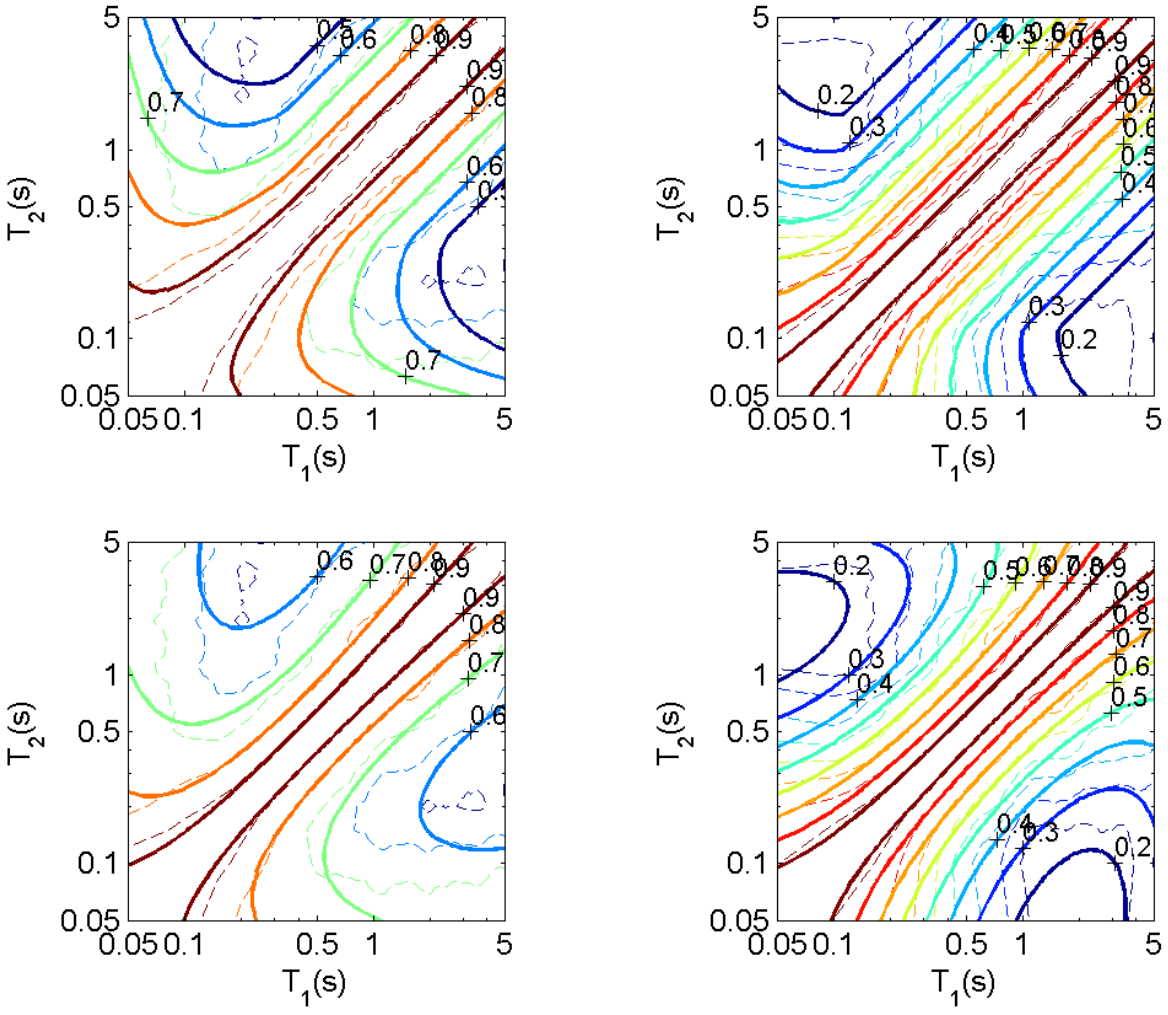

Fig. 5.5 Contour of observed (Dashed lines) and predicted (solid lines) correlation coefficients of V_{EIa} and V_{EIr} at two periods (T_1 and T_2) in the same component. Baker and Cornell (2006)

model for V_{EIa} (top left panel) and V_{EIr} (top right panel). Cimellaro (2013) for V_{EIa} (bottom left panel) and V_{EIr} (bottom right panel).

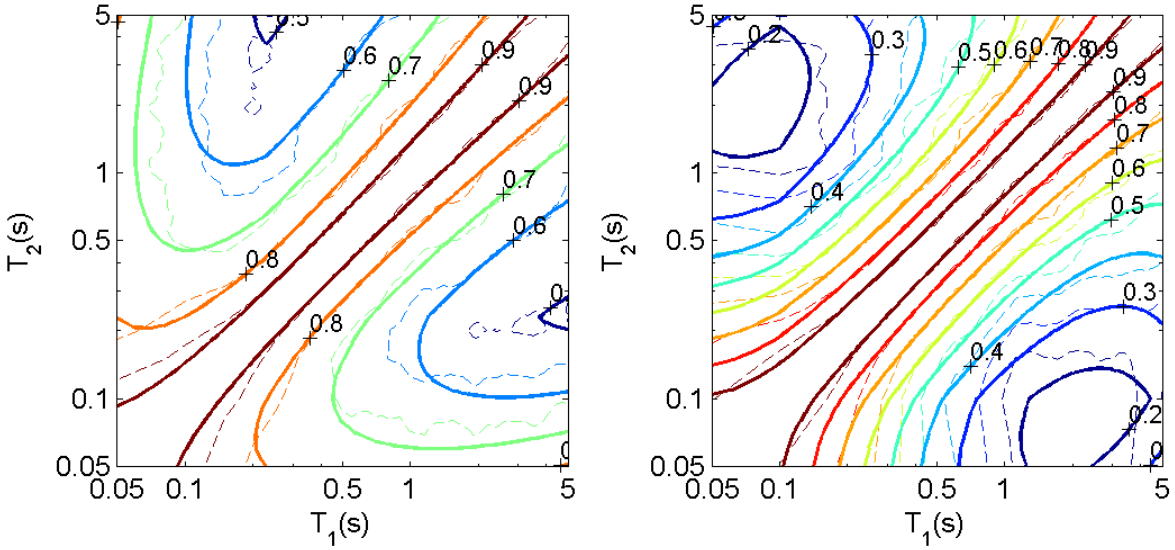

Fig. 5.6 Contour of observed (Dashed lines) and predicted (solid lines) correlation coefficients of V_{EIa} (left panel) and V_{EIr} (right panel) at two periods (T_1 and T_2) in the same component by using the proposed predictive model

5.3.3 Correlation of spectral values for the same period and different components

The observed correlation coefficients of epsilon for V_{EIa} and V_{EIr} at the same period in orthogonal orientations are fitted with linear model. The observed and predicted correlation coefficients are presented in Fig. 5.7. The left panel of Fig. 5.7 shows that the correlation coefficients of V_{EIa} do not vary significant with periods. Therefore the correlation coefficient of V_{EIa} at the same period in orthogonal components can be estimated by a constant, shown as following:

$$\rho_{\varepsilon_x(T),\varepsilon_y(T)} = 0.864 \tag{5.12}$$

where x and y represent two horizontal orthogonal orientation. On the other hand, the predicted correlation coefficient of V_{EIr} at the same period in orthogonal components is presented in the right panel of Fig. 5.7 and is described by

$$\rho_{\varepsilon_x(T),\varepsilon_y(T)} = 0.839 - 0.0288\ln(T) \tag{5.13}$$

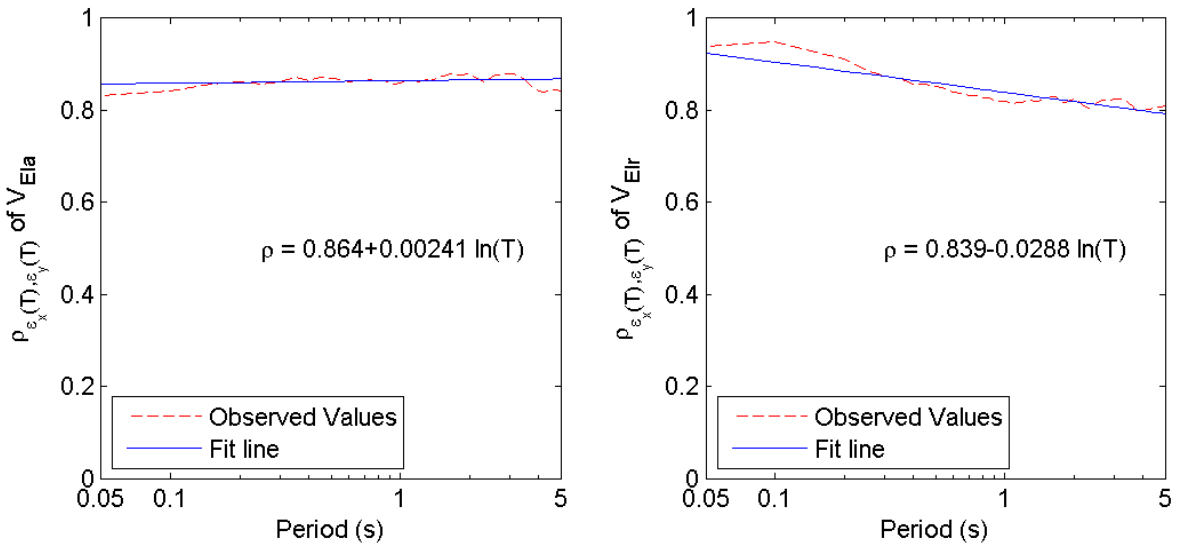

Fig. 5.7 Observed correlation coefficients and their fit lines for V_{EIa} (left panel) and V_{EIr} (right panel) at the same periods in different orientation

5.3.4 Correlation of spectral values for different periods and orthogonal components

With the same methodology as that used by Baker and Cornell (2006) and Baker and Jayaram (2008), the correlation coefficient of elastic input energy spectral values at different periods in the orthogonal orientations, $\rho_{\varepsilon_x(T_1),\varepsilon_y(T_2)}$, can be estimated by the production of the correlation coefficient at different periods in the same orientation, $\rho_{\varepsilon(T_1),\varepsilon(T_2)}$, and that at the same period in the orthogonal orientation $\rho_{\varepsilon_x(T),\varepsilon_y(T)}$. Therefore $\rho_{\varepsilon_x(T_1),\varepsilon_y(T_2)}$ of V_{EIa} is described with Equation 5.14 while $\rho_{\varepsilon_x(T_1),\varepsilon_y(T_2)}$ of V_{EIr} is evaluated with Equation 5.15, shown as following:

$$\rho_{\varepsilon_x(T_1),\varepsilon_y(T_2)} = 0.864\rho_{\varepsilon(T_1),\varepsilon(T_2)} \tag{5.14}$$

$$\rho_{\varepsilon_x(T_1),\varepsilon_y(T_2)} = (0.839 - 0.0288\ln\sqrt{T_1T_2})\rho_{\varepsilon(T_1),\varepsilon(T_2)} \tag{5.15}$$

, where $\rho_{\varepsilon(T_1),\varepsilon(T_2)}$ can be obtained from Equation 5.10 or 5.11; x and y indicate two horizontal orthogonal directions. In Equation 5.15 since two periods are of interest the arithmetic mean of the logarithmic periods is used. The contour of observed and predicted correlation coefficients of V_{EIa} and V_{EIr} are presented in Fig. 5.8. It illustrates that the predictive equations of correlation coefficients for different periods and orthogonal components, i.e., Equation 5.14 and 5.15, can well match the observed data.

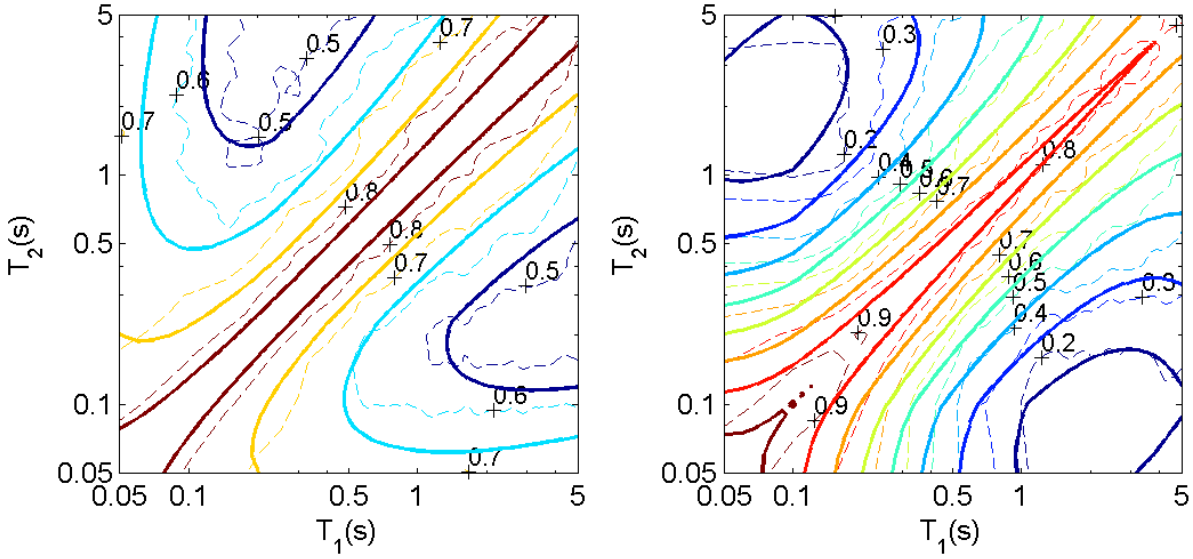

Fig. 5.8 Observed and predicted correlation coefficients of V_{EIa} (left) and V_{EIr} (right) for two different periods (T_1 and T_2) and orthogonal orientations. The predicted values are estimated with equation 5.14 (left) and 5.15 (right).

5.4 **Application in ground motion selection and modification**

In order to demonstrate the usefulness of the proposed predictive model of correlation coefficients associated with V_{EIa} and V_{EIr}, its applications in ground motion selection and modification in terms of spectrum-matched and amplitude-scaled methods are presented in the following.

5.4.1 Application in spectrum-matched method

Spectrum-matched approach is a commonly used method to select ground motions as input to dynamic analyses. In this method a group of ground motions are scaled to match a target response spectrum. The widely used ones include the Uniform Hazard Spectrum (UHS) and the Conditional Mean Spectrum (CMS) proposed by Baker (2010) recently. UHS has shown to be not suitable for matching in ground motions selection and modification and may cause conservative results. In fact UHS is an envelopment of spectral values, where the value at each period has the same exceeding probability. It does not represent a spectrum of any individual ground motion. CMS, estimating an expected response spectrum conditioned on occurrence of a target spectral value at the period of interest, deals with this issue. The evaluation of correlation of spectral values at different periods is a necessary step in the calculation of CMS. Therefore, the correlation coefficient predictive equations proposed in this study can be used for calculating the condition mean spectrum (CMS) of V_{EIa} and V_{EIr}, which reasonably accounts for the joint distribution of simultaneous spectral values. The process of calculating CMS of V_{EIa} and V_{EIr} is the same as that of S_a (Baker 2011). For example, the conditional mean values of $\ln(V_{EIr})$ at the period T_i conditioned on $\ln(V_{EIr})$ at the period T* can be computed using an equation given by

$$\mu_{\ln V_{EIr}(T_i)|\ln V_{EIr}(T^*)} = \mu_{\ln(V_{EIr}(T_i))}(\overline{M}, \overline{R}, T_i, \overline{\theta}) + \rho_{\varepsilon(T_i),\varepsilon(T^*)} \cdot \varepsilon(T^*) \cdot \sigma_{\ln V_{EIr}}(T_i) \tag{5.16}$$

, where $\mu_{\ln(V_{EIr}(T_i))}(\overline{M}, \overline{R}, T_i, \overline{\theta})$ and $\sigma_{\ln V_{EIr}}(T_i)$ are predicted mean value and dispersion of $\ln(V_{EIr}(T_i))$ obtained in GMPE. $\rho_{\varepsilon(T_i),\varepsilon(T^*)}$ is the correlation coefficients of epsilon at different periods in the same orientation, which can be obtained in Equation 5.10 and 5.11. Fig. 5.9 presents an example of CMS of V_{EIa} and V_{EIr}, while their UHS and predicted mean spectrum obtained with GMPE proposed by Chapter 4 are also plotted for comparison.

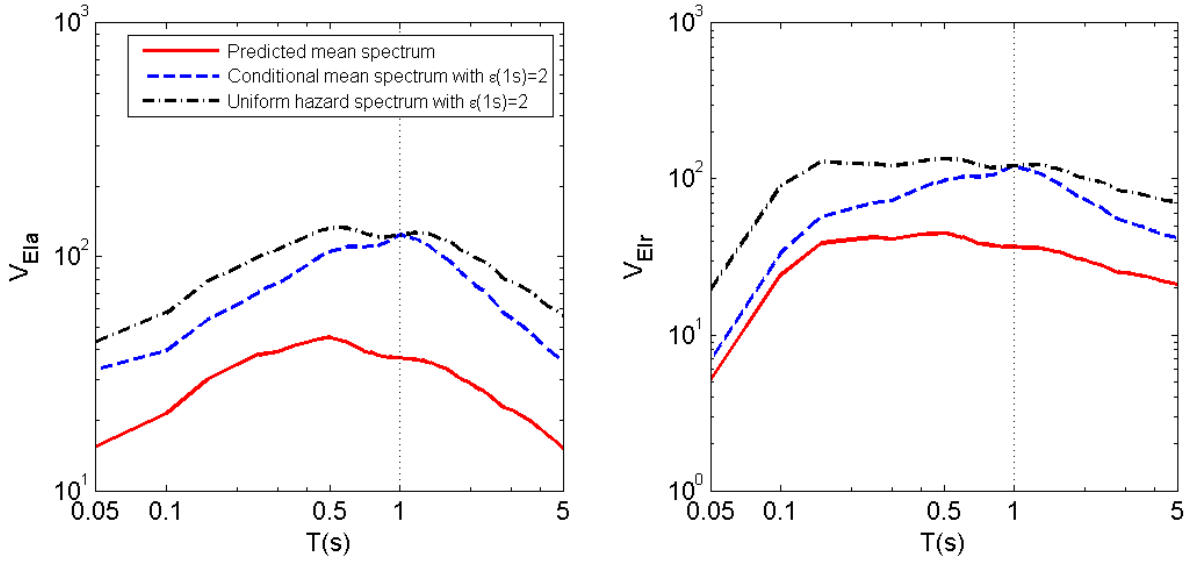

Fig. 5.9 Conditional mean spectrum conditioned on $\varepsilon(1s) = 2$, plotted with predicted mean spectrum obtained with GMPE proposed by Chapter 4 and Uniform hazard spectrum conditioned on $\varepsilon(1s) = 2$, for V_{EIa} (left panel) and V_{EIr} (right panel).

5.2 Application in amplitude-scaled method

The proposed predictive models of correlation coefficients in this study are also very useful in the calculation of predicted target values of some integral energy-based IMs, such as $V_{EIa}SI$, $V_{EIr}SI$, $MV_{EIa}SI$ and $MV_{EIr}SI$. The definitions of these IMs are shown in Table 2.3. The $V_{EIa}SI$, and $V_{EIr}SI$, obtained from integration of the V_{EIa} and V_{EIr} in the period range of 0.1-3.0 second, have been demonstrated to be appropriate for near-fault signals in the works of Decanini and Mollaioli (1998, 2001). On the other hand the Chapter 3 has shown that the $MV_{EIr}SI$ can be a potential IM for predicting the structural response of base-isolated buildings.

The predicted target value of the scalar IMs is the necessary parameter for selecting ground motions as input to dynamic analysis in terms of amplitude-scaled approach, where ground motions are scaled so that the value of the scalar intensity measure (IM) of GMs is equal to the predicted target value. The predicted target value of IMs is given by the seismic hazard curve in term of the IMs, where the mean value and standard deviation of predicted IMs are required. In general the mean value and standard deviation of the predicted integral energy-based IMs are obtained with their GMPEs, which are developed by directly performing the

regression analysis on these IM values of ground motions. However it's not the best choice first because the GMPEs of these integral energy-based IMs are in paucity, second because it will especially require much more effort when the GMPEs of $MV_{EIa}SI$ and $M_{VEIr}SI$ need to be developed since the integral period range of them is not fixed, which means the GMPEs of $MV_{EIa}SI$ or $M_{VEIr}SI$ need to be derived time and again when the fundamental period of considered structure changes.

To address this issue the approach proposed by Bradley et al. (2009) can be used to calculate the target values of integral energy-based IMs ($V_{EIa}SI$, $V_{EIr}SI$, $MV_{EIa}SI$ and $MV_{EIr}SI$) based on the GMPE of V_{EIa} or $V_{EIr.}$ Since the approach of Bradley et al. (2009) was originally proposed to calculate the mean and standard deviation of predicted Housner Intensity based on the GMPE of spectral acceleration in performance-based assessment and design, the equations in this approach have been modified and calibrated to calculate the mean and standard deviation of integral energy-based IMs, presented in Equation 5.17 and 5.18. The Equation 5.18 implies that the correlation coefficients of V_{EI} (V_{EIa} or V_{EIr}) at different periods (i.e. $\rho_{V_{EI}i,V_{EI}j}$) are indispensable for computing standard deviation of $V_{EIa}SI$, $V_{EIr}SI$, $MV_{EIa}SI$ and $MV_{EIr}SI$. Therefore the correlation coefficient equations proposed in this study addresses the issue of application of these integral energy-based IMs in the performance-based assessment and design to structures.

$$\mu_{V_{EI}SI} = \Delta T \sum_{i=1}^{n} w_i \mu_{V_{EI}i} \tag{5.17}$$

$$\sigma_{V_{EI}SI} = (\Delta T)^2 \sum_{i=1}^{n}\sum_{j=1}^{n} (w_i w_j \rho_{V_{EI}i,V_{EI}j} \sigma_{V_{EI}i} \sigma_{V_{EI}j}) \tag{5.18}$$

In equation 5.17 and 5.18, n is the number of periods at which V_{EI} is computed, ΔT is the size of the vibration period discretization (the step-size used in the integration). W_i and W_j are integration weights. The notation $V_{EI}SI$ represents $V_{EIa}SI$, $V_{EIr}SI$, $MV_{EIa}SI$ or $MV_{EIr}SI$, and V_{EI} indicates V_{EIa} or V_{EIr}. $\mu_{V_{EI}}$ and $\sigma_{V_{EI}}$ are the predicted mean and standard deviation (sigma) of V_{EIa} or V_{EIr}, respectively, which can be obtained from their GMPEs. The further formula derivation can be referred to the study of Bradley et al. (2009).

5.5 **Conclusion**

First, the empirical (observed) correlation coefficients of energy-based intensity measures (V_{EIa} and V_{EIr}) for ground motions are calculated. Then the predictive models for the correlation coefficients are proposed in this study. The proposed models are demonstrated to better fit the observed correlation coefficients of V_{EIa} and V_{EIr}, compared to the two existing models that have been used for spectral acceleration (S_a). Three cases associated with predictive models of correlation coefficients of V_{EIa} and V_{EIr} spectral values are investigated in this study: the case with two different periods and the same horizontal orientation; the case with the same period and two horizontal orthogonal orientations; the case with two different periods and two horizontal orthogonal orientations.

The proposed predictive models of correlation coefficients of V_{EIa} and V_{EIr} are very useful in application of ground motion selection and modification in terms of spectrum-matched and amplitude-scaled methods. They can be used not only to develop the conditional mean spectrum of V_{EIa} and V_{EIr} but also to calculate the target values of some energy-related scalar intensity measures, such as $V_{EIa}SI$, $V_{EIr}SI$, $MV_{EIa}SI$ and $MV_{EIr}SI$. Note that the resulting models are strictly empirical and thus should not be extrapolated beyond the range over which the observation values were fit. In other words the proposed predictive models of correlation coefficients should be used for period range of 0.05-5 s, earthquake magnitude range of 5-7.9, fault-to-site closest distance less than 200 km, and site class with B, C and D categorized according to NEHRP.

6 A Matlab implementation of Ground Motion Selection and Modification (GMSM)

6.1 Introduction

Due to the rapid development of computational power and evolution of engineering software, nonlinear dynamic analysis of structures, even of complex structures, has been made feasible in the last decade and becoming more and more prevalent in codes and regulatory documents prescribing design and analysis. In the procedure of performing nonlinear dynamical analyses, the uncertainty of nonlinear structural response usually originates from some aspects, e.g., the material properties, the design assumptions and the earthquake-induced ground motions. Among all these sources of uncertainty, the ground motions have the largest impact on the nonlinear dynamic structural response. Therefore the selection and modification method of ground motions is considered as a critical issue in the assessment of seismic structural response obtained from numerical nonlinear dynamic analyses of structures. Consequently, considerable efforts have been paid in these years in developing suitable Ground Motion Selection and Modification (GMSM) methods for selecting an appropriate set of ground motions that can be representative of the ground motions induced by the future earthquake. In this study we did not create new GMSM methods, but the practical application of ground motion selection using various widely used GMSM methods in terms of various IMs is underlined.

In order to facilitate engineers and researchers in selecting and modifying the real ground motions accelerograms using the IMs we have investigated in the previous chapters, the author herein in this chapter developed a Matlab implementation of GMSM, which is called RELACS (REaL ACcelerogram Selection). The RELACS compiled with the new database, consisting of NGA, SISMA and ESGM, was developed by the author was programmed with Matlab R2010b of Mathworks, creating a stand-alone application which can be run on PCs with or without Matlab installed. Selecting real accelerograms with GMSM methods in terms of energy-based IMs for structural dynamic analyses can be easily and conveniently achieved

using the RELACS. This Matlab implementation can be very useful in the application of structural seismic assign and assessment.

6.2 **GMSM methods used in the RELACS**

According to recent researches (e.g., Beyer and Boomer 2007, Buratti, 2008), the GMSM methods based on a given earthquake scenario and a given ground motion scenario (selection according to spectral matching or spectral ordinates) have been investigated in terms of the accuracy and precision of predicting EDPs of structures (see their definitions in Haselton et al., 2009). When earthquake scenario-based selection is conducted, records which fall in bins around central values of seismic parameters are selected. The three most seismic parameters are magnitude, source-to-site distance, and site class. By selecting according to spectral matching and duration one tries to identify records which match best the target spectra after scaling of records. In current aseismic codes uniform hazard spectra is considered as the target spectra. However the commonly used Uniform Hazard Spectrum (UHS) recently is shown to be an unsuitable target for this purpose, as it conservatively implies that large-amplitude spectral values will occur at all periods within a single ground motion (see Baker 2011). The conditional mean spectrum is proposed by Jack W. Baker to be as the target spectra, demonstrated to be an effective spectrum, to more accurately predict structural seismic response obtained from nonlinear dynamic analyses.

Therefore the RELACS is composed of two main steps: preliminary ground motion selection according to geophysical seismic parameters (earthquake scenario-based selection), and further ground motion selection and modification according to elastic structural response spectrum or ordinates (ground motion scenario-based selection). The GMSM methods used in the RELACS is firstly introduced in this subsection.

6.2.1 GMSM according to geophysical seismic parameters

The most traditional selection parameters used in earthquake-scenario selection are magnitude (M), source-to-site distance (R) and site classification(S). They are not only the most common parameters related to an earthquake, but also reflect the frequency content, spectral shape and

duration of the records, which have significant impact on the structural response. In this process ground motions whose magnitude and distance fall in bins around central values of the target values of them are selected in the format M±ΔM and R±ΔR. Stewart et al. (2001) recommended ΔM as a $0.25M_w$, while Bommer and Acevedo (2004) suggested as $0.2M_w$. The earthquake scenario pair (M, R) can be defined by performing and Probabilistic Seismic Hazard Analysis (PSHA) disaggregation for an investigated site in the framework of Probabilistic Performance-based earthquake engineering. The scenario pair (M, R), maybe more than 1 pair, dominating the hazard at the given site is chosen to be design earthquake scenario. The earthquake scenario can also be determined by conducting Deterministic Seismic Hazard Analysis (DSHA). This approach is straightforward, and strong motion parameters are estimated for maximum credible earthquake, which is assumed to occur at the closest possible distance from the investigated site. It should be noticed that for this approach nothing is being said about the probability of occurrence.

On the other hand some researchers (e.g. Bazzuro et. al. 1998, Shome et al. 1998 and Jalayer 2003) argued that design earthquake scenario of (M, R) pair matching is not important if the records are scaled in terms of S_a (T_1). Furthermore Baker and Cornell (2005) confirmed the above conclusion, and in particular it states that the closest source-to-site distance is statistically insignificant to the structural response, while the earthquake magnitude shows some significance. Based on the above observation the magnitude of can be considered as an acceptable criterion in the preliminary refinement of ground motion selection, while the distance in design earthquake scenario can be considered as a supplementary criterion in the preliminary selection of ground motions.

Since the site classification can affect both the amplitude and spectral shape of ground motion records, it is also taken into account as a criterion for selection of records. This parameter is generally measured by average shear-wave velocity at the uppermost 30m (V_{S30}) of the site. Bommer and scott (2000) noticed that additional matching criterion, namely, matching site classification, can significantly reduce the number of candidate records compared to that only using (M, R) pair to match. Based on this observation Boomer and Acevedo (2004) recommended that if a reasonable number of records matching the magnitude and distance

criteria cannot be found in record database it is advisable to relax the matching criterion for site classification by adding either side of site classification considered.

Some other criteria e.g. rupture mechanism and duration, could also be considered into the design earthquake scenario in the process of preliminary selection of records. However they are all less important compared to M, R and S.

6.2.2 GMSM according to elastic structural response spectrum or ordinates

This study just focuses on the elastic ground motion parameters, and the vertical component issue is not included herein. The following subchapter will give a review of some representative GMSM methods, which are involved in the RELACS. Four groups of GMSM methods are described in the following context: 1), $S_a(T_1)$ Scaling with Bin Selection; 2), Selection and Scaling Using Uniform Hazard Spectrum (UHS); 3), Selection and Scaling Using Conditional Mean Spectrum (CMS); 4), Selection and Scaling Using Proxy for CMS. The classification is consistent with the report of Curt B. Haselton et al. (2009).

6.2.2.1 S_a (T_1) Scaling with Bin Selection

One widely used ground motion selection and modification proposed by Shome et al. (1998) is $S_a(T_1)$ Scaling with Bin Selection, which is to aim to obtain a set of ground-motion records for nonlinear structural dynamic analysis that will result in an accurate estimate of the cumulative distribution function (CDF) and an accurate estimate of the median of the engineering demand parameter (EDP) of interest for a given structure, earthquake magnitude (M), source-to-site distance (R), site classification (S) and style of faulting (F) and first-mode spectral acceleration ($S_a(T_1)$).

Compared to the methods for which a suit of records are chosen from a narrow magnitude and distance interval displaying wide dispersion, it is observed from Shome et al. (1998) that when the records in each bin (within a magnitude or distance interval) are scaled to the spectral acceleration estimated by the established attenuation relationship (now it is preferred to term ground motion prediction equation, GMPE, described in chapter 4) at the fundamental frequency of the structure, the structural response evaluated with these scaled input records

displays the same mean and reduced variability. In the study of Shome et al. (1998) Scaling to $S_a(T_1)$ has been observed reducing the EDP (engineering demand parameter) dispersion by a factor of about 2, therefore reducing the number of runs required to estimate the median EDP by a factor of about 4.

The procedure of this method is as following: first, decide on an M-R-S-F bin that is consistent with the given scenario, shown as in Fig. 6.1. Then Select desired number of records randomly from the bin of records. Finally, scale the records to the target $S_a(T_1)$, shown as in Fig. 6.2. This GMSM method for nonlinear dynamic analysis can be also performed for calculating the annual probability of exceeding a specified EDP of interest.

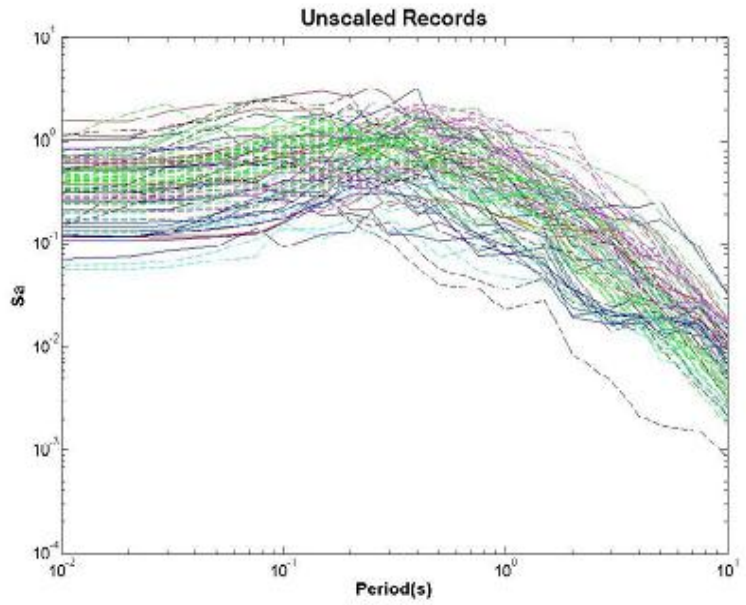

Fig. 6.1 (from Haselton et al.,2009). Spectrum of bin of records for earthquake events which have magnitude Mw= 7 and distance R = 10km at stiff soil sites (Vs ≈ 400 m/s).

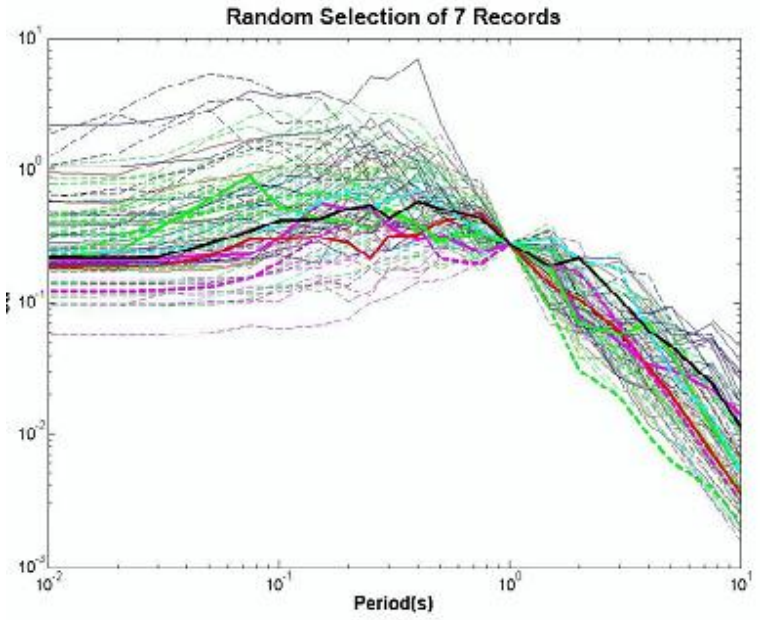

Fig. 6.2 (from Haselton et al.,2009): Records from the bin of records in Fig. 6.1 are scaled to a target spectral acceleration 0.28g at period, T =1 sec and 5% damping. Seven records are selected randomly from this bin for nonlinear time-history analysis of structures and are shown in thick lines.

6.2.2.2 Selection and scaling using uniform hazard spectrum

Uniform hazard spectrum is the acceleration amplitudes at series of time periods where the acceleration amplitudes at each time period has the same probability of exceedence in certain interval years, which could be computed by probabilistic seismic hazard analysis. This spectrum is usually used to define seismic hazard in many national seismic codes at a given site, and the ground motions whose response spectrum are close to this target uniform hazard spectrum are selected as loading for structural dynamic analyses. In the worldwide, the codes of many countries describe relatively similar procedures but not specific provision for selecting ground motions for nonlinear dynamic analysis using uniform hazard spectrum.

One representative method of Selection and Scaling Using Uniform Hazard Spectrum (UHS) is that proposed in the Eurocode 8 (2003). The provisions for the ground motion selection and scaling given by the code in prEN 1998-1 are described as the following:

Once the reference spectrum has been defined, EC8—Part 1(General rules, seismic actions and rules for buildings) allows the use of any form of accelerograms for structural assessment; i.e., real, artificial or obtained by simulation of seismic source, propagation and site effects.

To comply with Part 1 the set of accelerograms, regardless its type, should basically match the following criteria:

3.2.3.1.2 (4):

a) *a minimum of 3 accelerograms should be used;*
b) *the mean of the zero period spectral response acceleration values (calculated from the individual time histories) should not be smaller than the value of agS for the site in question.*
c) *in the range of periods between 0.2T1 and 2T1, where T1 is the fundamental period of the structure in the direction where the accelerogram will be applied; no value of the mean 5% damping elastic spectrum, calculated from all time histories, should be less than 90% of the corresponding value of the 5% damping elastic response spectrum.*

In the case of spatial structures：

3.2.3.2 (2) P Such spatial models shall be consistent with the elastic response spectra used for the basic definition of the seismic action in accordance with 3.2.2.2 and 3.2.2.3 (calculation of horizontal and vertical elastic response spectrum).

3.2.3.1.1 (2) P When a spatial model of the structure is required, the seismic motion shall consist of three simultaneously acting accelerograms. The same accelerogram may not be used simultaneously along both horizontal directions. Simplifications are possible in accordance with the relevant Parts of EN 1998.

4.3.3.4.3 (3) If the response is obtained from at least 7 nonlinear time-history analyses with ground motions in accordance with 3.2.3.1, the average of the response quantities from all of these analyses should be used as the design value of the action effect E_d in the relevant verifications of 4.4.2.2. Otherwise, the most unfavourable value of the response quantity among the analyses should be used as E_d.

6.2.2.3 Selection and scaling based on Conditional Mean Spectrum

The commonly used Uniform Hazard Spectrum (UHS) is found to not be a suitable target spectrum to match. In fact the UHS is an envelope of spectra from a suite of earthquakes with the same exceeding probability of spectral values in interval years for a certain site. So a single ground motion is unlikely to cause large-amplitude spectral values at all periods

simultaneously. The UHS may be dominated by two or more than two earthquake scenarios, so UHS spectral amplitudes at different periods are caused by differing earthquake events. Therefore the UHS can't be representative of spectra of an individual ground motion, and it can induce a conservative result for structural response when ground motions matching UHS are used for nonlinear dynamic analyses for structures.

Due to the disadvantage of UHS an alternative spectrum, Conditional Mean Spectrum (CMS), proposed by Jack Baker is used to be as target spectrum for matching. The CMS provides the expected response spectrum where the spectral acceleration values at all periods are conditioned on occurrence of a target spectral acceleration value at the period of interest. Therefore the CMS takes into account the correlation between response spectral values at different periods. The probability of exceeding some certain engineering demand parameter value (P[EDP]) can be consistently evaluated by integrating the results of structure dynamic analysis with seismic hazard curve resulted from probabilistic seismic hazard analysis (PSHA), where the target spectral acceleration at the period of interest serves as an important link for these two process (e.g., Bazzurro and Cornell 1994; Cornell et al. 2002; Cornell and Krawinkler 2000). The ground motion selection and modification method matching CMS is presented the most robust GMSM method to predict the accurate MIDR with low dispersion (Haselton et al., 2009), since the spectral shape of target spectrum matched is regarded to be able to more effectively capture hazard level. It also widens the range of acceptable records for analyses because the selected records do not necessarily have appropriate magnitude, distance and ε value. Conversely, the UHS does not allow for such statements.

The following is shortly introduction about the development of CMS and procedure to match CMS:

First the CMS should be calculated for CMS matching method. The spectral value of CMS at period Ti can be calculated with following equation:

$$\ln Sa(T_i) = \overline{\ln Sa}(M, R, T_i) + \sigma_{\ln Sa}(T_i) \cdot \bar{\varepsilon}(T_i) \tag{6.1}$$

,where $\overline{\ln Sa}(M, R, T_i)$ and $\sigma_{\ln Sa}(T_i)$ are predicted mean and standard deviation of logarithmic spectral acceleration at period T_i, which can be evaluated by ground motion prediction

equation (termed as attenuation relationship in the past) given magnitude, distance, period, etc. In the equation, $\bar{\varepsilon}(T_i)$ can be computed by the following two equations:

$\bar{\varepsilon}(T_i) = \rho \cdot \bar{\varepsilon}(T_1)$

$$\rho = 1 - \cos\left(\frac{\pi}{2} - \left(0.359 + 0.163 I_{(T_{\min} < 0.189)} \ln\frac{T_{\min}}{0.189}\right)\ln\frac{T_{\max}}{T_{\min}}\right) \tag{6.2}$$

, where $\bar{\varepsilon}(T_1)$ is target ε associated with $S_a(T1)$ resulted from PSHA disaggregation; T_{min} and T_{max} are the smaller and larger values of T_1 and T_i; and T_1 is the period of interest (e.g. first-mode period of structure, but it could be other period in some case such as floor accelerations are more sensitive to higher-mode excitation than to first-mode excitation); $I_{(T_{\min} < 0.189)}$ is an indicator equal to 1 if $T_{\min}$ is smaller than 0.189 and equal to 0 otherwise. The conditional mean spectrum could be developed by repeating computing $S_a(T_i)$.

Then after developing CMS, the acceleration spectrum of ground motion needs to be scaled for matching CMS. There are two ways mentioned by the Baker (2011) to scale the acceleration spectra of records to match the conditional mean spectrum. The first method is to scale each ground motion so that its $S_a(T_1)$ (T_1 could be the fundamental period of structure) is equal to the target $S_a(T_1)$ from the CMS. So the scaled factor (α) could be computed by the following equation.

$$scale\_factor(\alpha) = \frac{Sa_{CMS}(T_1)}{Sa(T_1)} \tag{6.3}$$

The other method is to scale each ground motion so that the average response spectrum over the periods of interest equals to the average of the target spectrum over the same periods. For this case, a given ground motion's scale factor is

$$scale\_factor(\alpha) = \frac{\sum_{j=1}^{n} Sa_{CMS}(T_j)}{\sum_{j=1}^{n} Sa(T_j)} \tag{6.4}$$

Finally the scaled ground motions are going to match CMS for selecting a suit of ground motions used to run nonlinear dynamic analyses. The SEE, sum of the squared difference

given by the following equation, is the criterion to determine the degree of matching to CMS. That is, a smaller value of SEE of a ground motion with respect to CMS indicates this ground motion is more compatibility with CMS.

$$SSE = \sum_{j=1}^{n} (\ln Sa(T_j) - Sa_{CMS}(T_j))^2 \tag{6.5}$$

6.2.2.4 Selection and Scaling Using Proxy for Spectral Shape

The selecting method using proxy for spectral shape is similar to the methods of selection and scaling using CMS, the only except is that it uses a proxy, that is ε, which has been found a good predictor of the spectral shape of CMS (Baker and Cornell 2006). This method is simpler than CMS method, since it does not need to match the response spectrum of ground motions to the target CMS other than simply use an indicator of spectral shape as a judgement of matching. For this method the ground motions whose ε of response spectrum is close to the target ε are selected and scaled to the target ε. The ε at a period is defined as the number of logarithmic standard deviations that S_a at this period of a ground motion subtracts its median value provided by the GMPE (ground motion prediction equation or attenuation law). Accordingly target ε can be determined through PSHA.

6.3 **Development of new ground motion database in the RELACS**

In the study three major databases, including NGA (Next generation attenuation) database, SISMA (Site of Italian Strong Motion Accelerograms) database and ESGM database (European Strong-motion Database, in this study it is referred to as ESGM), are compiled in order to make a larger available database for the Matlab implementation of GMSM. Besides the ground motions compiled in this RELACS, the users can also upload their own available database in the implementation for selecting and scaling ground motions.

The first database, NGA database, is the most widely used earthquake records database by worldwide researchers. In this author-developed GMSM Matlab implementation, the NGA database consists of the majority ground motions among the ground motion database. The NGA database (http://peer.berkeley.edu/nga/index.html) contains a large set of records and one of the most comprehensive groups of meta-data, including different magnitude and

distance measures, various site characterizations, earthquake source data, etc. Currently, this data set consists of 3551 available multi-component records from 173 shallow crustal earthquakes with magnitude range of 4.2-7.9. The more details about NGA database can be referred to the study of Chiou et al. (2008).

The second database is SISMA that is the abbreviation of Site of Italian Strong Motion Accelerograms. This database consists of 247 three-component corrected motions recorded at 101 stations from 89 earthquakes that only occurred in Italy from 1972 to 2002. This database is the researching result of cooperative project between Sapienza University of Rome and University of California at Los Angeles. The work of Scasserra et al. (2008) provides more details about this database.

The third database, that is ESGM, developed in the new CD ROM of European and Middle Eastern strong-motion data, contains 462 three-component records from 110 earthquakes recorded from 261 stations in European and Middle Eastern region. The further details can be referred to the research of Ambraseys et al. (2004).

In this research we did not create any ground motion database we only compile these three record databases to achieve more available ground motion records. However there are some recordings existing in more than one of these three databases. Since the NGA database provides more comprehensive meta-data, we considered NGA database as the priority, then SISMA is followed and finally ESGM. In particular: if the records recorded from the same station and the same earthquake not only exist in NGA but also present in SISMA and/or ESGM, we keep the records in NGA database and delete the records in SISMA and/or ESGM database; if the records simultaneously exit in the SISMA and ESGM, we remain those in SISMA and remove the records in ESGM.

Along these lines, in other words all the records from NGA database should be included in our new compiled database. However the author found that in NGA database the accelerograms of some records cannot be accessible even from the original resource, on the newest website of PEER NGA database. In addition, some records only have one horizontal

component of ground motion accelerogram. Therefore the author remained the records that have at least two horizontal components of accelerograms. In the end, 3518 records from NGA database have been remained as a part set of the author-compiled ground motion database rather than 3551 records. After removing the same records as those in NGA database, 232 records coming from the SISMA database are compiled in our new database. In the same way 307 recordings of ESGM are remained. The new compiled ground motion database is composed of 4057 records recorded from 265 Earthquake events. Note that in SISMA database the records which have only one horizontal component of accelerogram or lack both two horizontal components of accerograms are also removed from the new compiled database.

6.4 **Intensity measures in the RELACS**

A variety of intensity measures have been investigated in the previous chapters. In order to using them into practical ground motion selection, it is necessary to calculate the values of these intensity measures of ground motions. Therefore in the programmed Matlab implementation, RELACS, all values of various intensity measures of each record in the complied database (4057 records) have been calculated and are available for selecting. The intensity measures include the spectral values of three kinds of response spectra and the values of scalar IMs of ground motions. The three response spectra are acceleration spectrum, the spectrum of absolute input energy equivalent velocity and the spectrum of relative input energy equivalent velocity. The scalar IMs include PGA, PGV, PGD, AI, CAV, I_a, I_c, FI, I_v, CAD, SED, I_d, ASI, VSI, I_H, $V_{EIa}SI$, $V_{EIr}SI$. Their definitions are referred to Table 2.2 and Table 2.3.

Energy-based IMs have been initiatively applied in the GMSM methods in the RELACS. That is because most efforts of providing the necessity and possibility of selecting and scaling ground motions using the energy-based IMs have been done in the previous chapters. They are include: Chapter 2 and Chapter 3 investigating energy-based parameters in terms of efficiency, sufficiency and sensitivity of predicting the Engineering Demand Parameters (EDPs); Chapter 4 developing the Ground Motion Prediction Equation (GMPE) of these

parameters; and Chapter 5 evaluating the correlation of spectral values of these parameters for multicomponent ground motions.

6.5 **The application procedure of the RELACS**

As mentioned above the Matlab implementation of GMSM, RELACS, consists of two main steps: preliminary ground motion selection according to geophysical seismic parameters, and further ground motion selection and modification according to elastic structural response spectrum or ordinates. In this subchapter the use of the RELACS will be introduced.

The Fig.6.3 is the screenshot showing the first step of the RELACS, namely, Preliminary Ground Motion Selection. In this window users should first upload the three author-defined ground motion databases or user-defined ground motions database. And then users can select ground motions based on some geophysical parameters. In the bottom of the screenshot some information of the selected ground motion records are shown, including Sub-Database Name, Record Sequence Number in each Sub-Database, Name of Earthquake (Ground Motion), the Time of Earthquake Occurrence (Year/Month/Day And Hour/Minute), Hypocenter Latitude, Hypocenter Longitude, Station Name, Magnitude (equal to M_w or M_L if M_w is not available), M_w, M_s, M_L, M_b, M_o(Dyne. cm), Mechanism based on rake angle, Earthquake in Extensional Regime (1=Yes; 0=No), Epicenter Distance, Hypocenter Distance, Joyner-Boore Distance, Closest Distance, FW/HW Indicator, GMX's C1, GMX's C3, Depth, NEHRP Soil Type based on V_{S30}, Europe Soil Type, Preferred V_{S30} (M/S), HP-H1 (Hz), HP-H2 (Hz), HP-V (Hz), LP-H1 (Hz), LP-H2 (Hz), LP-V (Hz), Lowest Usable Freq-H1 (Hz), Lowest Usable Freq-H2 (Hz), H1-PGA, H1-PGV, H1-PGD, H2-PGA, H2-PGV, H2-PGD, V-PGA, V-PGV, V-PGD. In the mean while some other functions, such as plotting and outputting the outcome of ground motions, of the RELACS are available as well in this window.

Here is an example of processing the first step of the RELACS. Fig. 6.3 shows that using Preliminary Ground Motion Selection a set of 363 records meeting the limitation requirement for some geophysical parameters are selected. In particular: 310 records come from NGA database; 30 records come from SISMA database; and 23 records originate from ESGM

database. In the Fig.6.3 the main menu, located on the left-top of this screenshot, provides users options to plot time history and response spectrum of acceleration, velocity and displacement of three components. The Fig. 6.4(a) and Fig. 6.5(a) show the window of choosing the records to plot their time history and response spectrum, respectively. Then the corresponding plots of time history and response spectrum of the records chosen with Fig. 6.4(a) and Fig. 6.5(a) are presented in Fig. 6.4(b, c, d) and in Fig. 6.5(b, c, d), respectively. The data output of time history and response spectrum of records are provided as well in this window, shown in Fig. 6.6.

After filtering ground motions that do not satisfy the requirement of geophysical paramters, the RELACS come to the second step, namely selecting and scaling ground motions in terms of elastic response spectra or spectral ordinates. Fig. 6.7 shows the window where users choose which elastic response spectrum or spectral ordinate to follow. In this step the GMSM methods are categorized into three groups. The details of each group of GMSM methods are given by Table 6.1. In the Table 6.1 the procedure of Energy-based selection methods follows the same process of S_a-based selection methods that have been introduced in the subchapter 6.1.2. In particular: the methods of Scaling to V_{EIa}, V_{EIr}, $V_{EIa}SI$ and $V_{EIr}SI$ have the same procedure as the method of scaling to S_a (T_1) in the first group of GMSM methods; the methods of matching the Conditional Mean Spectrum of V_{EIa} and V_{EIr} have the same procedure as the method of matching Conditional Mean Spectrum of Sa. The whole third group of methods follows the same procedure of selection and scaling as the method of scaling to S_a (T_1) in the first group of methods.

Table 6.1 The list of GMSM methods in the RELACS

Main groups of GMSM methods	Sub-types of GMSM methods
Group one: S_a-based selection methods	1. Scaling to $S_a(T_1)$ 2.Matching Uniform Hazard Spectrum 3.Matching Conditional Mean Spectrum 4. Selection and scaling using Proxy for CMS
Group two:	1.Scaling to the Absolute Input Energy Equivalent

Energy-based selection methods	Velocity 2.Scaling to the Relative Input Energy Equivalent Velocity 3.Matching the spectrum of Absolute Input Energy Equivalent Velocity 4.Matching the spectrum of Relative Input Energy Equivalent Velocity 5.Scaling to $V_{EIa}SI$: Absolute Input Energy Equivalent Velocity Spectrum Intensity 6.Scaling to $V_{EIr}SI$: Relative Input Energy Equivalent Velocity Spectrum Intensity
Group three: Other methods for scalar IMs	Scaling to the value of scalar IMs of PGA: Peak Ground Acceleration AI: Arias Intensity CAV: Cumulative Absolute Velocity I_a: Compound Acceleration-Related IM I_c: Characteristic Intensity PGV: Peak Ground Velocity FI: Fajfar Intensity I_v: Compound Velocity-Related IM CAD: Cumulative Absolute Displacement SED: Specific Energy Density I_d: Compound Displacemnt-Related IM ASI: Acceleration Spectrum Intensity VSI: Velocity Spectrum Intensity I_H: Housner Intensity

The Figures from Fig. 6.8 to Fig. 6.11 are the screenshots of the RELACS windows, showing the examples of the second step of using RELACS with the first group of GMSM methods presented in Table 6.1. Regarding the windows of the second group of GMSM methods, only

the examples of GMSM methods associated with absolute Input energy are presented herein in Fig. 6.12, Fig. 6.13 and Fig. 6.14. For the third group of GMSM methods, that is other methods for scalar IMs, only the window of the RELACS with the method of scaling to I_H is presented, for taking into account that others in the third group of GMSM methods have the same selecting procedure.

The second step of the RELACS also provides the function of allowing users to choose the records from different earthquakes or not. Notice that when selecting ground motions in terms of energy-based or other scalar intensity measures is considered in the RELACS, all default response spectra of Energy-based IMs and default target values of Other Scalar IMs are calculated with the author-developed Ground Motion Prediction Equation (GMPE) proposed in chapter 4. However users also can upload their own target response spectra or set their own target values of these parameters in the RELACS. After finishing selection of ground motions, users can also remove some records that they do not like and select again with the remaining available record pool, where the records coming from the same earthquakes as the deleted ones are removed.

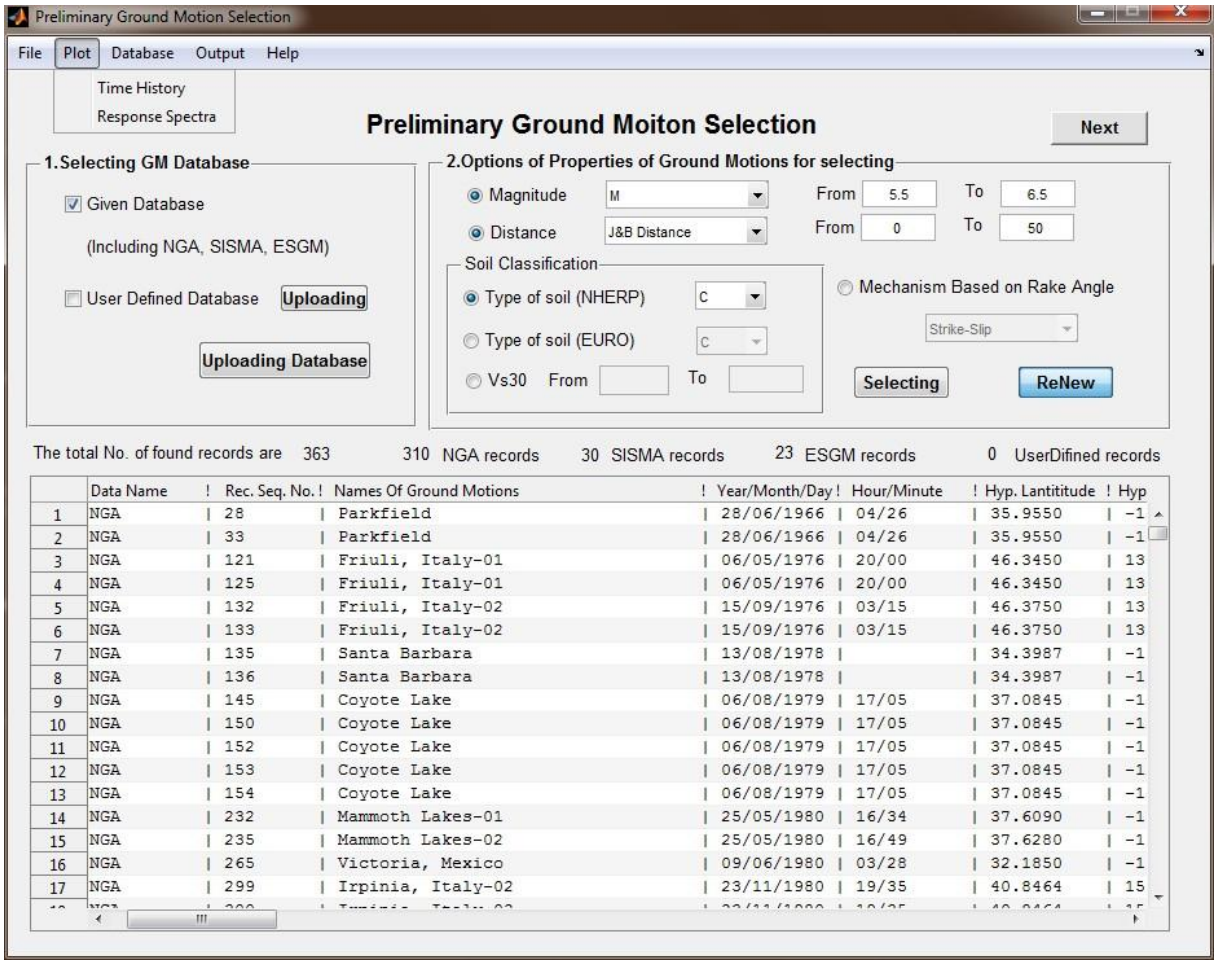

Fig. 6.3 Screenshot of the window of the first step of GMSM method, showing the result of an example of Priliminary Ground Motion Selection

(a)Window of plotting time history

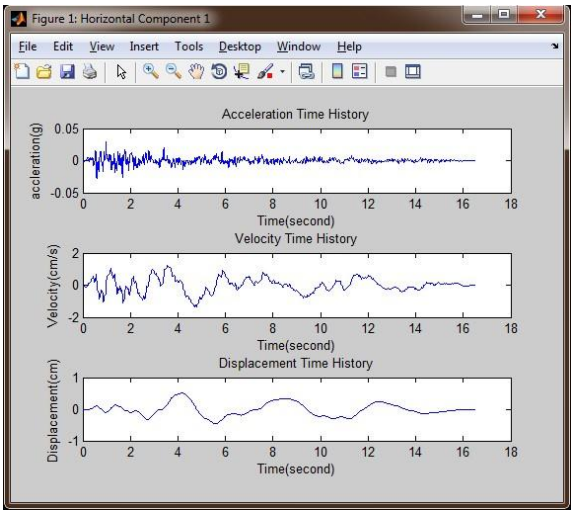

(b) Time history of acc., vel. and dis. of H1

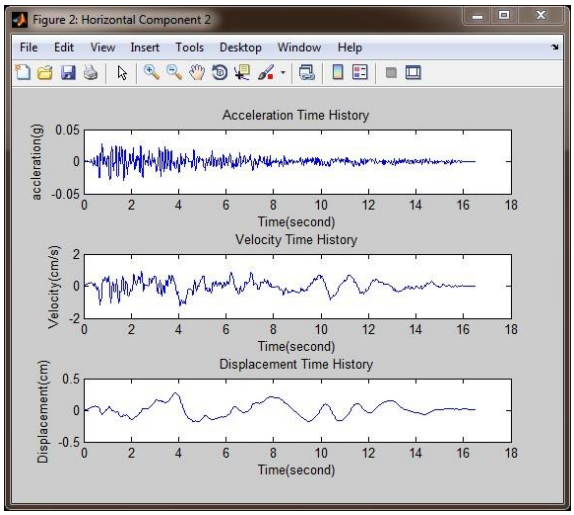

(c) Time history of acc., vel. and dis. of H2

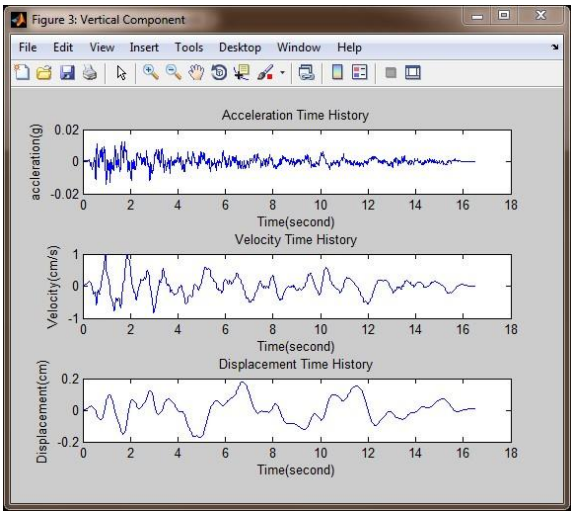

(d) Time history of acc., vel. and dis. of V

Fig. 6.4 Screenshot of function of plotting time history of ground motions

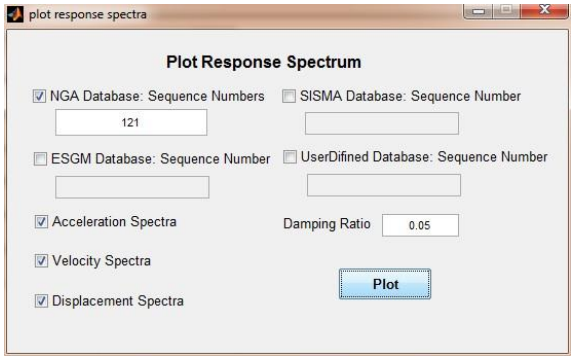

(a) window of plotting response spectrum

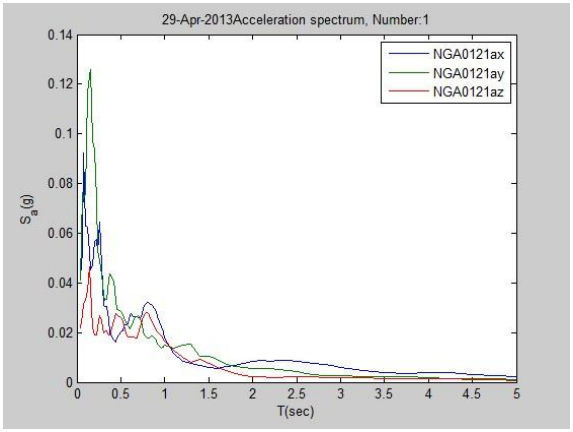

(b) Pseudo- acecleartion response spectrum

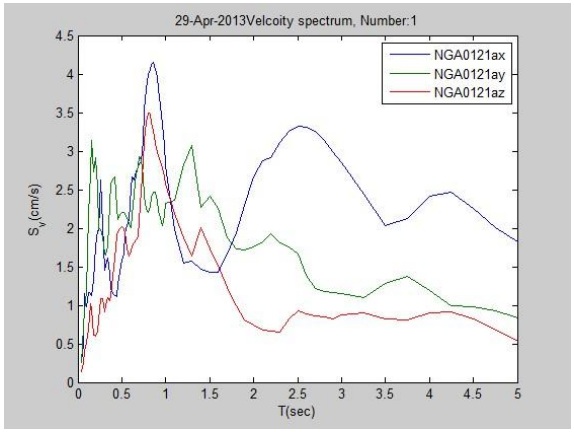

(c) Pseudo- velocity response spectrum

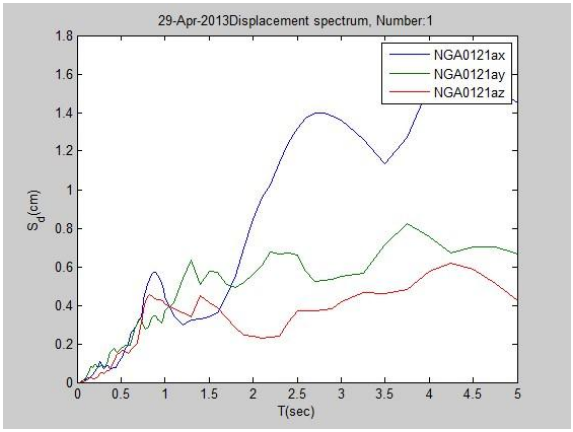

(d) Displacment response spectrum

Fig. 6.5 Screenshot of the widow of plotting response spectra of ground motions and its results

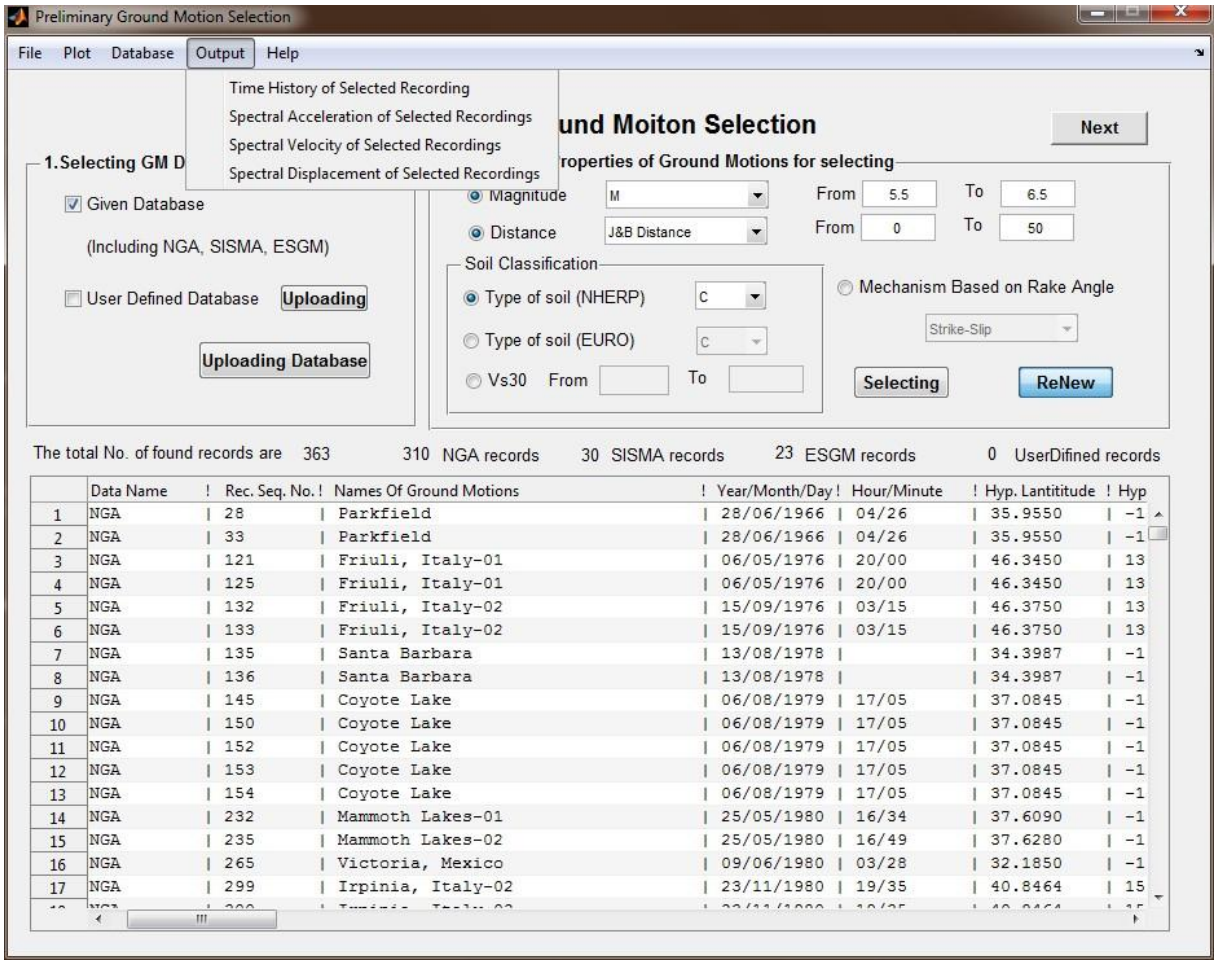

Fig. 6.6 Screenshot of the widow of showing the main menu of outputting time history and response spectrum

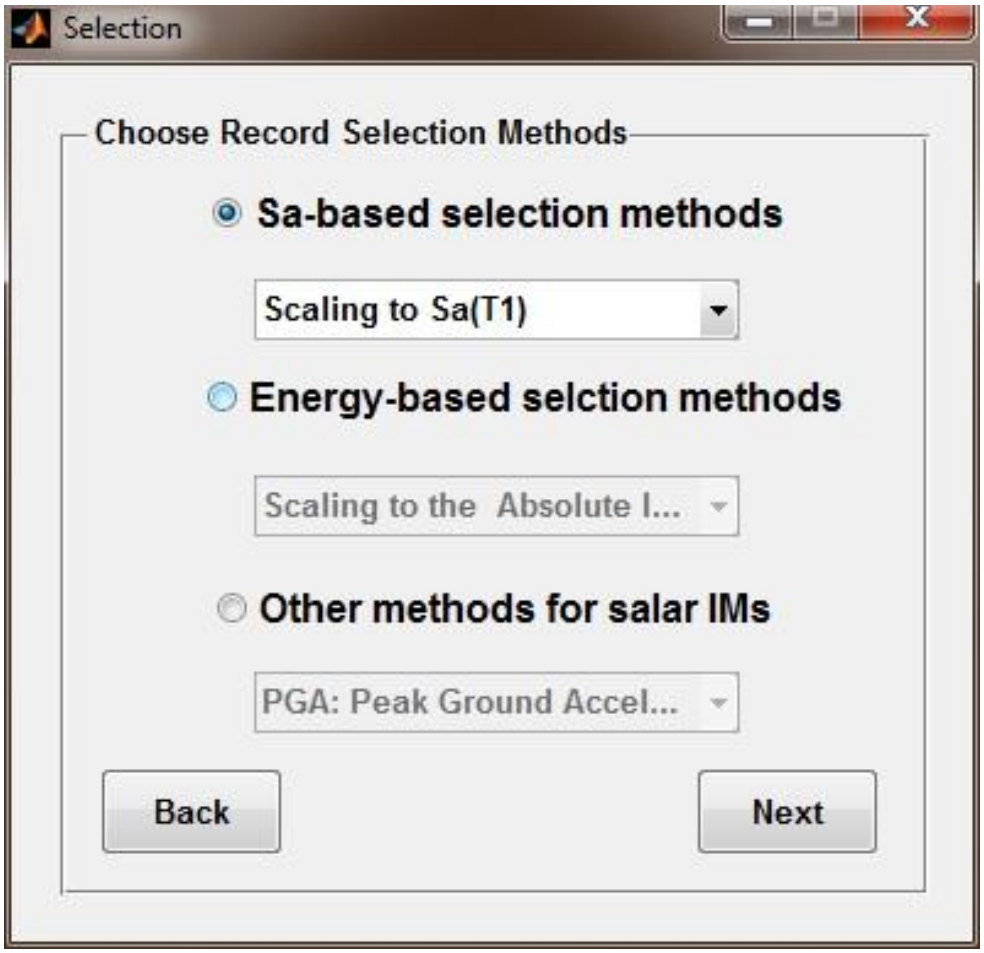

Fig. 6.7 Screenshot of the window of choosing the recording selection methods

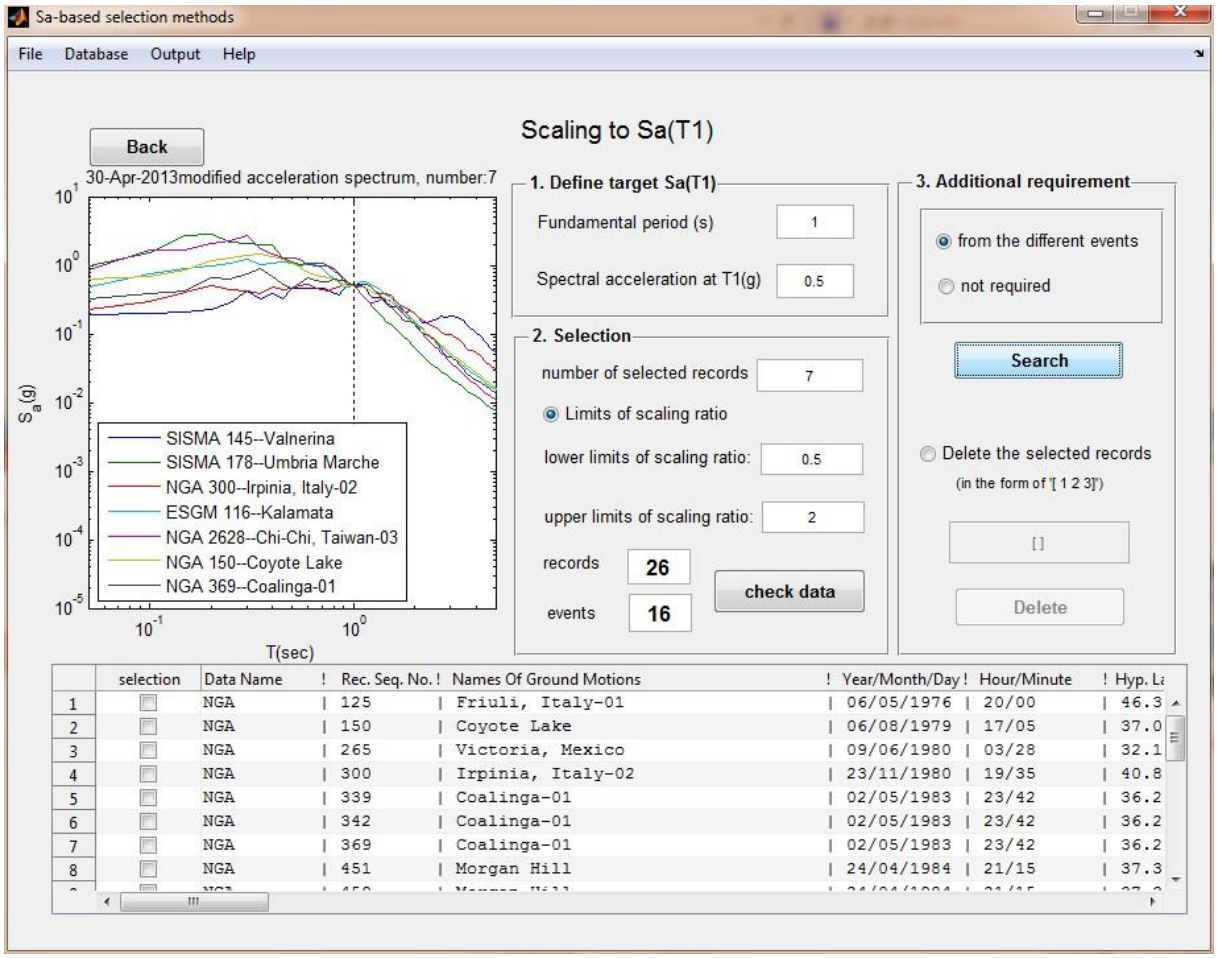

Fig. 6.8 Screenshot of the window of GMSM method of scaling to $S_a(T_1)$

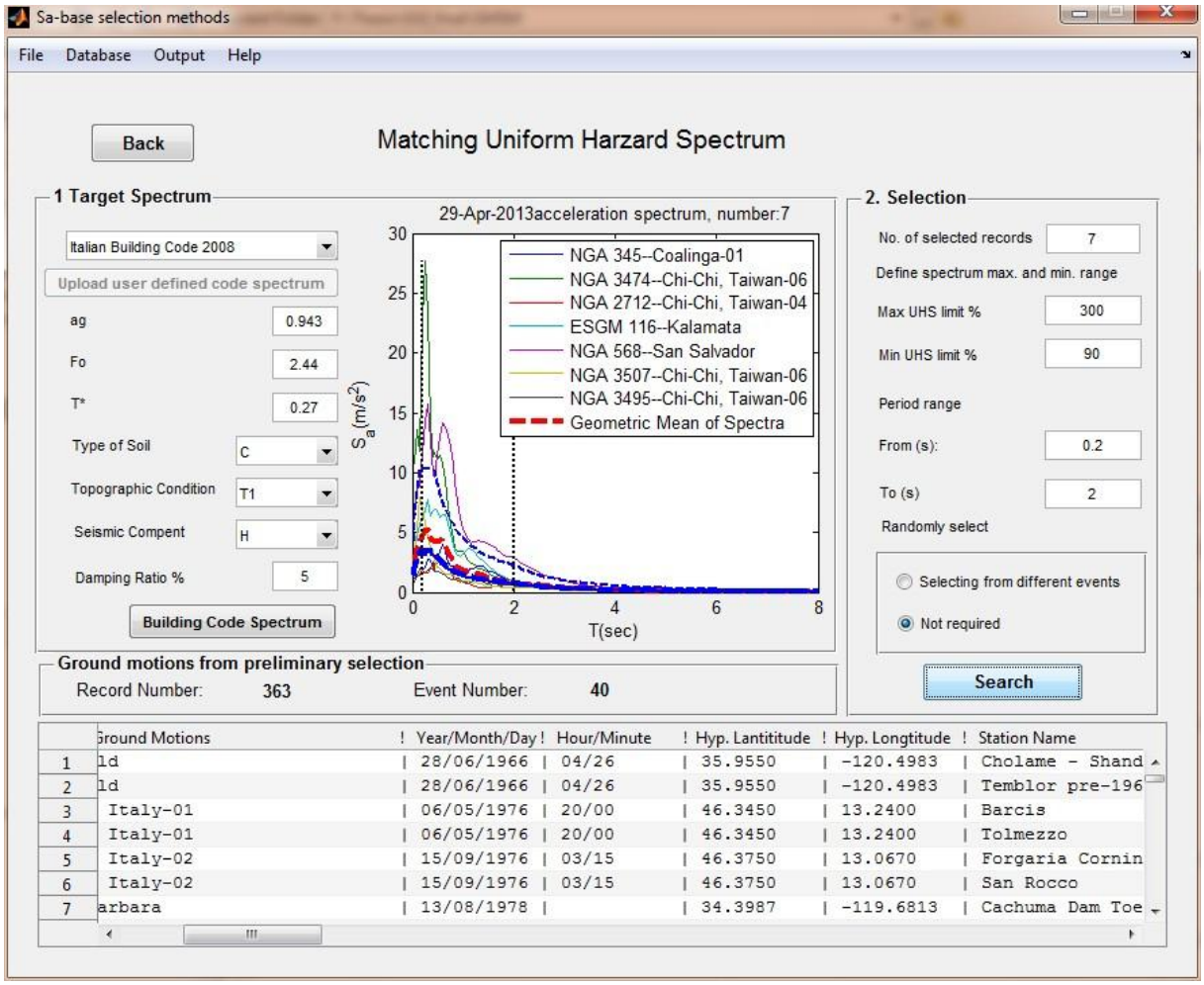

Fig. 6.9 Screenshot of the window of GMSM method of Matching Uniform Hazard Spectrum

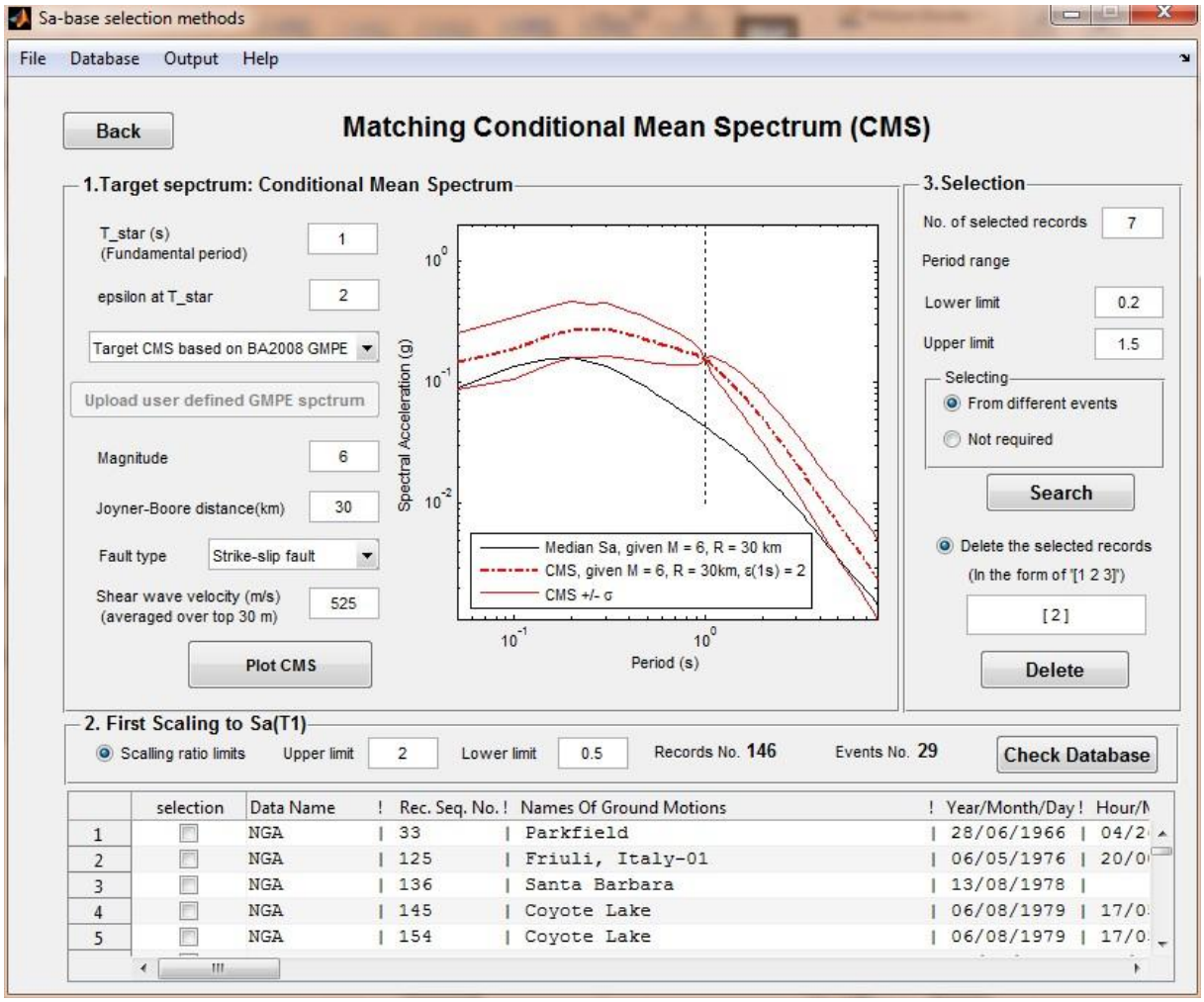
Sa-base selection methods
File Database Output Help
Back
Matching Conditional Mean Spectrum (CMS)
1.Target sepctrum: Conditional Mean Spectrum
T_star (s) (Fundamental period) 1
epsilon at T_star 2
Target CMS based on BA2008 GMPE
Upload user defined GMPE spctrum
Magnitude 6
Joyner-Boore distance(km) 30
Fault type Strike-slip fault
Shear wave velocity (m/s) (averaged over top 30 m) 525
Plot CMS
Spectral Acceleration (g)
Period (s)
Median Sa, given M = 6, R = 30 km
CMS, given M = 6, R = 30km, ε(1s) = 2
CMS +/- σ
3.Selection
No. of selected records 7
Period range
Lower limit 0.2
Upper limit 1.5
Selecting
From different events
Not required
Search
Delete the selected records
(In the form of '[1 2 3]')
[2]
Delete
2. First Scaling to Sa(T1)
Scalling ratio limits Upper limit 2 Lower limit 0.5 Records No. 146 Events No. 29
Check Database
selection Data Name Rec. Seq. No. Names Of Ground Motions Year/Month/Day Hour/M
1 NGA 33 Parkfield 28/06/1966 04/2
2 NGA 125 Friuli, Italy-01 06/05/1976 20/0
3 NGA 136 Santa Barbara 13/08/1978
4 NGA 145 Coyote Lake 06/08/1979 17/0
5 NGA 154 Coyote Lake 06/08/1979 17/0

(a)

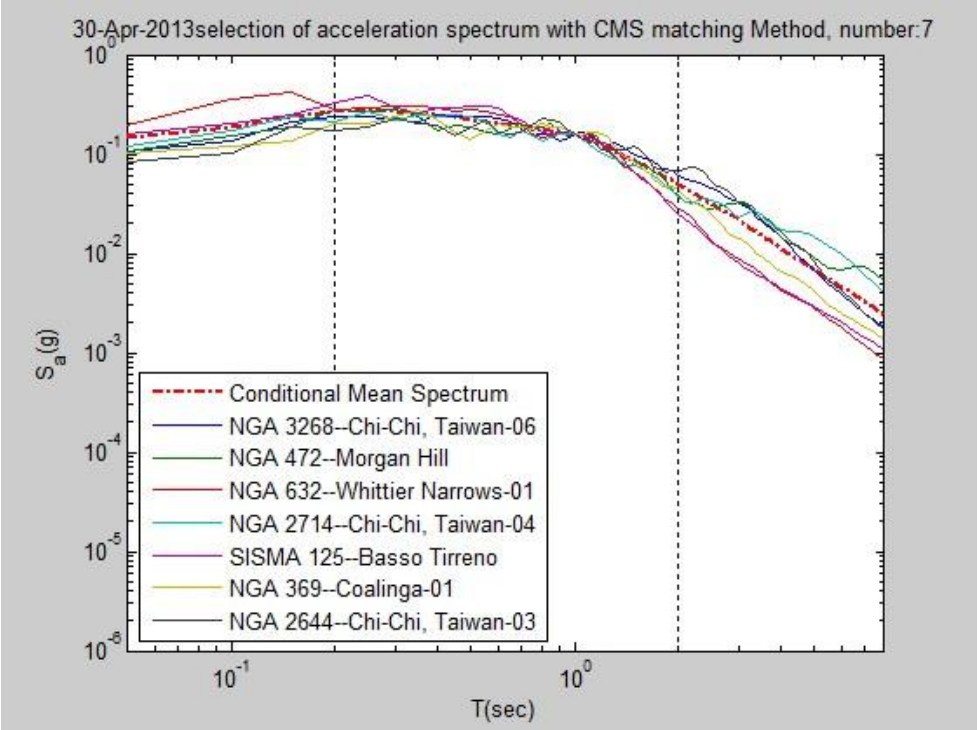

(b)

Fig. 6.10 Screenshot of the window of GMSM method of Matching Conditional mean spectrum (a) and the result of an example (b)

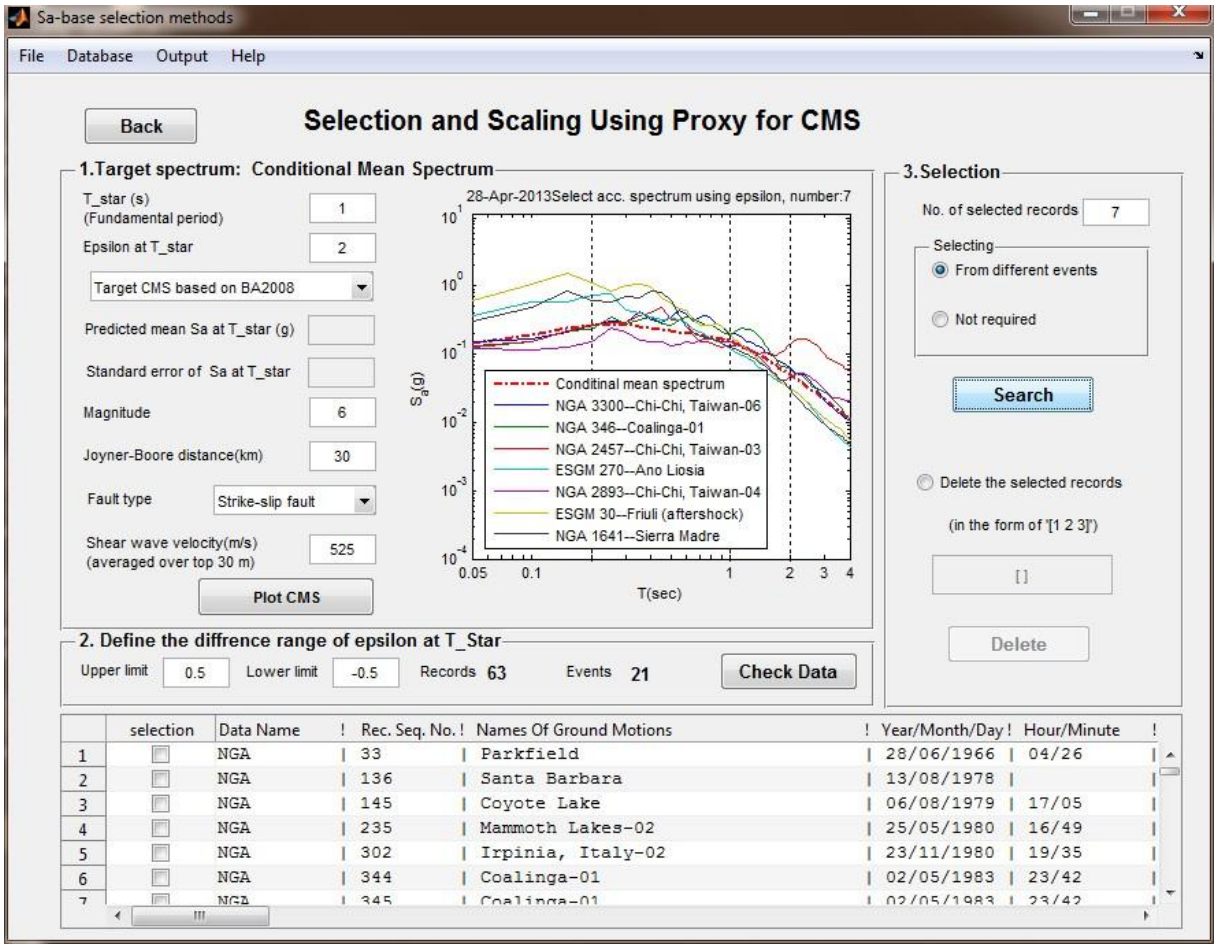

Fig. 6.11 Screenshot of the window of GMSM method of Selection and scaling using proxy for CMS

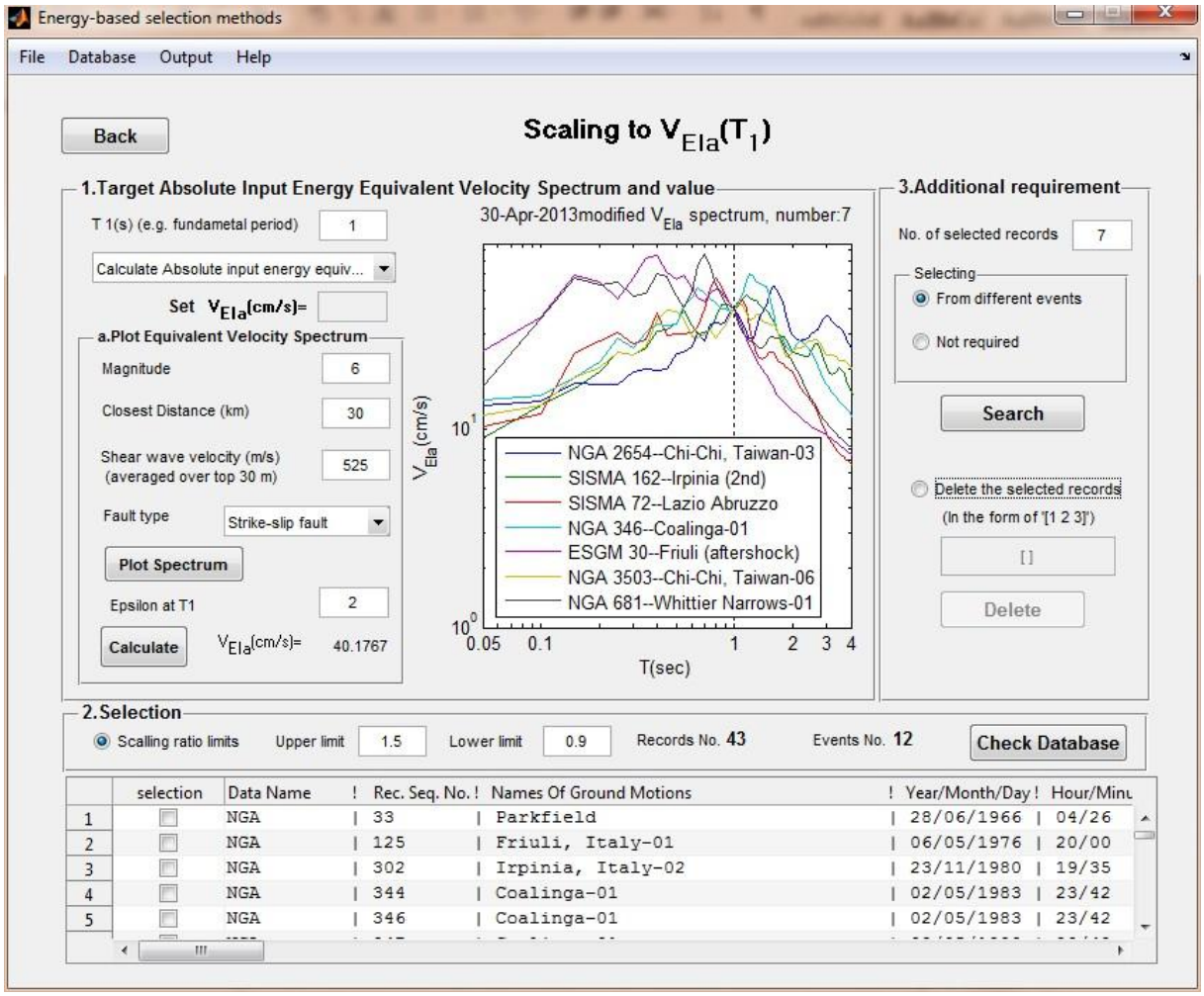

Fig. 6.12 Screenshot of the window of GMSM method of Scaling to $V_{Ela}(T_1)$

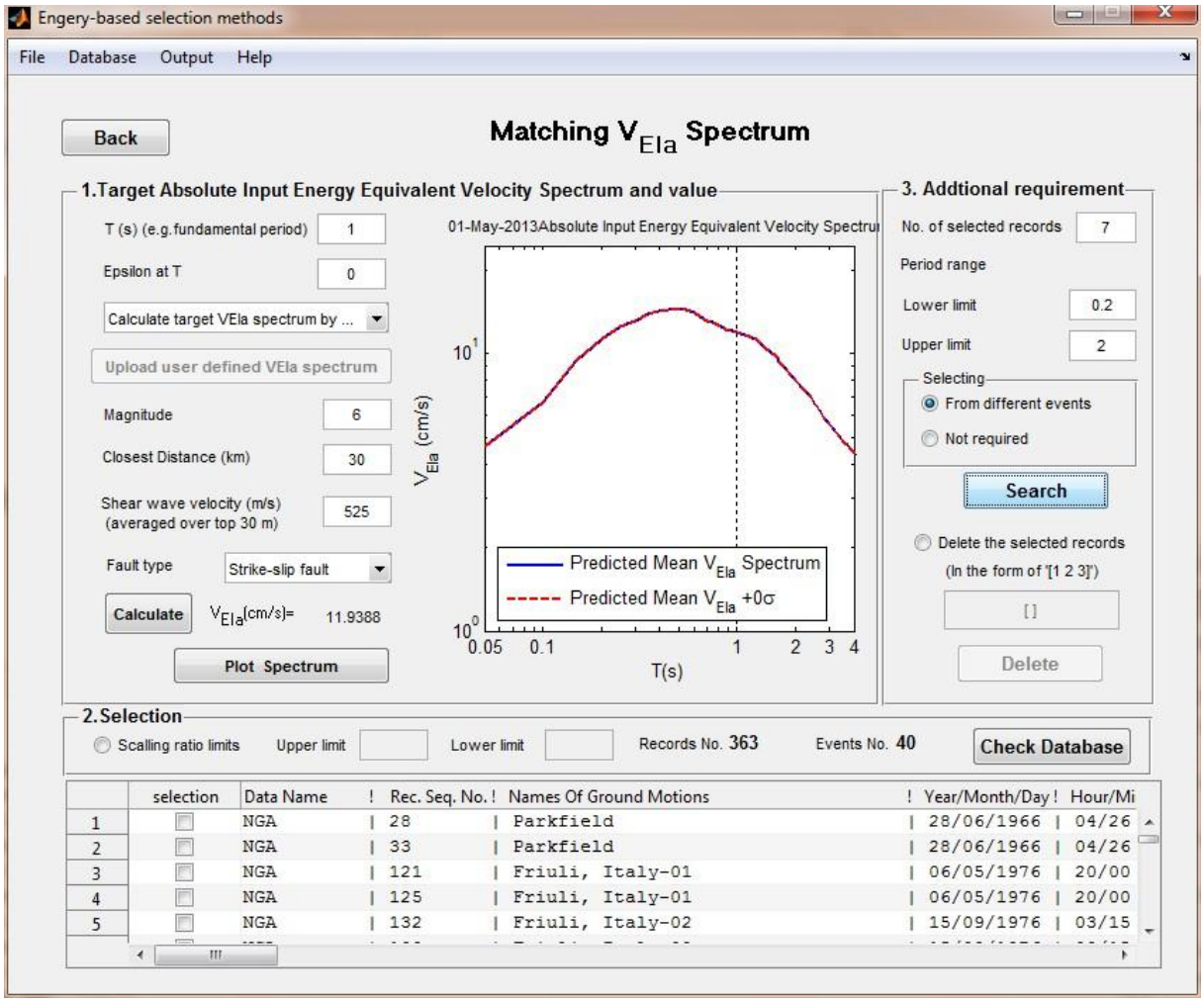
Engery-based selection methods
File Database Output Help
Back
Matching V_{Ela} Spectrum
1.Target Absolute Input Energy Equivalent Velocity Spectrum and value
T (s) (e.g.fundamental period) 1
Epsilon at T 0
Calculate target VEla spectrum by ...
Upload user defined VEla spectrum
Magnitude 6
Closest Distance (km) 30
Shear wave velocity (m/s) (averaged over top 30 m) 525
Fault type Strike-slip fault
Calculate V_{Ela}(cm/s)= 11.9388
Plot Spectrum
01-May-2013Absolute Input Energy Equivalent Velocity Spectru
V_{Ela} (cm/s)
T(s)
Predicted Mean V_{Ela} Spectrum
Predicted Mean V_{Ela} +0σ
3. Addtional requirement
No. of selected records 7
Period range
Lower limit 0.2
Upper limit 2
Selecting
From different events
Not required
Search
Delete the selected records
(In the form of '[1 2 3]')
[]
Delete
2.Selection
Scalling ratio limits Upper limit Lower limit
Records No. 363 Events No. 40
Check Database
selection Data Name ! Rec. Seq. No. ! Names Of Ground Motions ! Year/Month/Day ! Hour/Mi
1 NGA | 28 | Parkfield | 28/06/1966 | 04/26
2 NGA | 33 | Parkfield | 28/06/1966 | 04/26
3 NGA | 121 | Friuli, Italy-01 | 06/05/1976 | 20/00
4 NGA | 125 | Friuli, Italy-01 | 06/05/1976 | 20/00
5 NGA | 132 | Friuli, Italy-02 | 15/09/1976 | 03/15

(a)

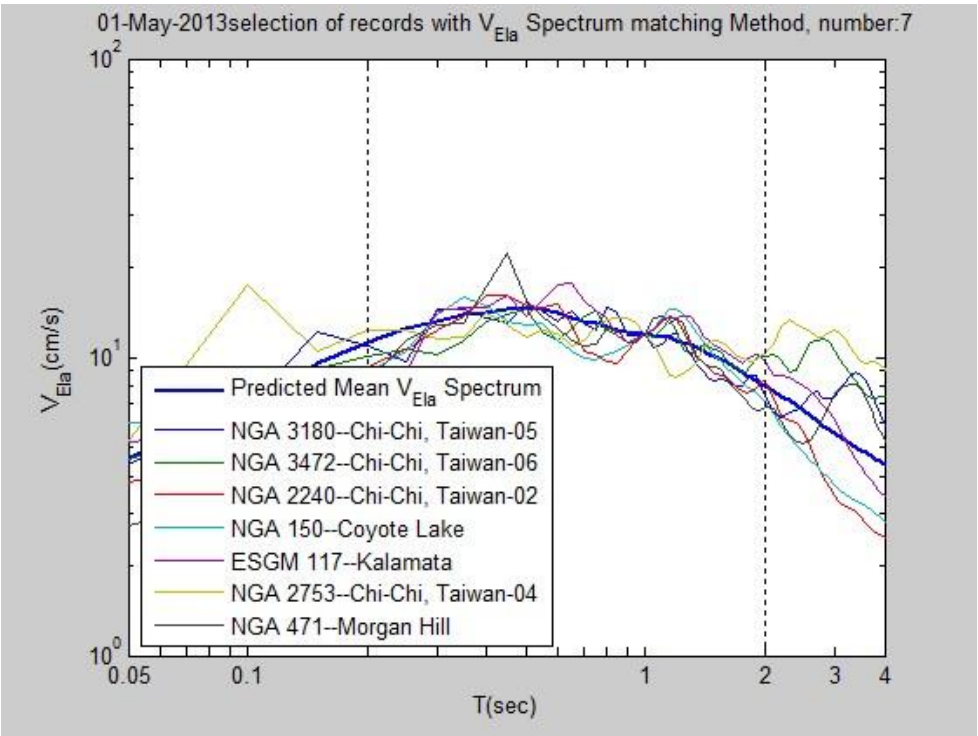

(b)

Fig. 6.13 Screenshot of the window of GMSM method of Matching V_{Ela} spectrum (a) and the resulting plot of an example (b)

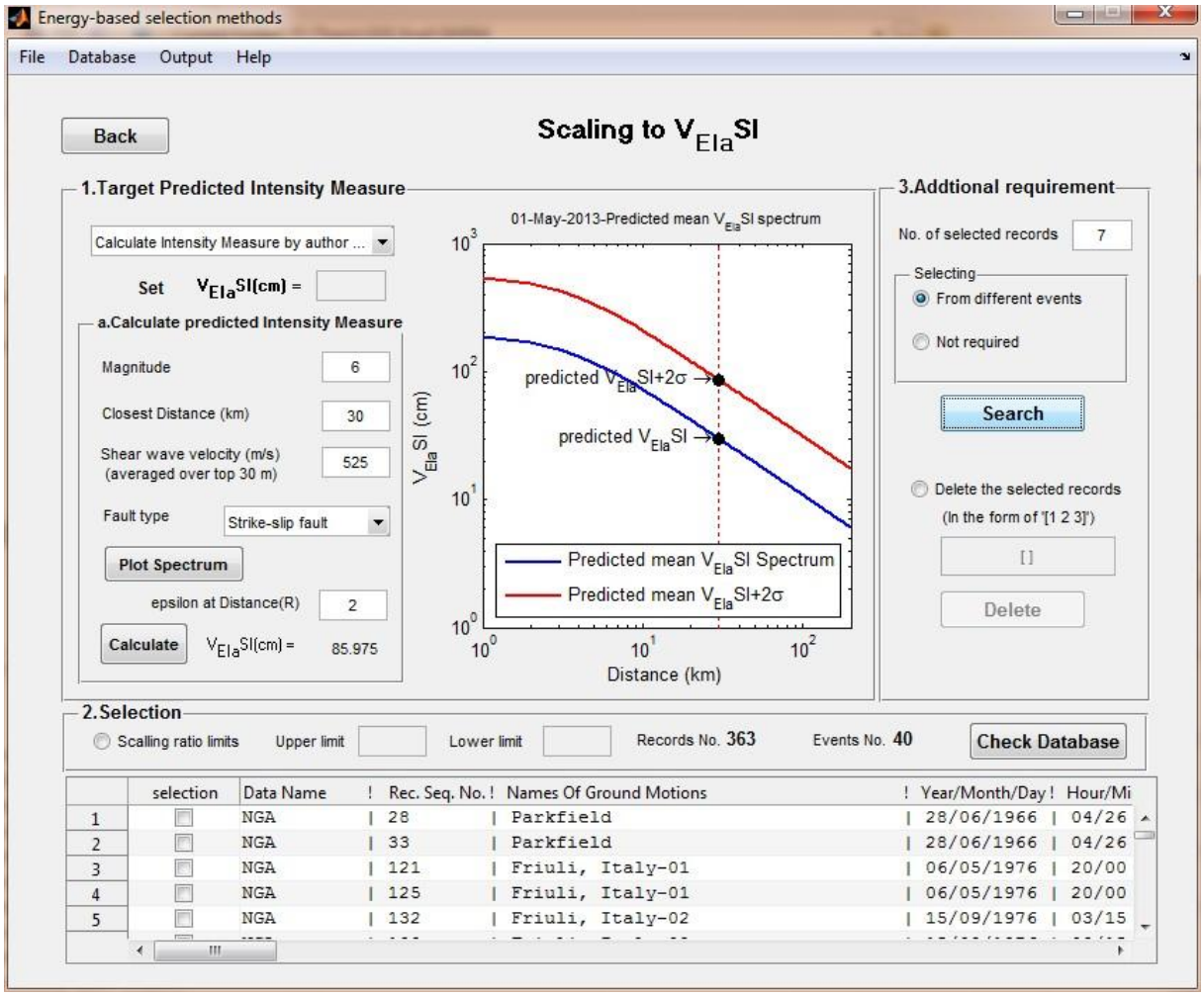

Fig. 6.14 Screenshot of the window of GMSM method of Scaling to $V_{Ela}SI$

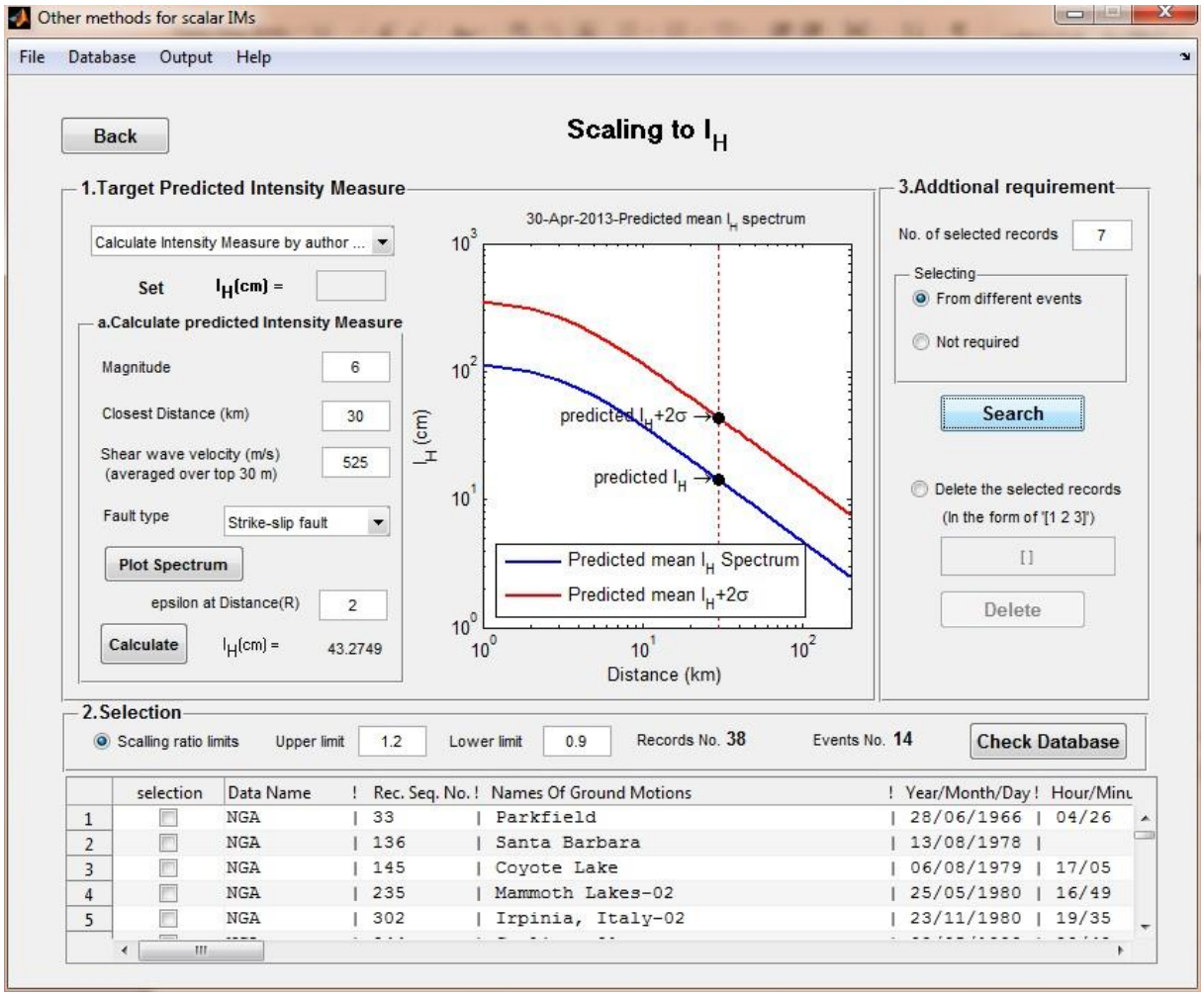

Fig. 6.15 Screenshot of the window of GMSM method of Scaling to I_H

6.6 **Conclusion**

A practical Matlab implementation for ground motion selection and modification is developed in this chapter. It is called RELACS (REaL ACcelerogram Selection). The total ground motion database in the RELACS, consisting of more available ground motion records, is compiled with three large ground motion database, i.e. NGA (Next Generation Attenuation) database, SISMA (Site of Italian Strong Motion Accelerograms) database, and ESGM (European Strong Ground Motion) Database. The values of a large variety of IMs of each ground motions in the database have been calculated. In addition to the GMSM methods with a widely used intensity measures, the methods with some energy-based intensity measures that have been approved good predictors for base-isolated buildings are also involved in the

Matlab implementation. Finally, users can easily obtain the acceleration time-history, the acceleration spectrum, the velocity spectrum, the displacement spectrum of the ground motion records selected with the RELACS.

7 Conclusion Remarks

7.1 **Conclusion**

In order to identify the Intensity Measures (IMs) that can better predict the seismic response of different types of structures (fixed base buildings and base-isolated buildings), a group of elastic intensity measures that consists of 27 IMs was investigated in the framework of PBEE in terms of their properties, efficiency, sufficiency and sensitivity (only latter is investigated for base-isolated structures). A series of nonlinear dynamic analyses are performed on 4-storey and 6-storey multi-storey RC frame structures and those protected with the base isolation systems characterized by different isolation properties subjected to a group of ground motions. They are composed of 80 ordinary and 59 pulse-like ground motion records. Some modified intensity measures, which are integral intensity measures with an integral period range dependent on the structural fundamental period for fixed base buildings and the isolation period for base-isolated buildings were proposed in this study. Some energy-based intensity measures were also proposed to explore IMs for better predicting EDPs of different structure types. EDPs extensively include Maximum Roof Drift Ratio (MRDR), Maximum Inter-story Drift Ratio (MIDR), Maximum Floor Acceleration (MFA) and Maximum Base Displacement (MBD, only for base-isolated buildings).

For fixed base buildings, it is demonstrated that $S_a(T_1)$ is the most efficient IM among all considered IMs for predicting MIDR and MRDR. But it may not be sufficient to distance and Magnitude. That implies that more attention should be paid to the distance and magnitude of the records when the record selection is performed in terms of $S_a(T_1)$. On the other hand the intensity measure, that MI_H, presents competitive efficiency, especially when higher storey buildings are considered. In the mean while the MI_H show the most sufficient property for predicting MIDR. Therefore the author suggest to use MI_H for predicting MIDR because of its satisfying efficiency and sufficiency, especially when the influences of the higher mode of vibration exist and the deep inelasticity of structures are significant. The intensity measure of PGA is suggested as a desired predictor of MFA because of its sufficiency and its simplicity

to evaluate. It is demonstrated that the proposed modified intensity measures are always more efficient than the corresponding spectrum intensity measures for predicting MRDR, MIDR and MFA. This is because the integral period range of the proposed modified intensity measure is dependent on the structural fundamental period, which could be more representative of the influence of higher-mode vibration and the inelastic effect of structures with respect to the fixed integral period range for the spectrum intensity measures.

For base-isolated buildings the properties of the IMs considered in the evaluation analyses were the efficiency, sufficiency and robustness. The latter was considered for studying the sensitivity of the IMs to varying isolation properties. The intensity measure that in the opinion of the authors can be considered as the best IM for predicting base-isolated building is overall $MV_{EIr}SI$. This IM is a proposed modified version of the relative Input Equivalent Velocity Spectrum Intensity. The analyses results showed that $MV_{EIr}SI$ is a very efficient predictor for the deformation response of both the superstructure and the isolation system. In particular, it was found that $MV_{EIr}SI$ is well correlated with the Maximum Inter-storey Drift Ratio (MIDR), the Maximum Roof Drift Ratio (MRDR) and the Maximum Base Displacement (MBD). This IM is also a good predictor for the acceleration response of the building (MFA). About the sufficiency, all the investigated IMs resulted to be dependent on magnitude and/or on distance. However, the p-values of the coefficients obtained with $MV_{EIr}SI$ were found to be lower than the limit value of 0.05 only in some cases. Finally, the results of the sensitivity investigations showed that $MV_{EIr}SI$ is a very robust IM, especially when the maximum displacement of the isolation system is predicted.

Trends about the variation of the IMs the predictive capabilities produced by the pulse-type properties of the exciting ground motions cannot be clearly identified. In most of the cases, both the efficiency and the sufficiency of the IMs reduce. For $MV_{EIr}SI$, it was found that the efficiency is actually not significantly influenced by the type of record. For most of the other considered IMs, instead, the efficiency considerably reduces, particularly when MIDR and MBD is predicted. Significant increases in the magnitude influence on the prediction of the regression residuals of MIDR, MRDR and MBD were observed, especially for the case of

$MV_{EIr}SI$. In general, the obtained results showed that frequently the IMs cannot predict properly the response of the base-isolated building when it is subjected to pulse-like records.

This study addressed Energy-based intensity measures, which have be shown in this study to be good alternatives with respect to standard intensity measures commonly used in performance-based earthquake engineering, such as the peak ground acceleration or the pseudo-spectral acceleration. In order to apply these energy-based intensity measures in practice of selecting ground motions for nonlinear dynamic analyses in the performance-based design and assessment to structures, chapter 4 and chapter 5 respectively did important works to achieve this. Chapter 4 proposed the necessary empirical Ground Motion Prediction Equations (GMPE) for estimating both the absolute input energy equivalent velocity (V_{EIa}) and the relative input energy equivalent velocity (V_{EIr}). Then chapter 5 evaluated and proposed the new predictive models of the correlation of V_{EIa} and V_{EIr} spectral values for multi-components of ground motions.

In particular, the GMPE developed based on a mixed-effect model has been calibrated through regression analyses using records selected from the NGA database. The proposed equations can be applied to predict V_{EIa} and V_{EIr} for shallow crustal earthquakes occurring in active tectonic region, with a magnitude range of 5 to 8, a distance less than 200 km, and a V_{S30} value in the range of 150-1500m/s. The improvements with respect to the prediction equations for input energy equivalent velocity spectra already available from the literature can be identified in the following: the proposed equations have been developed using a large number of records characterized by a wide range of magnitude and distance; they include a V_{S30} term that enables to better evaluate the effects of soil conditions than simple dummy variables; they also include terms to explicitly account for different types of fault mechanisms; a prediction equation for the relative input energy equivalent velocity, intensity measures that has not still received much research attention, has been also proposed.

The author calculated the correlation coefficients of V_{EIa} and V_{EIr} spectral values of ground, and proposed a new predictive model of them. The proposed predictive model was demonstrated to better fit the observed correlation coefficients of V_{EIa} and V_{EIr}, compared to

the two existing models that have been used to predict the correlation coefficient of spectral acceleration (S_a). Three cases associated with predictive equations of correlation coefficients of V_{EIa} and V_{EIr} spectral values are investigated in this study: the case with two different periods and the same horizontal orientation; the case with the same period and two horizontal orthogonal orientations; the case with two different periods and two horizontal orthogonal orientations. These correlations can be used not only to develop the conditional mean spectrum of V_{EIa} and V_{EIr} but also to calculate the target values of some energy-related scalar intensity measures, such as $V_{EIa}SI$, $V_{EIr}SI$, $MV_{EIa}SI$ and $MV_{EIr}SI$. All these target spectra or values are necessary in the application of ground motion selection and modification in terms of spectrum-matched or amplitude-scaled methods, respectively. The proposed predictive equations of correlation coefficients should be used for the period range of 0.05-5 s, the earthquake magnitude range of 5-7.9, the fault-to-site closest distance less than 200 km, and the site class with B, C and D categorized according to NEHRP.

Finally, in order to practically facilitate engineers and researchers to apply the investigated IMs in seismic structural design and assessment to structures, the Matlab implementation of processing Ground Motion Selection and Modification (GMSM) using the considered IMs is programmed in this study. This Matlab implementation is called RELACS (REaL ACcelerogram Selection). The energy-based IMs are also included in the Matlab implementation. It compiled three large record databases, i.e., NGA, SISMA and ESGM database. The values of the various investigated IMs of all records in the database are calculated and involved in it. Therefore users can select ground motions in larger record pool using the investigated IMs, including energy-based IMs. The Matlab implementation of GMSM (ground motion selection and modification) consists of two steps: the step of selection according to geophysical parameters; the step of selection according to elastic response parameters (IMs). With the RLACS users can easily plot and output acceleration time-history, acceleration spectrum, velocity spectrum, and displacement spectrum of the ground motion selected according to a variety of IMs.

7.2 **Further Researches**

This study explored some elastic intensity measures to identify IMs that better predict fixed base and base-isolated structures, developed the GMPE and GMSM Matlab implementation for their utilization in performance-based design and assessment to structures.

This study could be extended to inelastic intensity measures, as for example inelastic input energy intensity measures. In addition, a further extension of this study could be an exploration of other ground motion selection methods in terms of input energy intensity measures. The authors argue that a conditional mean spectrum input energy could be a potential criterion for selecting and scaling ground motions due to the their property that is dependent on not only the frequency content and duration of ground motions, but also the structural property (e.g. first-mode period). In addition, more comprehensive functions, such as PSHA of intensity measures and more GMSM methods, can be added in the GMSM Matlab implementation, in order to make users more conveniently select records with more extensive choices.

Reference

Abrahamson N A, Kammerer A, Gregor N (2003) Summary of scaling relations for spectral damping, peak velocity, and average spectral acceleration: Report for the PEGA-SOS project, Personal communication

Abrahamson NA, Silva WJ (2008) Summary of the Abrahamson & Silva NGA ground-motion relations. Earthq Spectra 24:67–97

Abrahamson NA, Youngs RR (1992) A stable algorithm for regression analysis using the ransom effects model. Bull Seism Soc Am 82: 505–510

Akkar S, Özen Ö (2005) Effect of peak ground velocity on deformation demands for SDOF systems. Earthq Eng Struct Dyn 34:1551-1571

Ambraseys NN et al. (2004) Dissemination Of European Strong-Motion Data, Volume 2. 13th World Conference on Earthquake Engineering Vancouver, B.C., Canada August 1-6, 2004 pp: 32

Anderson JC, Bertero VV (1987) Uncertainties in establishing design earthquakes. J Struct Eng 113(8):1709-1724

Araya R, Saragoni GR (1980) Capacidad de los movimientos de producir daño estructral. Publication SES I 7/80 (in Spanish), Division of Structural Engineering, Department of Engineering, University of Chile, Santiago

Arias A (1970) A measure of earthquake intensity. Seismic design for nuclear power plants, R.J. Hansen ed. MIT, Cambridge, Mass, pp 438–483

Asgarian B, Nojoumi RM, Alanjari P (2012) Performance-based evaluation of tall buildings using advanced intensity measures (case study: 30-story steel structure with framed-tube system). Struct Des Tall Special Build. doi: 10.1002/tal.1023

Avşar Ö, Özdenmir G (2011) Response of seismic-isolated bridges in relation with intensity measures of ordinary and pulse-like ground motions. J Bridge Eng. doi:10.1061/(ASCE)BE.1943-5592.0000340.

Baker J and Cornell CA (2006) Correlation of response spectral values for multicomponent ground motions. Bull Seismol Soc Am 96:215-227

Baker J and Jayaram N (2008) Correlation of spectral acceleration values from NGA ground motion models. Earthq Spec 24:299-317

Baker JW (2007) Quantitative Classification of Near-Fault Ground Motions Using Wavelet Analysis. Bull Seismol Soc Am 97(5):1486–1501

Baker JW (2011) Conditional Mean Spectrum: Tool for ground motion selection, J Struct Eng137(3):322-331

Baker JW, Cornell CA (2005) A vector-valued ground motion intensity measure consisting of spectral acceleration and epsilon. Earthq Eng Struct Dyn 34(10):1193–1217

Baker JW, Cornell CA (2006) Spectral Shape, Epsilon and Record Selection. Earthq Eng Struct Dyn 35 (9):1077-1095

Baker JW, Cornell CA (2007) Vector-valued ground motion intensity measures for probabilistic seismic demand analysis. Pacific Earthquake Engineering Research Center

Bazzurro P, Cornell CA (1994) Seismic hazard analysis of nonlinear structures. I: Methodology. J Struct Eng 120(11): 3320-3344.

Bazzurro P, Cornell CA, Shome N, Carballo JE (1998) Three proposals for characterizing MDOF nonlinear seismic response. J Struct Eng 124(11): 1281-1289

Bazzurro P, Cornell CA, Shome N, Carballo JE (1998) Three proposals for characterizing MDOF nonlinear seismic response. J Struct Eng 124(11):1281-1289

Benavent-Climent A, L ópez-Almansa F, Bravo-Gonz ález DA (2010) Design energy input spectra for moderate-to-high seismicity regions based on colombian earthquakes. Soil Dyn Earthq Eng 30(11):1129–1148

Beyer K, Bommer JJ (2007) Selection and Scaling of Real Accelerograms for Bi-Directional Loading: A Review of Current Practice and Code Provisions. J Earthq Eng11:13-45

Beyer K, Bommer JJ (2007) Selection and Scaling of Real Accelerograms for Bi-Directional Loading: A Review of Current Practice and Code Provisions. J Earthq Eng 11: 13-45

Bianchini M, Diotallevi PP, Baker JW (2009) Prediction of inelastic structural response using an average of spectral accelerations. 10th International Conference on Structural Safety and Reliability (ICOSSAR09), 13-17 September, Osaka, Japan

Bommer JJ, Acevedo A (2004) The use of real earthquake accelerograms as input dynamic analysis. J Earthq Eng 8(1):43–91

Bommer JJ., Scott SG. (2000) The feasibility of using real accelerograms for seismic design, Implications of Recent Earthquakes on Seismic Risk, Editor(s): Elnashai, Antoniou, Imperial College, pp:115-126

Boore DM, Atkinson GM (2008) Ground-motion prediction equations for the average horizontal component of PGA, PGV, and 5%-damped PSA at spectral periods between 0.01 s and 10.0 s. Earthq Spectra 24:99–138

Boore DM, Joyner, WB, Fumal TE (1993) Estimation of response spectra and peak accelerations from western North American earthquakes: An interim report U. S. Geological Survey Open-File Report 93-509, pp72

Bradley BA (2011) Empirical equations for the prediction of displacement spectrum intensity and its correlation with other intensity measures. Soil Dyn Earthq Eng 31(8): 1182–119

Bradley BA, Cubrinovski M, MacRae GA, Dhakal RP (2009) Ground-Motion Prediction Equation for SI Based on Spectral Acceleration Equations. Bull Seismol Soc Am 99(1): 277–285

Brillinger DR, Preisler HK (1984) An exploratory data analysis of the Joyner-Boore attenuation data. Bull Seism Soc Am 74:1441-1450

Brillinger DR, Preisler HK (1985) Further analysis of the Joyner-Boore attenuation data. Bull Seism Soc Am 75:611-614

Campbell KW, Bozorgnia Y (2008) NGA ground motion model for the geometric mean horizontal component of PGA, PGV, PGD and 5% damped linear elastic response spectra for periods ranging from 0.01 to 10s. Earthq Spectra 24:139–171

Campbell KW, Bozorgnia Y (2010) A Comparison of Ground Motion Prediction Equations for Arias Intensity and Cumulative Absolute Velocity Developed Using a Consistent Database and Functional Form. Earthq Spectra 28(3): 931–941

Campbell KW, Bozorgnia Y (2010) Ground Motion Prediction Equation for the Horizontal Component of Cumulative Absolute Velocity (CAV) Based on the PEER-NGA Strong Motion Database. Earthq Spectra 26(3):635–650

Chapman MC (1999) On the Use of Elastic Input Energy for Seismic Hazard Analysis. Earthq Spectra 15(4):607–635

Chiou B, Darragh R, Gregor N, Silva W (2008) NGA Project Strong-Motion Database. Earthq Spectra 24(1):23-44

Chiou BJ, Youngs RR (2008) An NGA model for the average horizontal component of peak ground motion and response spectra. Earthq Spectra 24(1):173–215

Chou CC, Uang CM (2000) Establishing absorbed energy spectra-an attenuation approach. Earthq Eng Struct Dyn 29(10):1441–1455

Cimellaro GP (2013) Correlation in spectral acceleration for earthquakes in Europe. Earthq Eng Struct Dyn 42:623-633

Cordova PP, Deirlein GG, Mehanny SSF, Cornell CA (2000) Development of a two-parameter seismic intensity measure and probabilistic assessment procedure. In: Proceedings of the 2nd U.S.-Japan Workshop on Performance-Based Earthquake Engineering of Reinforced Concrete Building Structures, 11-13 September, Sapporo, Hokkaido, Japan

Cornell CA (1970) Probability, Statistics, and Decision for Civil Engineers. McGraw-Hill, New York, pp684.

Cornell CA, Jalayer F, Hamburger RO, Foutch DA (2002) Probabilistic Basis for 2000 SAC Federal Emergency Management Agency Steel Moment Frame Guidelines. J Struct Eng 128(4):526-533

Cornell CA, Krawinkler H (2000) Progress and Challenges in Seismic Performance Assessment. PEER Center News 3(2)

Danciu L, Tselentis GA (2007) Engineering ground-motion parameters attenuation relationships for Greece. Bull Seismol Soc Am 97(1):162–183

Decanini L, Mollaioli F (2001) An energy-based methodology for the assessment of seismic demand. Soil Dyn Earthq Eng 21(2):113-137

Decanini L, Mollaioli F, (1998) Formulation of elastic earthquake input energy spectra. Earthq Eng Struct Dyn 27(13): 1503-1522

Decanini LD, Mollaioli F (2001) An energy-based methodology for the assessment of seismic demand. Soil Dyn Earthq Eng 21:113-137

Decreto Ministero (DM) dei Lavori Pubblici 16/01/1996 (1996) Norme Tecniche per le Costruzioni in Zone Sismiche (in Italian). Italian Ministry of Public Works, Rome, Italy

Electrical Power Research Institute (EPRI) (1988) A criterion for determining exceedence of the operating basis earthquake. EPRI NP-5930, EPRI, Palo Alto, California

Eurocode 8 (2003): Design Provisions for Earthquake Resistance of Structures, Part 1.1: General rules, seismic actions and rules for buildings, PrEN1998-1

Fajfar P, Vidic T, Fischinger M (1990) A measure of earthquake motion capacity to damage medium-period structures. Soil Dyn Earthq Eng 9(5):236–242

Foulser-Piggott R, Stafford PJ (2012) A predictive model for arias intensity at multiple sites and consideration of spatial correlations. Earthq Eng Struct Dyn 41(3):431–451

Giovenale P, Cornell AC, Esteva L (2004) Comparing the adequacy of alternative ground motion intensity measures for the estimation of structural responses. Earthq Eng Struct Dyn 33:951–979

Gong MS, Xie LL (2005) Study on comparison between absolute and relative input energy spectra and effects of ductility factor. Acta Seismol Sinic18(6):717–726

Haselton CB et al. (2009) Evaluation of Ground Motion Selection and Modification Methods: Predicting Median Interstory Drift Response of Buildings. PEER Report 2009/01 College of Engineering University of California, Berkeley

Housner GW (1952) Spectrum intensities of strong motion earthquakes. In: Proceedings of symposium of earthquake and blast effects on structures, EERI, Los Angeles, California, pp 21–36

Idriss I (2008) Annga empirical model for estimating the horizontal spectral values generated by shallow crustal earthquakes. Earthq Spectra 24(1):217–242

Jalayer F (2003) Direct probabilistic seismic analysis: implementing non-linear dynamic assessments. Stanford University, Stanford

Jangid RS, Kelly JM (2001) Base isolation for near-fault motions. Earthq Eng Struct Dyn 30(5): 691-707

Jayaram N, Mollaioli F, Bazzurro P, De Sortis A., Bruno S (2010) Prediction of structural response of reinforced concrete frames subjected to earthquake ground motions. 9th U.S.

National and 10th Canadian Conference on Earthquake Engineering, pp 428-437, 25-29 July, Toronto, Canada

Joyner WB, Boore DM (1981) Peak horizontal acceleration and velocity from strong-motion records including records from the 1979 Imperial Valley, California earthquake. Bull Seism Soc Am 71:201–38

Kaklamanos J, Baise LG, Boore DM (2011) Estimating unknown input parameters when implementing the NGA ground-motion prediction equations in engineering practice. Earthq Spectra 27(4):1219–1235

Kalkan E, Kunnath SK (2007) Effective cyclic energy as a measure of cyclic demand. J Earthquake Eng11(5):725-751

Kalkan E, Kunnath SK (2008) Relevance of absolute and relative energy content in seismic evaluation ofstructures. Adv Struct Eng 11(1):17–34

Katsanos EI, Sextos AG, Manolis GD (2010) Selection of earthquake ground motion records: A state-of-the-art review from a structural engineering perspective. Soil Dyn Earthq Eng 30: 157-169

Lee CT, Hsieh BS, Sung CH, Lin PS (2012) Regional Arias Intensity Attenuation Relationship for Taiwan Considering V_{S30}. Bull Seism Soc Am 102(1):129–142

López-Almansa F, Yazgan A, Benavent-Climent A (2013) Design energy input spectra for high seismicity regions based on turkish registers. Bull Earthq Eng 11(4): 885–912

Lucchini A, Cheng Y, Mollaioli F, Liberatore L (2013) Predicting floor response spectra for rc frame structures. In: 4th ECCOMAS Thematic Conference on Computational Methods in Structural Dynamics and Earthquake Engineering, Kos, Greece

Lucchini A, Mollaioli F, Monti G (2011a) Intensity measures for response prediction of a torsional building subjected to bi-directional earthquake ground motion. Bull Earthq Eng 9(5):1499–1518

Lucchini A, Mollaioli F, Monti G, Kunnath, S (2011b) Seismic response of asymmetric RC frames subjected to bi-directional ground motions. In: Proceedings of fib Syposium on Concrete Engineering for Excellence and Efficiency, 8-10 June, Czech Republic, Prague

Luco L, Manuel L, Bazzurro P (2005) Correlation of Damage of Steel Moment-Resisting Frames to a Vector-valued Ground Motion Parameter Set that Includes Energy Demands. Report prepared for U.S.G.S., Grant No. 03HQGR0057, February

Luco N (2006) Categorization of Ground Motion Selection and Modification Methods. 2006 COSMOS Annual Meeting Technical Session

Luco N, Cornell CA (2007) Structure-Specific Scalar Intensity Measures for Near-Source and Ordinary Earthquake Ground Motions. Earthq Spectra 23(2): 357-392

Mackie K, Stojadinovic B (2003) Seismic Demands for Performance-Based Design of Bridges. PEER Report. http://peer.berkeley.edu/publications/peer_reports/reports_2003/reports_2003.html

Moehle JP, Deierlein GG (2004) A framework methodology for performance-based earthquake engineering. In: Proceedings of the 13th World Conference on Earthquake Engineering,1-6 August, Vancouver, Canada, pp 679

Mollaioli F, Bruno S, Decanini L, Saragoni R (2011) Correlations between energy and displacement demands for performance-based seismic engineering. Pure Appl Geophys 168(1-2):237-259.

Narasimhan S, Wang M, Pandey MD (2009) Principal component analysis for predicting the response of nonlinear base-isolated buildings. Earthq Spectra 25(1):93–115

Nau JM, Hall WJ (1984) Scaling methods for earthquake spectra. J Struct Eng 110:1533-1548

Neter J, Kutner MH, Nachtsheim CJ, Wasserman W (1996) Applied Linear Statistical Models, McGraw-Hill, Boston, Massachusetts, pp 1408

Nicola Buratti (2008) Assessment of Seismic Safety: Response Surface Approach and Accelerogram Selection Issues. Ph.D. Thesis. University of Bologna

Open System for Earthquake Engineering Simulation Version 2.2.2 (OpenSees 2.2.2) (2010) Pacific Earthquake Engineering Research Center. http://opensees.berkeley.edu

Ozbey C, Sari A, Manuel L, Erdik M, Fahjan Y (2004) An empirical attenuation relationship for northwestern turkey ground motion using a random effects approach. Soil Dyn Earthq Eng 24(2):115–125

Özbey C, Sari A, Manuel L, Erdik M, Fahjan Y(2004) An empirical attenuation relationship for Northwestern Turkey ground motion using a random effects approach. Soil Dyn Earthq Eng 24(2):115-125

Pacific Earthquake Engineering Research (PEER) (2005) Next Generation Attenuation (NGA) project .http://peer.berkeley.edu/nga/

Padgett JE et al. (2008) Selection of optimal intensity measures in probabilistic seismic demand models of highway bridge portfolios. Earthq Eng Struct Dyn 37:711–725

Park YJ, Ang AHS, Wen YK (1985) Seismic damage analysis of reinforced concrete buildings. J Struct Eng 111(4):740–757

PEER (2005) Next Generation of Attenuation (NGA) database. PEER strong-motion database (http://peer.berkeley.edu/nga/index.html). Pacific Earthquake Engineering Research Centre, Berkeley.

Pinheiro J, Bates D, DebRoy S, Sarkar D (2011) Linear and nonlinear mixed effects models. R package version

Pousse G, Bonilla LF, Cotton F, Margerin L (2006) Nonstationary stochastic simulation of strong ground motion time histories including natural variability: application to the K-Net Japanese Database. Bull Seismol Soc Am 96: 2103–2117prEN 1998-1

Riddell R (2007) On Ground Motion Intensity Indice. Earthq Spectra 23(1): 147-173

Riddell R, Garcia J (2001) Hysteretic energy spectrum and damage control. Earthq Eng Struct Dyn 30(12):1791–1816

Ryan KL, Chopra AK (2004a) Estimation of seismic demands on isolators based on nonlinear analysis. J Struct Eng 130(3):392–402

Ryan KL, Chopra AK (2004b) Estimating the seismic displacement of friction pendulum isolators based on non-linear response history analysis. Earthq Eng Struct Dyn 33(3):359–373

Sabetta F, Pugliese A (1996) Estimation of response spectra and simulation of nonstationary earthquake ground motions. Bull Seismol Soc Am 86: 337–352

Scasserra G, Lanzo G, Stewart JP, D'Elia B (2008). "SISMA (Site of Italian Strong Motion Accelerograms): a web-database of ground motion recordings for engineering applications", Proceedings of the 2008 Seismic Engineering Conference commemorating the 1908 Messina and Reggio Calabria Earthquake, MERCEA'08, Santini & Moraci Editors, July 8-11, Reggio Calabria, Italy, 2: 1649-1656

Shome N (1999) Probabilistic seismic demand analysis of non-linear structures. Ph.D. Thesis, Stanford University

Shome N, Cornell CA, Bassurro P, Carballo JE (1998) Earthquakes, records, and nonlinear responses. Earthq Spectra 14:469–500

Somerville PG, Smith NF, Graves RW, Abrahamson NA (1997) Modification of empirical strong ground motion attenuation relations to include the amplitude and duration effects of rupture directivity. Seismol Res Lett 68(1):199–222

Stafford PJ, Berrill JB, and Pettinga JR (2009) New predictive equations for Arias intensity from crustal earthquakes in New Zealand. J Seismol 13:31–52

Stewart JP, Chiou SJ, Bray RW, Graves P, Somerville G, Abrahamson NA (2001) Ground motion evaluation procedures for performance-based design. PEER report 2001/09, Pacific Earthquake Engineering Research Center, University of California, Berkeley, 2001

Tothong P, Luco N (2007) Probabilistic seismic demand analysis using advanced ground motions intensity measures. Earthq Eng Struct Dyn 36(13):1837-1860

U.S. Geological Survey earthquake hazard maps. 2002. http://eqhazmaps.usgs.gov/

Uang CM, Bertero VV (1990) Evaluation of seismic energy in structures. Earthq Eng Struct Dyn 19(1):77-90

Von Thun JL, Roehm LH, Scott GA, Wilson JA (1988) Earthquake ground motions for design and analysis of dams. In: Proceedings of the Earthquake Engineering and Soil Dynamics II-Recent Advances in Ground Motion Evaluation, Geotechnical Special Publication, ASCE, New York, pp 463-481

Wang G, Youngs R, Power M (2009) Design Ground Motion Library (DGML). Report and Users Manual. Final Technical Report for Pacific Earthquake Engineering Research Center and California Geological Survey. Geomatrix Consultants, Inc.

Yakut A, Yilmaz H (2008) Correlation of deformation demands with ground motion intensity. J Struct Eng 134(12):1818-1828

Yang D, Pan J, Li G (2009) Non-structure-specific intensity measure parameters and characteristic period of near-fault ground motions. Earthq Eng Struct Dyn 38(11):1257-1280

Appendix

Cross-sections and reinforcement of the structural members

A schematic representation of the studied 4-storey and 6-storey frame structure is reported in Fig. A. 1 and Fig. A. 2, respectively. Dimensions of the structural members cross-sections with details about the bars used as longitudinal reinforcement are reported in Table A. 1 and Table A. 2.

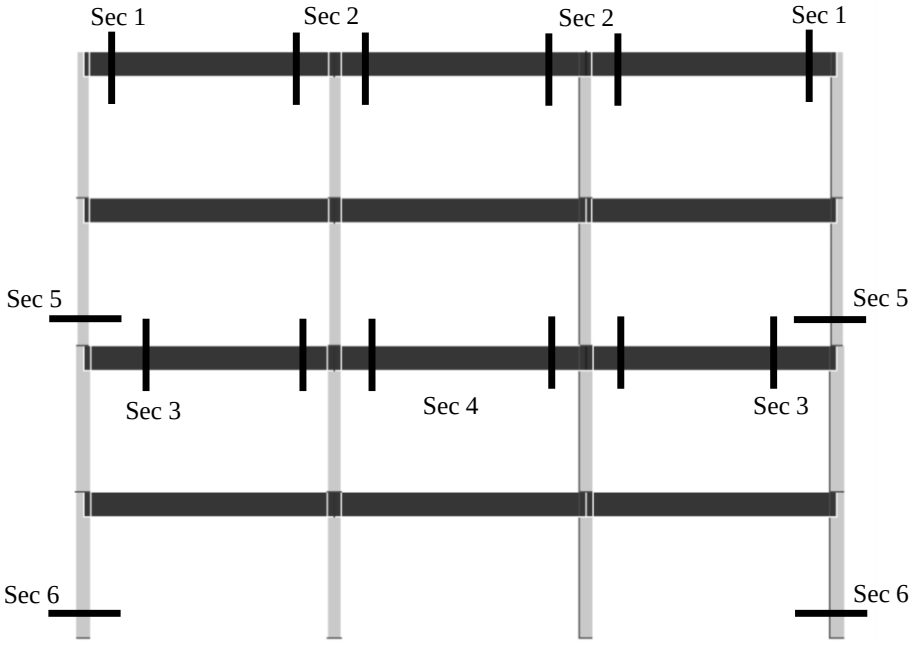

Fig. A. 1 Schematic representation of the 4-storey frame structure analysed in the study with names and location of the different cross-sections characterizing the structural members

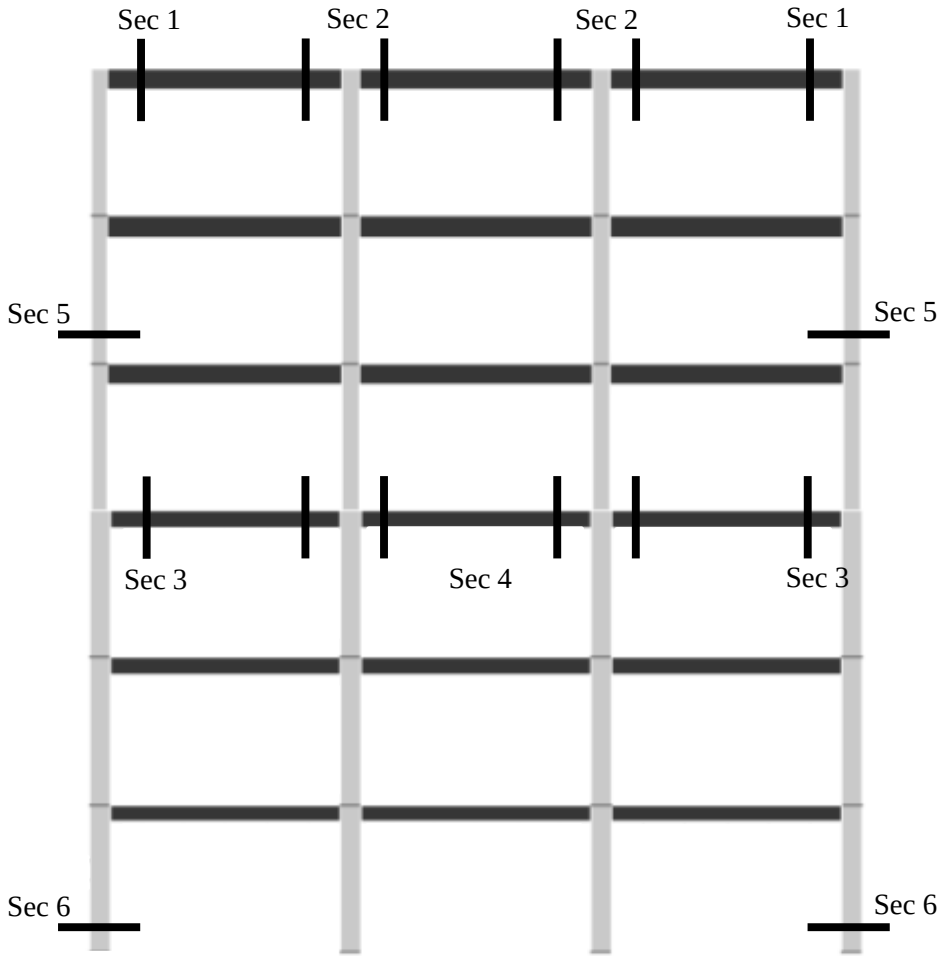

Fig. A. 2 Schematic representation of the 6-storey frame structure analysed in the study with names and location of the different cross-sections characterizing the structural members

Table A. 1 Structural members of the 4-storey frame building: cross-sections and longitudinal reinforcement

	Dimensions		**Reinforcement**					
Cross Section	**b**	**h**	**N top**	**ϕ top**	**N bot**	**ϕ bot**	**N lat**	**ϕ lat**
1	0.3	0.6	3	18	3	18	-	-
2	0.3	0.6	4	18	3	18	-	-
3	0.3	0.6	5	18	3	18	-	-
4	0.3	0.6	5	18	3	18	-	-
5	0.3	0.35	4	18	4	18	1	18
6	0.3	0.35	6	18	6	18	1	18

Table A. 2 Structural members of the 6-storey frame building: cross-sections and longitudinal reinforcement

	Dimensions		**Reinforcement**					
Cross Section	**b**	**h**	**N top**	**ϕ top**	**N bot**	**ϕ bot**	**N lat**	**ϕ lat**
1	0.3	0.6	3	20	2	20	-	-
2	0.3	0.6	3	20	2	20	-	-
3	0.3	0.6	4	20	3	20	-	-
4	0.3	0.6	4	20	3	20	-	-
5	0.3	0.45	4	20	4	20	1	20
6	0.3	0.45	6	20	6	20	1	20

The notation used in Table A. 1 and Table A. 2 is the following: b and h are the width and the height of the cross-section (both expressed in m), respectively; N is the number of longitudinal bars; ϕ is the bar diameter (expressed in mm); bot, top and lat denote the bar location which can be at the top, bottom and lateral side of the cross-section, respectively.

Details of selected ground motions

Details on the selected ground motions used in this study are given in Table A. 3 and Table A. 4.

Table A. 3 Pulse-like near-fault ground motions used in this study

NGA Seq. No.	**Earthquake name**	**Station name**	**Date D/M/Y**	**Eq. Mag.**	**Cl.Dist km**	**Ep.Dist. km**	**Pr.V_{S30} m/s**
150	Coyote Lake	Gilroy Array #6	06/08/1979	5. 74	3. 11	4. 37	663. 31
158	Imperial Valley-06	Aeropuerto Mexicali	15/10/1979	6. 53	0. 34	2. 47	274. 5
170	Imperial Valley-06	EC County Center FF	15/10/1979	6. 53	7. 31	29. 07	192. 05
171	Imperial Valley-06	EC Meloland Overpass FF	15/10/1979	6. 53	0. 07	19. 44	186. 21
173	Imperial Valley-06	El Centro Array #10	15/10/1979	6. 53	6. 17	26. 31	202. 85

174	Imperial Valley-06	El Centro Array #11	15/10/1979	6. 53	12. 45	29. 44	196. 25
179	Imperial Valley-06	El Centro Array #4	15/10/1979	6. 53	7. 05	27. 13	208. 91
180	Imperial Valley-06	El Centro Array #5	15/10/1979	6. 53	3. 95	27. 8	205. 63
181	Imperial Valley-06	El Centro Array #6	15/10/1979	6. 53	1. 35	27. 47	203. 22
182	Imperial Valley-06	El Centro Array #7	15/10/1979	6. 53	0. 56	27. 64	210. 51
183	Imperial Valley-06	El Centro Array #8	15/10/1979	6. 53	3. 86	28. 09	206. 08
184	Imperial Valley-06	El Centro Differential Array	15/10/1979	6. 53	5. 09	27. 23	202. 26
185	Imperial Valley-06	Holtville Post Office	15/10/1979	6. 53	7. 65	19. 81	202. 89
250	Mammoth Lakes-06	Long Valley Dam (Upr L Abut)	27/05/1980	5. 94	16. 2	14. 04	345. 42
292	Irpinia. Italy-01	Sturno	23/11/1980	6. 9	10. 84	30. 35	1000
316	Westmorland	Parachute Test Site	26/04/1981	5. 9	16. 66	20. 47	348. 69
407	Coalinga-05	Oil City	22/07/1983	5. 77	8. 5	4. 6	376. 07
415	Coalinga-05	Transmitter Hill	22/07/1983	5. 77	9. 5	5. 99	376. 07
418	Coalinga-07	Coalinga-14th & Elm (Old CHP)	25/07/1983	5. 21	10. 9	9. 57	338. 54
451	Morgan Hill	Coyote Lake Dam (SW Abut)	24/04/1984	6. 19	0. 53	24. 55	597. 12
459	Morgan Hill	Gilroy Array #6	24/04/1984	6. 19	9. 86	36. 34	663. 31
529	N. Palm Springs	North Palm Springs	08/07/1986	6. 06	4. 04	10. 57	345. 42
568	San Salvador	GeotechInvestig Center	10/10/1986	5. 8	6. 3	7. 93	545
615	Whittier Narrows-01	Downey - Co MaintBldg	01/10/1987	5. 99	20. 82	16. 04	271. 9
721	Superstition Hills-02	El Centro Imp. Co. Cent	24/11/1987	6. 54	18. 2	35. 83	192. 05
723	Superstition Hills-02	Parachute Test Site	24/11/1987	6. 54	0. 95	15. 99	348. 69
779	Loma Prieta	LGPC	18/10/1989	6. 93	3. 88	18. 46	477. 65

802	Loma Prieta	Saratoga - Aloha Ave	18/10/1989	6. 93	8. 5	27. 23	370. 79
821	Erzican. Turkey	Erzincan	13/03/1992	6. 69	4. 38	8. 97	274. 5
828	Cape Mendocino	Petrolia	25/04/1992	7. 01	8. 18	4. 51	712. 82
879	Landers	Lucerne	28/06/1992	7. 28	2. 19	44. 02	684. 935
982	Northridge-01	Jensen Filter Plant	17/01/1994	6. 69	5. 43	12. 97	373. 07
983	Northridge-01	Jensen Filter Plant Generator	17/01/1994	6. 69	5. 43	13	525. 79
1013	Northridge-01	LA Dam	17/01/1994	6. 69	5. 92	11. 79	628. 99
1044	Northridge-01	Newhall - Fire Sta	17/01/1994	6. 69	5. 92	20. 27	269. 14
1045	Northridge-01	Newhall - W Pico Canyon Rd.	17/01/1994	6. 69	5. 48	21. 55	285. 93
1063	Northridge-01	Rinaldi Receiving Sta	17/01/1994	6. 69	6. 5	10. 91	282. 25
1084	Northridge-01	Sylmar - Converter Sta	17/01/1994	6. 69	5. 35	13. 11	251. 24
1085	Northridge-01	Sylmar - Converter Sta East	17/01/1994	6. 69	5. 19	13. 6	370. 52
1086	Northridge-01	Sylmar - Olive View Med FF	17/01/1994	6. 69	5. 3	16. 77	440. 54
1119	Kobe. Japan	Takarazuka	16/01/1995	6. 9	0. 27	38. 6	312
1120	Kobe. Japan	Takatori	16/01/1995	6. 9	1. 47	13. 12	256
1182	Chi-Chi. Taiwan	CHY006	20/09/1999	7. 62	9. 77	40. 47	438. 19
1244	Chi-Chi. Taiwan	CHY101	20/09/1999	7. 62	9. 96	31. 96	258. 89
1489	Chi-Chi. Taiwan	TCU049	20/09/1999	7. 62	3. 78	38. 91	487. 27
1493	Chi-Chi. Taiwan	TCU053	20/09/1999	7. 62	5. 97	41. 2	454. 55
1494	Chi-Chi. Taiwan	TCU054	20/09/1999	7. 62	5. 3	37. 64	460. 69
1499	Chi-Chi. Taiwan	TCU060	20/09/1999	7. 62	8. 53	45. 37	272. 6
1503	Chi-Chi. Taiwan	TCU065	20/09/1999	7. 62	0. 59	26. 67	305. 85
1505	Chi-Chi. Taiwan	TCU068	20/09/1999	7. 62	0. 32	47. 86	487. 34
1510	Chi-Chi. Taiwan	TCU075	20/09/1999	7. 62	0. 91	20. 67	573. 02
1511	Chi-Chi. Taiwan	TCU076	20/09/1999	7. 62	2. 76	16. 03	614. 98
1519	Chi-Chi. Taiwan	TCU087	20/09/1999	7. 62	7	55. 64	473. 9
1529	Chi-Chi. Taiwan	TCU102	20/09/1999	7. 62	1. 51	45. 56	714. 27
1530	Chi-Chi. Taiwan	TCU103	20/09/1999	7. 62	6. 1	52. 43	494. 1
1550	Chi-Chi. Taiwan	TCU136	20/09/1999	7. 62	8. 29	48. 75	473. 9
1752	Northwest China-03	Jiashi	11/04/1997	6. 1		19. 11	274. 5

1853	Yountville	Napa Fire Station #3	03/09/2000	5	11. 4	9. 89	271. 44
2627	Chi-Chi. Taiwan-03	TCU076	20/09/1999	6. 2	14. 66	20. 8	614. 98

Table A. 4 Ordinary ground motions used in this study

NGA Seq. No.	**Earthquake name**	**Station name**	**Date D/M/Y**	**Eq. Mag.**	**Cl.Dist km**	**Ep.Dist. km**	**Pr.V_{S30} m/s**
6	Imperial Valley-02	El Centro Array #9	19/05/1940	6. 95	12. 99	6. 09	213. 44
65	San Fernando	Gormon - Oso Pump Plant	09/02/1971	6. 61	49. 83	46. 78	308. 35
70	San Fernando	Lake Hughes #1	09/02/1971	6. 61	26. 1	27. 4	425. 34
95	Managua. Nicaragua-01	Managua. ESSO	23/12/1972	6. 24	5. 68	4. 06	288. 77
154	Coyote Lake	San Juan Bautista. 24 Polk St	06/08/1979	5. 74	23. 24	19. 7	370. 79
158	Imperial Valley-06	Aeropuerto Mexicali	15/10/1979	6. 53	2. 47	0. 34	274. 5
159	Imperial Valley-06	Agrarias	15/10/1979	6. 53	2. 62	0. 65	274. 5
186	Imperial Valley-06	Niland Fire Station	15/10/1979	6. 53	68. 92	36. 92	207. 47
189	Imperial Valley-06	SAHOP Casa Flores	15/10/1979	6. 53	12. 43	9. 64	338. 6
265	Victoria. Mexico	Cerro Prieto	09/06/1980	6. 33	33. 73	14. 37	659. 6
289	Irpinia. Italy-01	Calitri	23/11/1980	6. 9	15. 04	17. 64	600
322	Coalinga-01	Cantua Creek School	02/05/1983	6. 36	30. 06	24. 02	271. 44
334	Coalinga-01	Parkfield - Fault Zone 1	02/05/1983	6. 36	52. 86	41. 99	338. 54
338	Coalinga-01	Parkfield - Fault Zone 14	02/05/1983	6. 36	38. 54	29. 48	338. 54
339	Coalinga-01	Parkfield - Fault Zone 15	02/05/1983	6. 36	37. 97	29. 38	376. 07
340	Coalinga-01	Parkfield - Fault Zone 16	02/05/1983	6. 36	36. 49	27. 67	338. 54
342	Coalinga-01	Parkfield - Fault Zone 3	02/05/1983	6. 36	47. 9	37. 22	370. 79
359	Coalinga-01	Parkfield - Vineyard Cany 1E	02/05/1983	6. 36	34. 35	26. 38	338. 54
368	Coalinga-01	Pleasant Valley P. P. - yard	02/05/1983	6. 36	9. 98	8. 41	257. 38
465	Morgan Hill	Hollister Diff Array #4	24/04/1984	6. 19	52. 82	26. 43	215. 54
495	Nahanni. Canada	Site 1	23/12/1985	6. 76	6. 8	9. 6	659. 6
496	Nahanni. Canada	Site 2	23/12/1985	6. 76	6. 52	4. 93	659. 6

504	Taiwan SMART1(40)	SMART1 E01	20/05/1986	6. 32	65. 48	64	274. 5
540	N. Palm Springs	Whitewater Trout Farm	08/07/1986	6. 06	4. 24	6. 04	345. 42
540	N. Palm Springs	Whitewater Trout Farm	08/07/1986	6. 06	4. 24	6. 04	345. 42
551	Chalfant Valley-02	Convict Creek	21/07/1986	6. 19	35. 24	31. 19	338. 54
558	Chalfant Valley-02	Zack Brothers Ranch	21/07/1986	6. 19	14. 33	7. 58	271. 44
571	Taiwan SMART1(45)	SMART1 E01	14/11/1986	7. 3	73. 43	39	274. 5
573	Taiwan SMART1(45)	SMART1 I01	14/11/1986	7. 3	76. 39	39	274. 5
576	Taiwan SMART1(45)	SMART1 M07	14/11/1986	7. 3	75. 25	39	274. 5
584	Taiwan SMART1(45)	SMART1 O12	14/11/1986	7. 3	78. 17	39	274. 5
642	Whittier Narrows-01	LA - W 70th St	01/10/1987	5. 99	20. 85	22. 17	294. 28
645	Whittier Narrows-01	LB - Orange Ave	01/10/1987	5. 99	20. 68	24. 54	270. 19
719	Superstition Hills-02	Brawley Airport	24/11/1987	6. 54	29. 91	17. 03	208. 71
738	Loma Prieta	Alameda Naval Air Stn Hanger	18/10/1989	6. 93	90. 77	71	190
741	Loma Prieta	BRAN	18/10/1989	6. 93	9. 01	10. 72	376. 07
757	Loma Prieta	Dumbarton Bridge West End FF	18/10/1989	6. 93	54. 99	35. 52	274. 5
758	Loma Prieta	Emeryville - 6363 Christie	18/10/1989	6. 93	96. 52	76. 97	198. 74
776	Loma Prieta	Hollister - South & Pine	18/10/1989	6. 93	48. 24	27. 93	370. 79
777	Loma Prieta	Hollister City Hall	18/10/1989	6. 93	47. 9	27. 6	198. 77
784	Loma Prieta	Oakland - Title & Trust	18/10/1989	6. 93	91. 68	72. 2	306. 3
786	Loma Prieta	Palo Alto - 1900 Embarc.	18/10/1989	6. 93	50. 17	30. 81	209. 87
787	Loma Prieta	Palo Alto - SLAC Lab	18/10/1989	6. 93	51. 2	30. 86	425. 3
790	Loma Prieta	Richmond City Hall	18/10/1989	6. 93	107. 45	87. 87	259. 9
829	Cape Mendocino	Rio Dell Overpass - FF	25/04/1992	7. 01	22. 64	14. 33	311. 75
848	Landers	Coolwater	28/06/1992	7. 28	82. 12	19. 74	271. 44
931	Big Bear-01	San Bernardino - E & Hosp.	28/06/1992	6. 46	45. 51	34. 6	271. 44
963	Northridge-01	Castaic - Old Ridge Route	17/01/1994	6. 69	40. 68	20. 72	450. 28
968	Northridge-01	Downey - Co MaintBldg	17/01/1994	6. 69	47. 48	46. 74	271. 9
987	Northridge-01	LA - Centinela St	17/01/1994	6. 69	25. 44	28. 3	234. 88
995	Northridge-01	LA - Hollywood Stor FF	17/01/1994	6. 69	23. 61	24. 03	316. 46
1003	Northridge-01	LA - Saturn St	17/01/1994	6. 69	25. 52	27. 01	308. 71

1010	Northridge-01	LA - Wadsworth VA Hospital South	17/01/1994	6. 69	19. 55	23. 6	413. 81
1026	Northridge-01	Lawndale - Osage Ave	17/01/1994	6. 69	39. 34	39. 91	361. 17
1031	Northridge-01	Leona Valley #5 - Ritter	17/01/1994	6. 69	52. 44	37. 8	445. 98
1052	Northridge-01	Pacoima Kagel Canyon	17/01/1994	6. 69	19. 28	7. 26	508. 08
1053	Northridge-01	Palmdale - Hwy 14 & Palmdale	17/01/1994	6. 69	56. 78	41. 67	551. 56
1054	Northridge-01	Pardee - SCE	17/01/1994	6. 69	25. 65	7. 46	345. 42
1061	Northridge-01	Rancho Palos Verdes - Hawth	17/01/1994	6. 69	53. 19	52. 18	477. 65
1077	Northridge-01	Santa Monica City Hall	17/01/1994	6. 69	22. 45	26. 45	336. 2
1107	Kobe. Japan	Kakogawa	16/01/1995	6. 9	24. 2	22. 5	312
1193	Chi-Chi. Taiwan	CHY024	20/09/1999	7. 62	24. 1	9. 64	427. 73
1197	Chi-Chi. Taiwan	CHY028	20/09/1999	7. 62	32. 67	3. 14	542. 61
1203	Chi-Chi. Taiwan	CHY036	20/09/1999	7. 62	44. 02	16. 06	233. 14
1231	Chi-Chi. Taiwan	CHY080	20/09/1999	7. 62	31. 65	2. 69	553. 4
1488	Chi-Chi. Taiwan	TCU048	20/09/1999	7. 62	43. 31	13. 55	473. 9
1504	Chi-Chi. Taiwan	TCU067	20/09/1999	7. 62	28. 7	0. 64	433. 63
1507	Chi-Chi. Taiwan	TCU071	20/09/1999	7. 62	15. 42	5. 31	624. 85
1508	Chi-Chi. Taiwan	TCU072	20/09/1999	7. 62	21. 42	7. 03	468. 14
1509	Chi-Chi. Taiwan	TCU074	20/09/1999	7. 62	19. 08	13. 46	549. 43
1545	Chi-Chi. Taiwan	TCU120	20/09/1999	7. 62	25. 57	7. 41	459. 34
1551	Chi-Chi. Taiwan	TCU138	20/09/1999	7. 62	24. 22	9. 79	652. 85
1595	Chi-Chi. Taiwan	WGK	20/09/1999	7. 62	31. 96	9. 96	258. 89
1628	St Elias. Alaska	Icy Bay	28/02/1979	7. 54	74. 84	26. 46	274. 5
1794	Hector Mine	Joshua Tree	16/10/1999	7. 13	52. 29	31. 06	379. 32
2113	Denali. Alaska	TAPS Pump Station #09	03/11/2002	7. 9	93. 43	54. 78	382. 5
2419	Chi-Chi. Taiwan-02	TCU120	20/09/1999	7.62	40. 62	36. 8	459. 34
2618	Chi-Chi. Taiwan-03	TCU065	20/09/1999	76. 2	32. 05	26. 05	305. 85
2655	Chi-Chi. Taiwan-03	TCU122	20/09/1999	76. 2	24. 47	19. 3	475. 46
2752	Chi-Chi. Taiwan-04	CHY101	20/09/1999	76. 2	27. 97	21. 67	258. 89

Details on modeling

The structures are modeled with OpenSees 2.2.2. In particular, Beam with Fibre-Hinges Elements are used for modeling beams and columns of the frames. The hinge length is fixed equal to the height of the element cross-section. The material model selected for concrete and steel is Concrete01 and Steel01, respectively. In Table A. 5 and
Table A. 6, the values of the models parameters are reported. The Young modulus used for the elastic portion of all the beam-column elements is equal to 15.5 GPa (equal to one-half the un-cracked concrete Young modulus value). The floor masses of the two superstructures are given in Table A. 7.

Table A. 5 Parameters of the OpenSees model used for concrete

Model	**f_c (MPa)**	**ε_{c0}**	**f_{cu} (MPa)**	**ε_{cu}**
Concrete01	27	-0.004	15	0.015

Table A. 6 Parameters of the OpenSees model used for steel

Model	**f_y (MPa)**	**E_0 (GPa)**	**b**
Steel01	440	210	0.01

Table A. 7 Floor masses (expressed in kg) of the 4-storey and 6-storey building

	Floor level						
Building	**0**	**1**	**2**	**3**	**4**	**5**	**6**
4-storey	42015	42015	42015	42015	33375	-	-
6-storey	43065	43065	43065	43065	42540	42540	33600

Elastomeric Bearing Elements are used for modeling the isolators. The unidirectional plasticity properties for the shear deformations of the elements are defined in accordance with the properties of the isolation systems reported in Table A. 2 of subsection 2.1 of the paper. A zero mass and a zero length is assigned to all the isolators. In order to avoid the introduction of artificial viscous damping in the isolation system, no contribution to the Rayleigh damping is considered for the bearing elements.